



universität
wien

DISSERTATION

Novel concepts and strategies in anticancer metallodrug development: Towards oral activity, peptide conjugation and mass spectrometric applications

Verfasser

Samuel M. Meier, MSc.

angestrebter akademischer Grad

Doktor der Naturwissenschaften (Dr. rer. nat.)

Wien, März 2013

Studienkennzahl lt. Studienblatt: A 791 419

Dissertationsgebiet lt. Studienblatt: Chemie

Betreut von: O. Univ. Prof. Dr. Dr. Bernhard K. Keppler
a./Prof. Dr. Christian G. Hartinger



universität
wien

Ph.D. THESIS

Novel concepts and strategies in anticancer metallodrug development: Towards oral activity, peptide conjugation and mass spectrometric applications

Author

Samuel M. Meier, MSc.

Submitted in partial fulfilment of the requirements for the degree of
Doctor of Sciences (Dr. rer. nat.)

Vienna, March 2013

Doctoral Subject:

Chemistry (A 791 419)

Supervisors:

O. Univ. Prof. Dr. Dr. Bernhard K. Keppler
a./Prof. Dr. Christian G. Hartinger

This Ph.D. thesis is based on the following publications and manuscripts:

Novel Metal(II) Arene 2-Pyridinecarbothioamides: A Rationale to Orally Active Organometallic Anticancer Agents

Samuel M. Meier, Muhammad Hanif, Zenita Adhireksan, Verena Pichler, Maria Novak, Elisabeth Jirkovsky, Michael A. Jakupec, Vladimir B. Arion, Curt A. Davey, Bernhard K. Keppler, Christian G. Hartinger

Chemical Science, **2013**, *4*, 1837-1846.

Identification of the Structural Determinants for Anticancer Activity of an Organometallic Ru^{II}(Arene)–Peptide Conjugate

Samuel M. Meier, Maria Novak, Wolfgang Kandioller, Michael A. Jakupec, Vladimir B. Arion, Nils Metzler-Nolte, Bernhard K. Keppler, Christian G. Hartinger

Chemistry – A European Journal, submitted.

Biomolecule Binding vs. Anticancer Activity: Reactions of Ru(arene)[(thio)pyr(id)one] Compounds with Amino Acids and Proteins

Samuel M. Meier, Muhammad Hanif, Wolfgang Kandioller, Bernhard K. Keppler, Christian G. Hartinger

Journal of Inorganic Biochemistry, **2012**, *108*, 91-95.

Fragmentation Methods on the Balance: Unambiguous Top-Down Mass Spectrometric Characterization of Oxaliplatin-Ubiquitin Binding Sites

Samuel M. Meier, Yury O. Tsybin, Paul J. Dyson, Bernhard K. Keppler, Christian G. Hartinger

Analytical and Bioanalytical Chemistry, **2012**, *402*, 2655-2662.

Zusammenfassung

Manche auf Ruthenium und Osmium als Zentralatomen basierende Koordinationsverbindungen haben sich als vielversprechende tumorhemmende Wirkstoffkandidaten erwiesen. Derzeit stellen organometallische Ru^{II} und Os^{II} Komplexverbindungen—durch einen η^6 -koordinierenden Arenliganden stabilisiert—die bis dato modernste Forschungsstrategie dar, um solche Wirkstoffe zu erhalten. Im Rahmen dieser Dissertation wurden neuartige, tumorhemmende Ru^{II}- und Os^{II}-Aren Verbindungen entdeckt und in Bezug auf ihre molekularen Wechselwirkungen mit Biomolekülen untersucht. Letzteres wurde vorab anhand klassischer Metallverbindungen etabliert.

Obwohl dieser Forschungsbereich bereits intensiv untersucht wird, wird hier das erste Mal von *S,N*-bidentaten organometallischen Ru^{II} und Os^{II} Wirkstoffkandidaten berichtet. Die Liganden basieren dabei auf 2-Pyridinkarbothioamiden, denen Magenschleimhaut-schützende Wirkung und sehr geringe *in vivo* Toxizität nachgewiesen wurde (*J. Med. Chem.*, **1990**, 33, 327–336). Koordination an den organometallischen Rest ergibt äußerst zytotoxische Verbindungen in chemoresistenten Kolonkarzinom- und multidrug-resistenten Lungenkarzinomzelllinien. Ihr Verhalten in wässriger Lösung und ihre ‚drug-likeness‘ legen den Schluss nahe, dass diese neuartige Familie von organometallischen tumorhemmenden Wirkstoffen zur oralen Applikation geeignet sein dürfte. Zudem zeigten Untersuchungen mit dem Nukleosompartikel, dass diese Metallverbindungen ausschließlich an Histon Dimer–Dimer und Dimer–Tetramer Grenzflächen der Histonproteine binden. Dies könnte auf eine Beeinträchtigung von Chromatindynamiken als möglichen Wirkmechanismus deuten.

Organometallische Ru^{II}-Aren Verbindungen, basierend auf *O,O*-bidentaten Pyronatoliganden, zeigen typischerweise eine sehr geringe antiproliferative Aktivität *in vitro*. Es wird hier jedoch gezeigt, dass Ru^{II}-*p*-Cymol Verbindungen mit Triazolyl-modifizierten Pyronatoliganden erhebliche zytotoxische Wirkung aufweisen. Die Strategie der Triazolyl-Modifikation wurde verfolgt, um das erste organometallische Ru–Peptid Biokonjugat mit zytotoxischer Aktivität im niederen mikromolaren Bereich zu erhalten. Dieses Biokonjugat wurde mittels verschiedener Methoden, einschließlich top-down Elektrosprayionisations-Massenspektrometrie (ESI-MS), umfassend charakterisiert.

Massenspektrometrie (MS) ist ein außerordentlich wertvolles Werkzeug zur molekularen Analyse von Wechselwirkungen zwischen Metallverbindungen und Biomolekülen, wie z.B. DNA, Proteinen und deren Bestandteilen. Die molekulare Reaktivität von metallbasierenden tumorhemmenden Wirkstoffen und Wirkstofffamilien kann Erkenntnisse über deren Wirkmechanismus liefern. Im Rahmen dieser Dissertation wurden MS-basierende Techniken neben der Charakterisierung von neuen Verbindungen oder wie oben beschrieben von Peptidkonjugaten auch zur Analyse der Reaktivität von repräsentativen tumorhemmenden (Thio)Pyr(id)onato Ru^{II}-*p*-Cymol Metallverbindungen gegenüber Aminosäuren, Nukleotiden und Proteinen verwendet. Eine inverse Korrelation zwischen dem Ausmaß der Proteinaffinität und der antiproliferativen Aktivität konnte für diese metallhaltigen Verbindungsfamilien festgestellt werden.

Die Bestimmung der Bindungsstelle von Metallionen an Proteinen durch massenspektrometrische Methoden stellt eine erhebliche analytische Herausforderung dar, die vielfach durch eine niedrige Effizienz der Addukt detektion bedingt ist. Es konnte gezeigt werden, dass top-down MS als eine vielversprechende Herangehensweise gelten kann, um z.B. die Bindungsstellen von Oxaliplatin an Ubiquitin (ub) zu bestimmen. Die Kombination der Fragmentierungsmethoden höher energetischer C-Fallen Dissoziation (HCD) und Elektrontransferdissoziation (ETD) erzielte dabei den höchsten Informationsgehalt. Dadurch konnte Methionin-1 als primärer und Histidin-68 als sekundärer Bindungspartner bestätigt werden.

Abstract

Some ruthenium and osmium complexes are promising anticancer drug candidates and the preparation of organometallic Ru^{II} and Os^{II} complexes, stabilized by a η^6 -coordinating arene, represents the latest strategy for obtaining anticancer active metallodrugs with an intriguing activity profile. This PhD thesis reports on the discovery of novel tumour-inhibiting Ru^{II}- and Os^{II}-arene metallodrugs and on studies aimed at understanding the molecular interactions of established anticancer agents and drug candidates with biomolecules.

Although this field of research is intensely investigated, *S,N*-bidentate ligand-containing Ru^{II} and Os^{II} metallodrugs are reported for the first time. The ligands are based on 2-pyridinecarbothioamides, which show activity as gastric mucosal protectants and are largely non-toxic *in vivo* (*J. Med. Chem.*, **1990**, *33*, 327–336). Complexation to the organometallic moiety, however, yields highly cytotoxic metallodrugs in the chemoresistant colon carcinoma and multidrug-resistant non-small lung cancer cell lines. Their aqueous behaviour and drug-likeness properties suggest that this novel family of organometallic anticancer agents may be suitable for oral administration. Additionally, studies with the nucleosome core particle showed that these metallodrugs bind exclusively to the histone proteins at histone dimer–dimer and dimer–tetramer interfaces and therefore, may interfere with chromatin dynamics as a possible mode of action.

Organometallic Ru^{II}-arene metallodrugs based on *O,O*-bidentate pyronato ligands typically show low antiproliferative activity. Intriguingly, triazolyl-modified pyrones coordinated to Ru^{II}-*p*-cymene yield highly cytotoxic agents *in vitro*. The strategy of triazolyl modification was followed to prepare the first organometallic Ru–peptide bioconjugate with cytotoxic activity in the low micromolar range in an ovarian cancer cell line. The metal–peptide bioconjugate was thoroughly characterized by different methods including top-down electrospray ionization-mass spectrometry (ESI-MS).

Mass spectrometry is an invaluable tool in the analysis of molecular interactions between metallodrugs and biomolecules, such as DNA or proteins and their constituents. Furthermore, the molecular reactivity may give insight into the mode of action of a particular metallodrug or family of metallodrugs. Within the frame of this Ph.D. thesis, mass spectrometric techniques have been used to characterize the reactivity of representative (thio)pyr(id)onato Ru^{II}-*p*-cymene metallodrugs towards amino acids, nucleotides and proteins and an inverse correlation was found between extent of protein binding and antiproliferative activity, at least for these families of metallodrugs.

Furthermore, the analysis of metallation sites of metallodrugs on proteins by mass spectrometric methods poses significant challenges in many cases due to low adduct detection efficiencies. Top-down mass spectrometric analysis is a promising approach to determine oxaliplatin binding sites on ubiquitin and different fragmentation techniques were investigated with the combination of higher energy C-trap dissociation (HCD) and electron transfer dissociation (ETD) tandem mass spectrometry yielding the highest information content. This approach led to the confirmation of methionine-1 as the primary and histidine-68 as the secondary binding site.

I would like to express my sincere gratitude to

Bernhard K. Keppler for giving me the opportunity to perform my Ph.D. in his group, for his guidance and generous support.

Christian G. Hartinger for his guidance, insightful and inspiring discussions, for correcting many written pages and for his support 24/7 even from his new home in Auckland.

Yury O. Tsybin at the EPFL for valuable discussions on the topic of mass spectrometry.

Nils Metzler-Nolte, together with **S. David Köster**, **H. Bauke Albada** and **Kathrin Klein** at the RUB for their thorough introduction into the synthesis of metal-peptide conjugates.

Elfriede Limberger for her sedulous administrative aid.

Wolfgang Kandioller, **Andrea Kurzwernhart**, **Masha Babak**, **Stefan Mokesch**, **Mario Kubanik**, **Britta Fischer**, **Evelyn Balsano** and all the remaining and former members of Lab6@AT and Lab6@NZ for their support.

Gerlinde Grabmann and **Sarah Theiner** of Lab2 for critically discussing countless questions and topics in analytics.

Vladimir B. Arion and **Alexander Roller** for X-ray data collection and refinement.

Markus Galanski, **Verena Pichler**, **Wolfgang Kandioller**, **Amitava Kundu**, **Sergey Abramkin**, **Michael Primik** and **Paul-Steffen Kuhn** for reliable NMR measurements.

Michael A. Jakupec and **Maria Novak** for performing and interpreting cell culture assays.

Johannes Theiner for the elemental analysis of numerous compounds.

My former colleagues **Sergey Abramkin**, **Gabriel E. Büchel**, **Anna K. Bytzek**, **Alexander Egger** and **Muhammad Hanif** for their introduction to the institute and kind support in various aspects.

Elisabeth Jirkovsky for her commitment to my projects.

My **family** and **friends**, especially Katharina, my four parents, my parents in law and my godfather for their invaluable support, motivation, understanding and patience throughout my life.

– S.M.M.

Table of Contents

1. Abbreviations	XII
2. Introduction	1
2.1. Medicinal Chemistry	1
2.1.1. Drug Discovery	2
2.1.2. Drug Design	2
2.1.3. Drug Development	3
2.2. Cancer	3
2.2.1. Biology of Cancer	3
2.2.2. Cancer Therapy	4
2.3. Ruthenium and Osmium Metallopharmaceuticals	5
2.3.1. Ruthenium(III) Anticancer Agents	5
2.3.2. Ruthenium(II) Anticancer Agents	7
2.3.3. Osmium Anticancer Agents	9
2.3.4. Organometallic Ruthenium and Osmium Anticancer Agents: State-of-the-Art	10
2.3.5. Pharmacodynamics of Ruthenium and Osmium Anticancer Agents	17
2.3.6. Pharmacokinetics and Toxicology of Ruthenium and Osmium Anticancer Agents	21
2.4. Mass Spectrometry for Investigating Metal-Based Anticancer Agents	22
2.4.1. Instrumental Setup of a Mass Spectrometer	22
2.4.2. Application of Mass Spectrometry in Metallodrug Research	25
2.5. Research Justification	27
2.6. References	27
3. Results and Discussion	33
3.1. Novel Metal(II) Arene 2-Pyridinecarbothioamides: A Rationale to Orally Active Organometallic Anticancer Agents	33
3.2. Identification of the Structural Determinants for Anticancer Activity of an Organometallic Ru ^{II} (Arene)–Peptide Conjugate	45
3.3. Biomolecule Binding <i>vs.</i> Anticancer Activity: Reactions of Ru(arene)[(thio)pyr(id)one] Compounds with Amino Acids and Proteins	57
3.4. Fragmentation Methods on the Balance: Unambiguous Top-Down Mass Spectrometric Characterization of Oxaliplatin-Ubiquitin Binding Sites	65
4. Conclusions	75
5. Supporting Information	77
5.1. Novel Metal(II) Arene 2-Pyridinecarbothioamides: A Rationale to Orally Active Organometallic Anticancer Agents	77
5.2. Identification of the Structural Determinants for Anticancer Activity of an Organometallic Ru ^{II} (Arene)–Peptide Conjugate	107
5.3. Biomolecule Binding <i>vs.</i> Anticancer Activity: Reactions of Ru(arene)[(thio)pyr(id)one] Compounds with Amino Acids and Proteins	119
5.4. Fragmentation Methods on the Balance: Unambiguous Top-Down Mass Spectrometric Characterization of Oxaliplatin-Ubiquitin Binding Sites	121
6. Personal Information	130
6.1. Curriculum Vitae	130
6.2. List of Publications	131
6.3. List of Oral Contributions	131
6.4. List of Poster Contributions	131

1. Abbreviations

ADME – absorption, distribution, metabolism and elimination; 5'-AMP – adenosine 5'-monophosphate; ATP – adenosine 5'-triphosphate; bip – biphenyl; ^tBu – *tert*-butyl; CDK – cyclin-dependent kinase; CID – collision-induced dissociation; CL – total clearance; ClogP – calculated partition coefficient; C_{max} – maximum concentration; cNMP – nucleotide 3',5'-cyclic monophosphate; cym – p-cymene; Cys – L-cysteine; cyt – cytochrome C; CZE – capillary zone electrophoresis; Da – Dalton, atomic mass unit; dG – 2-deoxyguanosine; DNA – 2-deoxyribonucleic acid; 5'-dNMP – 2-deoxyribonucleotide 5'-monophosphate; dmsO – dimethyl sulfoxide; dT – thymidine; EAC – Ehrlich's ascite carcinoma; ECD – electron capture dissociation; en – ethylenediamine; EPR – electron paramagnetic resonance; ESI – electrospray ionization; Et – ethyl; ETD – electron transfer dissociation; *f*_{MF} – fraction of the molecular framework; Fsp³ – fraction of sp³-hybridized carbon atoms; FT – Fourier transform; 5'-GMP – guanosine 5'-monophosphate; GSH – glutathione; HBA – hydrogen bond acceptor; HBD – hydrogen bond donor; HCD – higher energy C-trap dissociation; His – L-histidine; HPLC – high performance liquid chromatography; HSA – human serum albumin; IC₅₀ – concentration at which an inhibitory effect of 50% is obtained; ICP – inductively coupled plasma; ICR – ion cyclotron resonance; IEC – ion exchange chromatography; IM – ion mobility; i.p. – intraperitoneal; IRMPD – infrared multiphoton dissociation; IT – ion trap; i.v. – intravenous; K_a – acidity constant; LA – laser ablation; LOD – limit of detection; LTQ – linear triple-quadrupole; *m/z* – mass-to-charge ratio; MALDI – matrix-assisted laser desorption ionization; Me – methyl; Met – L-methionine; MlogP – measured partition coefficient; μM – micromolar; MMP-2 – matrix metalloproteinase 2; MS – mass spectrometry; MS² – tandem mass spectrometry (also MS/MS); MSⁿ – multi-stage mass spectrometry; MTD – maximum tolerated dose; MudPIT – multidimensional protein identification technology; NAD⁺ – nicotinamide adenine dinucleotide, oxidized form; NADH – nicotinamide adenine dinucleotide, reduced form; NCP – nucleosome core particle; 5'-NMP – nucleotide 5'-monophosphate; PDT – photodynamic therapy; pH – negative common logarithm of the H⁺ activity; p.o. – oral; PSA – polar surface area; PTM – post-translational modification; QED – quantitative estimate of drug-likeness; RNA – ribonucleic acid; ROS – reactive oxygen species; SAR – structure-activity-relationship; SEC – size-exclusion chromatography; T/C – survival time or tumour growth with respect to a control group; t_{1/2} – half-life; Tf – transferrin; 5'-TMP – thymidine 5'-monophosphate; TOF – time-of-flight; TP53 – tumour protein 53; ub – ubiquitin; V_{ss} – volume of distribution at steady state.

2. Introduction

2.1. Medicinal Chemistry

The discovery and development of pharmaceutical compounds for application in diagnosis and treatment of diseases or adverse conditions in humans is the main task of medicinal chemists. Any pharmaceutical should ideally display highly selective bioactivity, meaning that the pharmaceutical should be effective only against the disease and avoid harming the healthy parts of the body [1]. Unfortunately, adverse effects of therapeutic agents are quite commonly observed, always depending on the applied dose. This was already recognized in the mid 15th century AD by Paracelsus, who stated that “*all things are poison and nothing [is] without poison. Only the dose makes a thing not to be poison*” [2]. Today, the therapeutic index is one way of measuring the safety of a pharmaceutical and it is defined by the ratio of the dose leading to toxic effects and the dose required for a beneficial response, *i.e.* the larger the therapeutic index, the “safer” the drug [1]. But how can a small molecule evoke a therapeutic or toxic effect in a highly complex setting such as in animals or humans?

In fact, all mammals (including humans) are extraordinary large assemblies of eukaryotic cells, which specialize and cluster to form the diverse tissues of their bodies with very specific functions [3]. For example, the liver and kidneys filter the blood, muscles allow us to move and are responsible for circulating the blood (heart), the lungs allow the passage of oxygen into the blood and the eyes allow us to perceive our environment even in colour. Eukaryotic cells contain common components independently of their degree of speciation. First, all cells are surrounded by a membrane – a lipid bilayer – that separates them from their environment and that manages the passage of nutrients and other compounds into and out of the cell. Besides the highly crowded cytoplasm [4], a cell contains

organelles, which are themselves surrounded by a membrane, *e.g.* the energy generating mitochondria, acidic endosomes, peroxisomes and lysosomes, but also the protein manufacturing endoplasmic reticulum and the Golgi apparatus. Furthermore, the cytoskeleton is responsible for trafficking. In contrast to prokaryotes, eukaryotic cells contain a nucleus, which stores the 2-deoxyribonucleic acid (DNA) and is itself surrounded by the nuclear membrane. All the necessary information of cell survival, adaption and specification is encoded in the DNA sequence. DNA information can be transiently transcribed into messenger ribonucleic acid (mRNA), which is then translated into proteins with the latter being the executors of the DNA information. Proteins have many different functions in the cell including transport, structural, signalling and catalytic roles. The process of transcription and translation is known as gene expression and guides the behaviour, form and virtually all activities of a cell. Since DNA, proteins and also the lipid bilayer are made of discrete molecules with distinct structures and specific functions at different stages of the cellular life cycle (Figure 1), medicinal chemists aim at targeting such molecules in a way to cause the cells to behave differently or even forcing them to trigger apoptosis (programmed cell death). Therefore, a therapeutic or toxic effect is caused by a *molecular* interaction of a pharmaceutical with a drug target such as DNA or a protein on the cell membrane or inside the cell and is characterized by covalent (coordinative) or non-covalent bonding (electrostatic, dipole – dipole, van-der-Waals, hydrophobic or hydrogen bonding) [1].

The process from discovery of a bioactive substance to marketing can be divided into three stages (Figure 2), namely drug discovery, design and development, which will be

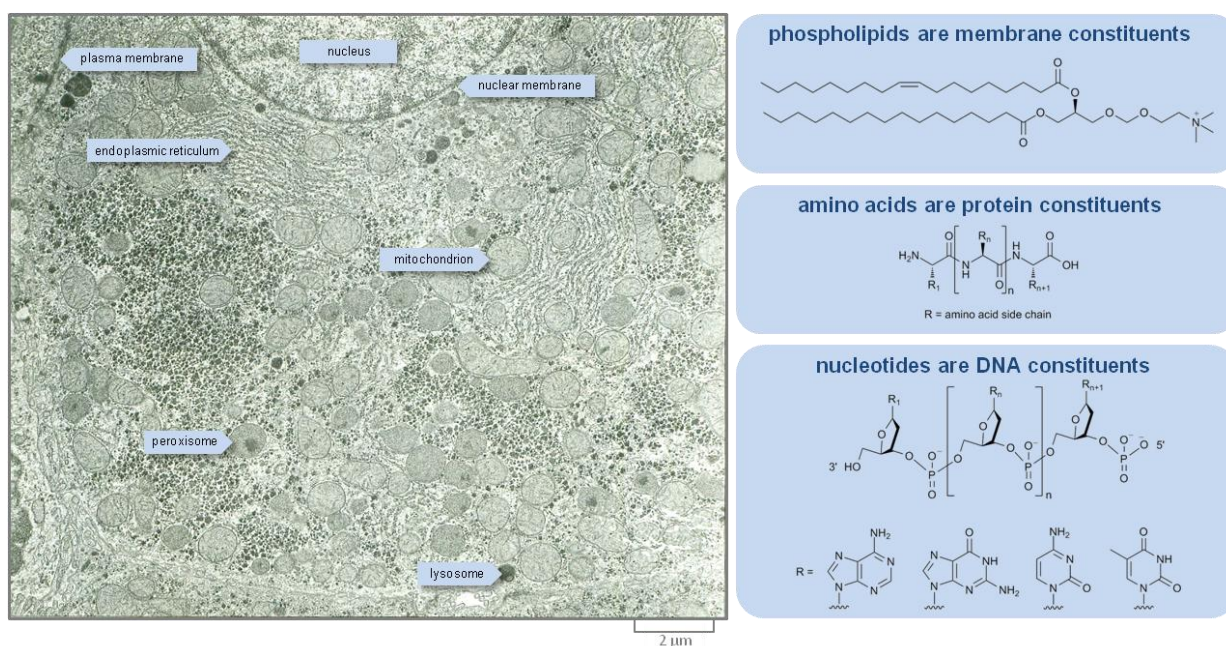


Fig. 1 (left) A section of a liver cell shows the densely packed cytoplasm with cellular compartments, adapted from Ref. [3]. (right) The basic molecular components of the cell can largely be reduced to phospholipids (phosphatidylcholine is shown as an example), amino acids and nucleotides, which are the building blocks of the membranes, proteins and DNA, respectively.

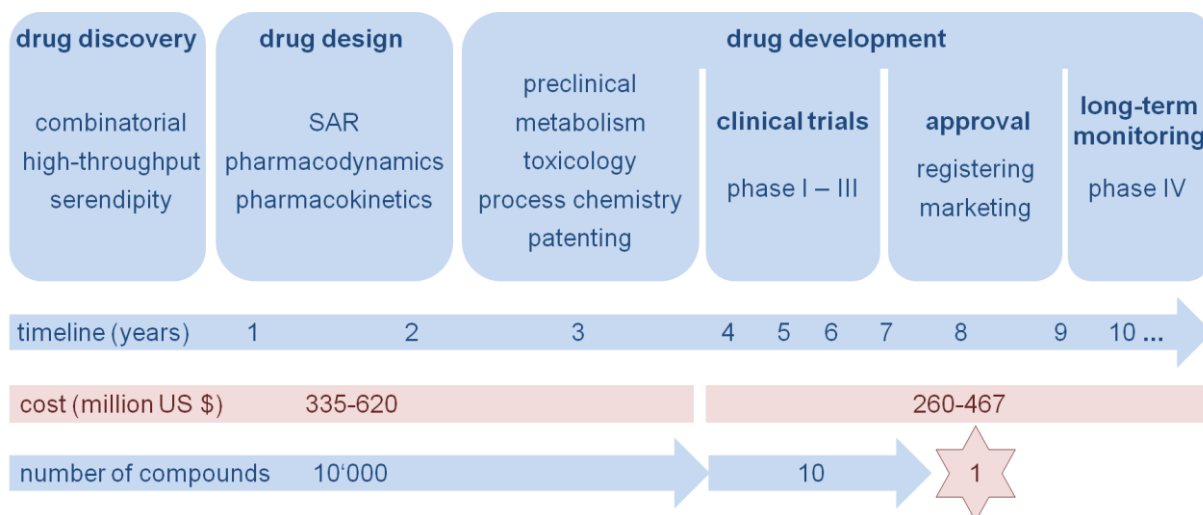


Fig. 2 An overview on the stages from drug discovery to drug development. Each stage is characterized by the evaluation of certain key properties of a potential drug candidate. The bottom lines illustrate the timeline, the cost and the number of compounds studied at each stage and are adapted from Refs. [1,7].

discussed in the following sections. In practice, the boundaries between the three stages are quite diffuse and they may partly evolve in parallel [1,5].

2.1.1. Drug Discovery

The aim of drug discovery is to identify a lead compound, which shows biological activity in a bioassay with relevance to a chosen disease [1]. Such assays can be performed using cell cultures (*in vitro*) or in animal models (*in vivo*). Cell cultures are generally preferred because they are faster, cheaper and less controversial in terms of ethics. It must be noted that high potency *in vitro* does not necessarily translate to high potency *in vivo* due to unpredictable absorption and distribution of a pharmaceutical [5]. A lead may be identified either by serendipity or by screening a library of natural or synthetic compounds. Upon selection of a lead, a reliable synthetic pathway must be established. Similarly, the structure and purity must be thoroughly characterized at the molecular level. Chemicals are never 100% pure and if a chemical is intended for clinical use, it is of high importance to characterize the impurities as accurately as possible [6], especially if their concentration exceeds a certain threshold level.

High throughput screenings [8] and combinatorial synthesis [9] of very large compound libraries experienced a considerable boost in recent years due to the possibility of screening thousands of compounds in a relatively short amount of time by automated *in vitro* assays. It was hoped that increasing the number of screened molecules would increase the probability of identifying leads. However, these methods did often not meet the expectations and success was scarce [10]. Computational chemistry is also making its way as an increasingly important tool for predicting lead structures, in particular when X-ray structures of drug targets are available [11].

2.1.2. Drug Design

If a pharmaceutical is planned to undergo clinical studies, it should display high potency with respect to its biological effect but also accumulate at therapeutically relevant concentrations at the desired site in the body, ideally without affecting off-targets. The optimization of these parameters is a tricky process and the medicinal chemist summarizes these

investigations by pharmacodynamics and pharmacokinetics [1].

Pharmacodynamics. Pharmacodynamics is mainly characterized by lead optimization with respect to the interaction with a drug target and the resulting improvement of the biological activity, *i.e.* the cytotoxic activity or enzyme inhibition. Optimization is achieved by preparing a set of slightly structurally-different compounds and evaluating their effect in bioassays, which are most often *in vitro*-based. Structure-activity relationships (SAR) can then be derived from these studies, which help predicting the influence of chemical modifications on the biological effect. Importantly, polar and hydrophobic interactions, functional groups and the rigidity of the molecule often directly influence the degree of potency of the pharmaceutical in the assay.

Pharmacokinetics. The most potent representative from pharmacodynamic (*in vitro*) studies is not always the best drug for further drug development because absorption and distribution effects are not considered. Pharmacokinetic studies deal with the fate of the drug in the body, once it is administered *in vitro* and/or *in vivo* and encompass mainly ADME profiling, *i.e.* the evaluation of absorption, distribution, metabolism and excretion. Pharmacokinetics highly depend on the route of administration. For example, orally active drugs must be stable enough to survive the acidic conditions in the stomach and must be able to cross the gut wall or tight junctions in order to reach the blood stream. An orally active pharmaceutical must also cope with a substantial pH increase between stomach and blood ($\Delta\text{pH} \approx 6$), which is critically influenced by the presence of functional groups in the drug's molecular structure. Polar or charged compounds are under these conditions only poorly absorbed and are unlikely to cross cellular membranes by passive diffusion. Furthermore, such compounds tend to be rapidly excreted from the blood stream, while uncharged and hydrophobic compounds can cross membranes more easily but tend to accumulate in fatty tissues. The polarity (lipophilicity) and acidity (pK_a) are crucial parameters affecting not only absorption of a drug, but also its distribution and elimination.

Once a drug is administered, it may be extensively metabolized by the body, which thereby modifies the physicochemical properties of a pharmaceutical. Metabolism

generally renders foreign molecules more polar to facilitate rapid excretion. During pharmacokinetic studies, drugs can be made more or less resistant to metabolic reactions in order to optimize distribution and excretion parameters. Metabolism is generally characterized by two phases: Phase 1 modifies a foreign molecule by adding a polar group to a hydrophobic region *via* oxidation, while during phase 2 large polar molecules are added to the already metabolized drug, such as by glucuronidation. Finally, pharmaceuticals should accumulate in the desired tissue or organ because selective distribution is generally associated with reduced side effects [1].

2.1.3. Drug Development

Once an optimized lead compound exhibiting promising pharmacodynamic and pharmacokinetic properties was selected, it may enter drug development [1]. This is the most time- and cost-expensive of all three stages. Typically, of a total of 10'000 synthesized molecules during drug design, only 10 will reach drug development and clinical trials, while only one will be successfully registered and marketed. The average cost for the overall research and development of one successful drug is estimated to be close to \$1 billion [7]. Drug development comprises three important phases, namely patenting, process development and (pre-)clinical trials [1]. To be able to refund such astronomical amounts for further drug discovery and development programs, novel substance families including the drug candidate need to be patented with respect to their structures, synthesis and biological effect. Moreover, at the edge of clinical trials, large amounts of the drug candidate are needed. This involves chemical and process development following strict guidelines for good manufacturing procedures yielding reliable batches with consistent composition and purity.

Preclinical experiments. A promising drug candidate from drug design undergoes *in vivo* toxicity tests during preclinical trials. The main focus lies on determining the acute and chronic toxicity as well as carcinogenicity and mutagenicity. Additionally, the therapeutic index of the drug candidate is determined *in vivo* and gives an estimate of the initial dosage during clinical trials. Furthermore, drug metabolites are characterized and separately tested for their activity and toxicity because one drug metabolite may potentially show a therapeutic effect, while others rather exert toxic effects. Detailed investigations on the mechanism of action and interactions with off-targets may also be carried out at this stage. Preclinical trials finally involve stability and formulation tests in order to estimate the shelf-life of a drug candidate and to find an appropriate route of administration.

Clinical trials. If the preclinical experiments show the desired safety and therapeutic properties, a drug candidate may enter clinical trials, where it is finally evaluated for its efficacy in humans. Clinical trials have an average duration of 5–7 years and contain four phases with specific endpoints. Many drug candidates fail at this final hurdle in drug development and in many cases additional chemical modifications must be envisioned in order to save the drug candidate from attrition [12].

Phase I studies are usually performed on a small number of healthy volunteers with the purpose of evaluating the safety, dosage and pharmacokinetics of the drug candidate [1]. In cases of life-threatening diseases such as cancer, volunteer patients are recruited rather than healthy volunteers due to the potential toxic side effects of anticancer agents.

Phase II studies are carried out to establish whether the drug candidate is actually effective in patients and whether it causes adverse effects. In general, clinical phase II trials are performed as double-blind placebo-controlled studies. This means that neither the doctors, nor the patients know who obtains a placebo or the real drug. With regard to life-threatening diseases, the administration of a placebo would be unethical and the effect of the drug candidate is compared to an established therapeutic drug. Additionally, the final dosage needs to be determined.

During phase III, the drug candidate is evaluated in a large cohort of patients (~1000), which are screened for the drug's effectiveness and potential long-term toxicities. The drug candidate is also compared to already established drugs and should display an improved effectiveness in order to obtain approval.

Finally, phase IV studies include long-term monitoring of the drug with respect to the effectiveness and rare side effects after approval and marketing. Clinical trials can be terminated at each phase as soon as toxic side effects are observed. Even drug-withdrawal from the market occurred in some cases if rare, but serious adverse effects were reported [1].

2.2. Cancer

Our body maintains various signalling and communication systems among the cells of our tissues, which are responsible for their social behaviour supporting the whole organism. In order to grow and maintain their function, cells constantly renew themselves. During this replication process, errors (mutations) may occur that normally trigger apoptosis of the affected cell, *i.e.* such cells are usually not viable. However, there are cases, where a mutation may inhibit apoptosis leading to an advantage over the neighbouring cells. Cancer may then develop after several mutation steps and the affected cells start to display unsocial character, which is characterized among others by sustained proliferation and invasion of other tissues that may eventually cause the death of the whole organism. The severity and prognosis of cancer depends on the cell type that is affected. The World Health Organization reports that in Austria in 2010, 19'761 deaths were caused by cancer, which amounts to 26% of all deaths of that year [13,14]. Men (10'465) were slightly more affected than women (9'296). Cancers of the lung, intestine, colon (including rectum and anus), pancreas and prostate, breast and ovary were the deadliest. Cancer mortality is highly age-dependent and only about 5% (1'040) of cancer deaths account for people younger than 50 years in Austria [13]. This situation is characteristic of countries of the developed world, where cancer mortality is only second to cardiovascular diseases [15]. Finally, it seems that cancer is rather caused by the way of life of an individual, *e.g.* smoking and diet [16], than by environmental factors [3].

2.2.1. Biology of Cancer

Carcinogenesis describes the evolution of a normal cell into a malign tumour and involves multiple mutations accompanied by proliferation (Scheme 1) [3]. Cancer cells are often characterized by their genomic instability [17] but also by sustained inflammation [18]. The notion of tumour microenvironment refers to the idea that tumours are highly diverse and complex tissues that can recruit normal surrounding cells, which form the tumour-associated stroma [19]. The whole microenvironment was suggested to include

cancer cells, cancer stem cells, endothelial cells, pericytes, immune inflammatory cells and cancer-associated fibroblast as well as stem and progenitor cells of the stroma.

During recent years, several hallmarks of cancer have been proposed (Figure 3) [19,20]:

- 1) Cancer cells can control their own proliferation. This is either achieved by autocrine proliferation or stimulation of tumour-associated stroma cells for supplying growth factors to cancer cells. Although sustained proliferative signalling seems to be necessary, over-expression of growth factors forces the cells into a non-proliferating state called senescence. Cancer cells seem able to tightly control the abundance of growth factors.
- 2) Cancer cells tend to evade growth suppressors by inhibiting negative regulators of proliferation. Inhibition of such negative regulators alone does not result in acute carcinogenesis, but may lead to late-life leukaemia and sarcomas in mice.
- 3) Cancer cells resist apoptosis by inhibiting the tumour suppressor function of tumour protein 53 (TP53), a protein that can detect DNA damage. Additionally, cancer cells can display some degree of autophagy to resist apoptosis, for example in the case of nutritional shortage.
- 4) Cancer cells enable replicative immortality. Telomere erosion at the DNA-ends usually dictates the life-span of a normal cell. Cancer cells can up-regulate telomerase activity in order to keep the telomeres at a viable length.
- 5) Tumours constantly activate angiogenesis. Due to sustained angiogenesis, the formed blood vessels are usually aberrant and leaky. Angiogenesis is already induced early in the development of cancer and contributes to the microscopic premalignant phase of neoplastic progression. The innate immune system infiltrates such premalignant lesions causing inflammation, which actually helps triggering angiogenesis. Moreover, angiogenesis may also be activated by hypoxia.
- 6) Cancer cells can actively invade the surrounding tissues and metastasize. Importantly, inhibition of E-cadherin proteins causes loss of cell-to-cell adhesion. Invasion and metastasis is a multistage process and involves local invasion, intravasation, transit through the lymphatic and haematogenous system, escape from the vessels into the parenchyma of distant tissues (extravasation) and survival.

Recently, two new hallmarks were suggested involving reprogramming of energy metabolism and evading immune destruction [19].

2.2.2. Cancer Therapy

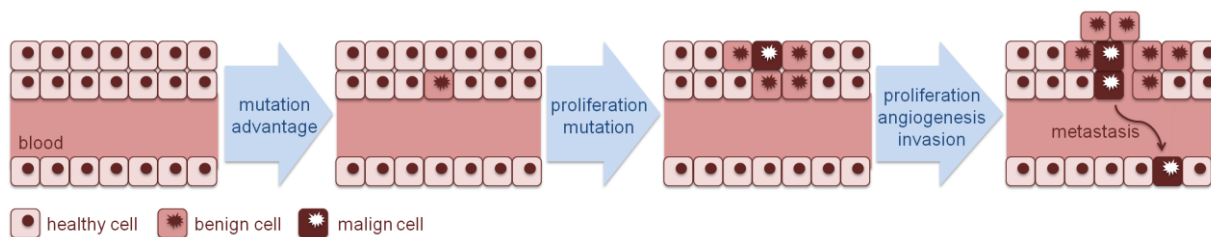
The current standard therapies for treating cancer are surgery, radiation- [21,22], chemo- [23], immuno- [24] or antibody [25] therapy. Depending on the location, type and



Fig. 3 The extended hallmarks of cancer proposed by Hanahan and Weinberg. Adapted from Ref. [19].

size of the tumour, two or more of the mentioned methods are combined to improve the chance of curative cancer therapy. The most common combination is surgery with chemotherapy. After surgical removal alone cancer recurrence is often observed due to unrecognized microscopic lesions or metastases [21]. The main purpose of chemotherapy is to assist in the treatment of such lesions and help improving the curative effect. Most commonly, the drug design strategy for cancer chemotherapeutics involves DNA damage [26,27], since cancer cells are rapidly proliferating cells. DNA may be damaged by alkylation (dacarbazine, lomustine, cisplatin, carboplatin, oxaliplatin) while DNA replication may be hindered by anti-metabolites (methotrexate, 5-fluorouracil) or by inhibition of proteins involved in replication or transcription (etoposide). Furthermore, effective cytotoxic antibiotics (anthracyclines such as doxorubicin) are also known, which intercalate into DNA. However, a tumour-selective chemotherapy is very hard to realize since cancer and healthy cells are (bio)chemically virtually identical. Therefore, healthy cells are often severely damaged during classical chemotherapy, which is usually accompanied by well-known side effects, such as nausea, hair loss, myelosuppression, nephro-, hepato- and ototoxicity as in the case of cisplatin [28]. Consequently, the quality of life [29] of cancer patients is drastically reduced. Targeting of tumour-selective oncoproteins (imatinib) represents a recent strategy for reducing side effects and improving the quality of life of cancer patients [27].

Although only three Pt^{II} chemotherapeutics are approved for worldwide clinical use, namely cisplatin, carboplatin and oxaliplatin, Pt^{II}-based anticancer agents are used in almost 50% of all cancer therapy schemes and are among the best known anticancer agents [30]. The most recent Pt-anticancer complex, oxaliplatin, was approved for worldwide clinical



Scheme 1 A multistage mutation process forms the basis of carcinogenesis. Initial mutations afford the affected cell an advantage over the surrounding cells with respect to growth. Further mutations cause DNA instability leading to uncontrolled proliferation, angiogenesis and finally to invasion and metastasis formation.

application in 2002. In spite of the success of Pt^{II} cancer chemotherapeutics, they are selective only with respect to a few cancer types and also cause severe side effects [31], which definitely opened room for research and development of alternative metal-based anticancer agents with an improved activity profile and reduced general toxicity. In particular, ruthenium and osmium complexes hold great promise in this regard [30,32] and are discussed in detail in the following sections.

2.3. Ruthenium and Osmium Metallopharmaceuticals

Probably one of the earliest investigations on the anticancer effect of inorganic metal salts and complexes was reported by Collier and Krauss in 1931 [33]. In their work, they infected white mice with Ehrlich's mouse carcinoma and analyzed the effect of single-dose subcutaneous administrations of Cu, Pb, Cr, Mn, Fe, Ni, Co, Ru, Rh and Os compounds on tumour growth. Most of the compounds were inactive, but significant activities were observed for some Pb-compounds, K₂Mn(SO₄) and importantly Cs₂[Ru^{IV}Cl₆] hydrate. They concluded that the biological effect of a metal on the mouse carcinoma was not solely caused by the metal centre, but also by its structure and type of ligands: "Die Wirkung eines *Schwermetalls* gegen den experimentellen Mäusekrebs ist *nicht nur durch das Metall allein, sondern auch durch den Aufbau der Verbindung und die Verbindungsgenossen bedingt*". However, it was not before the pioneering work of Rosenberg some 34 years later that metallopharmaceuticals, in particular platinum-based complexes, received broad scientific attention [34]. In his first report on the inhibition of cell division by electrolysis products from a platinum electrode in *E. coli*, Rosenberg demonstrated that several Pt^{IV} halogenides, Rh^{III} chlorides, but also [Ru^{III}(NH₃)₄Cl(OH)]Cl were actively causing filamentous growth of the bacteria. Consequently, these types of metals interfere with cell division and their effect was assumed to be caused by interaction with DNA on a molecular level. Rosenberg's question of whether these metal ions would inhibit cell division in other bacteria, or even mammalian cells was answered in 1969, where he showed *in vivo* inhibition of sarcoma and leukaemia tumours by platinum compounds and claimed the platinum compounds as a new class of potent antitumour agents [35,36]. Four platinum compounds, namely *cis*-[Pt^{IV}(NH₃)₂Cl₄], *cis*-[Pt^{II}(NH₃)₂Cl₂] (cisplatin), [Pt^{IV}Cl₄(en)] and [Pt^{II}Cl₂(en)], where en is ethylenediamine were reported and showed antineoplastic effects after intraperitoneal administration. A decade later, Pascoe showed that DNA seems indeed to be the cellular target for cisplatin [37].

2.3.1. Ruthenium(III) Anticancer Agents

In his first report, Rosenberg also investigated other metals and Rh and Ru complexes were of particular interest since they were causing filamentous growth in *E. coli*. [34]. While Rh was also found to be toxic to the cells, Ru was selected by researchers as the most promising non-platinum metal for further development. Consequently, investigations were conducted with am(m)ine and chlorido Ru^{III} complexes because of their well-established chemistry and similarity to cisplatin. In 1976, *fac*-[Ru^{III}Cl₃(NH₃)₃] was shown to induce filamentous growth in *E. coli* indicating a similar effect as observed for cisplatin [38]. This triggered research to focus on the mode of action and molecular interactions of Ru complexes in particular with DNA and models thereof. The

early work by Clarke reported such interactions employing the monofunctional [Ru^{III}(NH₃)₅Cl]Cl₂ as a precursor [39,40]. He demonstrated the synthesis of guanine [39], as well as cytidine and adenosine [40] adducts with the penta(ammine)ruthenium^{III} moiety *via in situ* reduction of [Ru^{III}(NH₃)₅Cl]²⁺ followed by reoxidation. He also showed that guanine binds *via* N7, while adenosine and cytidine seem to coordinate *via* the exocyclic amines to the metal, which is believed to be stabilized by hydrogen bonding. Furthermore, the *in vitro* cytotoxicity of several [Ru(NH₃)₅(P)]Cl₃ complexes, where P is a purine, was tested in human nasopharyngeal carcinoma cells [41]. At concentrations of 0.1 mM, they observed inhibition of DNA synthesis and to some extent inhibition of protein synthesis. Importantly, the same article describes the "activation-by-reduction" hypothesis, *i.e.*, substitution-inert Ru^{III} complexes are believed to be activated by reduction to a Ru^{II} species in the cellular environment, which then react with DNA resulting in the anticancer activity. Reduction from Ru^{III}→Ru^{II} decreases the π-acceptor property of the metal leading to a labilization of π-donating ligands such as chlorides, which facilitates hydrolysis. Reduction should be facilitated in the hypoxic tumour environment and should result in some selectivity for tumour tissue [41,42]. In 1980, Clarke investigated the activation-by-reduction hypothesis further with [Ru(NH₃)₅Cl]Cl₂, leading to the conclusion that the reduction might be catalyzed by cellular components such as glutathione (GSH) or microsomal proteins and that the presence of air decreases the rate of heterocyclic ligand binding, *i.e.* to DNA [43].

In the same year, he commented on the mutagenicity of these Ru^{III} complexes due to their ability to form stable metal–nucleotide bonds [44]. Again, he pointed at the importance of the oxidation state of the metal, which influences binding to nucleic acids and nucleosides. His emphasis was on developing "substitution-inert metal ions [which] can cause recognizable lesions in cellular chromatin and so induce the cell to attempt to repair its DNA by error-prone methods." [44]. His letter must also be viewed as a call for research activities in the area of metal-based anticancer agents, which was boosted by the approval of cisplatin as a first-line drug to treat testicular and ovarian cancer two years earlier [28]. However, as mentioned above, platinum-based chemotherapy suffers from several severe side effects [28]. Furthermore, no or insufficient activity of cisplatin is observed in slow growing adenotumours occurring in the lung, colon or rectum [31], *i.e.* adenocarcinoma of the colon is still among the four deadliest cancer types and was responsible for 608'000 deaths worldwide in 2008 [45]. The main motivation for the development of Ru^{III} anticancer agents was the effective targeting of these tumour types.

KP1339. In 1986, Keppler communicated the first representative of a novel class of active Ru^{III} antitumour agents based on (H₂Im) *trans*-[RuCl₄(HIm)₂], where HIm is imidazole (KP418) [46]. In the full paper the year after [47], he wrote: "The reported activity against the transplantable tumour models described above indicates tumour-inhibiting properties in general, but it cannot guarantee activity of the test compound against specific human organ tumours. Within the range of human tumours, gastrointestinal cancers are one of the major causes of cancer mortality in the western world. No really sufficient chemotherapy against this type of tumours could be established until now." In fact, (HB) *trans*-[RuCl₄B₂] and (HB)₂ [RuCl₅B], where B is a N-containing heterocycle,

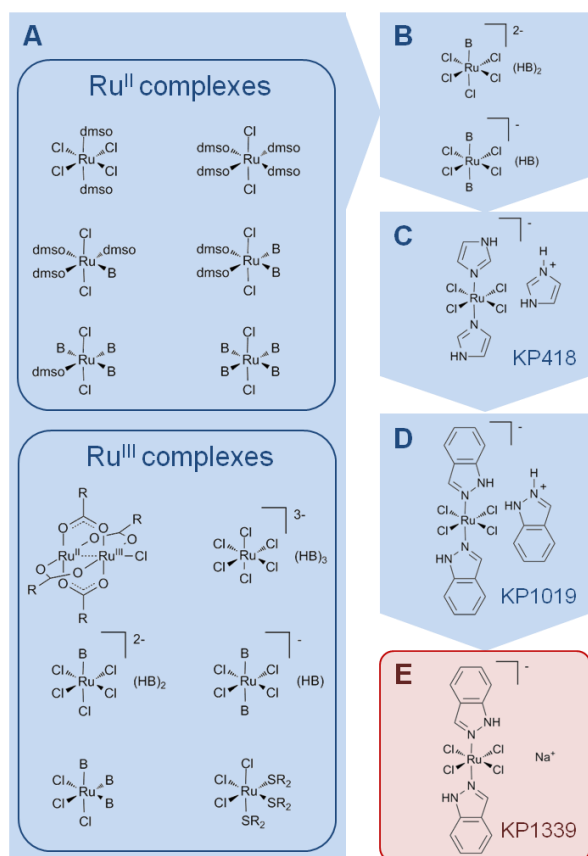


Fig. 4 The design of KP1339: From drug discovery to lead optimization. (A) *In vivo* screening of several compound families in the P388 leukaemia mouse model yielded the most promising families (B) and the lead compound KP418 (C). However, KP418 showed toxic effects in the more developed colorectal tumour model. KP1019 (D) turned out less toxic but equally active. The low solubility of KP1019 was improved by exchanging the indazolium counter cation with sodium resulting in the optimized lead compound KP1339 (E), which is currently in clinical phase I/II studies. R denotes an organic rest and B a nitrogen donor.

were the most promising classes from a large *in vivo* screening in the P388 leukaemia mouse model (Figure 4) [31]. The effect of KP418 was then investigated in an autochthonous colorectal carcinoma model in rats [48]. The compound caused a significant tumour growth inhibition of >90%, while cisplatin was completely inactive. However, this beneficial effect was accompanied by 34% loss of body weight and 55% mortality indicating dose-related toxicities in the animals. In the same work, a reduction of these side effects while retaining the antitumor activity was obtained with (H₂Ind) *trans*-[RuCl₄(HInd)₂], where HInd is indazole (KP1019) [48], where 3% loss of body weight and 0% mortality were observed at a dosage of 22 mmol/kg. However, this came at the cost of lower water solubility. In the following years, both compounds were investigated for their hydrolysis behaviour [49,50], their plasma protein binding capability [51,52] and in particular KP1019 for its preclinical activity in freshly explanted human tumour *in vitro* models [53]. Following these reports, the mode of action of KP1019 is believed to involve hydrolysis of a Ru–Cl bond to yield the corresponding aqua complex, which binds extensively to serum proteins in the blood. Besides coordinative protein binding, the rapid formation of transient hydrophobic interactions between KP1019 and HSA was also detected using electron paramagnetic resonance (EPR) experiments, which slowly

convert to coordinative interactions [54]. In the same report, Tf binding was characterized by the direct formation of covalent interactions. The hypoxic environment of cancer cells would then be responsible for generating the more reactive Ru^{II} species, which would ultimately bind to DNA resulting in cancer cell death. The preclinical report stated “if appropriate plasma levels can be achieved in patients, KP1019 may have significant clinical activity against a variety of different tumour types” [53]. However, additional or supplementary mechanisms were also thought to be possible but not further elaborated at this time [55].

It was later shown that KP418 and KP1019 induce apoptosis via the mitochondrial pathway in colorectal carcinoma (SW480) cell lines [56]. KP1019 was by then the most advanced and promising ruthenium-based anticancer agent to treat primary tumours but suffered from low solubility. It was the second Ru^{III} anticancer agent to enter clinical trials and a preliminary phase-I study was completed in 2008 [57]. KP1019 showed promising results in phase I, which was designed as an open-label dose-escalation study. Five out of six patients experienced disease stabilization independently of the dose, which was between 25 and 600 mg. Importantly, disease stabilization was obtained in adenocarcinoma of the colon and carcinomas of the liver, endometrium and tongue. Only mild toxicities were observed, while the maximum tolerated dose (MTD) could not be determined due to the relatively low solubility of KP1019 limiting the total amount to be administered. The endpoint was met at a final dose of 600 mg, administered twice a week, which represents the plasma concentration at which approximately one Ru moiety is bound to Tf. In preclinical models, it was found that a Ru : Tf ratio of 1 : 1 was the optimal concentration for efficient cellular uptake [57,58].

Exchanging the indazolium counter cation with sodium giving sodium *trans*-[RuCl₄(HInd)₂] (KP1339 or NKP-1339) allegedly increased the solubility 30-fold and this compound is currently undergoing phase-I/II clinical studies in the US as a GRP78 inhibitor for the treatment of primary tumours [55,59]. The drug is infused in a 90 min session once a week [60]. Grade 1 fever/chills were observed above 420 mg/m², while the dose limiting toxicity was grade 2–3 nausea and vomiting at a weekly dose of 780 mg/m². This led to the definition of an MTD of 625 mg/m² [61]. Single agent activity was obtained in particular in neuroendocrine tumours [61].

NAMI-A. Besides *N*-donors, *S*-donor containing Ru^{III} anticancer agents were also investigated for their biological activity. The first studies using [RuCl₂(dmsO)₄], where dmsO is dimethylsulfoxide, were carried out in *E. coli* in 1975 and it was claimed that this Ru compound possesses similar properties of inducing filamentous growth compared to cisplatin [62]. A systematic investigation on *cis*- and *trans*-isomers and different halides was undertaken thirteen years later [63], which showed the superior activity of *trans*-[RuCl₂(dmsO)₄] over the *cis*-isomer against a metastasizing Lewis lung carcinoma model. Additionally, the chlorido complex was also more active than the bromido analogue. In contrast to previous examples, the Ru centre of the investigated compounds is in oxidation state +II. Furthermore, *trans*-[RuCl₂(dmsO)₄] was shown to have only a marginal effect on primary tumours, but reduced significantly the volume of lung metastases [64]. Similar investigations were also carried out with hydrogen *trans*-[Ru(dmsO)₂Cl₄], the analogous Ru^{III} complex [65]. However, it turned out that these species are not stable in aqueous solution and

immediately release one dmsoligand. After structural optimization, sodium *trans*-[RuCl₄(dmsol)(HIm)] (NAMI), where HIm is imidazole, was selected as the most promising candidate for further development [66]. The selection was based on the increased stability, good solubility and effective inhibition of spontaneous metastasis formation compared to *inter alia mer*-[RuCl₃(dmsol)₂(HIm)], hydrogen *trans*-[RuCl₄(dmsol)₂] and *trans*-[RuCl₂(dmsol)₄]. Further *in vivo* studies in the metastasizing MCA mammary carcinoma xenograft model showed specificity for the reduction of lung metastases and no effect on primary tumour growth [67]. It was found that NAMI inhibited both the formation of metastases as well as growth of the existing ones. The life-span of the mice was significantly prolonged in particular in combination with surgical removal of the tumour. The effect of the sulfoxide on the chemical properties of NAMI compared to KP418 amounts to a decrease of the Ru^{III}→Ru^{II} reduction potential due to the π-acceptor properties of the S-donor. Furthermore, the S-donor exhibits a kinetic *trans*-effect. Together, this leads to an increased lability of NAMI in biological media compared to KP418. Hydrolysis of NAMI is believed to be preceded by a reduction of the metal, which may be catalyzed by biological reductants [68]. It seems that NAMI is also activated by reduction. Finally, the relative air instability of NAMI led to the replacement of the counter cation from sodium to imidazolium. The resulting compound imidazolium *trans*-[RuCl₄(dmsol)(HIm)] (NAMI-A) showed higher stability in air than NAMI and similar pharmacological effects [69]. NAMI-A was the first Ru-based anticancer agent to enter clinical trials and phase I studies were completed in 2004 [70]. These studies were designed as an open-label dose-escalation study with the aim of determining tolerability and the MTD. Disease stabilization was observed for patients with advanced non-small cell lung carcinoma (NSCLC). Painful blister formation on the extremities at doses of >400 mg/m² per day determined the MTD. Consequently, a dose of 300 mg/m² per day for 5 days every 3 weeks was recommended for further studies. Today, NAMI-A is in clinical phase-I/II studies as a second-line treatment for NSCLC in combination with gemcitabine [71].

2.3.2. Ruthenium(II) Anticancer Agents

Following the “activation-by-reduction” hypothesis for Ru^{III} metallodrugs, it seems intuitive to directly prepare potential antineoplastic Ru^{II} compounds. As mentioned above, the first reports on the biological activity of Ru^{II} complexes were encouraging [62,72] but seemed to be hampered by the stability of the Ru^{II} species, which underwent rather fast ligand substitution reactions [63]. While it was soon realized that N-heterocycles seem to stabilize the lower oxidation state [64], it was only in 2000, that the first active Ru^{II} coordination compound was reported by the group of Reedijk [73]. The chiral complex [Ru^{II}(azpy)₂Cl₂], where azpy is 2-phenylazopyridine, showed promising *in vitro* results depending on the isomer (Figure 5) [73]. While the reported β- and γ-isomers showed cytotoxic activity in the low micromolar (μM) range in various cell lines, the α-isomer exhibited *in vitro* activities in the sub-μM range, e.g. particularly in the breast cancer (MCF-7 and EVSA-T) and melanoma (M19 MEL) cell lines. The activity of the α-isomer was similar to cisplatin and 5-fluorouracil. It is believed that the hydrolysis of the M–Cl bonds is less favourable in the sterically crowded octahedral Ru^{II}, compared to cisplatin [73]. Consequently, the contrasting activity profile suggested that

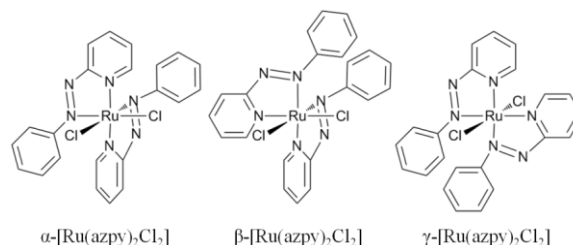


Fig. 5 The α-, β- and γ-isomers of the Ru^{II} coordination compound [Ru(azpy)₂Cl₂], where azpy is 2-phenylazopyridine.

cytotoxic activity is only obtained when the chlorides are in *cis*-position and the arrangement of the 2-phenylazopyridine chelates allows the hydrolysis of both chlorido ligands, which is only met with the α-isomer. Unfortunately, the low solubility of these complexes prevented the performance of *in vivo* tests, which were neither reported with the more soluble α-[Ru^{II}(azpy)₂(NO₃)₂] [74]. A completely novel approach aimed at stabilizing Ru^{II} by an η⁶-arene moiety, which occupies three coordination sites and was already reported in 1999 [72]. Importantly, the isomeric complexity is reduced to a maximum of two isomers, when employing a symmetric η⁶-arene, in contrast to the coordination compound [Ru^{II}(azpy)₂Cl₂], which may be present in five isomeric forms [73]. The organometallic so-called “half-sandwich piano-stool” compounds feature three remaining binding sites in *fac*-position, which can be occupied by inert and/or labile ligands [75,76]. The resulting pseudo-tetrahedral compounds are in general stable in water and in biological media, contradictory to a general paradigm against organometallics [32]. This novel class of organometallic anticancer agents represents the latest generation of ruthenium-based metallodrugs up to date and was initiated by Dyson *et al.* [76,77] and Sadler *et al.* [78] in 2001 (Figure 6).

RAPTA-T. The group of Dyson published one of the first reports describing biologically active organometallic Ru^{II} agents [77]. They reported [RuCl₂(cym)(pta)] (RAPTA-C), where cym is η⁶-p-cymene and pta is 1,3,5-triaza-7-phosphaadamantane, to be a metallodrug, which showed DNA degradation specifically at pH < 6.5 [77]. As mentioned above, solubility is a crucial issue with Ru metallopharmaceuticals and the employment of a pta ligand aimed at increasing this parameter. Furthermore, the activation of the drug in slightly acidic medium was recognized as a potential targeting possibility for diseased cells, such as hypoxic tumour tissue. This prochiral Ru^{II} metallodrug was investigated in particular as an antimetastatic agent [76]. Extensive *in vitro* and *in vivo* studies followed for a number of RAPTA compounds [79] and it turned out that these species are non-toxic to normal cells. For example, RAPTA-T (Figure 6), where the arene is η⁶-toluene, was found to exhibit cytotoxic activity against the TS/A mouse adenocarcinoma cancer cell line while being non-toxic to the non-tumour HBL-100 human mammary cell line up to 0.3 mM. *In vivo* experiments with MCA mammary carcinoma xenografts in CBA mice showed that RAPTA-C reduces the growth of lung metastases but does not affect the primary tumour similarly to NAMI-A, although being slightly less effective. It seems that hydrolysis of both Ru–Cl bonds occurs in water within minutes, whereas hydrolysis is inhibited in 100 mM aqueous NaCl. Hydrolysis is believed to be important for activation of the metallodrug as well as protonation of the pta ligand [79], which is believed to assist binding to DNA by electrostatic

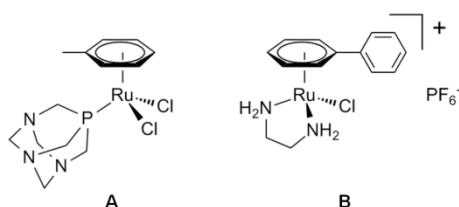


Fig. 6 The structures of the face-capped Ru^{II}-arene organometallics RAPTA-T (A) and RM175 (B).

interactions and to retain the compound in the cell. The coordinated pta ligand is more acidic than the free pta and pK_a values of the former were determined in the range of pK_a = 3.2 ± 0.2. Due to the relatively fast hydrolysis kinetics, second-generation RAPTA derivatives were prepared that resist hydrolysis [80]. These compounds contained a bidentate dicarboxylate leaving group instead of the chlorido ligands, as also present in the Pt^{II} compounds carboplatin and oxaliplatin. Indeed, these biscarboxylato-Ru species showed lower aquation kinetics and were also stable at lower pH, while preserving similar *in vitro* activity compared to the parent compound RAPTA-C.

The mode of action of the antimetastatic RAPTA family was investigated using Ehrlich's ascite carcinoma (EAC) xenograft model *in vitro* and *in vivo* [81]. EAC cells resemble the most chemosensitive human tumours because the tumour cells are fast growing and non-differentiated [82]. Intraperitoneal (i.p.) administration of 40 mg/kg per week led to reduction of tumour growth by 50%. Interestingly, RAPTA-C seems to trigger G2/M cell cycle arrest, apoptosis *via* the mitochondrial pathway and up-regulation of c-Jun NH₂-terminal kinase (JNK) indicating apoptosis induction *via* DNA damage. This led to the deduction that DNA damage is likely not the only mode of action of this Ru^{II} anticancer agent and may induce apoptosis in multiple pathways, which was believed to be beneficial for avoiding drug resistance. In a further study, the antimetastatic properties of RAPTA-T were investigated in more detail [83], showing that this compound effectively hinders metastasis formation by inhibiting detachment from the primary tumour and re-adhesion to a new substrate. These effects were particularly prominent in the highly aggressive MDA-MB-231 breast cancer model. Furthermore, it was shown that RAPTA-T and RAPTA-C exhibit antiangiogenic properties [84]. Recently, crystallographic studies showed that RAPTA-C forms specific adducts with nucleosome core

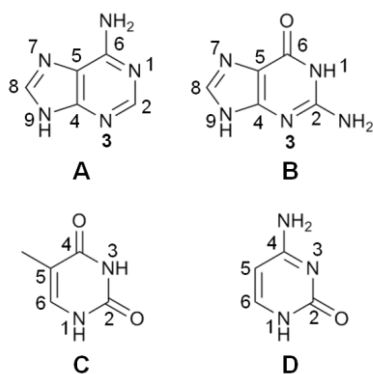


Fig. 7 The atom numbering of the purine and pyrimidine nucleobases: (A) Adenine (B) Guanine (C) Thymine (D) Cytosine.

particles (NCP) [85]. The NCP consists of 145 base-pair double-stranded DNA wrapped around a histone protein octamer. It represents an ideal model to test the target tendency of a metallodrug at the molecular level. RAPTA-C was found to bind at three distinct sites exclusively on the histone proteins. Therefore, the primary target of RAPTA-C is believed to involve proteins rather than DNA, contrary to Pt^{II} metallodrugs [86]. Currently, out of the RAPTA-family RAPTA-T is the most promising representative for further investigations combining antimetastatic and antiangiogenic properties with some activity against primary tumours [87].

RM175. Sadler and his group were also among the first to introduce diamine-based Ru^{II}-arenes as a novel type of organometallic anticancer agent [88,89]. Their strategy of coordinating an inert bidentate ethylenediamine (en) moiety and one chlorido leaving group to the metal-arene core, *e.g.* [(η⁶-arene)RuCl(en)]PF₆, where arene is a substituted arene, was reported to yield highly cytotoxic agents in the human ovarian cancer cell line A2780 *in vitro* [78]. In particular, [(η⁶-bip)RuCl(en)]PF₆, where bip is η⁶-biphenyl (RM175, see Figure 6), showed cytotoxic activity comparable to carboplatin. It must be noted that RM175 and also its hydrolysis products are achiral. In the same study, [RuCl₂(cym)(isonicotinamide)]PF₆ and [Ru(CH₃CN)₂(cym)X]PF₆, where X is chloride or bromide, were evaluated on their cytotoxic properties and both were found to be inactive in the A2780 cell line. RM175 was further investigated in human ovarian cancer models *in vivo*, *i.e.* A2780 and A2780cis xenografts [90]. RM175 showed non-cross resistance and tolerability at higher doses than cisplatin, although being about half as active as cisplatin. The compound was administered at single-doses of 25 mg/kg i.p. after 1 and 5 days compared to 10 mg/kg for cisplatin. It was concluded that an inert chelating ligand as well as one mono-functional leaving group yield the most active representative of the compound class [78,90]. In 2006, RM175 and its analogue HC11, [RuCl(en)(η⁶-tetrahydroanthracene)]PF₆, were investigated in a panel of 13 cell lines [91]. The two metallodrugs were particularly active in breast cancer and non-small cell lung cancer (A549) cell lines, while HC11 showed higher activity *in vitro*. In A549 *in vivo* xenograft models, both compounds exhibited a significant tumour growth delay after i.p. single-dose administration [91]. However, HC11 led to increased hepatotoxicity compared to RM175, probably caused by the more lipophilic polyaromatic arene. Finally, RM175 has been investigated for its antimetastatic effect in MCA mammary carcinoma xenograft models *in vivo* [92]. At a daily dose of 10 mg/kg for 5 days, RM175 was shown to reduce the growth of the primary as well as secondary tumours. Furthermore, MDA-MB-231 cells were inhibited from detachment from the primary tumour. The inhibition of the formation of matrix metalloproteinase 2 (MMP-2) further underlined the potential antimetastatic activity of RM175.

On the molecular level, RM175 contains only one halido leaving group and is believed to follow a different mode of action than the established Ru^{III} anticancer agents and RAPTA-T, by only binding mono-functionally to DNA, especially to guanine-N7 [78,93]. The possibility of hydrogen-bonding between en protons of RM175 and guanosine-O6 seems to be responsible for the selectivity over adenosine and thymidine [93,94], while the order of reactivity with nucleosides was determined as guanosine-N7 > thymidine-N3 > adenosine-N7/N1 (see Figure 7 for atom numbering of the

nucleobases) [94]. In addition, the reaction with nucleotide 5'-monophosphates (5'-NMPs) also yielded 5'-phosphate bound species for thymidine and adenosine, but not for guanosine, nor for 3',5'-cyclic nucleotide monophosphates (cNMPs). Furthermore, it is believed that the hydrophobic arene moiety facilitates passage across cell membranes and intercalation into DNA [93]. Ru^{II}-arene metallodrugs are activated only by hydrolysis, which is a crucial parameter in drug design [95]. It was found that hydrolysis of the Ru-Cl bond occurs in water, but is slowed down in the presence of elevated chloride levels in solution [78,96]. Further studies were performed on the interactions between RM175 and biological nucleophiles, which are not believed to be the primary targets for the compound, *i.e.* L-cysteine (Cys) and L-methionine (Met) [97] but also L-histidine (His) and cytochrome C (cyt) [98]. It was found that adduct formation is preceded by hydrolysis of the Ru-Cl bond followed by coordination of a nucleophilic heteroatom, preferably *N*- or *S*-donors and preferentially at acidic pH. Cys was even able to displace the inert ethylenediamine ligand forming dinuclear Ru-Cys adducts. In contrast, the reaction between RM175 and Cys was suppressed in buffered solutions at pH > 5 or in solution containing 100 mM NaCl. The reactivity of RM175 towards the protein cyt was characterized by mono-adduct formation corresponding to [cyt + Ru(bip)(en) + *n*PF₆], where *n* = 0–3. Adduct formation is thought to involve most probably the *N*-terminus or carboxylic side chains on the protein, while His coordination was not observed. Importantly, RM175 reacts primarily with a 14-mer oligonucleotide, even in the presence of an excess of His or cyt. Competitive nucleotide binding studies of RM175 in the presence of GSH, a cellular reducing agent and metal detoxifier, revealed transient formation of an *S*-coordinated GSH-Ru^{II} adduct [99]. However, this thiolato adduct is prone to oxidation to the sulphenato adduct, which weakens the Ru-S bond, allowing the formation of a guanine-N7 adduct as the thermodynamically stable product. This has relevance to the mode of action and detoxification of RM175. It seems that GSH, the prototypic metal detoxifier, is not able to capture efficiently RM175, which seems to target preferentially DNA.

2.3.3. Osmium Anticancer Agents

An exchange of the metal centre to osmium, the heavier congener of ruthenium, proved to be an interesting strategy to alter the aquation rate, but also the reactivity of a metallodrug. Os^{II} shows generally an increased inertness towards ligand substitution compared to Ru^{II} and therefore often results in reduced or even suppressed hydrolysis [95,100]. Moreover, upon hydrolysis, the formed Os^{II}-aqua species tend to be more acidic than the analogous Ru^{II}-aqua species, *i.e.* a pK_a drop of 1.5 pH units is often observed [95]. Consequently, if hydrolysis occurs, the Os^{II} complexes tend to be found as unreactive hydroxido species under physiological conditions (pH = 7.4), while hypoxic and slightly acidic tumour tissues may lead to predominant aqua complexes if the pK_a of the aqua ligand is adjusted accordingly by selection of the ancillary ligands [95]. According to the HSAB principle, Os^{II} is slightly softer than Ru^{II}, which is expected to result in slightly different coordination preferences. It is not surprising that Os analogues were initially prepared of the already existing lead structures, *e.g.* of RAPTA-C [101,102] (2005), RM175 [103,104] (2006) and NAMI-A [105] (2007), while the osmium analogue of KP1019 is still elusive [106]. Investigations on the aqueous chemistry of the Os^{II}-arene

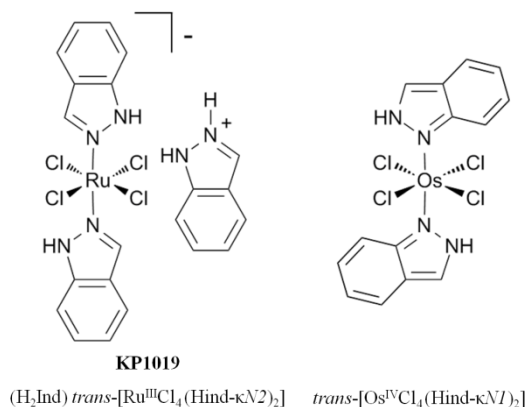


Fig. 8 KP1019 features a indazole-κN2 coordination (*left*), while the unprecedented indazole-κN1 coordination was found with the Os^{IV} complex (*right*).

moiety are scarce [107,108].

The osmium analogue of NAMI-A is more inert and stable towards hydrolysis in aqueous and physiological media and does not interact with 8-methyladenine in contrast to NAMI-A derivatives [109]. *In vitro* cytotoxicity tests revealed that the osmium analogue exhibited modest cytotoxic activity, while showing an altered activity profile, *i.e.* Os-NAMI-A showed a three-fold higher activity in colon carcinoma (HT-29) and a two-fold decrease in mammary carcinoma (SK-BR-3) cell lines compared to NAMI-A [105].

The reactivity of the osmium analogue of RAPTA-C was investigated towards a single-stranded 14mer DNA. While RAPTA-C formed mainly mono-adducts accompanied by arene cleavage, Os-RAPTA-C yielded mono- and bis-adducts with arene retention owing to the increased inertness of Os^{II} towards ligand substitution [101]. Furthermore, Os-RAPTA-C did not undergo excessive aquation and was inactive up to the maximum solubility in colon (HT29), non-small cell lung (A549) and breast (T47D) carcinoma cell lines [102].

The osmium analogue of RM175 (AFAP51) showed 40-fold lower hydrolysis kinetics, a lower pK_a than RM175, as well as reduced reactivity towards 9-ethylguanine. It was proposed that at physiological pH, the main form of AFAP51 corresponds to the hydroxido complex and correspondingly, it was characterized by low cytotoxicity in the ovarian cancer cell line (A2780) [103]. In contrast, AFAP51 showed DNA-binding ability in cell-free media and some cytotoxic activity in cisplatin-sensitive and -resistant ovarian cancer cell lines [110]. Interestingly, in a further study [92], AFAP51 was found to be up to six-fold more active in the aggressive breast cancer cell line MDA-MB-231 compared to RM175, but was inactive *in vivo* in the MCa mammary carcinoma model. An attempt of synthesizing precursors for Os-KP1019 was reported by Büchel *et al.*, who prepared *trans*-[Os^{IV}Cl₄(HInd)₂], where HInd is indazole (Figure 8) [106]. Interestingly, the coordination mode of indazole to osmium involves the unprecedented stabilization of the 2*H*-indazole tautomer. Compared to KP1019, *trans*-[Os^{IV}Cl₄(HInd)₂] showed suppressed hydrolysis in aqueous solution and similar cytotoxic activity in the ovarian cancer cell line (CH1), while being about twice as active in the colon carcinoma cell line (SW480).

The chemistry of Os anticancer agents in aqueous solution and biological media is not completely understood [100] yet predictable and therefore, clear-cut correlations of the cytotoxic activity with Ru have yet to be established [32].

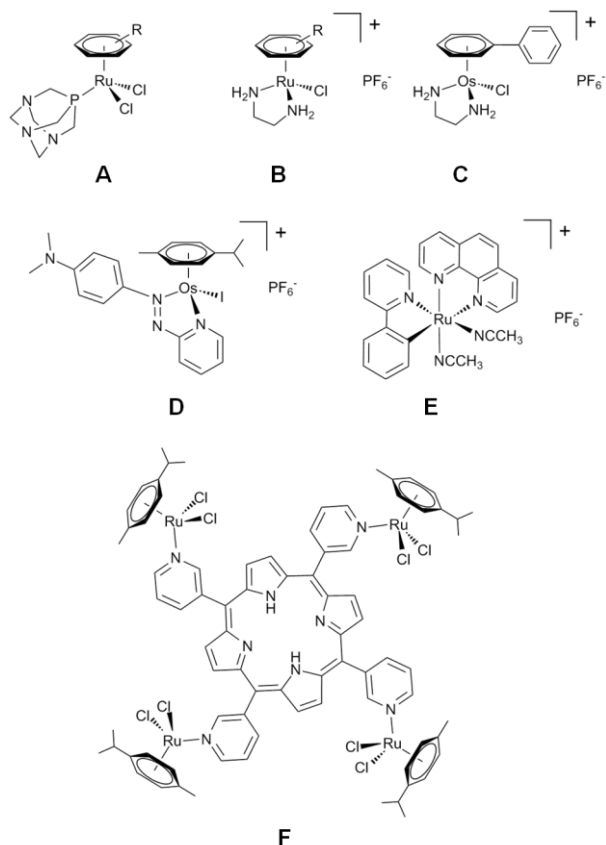


Fig. 9 The chemical structures of the *in vivo*-tested organometallic Ru^{II}- and Os^{II}-arene anticancer agents. (A) RAPTA derivatives, (B) RM175 derivatives, (C) AFAP51, (D) FY026, (E) RDC11 and (F) Ru^{II}-arene porphyrin derivatives.

2.3.4. Organometallic Ruthenium and Osmium Anticancer Agents: State-of-the-Art

According to the general paradigm, organometallic compounds were thought to be toxic and unstable in aqueous solution [32]. This view was contradicted by the initial reports on biologically active organometallic Ru^{II}-arene compounds [76-78,88,89], which opened up an exciting new area of research in inorganic medicinal chemistry. Today, many research groups worldwide are focusing their research efforts on optimizing these compounds for primary application as anticancer agents and a number of excellent reviews and perspectives are available related to this topic [32,71,75,87,112-119]. It must be noted that organometallic anticancer agents are at an early stage of drug design and *in vivo* data on such chemotherapeutics are scarce. To the best of my knowledge, such studies exist for RM175 analogues and AFAP51 [88-92]; RAPTA-C analogues [79,81]; [Os(azpy-NMe₂)(cym)I] (FY026), where azpy-NMe₂ is *p*-dimethylaminophenylazopyridine [120,121]; [Ru(NCMe)₂(phenanthroline)(2-phenyl-pyridine-κ²C,N)]PF₆ (RDC11) [122]; [MCl(cym)(IQ)]Cl, where M is Ru^{II} or Os^{II} and IQ is an indoloquinoline derivative [123] and [Ru₄(cym)Cl₈(PTP)], where PTP is a tetra(3-pyridyl)porphyrin, for application in photodynamic therapy (Figure 9) [124].

This section aims at delineating strategies in designing potent M^{II}-arene metallodrugs, where M is Ru or Os. Due to the vast body of research [125], metal-based anticancer agents will be introduced by compound families, which will be followed by alternative targeting strategies and activation

mechanisms. The first *in vivo* studies on Ru^{II}-arene metallodrugs suggested that bidentate ligands lead to favourable *in vivo* properties against primary tumours [90]. It is not surprising that the most promising Ru^{II}- and Os^{II}-arene metallodrug families involve chelating ligands. Figure 11 summarizes the evolution of Ru and Os metallopharmaceuticals with selected examples.

N-Phenylpicolinamides. Early *in vitro* structure-activity investigations on different chelating systems showed that neutral Ru^{II}(arene) metallodrugs containing *N,O*-chelating ligands such as amino acids or hydroxyquinoline were inactive in cisplatin-sensitive ovarian carcinoma cell lines [126]. This inactivity was mainly attributed to fast hydrolysis and ligand cleavage from the metal. Os^{II}(arene) metallodrugs containing *N,O*-chelating amino acids were also inactive, but the respective oxoquinolinato and picolinato complexes showed activity in the low μM range in ovarian and lung cancer cell lines (A2780 and A549, respectively) [110,127]. The increased anticancer activity over amino acid ligands was rationalized by the coordinating pyridine, a σ-donor/π-acceptor, which decreases the hydrolysis rate particularly for the picolinato ligand. Furthermore, the Os^{II}-picolinato complex showed a preference for guanosine binding over adenosine [127] and it was suggested that DNA binding may be responsible for the mode of action [110]. The advantageous properties of the Os^{II}-picolinato complex prompted a more detailed investigation, in particular with respect to substitutions at the pyridine ring [128]. Notably, *para*-substitution with chloride or methyl improved the cytotoxic activity substantially, while substitution with an ester or carboxylate did not, nor did any *ortho*-substitution. The resulting antiproliferative activity *in vitro* was comparable to that of cisplatin exhibiting no cross-resistance with cisplatin-resistant cell lines. A correlation between 9-ethylguanine binding and cytotoxicity was observed indicating that DNA binding may indeed be crucial for the cytotoxic activity [128]. Generally, the aqua complexes show pK_a values between 6.3 and 6.6 and therefore, these species are largely deprotonated at physiological pH. Importantly, the *para*-substituted carboxylate was inactive *in vitro*. It was speculated that the negative overall charge of the aquated hydroxido complex is responsible for the inactivity due to electrostatic repulsion with DNA [128].

In a further study, the mechanism of action of [Os(η⁶-arene)Cl(4-methyl-picolinate)], where the arene is benzene, *p*-cymene, biphenyl or tetrahydroanthracene, was investigated in ovarian carcinoma cells (A2780) [129]. It was found that the efficiency of cellular uptake was increased with increasing lipophilicity of the compound and similarly the cytotoxic activity increased. Cell fractionation revealed that these

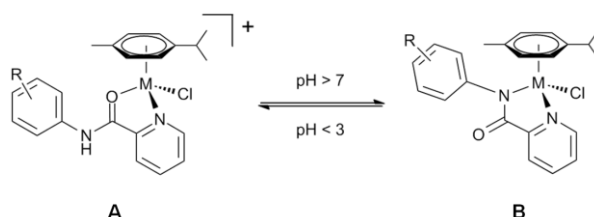


Fig. 10 The pH-dependent amide linkage isomerism of M^{II}-picolinamido anticancer agents, where M is Ru or Os as reported in ref [111]. Low pH favours the picolinamido-κ²N,O (A) and high pH favours picolinamido-κ²N,N organometallics (B).

metallo drugs mainly accumulate in the cytosol, while DNA binding did not correlate with cytotoxicity, contradictory to the previous hypothesis. These metal-based anticancer agents probably lead to apoptosis *via* the mitochondrial pathway [129].

In an attempt to extend the structure-activity relationship for this family of *N,O*-chelating ligands, a series of 2-phenylpicolinamido complexes were synthesized using both Ru^{II} and Os^{II} precursors [111]. Intriguingly, it was revealed that the picolinamido ligands may interconvert between *N,N*- and *N,O*-coordination modes (Figure 10). While electron-withdrawing substituents on the phenyl ring tend to yield *N,N*-coordinated complexes, electron-donating substituents rather yield *N,O*-coordinated complexes. The interconversion of the coordination mode seems to be reversible and pH-dependent when employing electron-withdrawing groups, favouring *N,N*-coordination at physiological pH. The *N,N*-coordination mode involves deprotonation of the *N*-amide resulting in a neutral complex. Importantly, the two coordination modes display rather contrasting activity profiles. While the *N,N*-coordinated complexes showed fast hydrolysis ($t_{1/2} < 5$ min), guanine binding and potent activity *in vitro*, the inverse was found for the *N,O*-coordinated complexes [111]. In contrast to the Os^{II} complexes, their Ru^{II} analogues were inactive *in vitro* even in the *N,N*-coordinated mode.

2-Phenylazopyridines. The family of [Ru^{II}(η^6 -arene)(azpy)X]PF₆, where azpy is 2-phenylazopyridine and X is chloride or iodide, was probably inspired by the promising cytotoxic properties of α -[Ru^{II}(azpy)₂Cl₂], as mentioned earlier [73]. The early investigations on this family reported Ru^{II}-arene complexes with azpy derivatives and chloride as a leaving group [130]. Importantly, the ligand acts as a σ -donor/ π -acceptor and competes with the η^6 -arene for electron density of Ru^{II}. This may lead to arene cleavage and consequently, the majority of the compounds were inactive in ovarian and non-small cell lung cancer cell lines (A2780 and A549, respectively) [130]. Some improvements in cytotoxic activity were obtained with electron-withdrawing substituents in *para*-position of the phenyl ring and in particular by exchanging pyridine with pyrazole. It was argued that pyrazole is a much weaker π -acceptor and consequently, yields complexes resistant to arene-cleavage but more labile to hydrolysis [130]. Exchanging the chlorido with an iodido leaving group leads to suppression of hydrolysis and simultaneously to a drastically increased cytotoxicity in the low μ M range [131]. The mode of action seems to involve catalytic induction of reactive oxygen species (ROS) inside the tumour cell. In particular, it seems that the intact (non-hydrolyzed) metallodrug catalyzes the oxidation of GSH to glutathione disulfide. It was suggested that GSH attacks the metallodrug at the azo group, since this moiety bears the lowest reduction potential. With attack of a second GSH, glutathione disulfide is released and the resulting hydrazine complex may then be able to produce ROS in the presence of dioxygen. Complexation of phenylazopyridines to Ru^{II}-arenes lowers the first reduction potential of the ligand to a biologically accessible range compared to the free ligand, which is itself biologically inactive [131]. For example, the reduction potential of the *p*-dimethylaminophenylazopyridine (azpy-NMe₂) ligand was found at -1.28 compared to -0.40 for [Ru^{II}(azpy-NMe₂)(cym)I]⁺.

Although initially reported as biologically inactive [104], a further improvement in cytotoxic activity was obtained for the Os^{II} analogues, which yielded IC₅₀ values of 140 nM in the

ovarian cancer cell line A2780 for [Os(azpy-NMe₂)(cym)I]PF₆ (FY026) and [Os(azpy-OH)(bip)I]PF₆ [121], where azpy-OH is *p*-hydroxyphenylazopyridine. The Os organometallics showed a 10-fold activity increase compared to the ruthenium analogues, but seem to follow a different mode of action since they do not catalyze the oxidation of GSH and do not seem to increase ROS levels [121,132]. Furthermore, FY026 and [Os(azpy-OH)(bip)I]PF₆ were non-toxic in a preliminary *in vivo* screen using a colon tumour xenograft model at single doses of 40 mg/kg, which were administered intravenously. In a following study on *in vitro* structure-activity relationships (SAR) the Os^{II}-azpy organometallics were reported to be inert towards hydrolysis and stable in water for at least 24 h [132]. The cytotoxicity was optimized using an iodido leaving group, electron-withdrawing substituents at the *para*-position of the phenyl ring or at the *meta*-position of the pyridine ring, while the lipophilicity does not seem to influence the antiproliferative activity [121,132]. Furthermore, cellular uptake is increased 30-fold when introducing a halide in the *para*-position of the pyridine ring [132]. FY026 showed the most promising results and was selected for *in vivo* investigations in the HCT116 human colon cancer xenograft model [120]. As a matter of fact, it was the first organometallic osmium compound to be tested *in vivo*. A single dose of 40 mg/kg, which represents the maximum solubility of the metallodrug, significantly delayed the tumour growth with negligible toxicity. Redox processes were suggested to play an important role in the biological activity, but knowledge on the exact mode of action of the Os^{II}-azpy series is still elusive.

Lastly, a series of Os^{II}-2-phenyliminopyridine (impy) metallodrugs were prepared, which are bioisosters of the Os^{II}-azpy anticancer agents [133]. While the new series exhibits similar *in vitro* anticancer activity, exchanging the azo with an imino moiety exerts dramatic effects on the chemical properties of the metallodrugs. In contrast to Os^{II}-azpy, the Os^{II}-impy bioisosters undergo aquation, bind to 9-ethylguanidine and induce ROS in cancer cells. Furthermore, the 2-phenyliminopyridine ligand is a weaker π -acceptor than the 2-phenylazopyridine ligand and correspondingly, the reduction potentials are higher for the former. For example, the reduction peak for [Os(cym)(impy-NMe₂)I]⁺ is -0.65 V, but -0.40 V for [Ru(cym)(azpy-NMe₂)I]⁺. This may explain why the Os^{II}-impy compounds do not react with GSH in contrast to the Ru^{II}-azpy analogues in a biological environment. However, reactions were observed with the stronger reducing agent nicotinamide adenine dinucleotide (NADH), which was oxidized by Os^{II}-impy to NAD⁺ *via* transient formation of an Os-hydride species as evidenced in ¹H NMR experiments. The chemical shift of the hydride was found at -4.2 ppm [133].

(Thio)Pyr(id)ones. Employing *O,O*-bidentate ligands for obtaining potent metal-based anticancer agents has also attracted interest as an alternative to the established *N,N*- or *N,O*-bidentate metallodrugs. Initial studies on this ligand system involved β -diketonates and the resulting Ru^{II}- and Os^{II}-arene complexes were inactive *in vitro* probably due to fast hydrolysis and acid-induced ligand cleavage from the metal [103,126,134]. Only the organometallic Ru^{II}-diphenyldiketonate derivative exhibited some antiproliferative activity, but suffered from very low solubility and further investigations on this family were abandoned. Instead, research activities focused on pyr(id)ones for obtaining effective Ru^{II}- and Os^{II}-arene metallodrugs containing *O,O*-

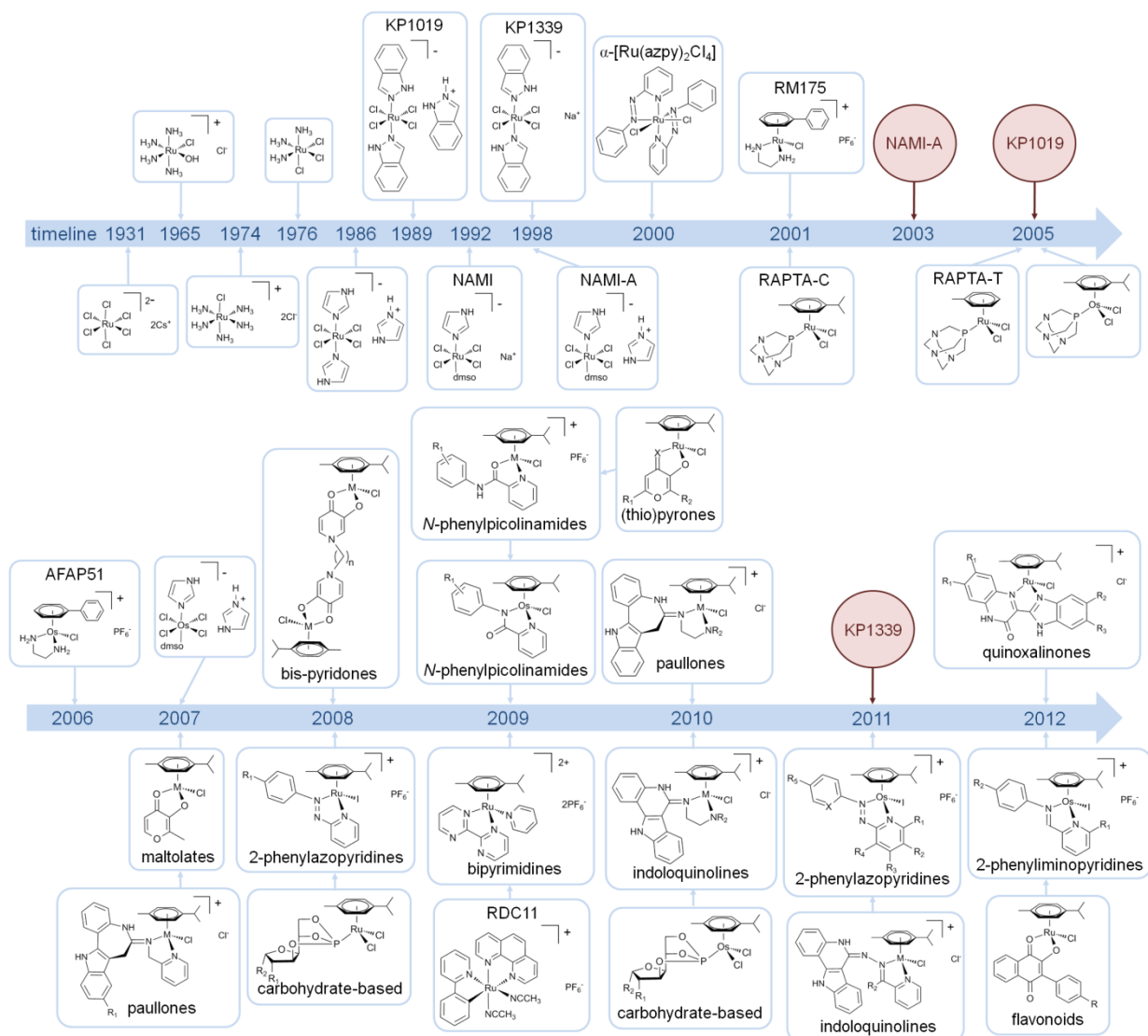


Fig. 11 The chronological appearance of various anticancer Ru and Os compound families and selected examples are displayed. They were all investigated for their antiproliferative activity and are discussed in the text. M denotes Ru^{II} and Os^{II} metal centres, R₁₋₅ is an organic fragment or a halide, X a sulfur or oxygen with (thio)pyrones and carbon or nitrogen with 2-phenylazopyridines, n = 2–12. The circles represent compounds entering clinical trials.

bidentate ligands. Pyr(id)ones are non-toxic and were already investigated for their iron-scavenging and releasing properties [135], as insulin mimetics and anticancer agents, when coordinated to gallium [136], while thiopyridones were found to be MMP-2 inhibitors [137]. The neutral maltolato complexes [MCl(cym)(maltolato)], where M is Ru^{II} or Os^{II}, were among the first representatives of this family of organometallic anticancer agents [138], but were inactive in ovarian cancer cell lines. Both species showed rapid hydrolysis and binding to 9-ethylguanine, similarly to the complexes based on β -diketonates. Ligand cleavage from the metal and formation of hydroxido-bridged dimers of the general formula [M₂(η^6 -arene)₂(μ -OH)₃]⁺ were observed for M = Ru and Os in aqueous solution, which was suggested to be responsible for the inactivity of these metallodrugs [103]. Importantly, an equilibrium seems to exist between the intact complex and the dimer, favouring the dimer when the complex is diluted to μ M concentrations in aqueous solution, even in the presence of 100 mM NaCl, whereas millimolar concentrations favour the intact complex. Ligand cleavage is more prominent for the Os^{II} analogue, which was explained by the higher acidity of the respective aqua complex with a pK_a

of 7.60 compared to 9.23 of the Ru analogue. Therefore, about 40% of the Os species are present as dinuclear hydroxido complexes under physiological conditions and formation of this species liberates protons that may weaken the metal-pyrene coordination of the complexes [138]. Consequently, Ru represents the more promising metal for obtaining cytotoxic pyronato complexes.

Around the same time, structure-activity relationships (SAR) were reported for Ru^{II}-arene metallodrugs containing pyrene-derived ligands [139-143]. Similarly to Ru^{II}-maltolato compounds discussed before, *O,O*-bidentate pyronato complexes hydrolyze instantaneously and react with 5'-GMP within minutes. However, they showed very low activity *in vitro* [138-140]. The lack of antiproliferative activity was again explained by ligand cleavage and was observed in the case of kojic acid, (allo)maltol and pyromeconic acid. Intriguingly, addition of imidazole stabilized the pyronato complexes in aqueous solution [139,141]. On the other hand, the Ru^{II}-ethylmaltolato complex showed increased stability against ligand cleavage [139]. Due to this finding, it was argued that ligand cleavage is not solely responsible for the low activity of these metallodrugs [139]. Reactions of the

pyronato-derived complexes with amino acids revealed that in particular His, Met and Cys form stable adducts *via* pyrone cleavage [139]. Therefore, the reactivity towards potentially chelating biological nucleophiles seems to constitute another pathway of deactivation, since it was shown that amino acid complexes do not possess cytotoxic properties [126].

The example of ethylmaltol suggested that electron-donating substituents at the pyrone ring might increase the stability of the resulting complexes [139]. The SAR study was then extended to a series of 2-substituted allomaltolato Ru^{II} complexes, which were obtained by an aldol addition of benzaldehyde derivatives to allomaltol [140]. The resulting compounds were more lipophilic, yet less soluble and displayed improved cytotoxic activity, *i.e.* IC₅₀ values were found between 25 and 50 μM in the ovarian cancer (CH1) cell line and the activity was selective for this cell line [140]. In an attempt to increase the solubility of these compounds, a series of 2-substituted kojic acid derivatives were reported, which were obtained by a Mannich reaction with secondary amines [143]. Unexpectedly, the resulting Ru^{II}-arene complexes were too unstable in aqueous solution for performing *in vitro* screenings [143].

Finally, variations of the η⁶-arene and of the leaving group seem to have distinct effects on the antiproliferative activity of the Ru^{II}-maltolato complex in the ovarian cancer cell line CH1 [142]. Exchange from η⁶-p-cymene to η⁶-biphenyl led to a 3-fold increase in anticancer activity, while the exchange from the chlorido to an iodido leaving group led to 2-fold higher anticancer activity.

A substantial enhancement of antiproliferative activity was obtained by exchanging the *O,O*-bidentate pyrone with an *S,O*-bidentate thiopyrone. Although hydrolysis rates and binding to 5'-GMP are similar to the pyronato analogues, the thiopyronato complexes are characterized by increased stability in aqueous solution, *i.e.* ligand cleavage is not observed for at least 18 h [139,141,142]. Furthermore, they show lower kinetics of amino acid binding and associated ligand cleavage [139]. For the thiopyronato complexes, variation of the η⁶-arene results only in marginal effects on the antiproliferative activity in the ovarian cancer cell line CH1 [142].

Inspired by the multinuclear platinum compound BBR3464, which showed promising results by following an alternate mode of DNA binding to classical Pt^{II} chemotherapeutics and even entered clinical trials [144-147], it was aimed to improve the *in vitro* anticancer activity of Ru^{II}-arene metallodrugs by the same concept of multinuclearity. Trinuclear Ru^{II}-arenes were already investigated as ionophoric molecules with high selectivity for Na⁺ over K⁺ [148,149]. These species were based on pyridones and consequently, dinuclear bispyridonato complexes were investigated for their antiproliferative activity [150-152]. The pyridonates were linked by an alkane spacer and it was found that the resulting dinuclear Ru^{II} metallodrugs exhibited antitumor activity depending on the spacer length, *i.e.* a compound featuring a hexane spacer yielded only moderately active species whereas the complex containing the dodecane spacer displayed an *in vitro* activity in the nanomolar range even in the intrinsically cisplatin-resistant SW480 colon cancer cell line [150]. Similar to the pyronato complexes, the pyridonato complexes hydrolyze quantitatively within minutes by replacing the chloride with an aqua ligand. However, the pyridonato ligand seems to stabilize the resulting aqua complex, since ligand cleavage and formation of hydroxido-bridged dimers were not observed [152].

Furthermore, these dinuclear metallodrugs showed affinity for DNA and transferrin, but not for ubiquitin or cytochrome-c, indicating that DNA may be a possible target for this family of Ru^{II} metallodrugs.

Mono-, di- and trinuclear Ru^{II}-arene pyridone metallodrugs were prepared in an additional structure-activity relationship study and it was shown that the dinuclear compounds were most effective [153]. Variation of the η⁶-arene from p-cymene to biphenyl did not alter the anticancer activity, nor did the exchange of the leaving group from chloride to bromide or iodide. The Os analogues were about three-fold less active than the Ru^{II} complexes while their *in vitro* activities were similarly dependent on the spacer length [153]. The dinuclear Ru^{II}-arene pyridones were found to interact strongly with DNA forming intra- and interstrand crosslinks [154]. More importantly, these metallodrugs were also able to form protein-DNA ternary adducts as well as adducts involving two DNA duplexes to a higher account than observed for other Ru metallodrugs. A study on related mononuclear 3-hydroxy-2-pyridonato complexes showed that these species are largely inactive *in vitro* [155]. It was found that the mononuclear complexes interact with ubiquitin by forming [ub + M(cym)] adducts, where M is Ru^{II} or Os^{II}. In the presence of amino acids, the pyridonato complexes form amino acid adducts similarly to the pyronato complexes.

Paullones. The incorporation of bioactive ligands into the Ru^{II} scaffold is another promising strategy for obtaining metallodrugs with unprecedented activity profiles. In particular, kinetically inert Ru^{II}-based staurosporine analogues developed in the group of Meggers were among the first representatives to show promise as highly effective metal-based Pim1, MSK1 and GSK3α inhibitors with biological relevance [156-158]. Metal-based protein kinase inhibitors offer the advantage of accessing chemical space in terms of structural diversity that is not possible with purely organic compounds. Notably, kinetically labile RAPTA-type inhibitors of glutathione transferase were also reported [159].

Of interest is also the family of paullones, which were found to be cyclin-dependent kinase (CDK) inhibitors similar to flavopiridol [160]. Especially, kenpaullone is a potent inhibitor of CDK1/cyclin B in the sub-μM range, while showing 10-fold reduced activity against CDK2/cyclin E [160]. Since these organic drugs are only poorly water soluble, it was aimed to increase their solubility by metallation. Paullones, which do not feature a thermodynamically-favoured metal coordination site, were modified at the lactam moiety with picolylamine to allow for *N,N*-bidentate coordination (position 6, see Figure 12) [161]. The first examples involving coordination compounds prepared from [RuCl₂(dmsO)₄] as a precursor showed encouraging results [161]. While the ligands were not sufficiently soluble for evaluation of their antiproliferative activity, the complexes [RuCl₂(dmsO)₂(PL)] and [RuCl(dmsO)(PL)₂]Cl, where PL is the modified paullone, were cytotoxic in the low μM range, but their solubility was still low (12.5 – 25 μM). Furthermore, DNA intercalation was proposed as an additional mode of action to CDK inhibition as revealed by studies with plasmid DNA [161].

Paullone derivatives were then tethered to a M^{II}-arene moiety in a following SAR study [162]. The resulting complexes [MCl(cym)(PL)]Cl, where M is Ru^{II} or Os^{II} and PL is a modified paullone, are charged species and hydrolyze slowly in aqueous solution. To obtain SARs, the paullones were modified at two positions for subsequent metallation, *i.e.*

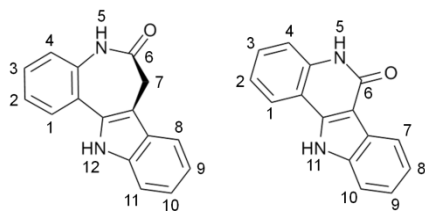


Fig. 12 The structure and atom numbering of the paullone (*left*) and indoloquinoline backbone (*right*).

at the lactam unit (position 6) and at position 9 (see Figure 12). Lactam modification yielded metallodrugs with higher antiproliferative activity than modifications at position 9. Additionally, electron-withdrawing substituents at position 9 seemed to decrease the anticancer activity of lactam-modified paullones, contrary to the activity of the ligand alone. The Os analogues were approximately half as active as the Ru organometallics. Both Ru^{II} and Os^{II} compounds were shown to lead to a G₀/G₁ cell cycle arrest, while only the lactam-modified analogues partially inhibited DNA synthesis [162].

Furthermore, potentially *N,N,O*-tridentate paullones were synthesized and tethered to organometallic Ru^{II}- and Os^{II}-arenes [163]. However, these species were found to bind exclusively in a *N,N*-bidentate coordination mode. Due to the free hydroxyl group(s) they showed improved water solubility but also improved cytotoxicity in the lung and ovarian cancer cell lines. In contrast to the Ru complex, the Os analogue did not react with 5'-GMP. Despite this chemical difference, the metal had no effect on the antiproliferative activity, suggesting that coordinative binding to DNA is not a primary effect in their mode of action. Similarly, in a recent study with Ru^{II} and Os^{II} complexes containing a free radical carrying paullone, it was also concluded that DNA is not the primary target of paullone-based metallodrugs [164].

Further research was directed into the comparison of organometallics containing paullone ligands with their indoloquinoline analogues. Indoloquinolines are planar in contrast to the nicked seven-membered azepine ring of the paullone [165]. Interestingly, organometallic indoloquinoline complexes showed a 3–10-fold higher antiproliferative activity compared to the paullone analogues, which was related to the better DNA-intercalating properties of the flat quinolone, when the metal binding site is introduced at position 6. Again, the metal centre of indoloquinoline complexes does not seem to exert a substantial effect on the anticancer activity *in vitro*. While the paullone derivatives exhibited only minor influence on the cell cycle, the indoloquinolines caused heavy cell cycle perturbation at biologically relevant concentrations [165]. The indoloquinoline complexes seem to inhibit CDK2/cyclin E activity, whereas the paullone complexes rather inhibit CDK1/cyclin B activity. However, the necessary concentrations for obtaining a biological effect suggested that CDK inhibition is not the primary mechanism of action [165]. The limitation of the indoloquinoline complexes in this study was their low stability in organic and aqueous solution, which was improved by exchanging the ethylenediamine-type chelating ligand for sp²-hybridized nitrogen donors [166], *i.e.* iminopyridines as already employed with the paullone complexes [163]. The resulting iminopyridine-modified indoloquinoline metallodrugs showed high stability in aqueous solution and potent *in vitro* cytotoxicity at sub- μ M

concentrations [166]. Small substitutions at position 2 did not result in pronounced effects on the antiproliferative activity, although electron-donating groups seem to be slightly advantageous with respect to *in vitro* activity [166]. Introducing an iminopyridine metallation site at position 2 of indoloquinolines resulted in an overall lower cytotoxic activity compared to the former reports [123]. Although direct SARs of these indoloquinolines could not be established, the cellular accumulation and intensity of cell cycle perturbation seemed to correlate with the antiproliferative activity of this series. Finally, the primary mode of action of paullone-derived metallodrugs is still under debate [167].

Carbohydrate-based Phosphites. The family of carbohydrate-based 3,5,6-bicyclic phosphite- α -D-glucofuranoside metallodrugs was designed as an alternative to the structurally similar RAPTA metallodrugs [168]. Additionally, since fast growing and hypoxic tumourigenic tissues rely increasingly on glucose uptake due to upregulation of glycolysis [169], employing carbohydrate-based ligands was expected to display favourable properties for tumour accumulation [170]. Hydrolysis of the first chloride of the neutral complexes [(cym)RuCl₂(P)], where P is a 3,5,6-bicyclic phosphite- α -D-glucofuranoside derivative, occurs within minutes [168]. The formed mono-aqua species undergoes an unexpected hydrolysis of the P–O(C5) bond prior to hydrolysis of the second chlorido leaving group, which was not observed for the free ligand (Figure 13). Dimer formation may occur slowly after the first hydrolysis step yielding [Ru₂(cym)₂Cl(P_{hydr})₂]⁺, where P_{hydr} is the hydrolyzed carbohydrate-based ligand. Furthermore, hydrolysis in phosphate buffer are approximately on the same order as binding kinetics to human serum albumin and transferrin, displaying t_{1/2} \approx 1 h. The carbohydrate-based metallodrugs were also found to form specifically mono- and bis-adducts with transferrin and the mass differences indicated binding of the [Ru(cym)Cl(P)] moiety to the protein, while binding to the smaller proteins ubiquitin and cytochrome C was not observed. These compounds are also able to bind to N7 of 9-ethylguanine forming exclusively mono-adducts. Substitution of the chlorido ligands by bromide or iodide gave largely insoluble products in aqueous solution, unsuitable for biological evaluation. Finally, this series of metallodrugs was only moderately cytotoxic *in vitro* with the most potent compound being the cyclohexyl-derivative with an IC₅₀ value of 29 \pm 4 μ M in the ovarian cancer cell line CH1. Notably, these carbohydrate-based metallodrugs display a comparable selectivity for tumourigenic tissue to the RAPTA compounds, but were more cytotoxic towards primary tumour models *in vitro* [79].

Substitution of the leaving groups by an oxalato moiety led to suppression of hydrolysis but also to a decrease in cytotoxic

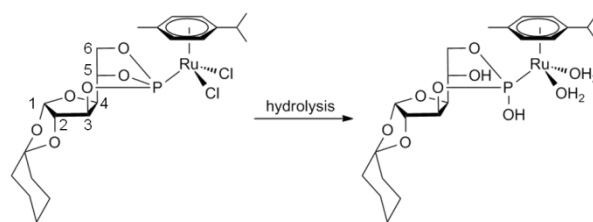


Fig. 13 Ru^{II}-arene carbohydrate-based phosphites hydrolyze both Ru–Cl bonds and additionally, hydrolysis of the P–O(C5) bond was observed.

activity suggesting that coordinative binding is crucial for the anticancer activity of carbohydrate-based metallodrugs [171].

The analogous carbohydrate-based Os^{II}-arene complexes showed a similar hydrolysis behaviour also involving hydrolysis of the P-O(C5) bond, but at a much lower rate [170]. The carbohydrate-based Os^{II} complexes were approximately half as active as the Ru^{II} analogues. Again, the cyclohexyl derivative was the most potent derivative with an IC₅₀ of 50 ± 6 μM in the ovarian cancer (CH1) cell line. The Os^{II}-based oxalato derivatives showed suppression of hydrolysis and were less active than the chlorido analogues, similar to the observations for the respective Ru^{II} compounds. Although hydrolysis is observed to some degree for the carbohydrate-based Os complexes, they did not bind to 9-ethylguanine. Finally, coordination of triphenylphosphine instead of the carbohydrate-based ligand led to insoluble compounds, which prevented the performance of *in vitro* assays [172]. Although developed as an alternative to the RAPTA family, the carbohydrate-based organometallics were not yet investigated for their antimetastatic activity.

Quinoxalinones. Quinoxalinones show activity as ATP-competitive kinase inhibitors similar to indirubin [173]. The complexation of these species to organometallic Ru and Os moieties was just recently reported [174]. The emphasis was on developing potent kinase inhibitors by non-covalent interactions combined with the potential antiproliferative effect of M^{II}-arene tethering. The resulting complexes [M(cym)Cl(Q)]Cl, where M is Ru^{II} or Os^{II} and Q is a quinoxalinone, contain one chlorido leaving group and are inert towards hydrolysis in 100 mM NaCl, while low salt concentrations led to partial hydrolysis and formation of the aqua complex. Importantly, the quinoxalinonato metallodrugs showed up to a 30-fold increase in anticancer activity compared to the free ligands, indicating synergistic effects of complexation. The complexes are highly cytotoxic, most of them in the low μM range in ovarian and the widely chemoresistant non-small cell lung cancer cell lines. It seems that coordination to the Os^{II}-arene moiety leads to slightly more potent anticancer agents *in vitro* although no clear-cut relationship was obtained. Exchange of the η⁶-*p*-cymene with η⁶-benzene resulted in a 10-fold reduction of the antiproliferative activity, probably due to the instability of the benzene complex in aqueous solution. Furthermore, benzimidazole was substituted with benzothiazole or benzoxazole and the benzothiazole derivatives were most cytotoxic upon complexation (see Figure 14 for ligand structure). The reduced activity of the benzoxazole derivatives was related to the lower kinetic and thermodynamic stability of the complexes. Intriguingly, the ligands led to a G₂/M cell cycle arrest similarly to indirubin [173], while the complexes do not perturb the cell cycle, although being more cytotoxic. This indicates that also other targets might be involved in the mode of action of this novel family of metallodrugs.

Flavonoids. Flavonoids are secondary metabolites in plants, which also display anticancer activity and it was suggested that their mode of action involves inhibition of human topoisomerases [175]. Topoisomerases can cut DNA strands and are responsible for DNA supercoiling. Topoisomerase II thereby simultaneously cleaves both DNA strands. 3-Hydroxyflavones are known as *O,O*-chelating ligands and coordination to a Ru^{II}-arene moiety was recently reported, which aimed at a dual-targeted approach, *i.e.* exerting anticancer activity by inhibiting topoisomerase IIα and by forming DNA adducts [176-178]. The resulting

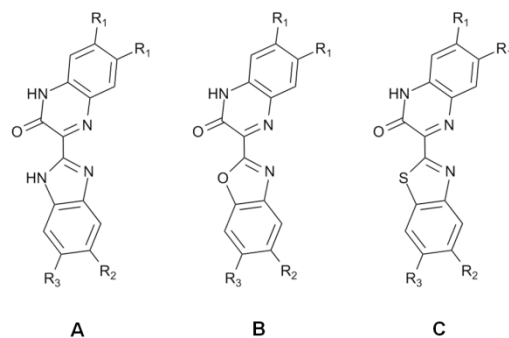


Fig. 14 The structure of quinoxalinones based on benzimidazole (A), benzoxazole (B) and benzothiazole (C). Especially the benzimidazole and -othiazole organometallics were anticancer active *in vitro*.

organometallic anticancer agents of the form [Ru(η⁶-arene)Cl(Flav)], where Flav is a flavonato ligand, were highly cytotoxic at low μM concentrations in the ovarian cancer cell line CH1 and also better soluble than the free ligands. Substitutions at the phenyl ring of the flavonoid yielded the following trend in terms of cytotoxicity: para > meta > ortho. Ortho-substitution results in a distorted delocalized system in the flavonoid ligand, which may be responsible for reduced enzyme inhibition or DNA intercalation and consequently, a reduced antiproliferative activity. Since CDK2 inhibition did not correlate with the *in vitro* cytotoxicity, it was suggested that this kinase is not a primary target of this compound family [177]. On the other hand, the metallodrugs were potent inhibitors of human topoisomerase IIα and even showed higher activity than the free ligands. Topoisomerase inhibition correlated well with the cytotoxic activity and the cell cycle arrest in the S-Phase [177]. Additionally, the flavone metallodrugs showed rapid binding to 5'-GMP. Binding to the model nucleobase is characterized by retention of the ligand, which may preserve the inhibitory effect of the metallodrug on topoisomerase IIα. Fluorescent staining of colon carcinoma cells indicated that the flavonoids seem to accumulate in the endoplasmic reticulum, being a common feature for lipophilic compounds [176]. SAR of this compound family indicated only a marginal effect of the η⁶-arene and the halido leaving group on the cytotoxic activity [178]. Exchanging the 3-hydroxyflavone with a 3-hydroxyquinolinone backbone (Figure 15) resulted in a slightly lower antiproliferative activity probably due to lower stability in aqueous solution. It was shown that the organometallics of both ligand systems interact similarly with 5'-GMP and with amino acids suggesting that small biomolecule binding is not essential in the mode of action of this compound family [178].

Photoactivation. Photodynamic therapy (PDT) represents a promising strategy in the treatment of cancer [179]. Potential chemotherapeutics are activated by irradiation selectively at the target site, which is anticipated to drastically reduce side effects. The mode of action of classic photosensitizers seems to involve generation of reactive (singlet) oxygen or free

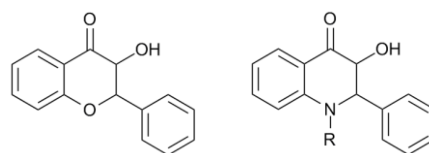


Fig. 15 The backbone of 3-hydroxyflavones (left) and 3-hydroxyquinolinones (right). R is hydrogen or methyl.

radicals mainly from the excited triplet state of the photosensitizer [179,180]. Porphyrin-systems and transition metals are particularly effective photosensitizers in this regard, since the extensive delocalized systems and d-orbitals offer electronic transitions and therefore, activation in the region of visible light [180]. Ideally, potential photosensitizers display a strong absorption band in the (infra)red region (620–850 nm) because light with longer wavelengths travels deeper into tissues and is less energetic [180].

Besides Ru^{II}-polypyridine complexes [180], *cis/trans*-[Ru^{II}Cl₂(dmsO)₄] were among the first Ru-based metallodrugs to be investigated on the effect of irradiation on their antiproliferative activity *in vitro* [181]. It was found that irradiation for 2–30 min with UV_A light ($\lambda = 365$ nm) approximately doubled the cytotoxic activity of both isomers compared to experiments in the absence of light, probably by facilitating DNA binding [181]. The ability of photoactivation was further investigated in organometallic Ru^{II} compounds under cell-free conditions (Figure 16) [182]. The dinuclear compounds [Ru₂(η^6 -arene)₂Cl₂(μ -2,3-dpp)](PF₆)₂, where 2,3-dpp is 2,3-bis(2-pyridyl)pyrazine, showed cleavage of the η^6 -arene in particular for η^6 -indan and η^6 -benzene upon irradiation with UV_A light ($\lambda = 360$ nm). The irradiated species showed marked DNA-adduct formation that blocked RNA polymerases, whereas the non-irradiated species did not show this behaviour. An additional beneficial feature represents the higher fluorescence of the free η^6 -arene compared to when coordinated to the metal centre, which might allow tracking of the cleavage efficiency [182].

Recently, Ru complexes of the type [Ru(η^6 -arene)(N,N')(L)](PF₆)₂, where N,N' is an *N,N*-bidentate π -acceptor and L is a pyridyl- or imidazolyl-based π -acceptor, were reported to photocleave the pyridyl ligand upon irradiation with UV_A and visible light [183,184]. While the precursors showed no binding to DNA models in the dark, irradiation led to preferential binding to 9-ethylguanine. Studies of irradiated complexes with calf thymus DNA under cell-free conditions resulted in extensive metallation, whereas DNA adducts with non-irradiated complexes were only observed to a negligible degree. Several compounds showed anticancer activity in the ovarian cancer cell line A2780 in the dark, but the effect of irradiation on the antiproliferative

activity of these potential anticancer agents was not investigated [184].

An attempt to combine the photosensitizing effect of porphyrins with the potential anticancer activity of Ru^{II} compounds was also reported [124,185,186]. Up to four [Ru(9]aneS3)]²⁺ moieties, where [9]aneS3 is 1,4,7-trithiacyclonane, were attached to a modified porphyrin containing either *N*-mono- or *N,N*-bidentate binding partners. The resulting species, which were up to +8 positively charged, showed a 10-fold enhanced *in vitro* anticancer activity upon irradiation using visible light (590–700 nm) compared to non-irradiated samples, in particular *in vitro* activity in the sub- μ M range was observed. Notably, an attempt to insert polyethylene-glycols in order to increase the solubility of the Ru-porphyrinoids decreased their antiproliferative activity.

Finally, hexa- and octanuclear Ru^{II}-arene metallacages were employed for the delivery of porphyrins to cancer cells [187]. Porphyrins were trapped in the metallacages by hydrophobic interactions. The metallacages showed antiproliferative activity in the low μ M range independent of porphyrin load. Interestingly, the porphyrin-metallacages displayed high stability in culture medium accompanied by fluorescence quenching of the porphyrin when trapped in the metallacage. A drastic increase in fluorescence was then detected inside HeLa cells indicating selective intracellular porphyrin release. The octanuclear Ru^{II}-arene metallacage thereby displayed higher porphyrin liberation ability than the hexanuclear metallacage [187].

Bioconjugation. Bioconjugation of organometallics, *i.e.* tethering to a peptide, protein or other biomolecules, represents a promising strategy for the selective delivery of metallodrugs to a desired site of action [188,189]. The synthesis of peptides is well established, and therefore, metal-peptide bioconjugates are usually obtained by solid-phase peptide synthesis or by postsynthetic modification. Although there are many examples of metals conjugated to peptides for diagnostic or therapeutic purposes, bioconjugates with half-sandwich Ru^{II} or Os^{II} anticancer agents are only scarcely reported up-to-date [189-191]. To the best of my knowledge, the first representative was prepared in the group of Metzler-Nolte in 2008 (Figure 17) [192]. The synthetic strategy involved the incorporation of a non-natural procarbene-

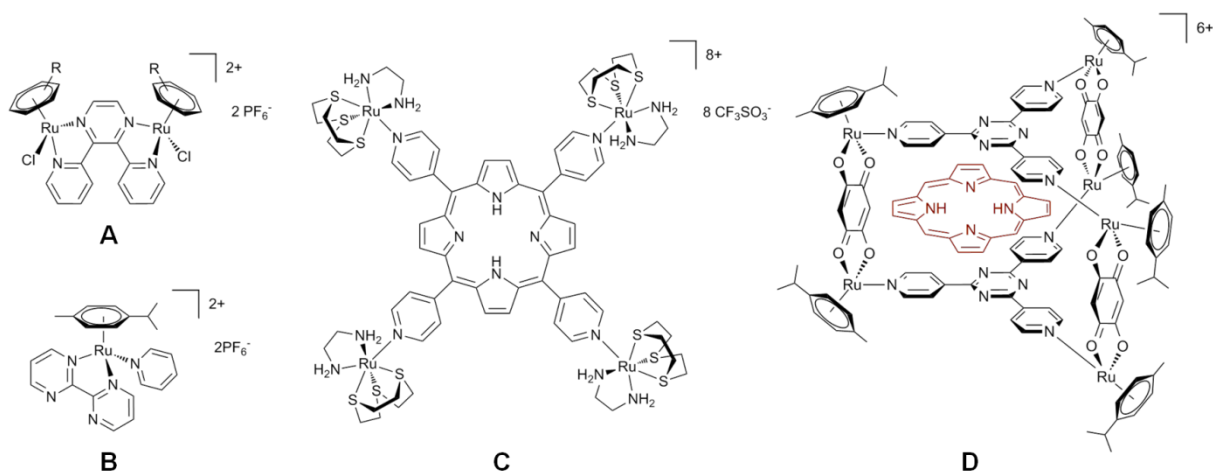


Fig. 16 Different strategies have been pursued for obtaining photoactive metallopharmaceuticals: (A) Irradiation of dinuclear Ru^{II}-arene bispyridylpyrazines leads to arene cleavage and extensive DNA binding depending on the π -acceptor ability of the η^6 -arene, (B) irradiation of heteroleptic Ru^{II}-arene bipyrimidine-pyridine organometallics led to pyridyl release and DNA binding, (C) porphyrin-based multinuclear Ru^{II}-[9]aneS3 complexes generate singlet oxygen and other ROS, (D) polynuclear Ru^{II}-arene metallacages can trap porphyrins but also other flat molecules for cellular delivery. The porphyrins are liberated inside the cells and generate singlet oxygen upon irradiation. The empty hexanuclear cages are also cytotoxic to some extent.

bearing amino acid into a short peptide and subsequent coordination of the carbene to the $[\text{Ru}^{\text{II}}\text{Cl}_2(\text{cym})]$ moiety. A similar route was followed to access thiazole-based carbene complexes [193]. It must be noted that these first representatives were not investigated for their biological activity. In 2011, a half-sandwich Os^{II} picolinato complex was reported, which was conjugated to polyarginines by 4-substitution of the *N,O*-bidentate picolinate [194]. The synthesized organometallic bioconjugates contained 1, 5 (Arg5) or 8 (Arg8) arginines. In contrast to $[\text{Os}^{\text{II}}\text{Cl}(\text{cym})(\text{picolinate})]$, which showed anticancer activity in the low μM range in the ovarian cancer cell line A2780 [127], the polyarginine bioconjugates were only moderately cytotoxic, with IC_{50} values of $71.5 \pm 2.5 \mu\text{M}$ (Arg5) and $32.9 \pm 3 \mu\text{M}$ (Arg8). The increased activity of the Arg8 bioconjugate was mainly ascribed to a 10-fold increased cellular uptake and a 15-fold higher DNA load. Intriguingly, low concentrations of the Arg5- and Arg8-bioconjugates led to fast precipitation of calf thymus DNA probably due to the formation of insoluble salts between the polycationic arginines-peptide and the negatively-charged DNA [194]. Furthermore, a half-sandwich Ru^{II} bioconjugate with a dicarba analogue of octreotide was prepared by conjugation of a pyridyl-derived octreotide to $[\text{Ru}(\text{bpm})(\text{cym})]^{2+}$, where bpm is bipyrimidine [195]. As mentioned before, pyridyl derivatives can be photocleaved from the metal centre by UV_A and visible light [183]. Since somatostatin receptors are over-expressed in cancer cells, conjugation to dicarba octreotide, a somatostatin agonist, might lead to specific tumour accumulation. After internalization, irradiation would then generate the active Ru species leading to apoptosis of cancer cells [195]. DNA interaction studies were performed showing that the $[\text{Ru}(\text{bpm})(\text{cym})]^{2+}$ -moiety possesses DNA-binding capabilities by favouring adjacent guanines even in the presence of L-histidine and L-methionine. In some cases, arene cleavage from the metal was also observed [195]. Octreotide was tethered to other metal systems involving M-peptide bioconjugates, where M is Pt^{II} , Ru^{II} and Os^{II} [196]. However,

the $[\text{RuCl}(\text{cym})(\text{PPh}_3)]^+$ -imidazolyl octreotide bioconjugate was the only conjugate with at least moderate antiproliferative activity in the human prostate tumour cell line DU-145, with an IC_{50} value of $26.0 \pm 2.0 \mu\text{M}$, however, it was equally cytotoxic to non-tumour Chinese hamster ovary cells (CHO).

Other delivery strategies involved η^6 -arene functionalization of organometallic phosphoadamantane- or carbohydrate-based Ru^{II} anticancer agents [197,198]. The functionalization of the η^6 -arene with a free aldehyde was employed to tether up to three RAPTA-type anticancer agents to hydrazone-modified human serum albumin (HSA) [197]. Importantly, the protein-RAPTA bioconjugate displayed antiproliferative activity in the low μM range in the ovarian cancer (A2780) cell line, whereas the free RAPTA derivative and the hydrazone-functionalized protein were inactive. Similarly, the η^6 -arene of RAPTA-type and carbohydrate-based Ru^{II} anticancer agents was modified with maleimide [198]. The selective reaction of the maleimide moiety with thiol-groups present in HSA was believed to provide a means for exploiting the enhanced permeability and retention effect (EPR). Indeed, the maleimide-derivatives were markedly more cytotoxic on primary tumour models than RAPTA-C.

2.3.5. Pharmacodynamics of Ruthenium and Osmium Anticancer Agents

In order to optimize drug lead structures with respect to potency, selectivity and safety, medicinal chemists often prepare a set of structurally slightly different compounds based on a lead compound. With such a library SARs can be derived by relating the chemical changes to differences in biological effects [5]. The aim of this section is to summarize SARs of Ru/Os anticancer agents with respect to their *in vitro* and *in vivo* activity against primary tumours.

Notably, for organometallic anticancer agents there were only a few *in vivo* SAR studies reported, but a huge body of *in vitro* data is available (*vide supra*). Interestingly, there seems to be a historical event for this development. With the enacting of the Council of Europe Treaty Series No. 123 ‘for the

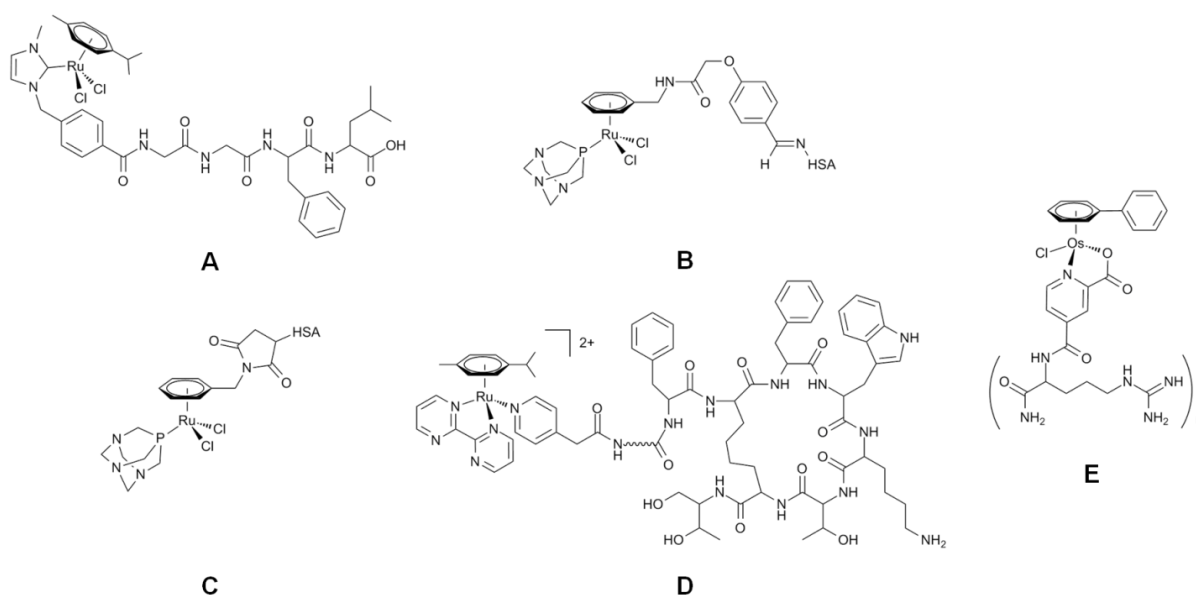


Fig. 17 Several studies reported the conjugation of Ru^{II} - and Os^{II} -arenes to biomolecules. (A) The first Ru^{II} -arene representative was obtained by solid-phase synthesis. The antiproliferative activity of this bioconjugate was not evaluated (B) An aldehyde-containing RAPTA-derivative reacted with hydrazine-modified HSA (C) A maleimide-containing RAPTA-derivative was also tethered to HSA (D) An octreotide-derivative was conjugated to a Ru^{II} -arene moiety with the aim of selective tumour accumulation (E) An Os^{II} arene polyarginine ($n = 1, 5, 8$) bioconjugate was reported with medium antiproliferative activity.

Table 1 Results of the Ru^{III} compound families are shown which were obtained in studies using the *in vivo* P388 leukaemia mouse model during the 1980s. The range of the survival time with respect to the control group (T/C, %) is given. A T/C of 200 % is desirable. B denotes an *N*-donor and R an organic group. Adapted from Ref. [31].

Compound	T/C (%)
[Ru ^{II} (dmsO) _{4-n} B _n Cl ₂]	100-125
[Ru ^{II} (dmsO) ₄ Cl ₂]	125
[Ru ^{II} Ru ^{III} Cl(RCOO) ₄]	125-135
[Ru ^{III} (RSR) ₃ Cl ₃]	130-135
<i>fac</i> -[Ru ^{III} B ₃ Cl ₃]	100-190
<i>trans</i> -[Ru ^{III} B ₂ Cl ₄](HB)	140-200
[Ru ^{III} BCl ₅](HB) ₂	140-200
[Ru ^{III} Cl ₆](HB) ₃	100-120
[Ru ^{IV} Cl ₆](HB) ₂	100-120

protection of vertebrate animals used for experiments and other scientific purposes' in 1991, animal tests needed to be approved by the authorities and are allowed only after ethical justification and explanation of their necessity [199]. The act includes experiments with mice, rats, guinea pigs, golden hamsters, rabbits, dogs, cats and quails, while the use of primates was generally prohibited. In Austria, a similar animal test act – *Tierversuchsgesetz* – was already proclaimed in 1989 [200]. In parallel, the first colorimetric *in vitro* assays for the assessment of cell proliferation and compound cytotoxicity were developed in 1983 [201] and routinely applied only since the mid 1980s. Consequently, the first Ru^{III} metallopharmaceuticals developed in the 1980s underwent extensive *in vivo* screenings [31], while there are only a limited number of *in vivo* studies of organometallic Ru/Os anticancer agents since 2001. This trend may prove to be double-edged since a predominate reliance on *in vitro* screenings for predicting SARs bears a significant risk of failure in later stages of drug development due to unpredictable toxicity and pharmacokinetics *in vivo* [5].

In vivo SARs. The most extensive *in vivo* study of different families of Ru^{II} and Ru^{III} coordination compounds was summarized by Keppler *et al.* in 1989 [31]. The anticancer activity was measured as a T/C ratio, which represented either the survival time (T/C >> 120% desirable) or tumour growth (T/C < 10% desirable) with respect to the control groups. At that time, the highly cisplatin-sensitive P388 leukaemia mouse model was most frequently employed. It was suggested that this *in vivo* model is suitable for selecting Ru metallodrugs for more sophisticated tumour models by comparing their activity to cisplatin. Additionally, the water solubility of the test compound needed to be appropriate in order to allow *in vivo* screenings typically at doses of 0.1–0.15 mmol/kg.

Among the initial Ru families tested were [Ru^{II}Cl₂(dmsO)_{4-n}B_n], where n = 1–4 and B = *N*-heterocycle, [Ru^{III}Cl₃(R₂S)₃], [Ru^{III}Cl₃B₃] and [Ru₂^{III/II}Cl₂(μ-RCO₂)₄], which all showed T/C < 135% (Table 1, see also Figure 4 for chemical formulas). Only *cis*-[Ru^{III}(NH₃)₄Cl₂]Cl and *fac*-[Ru(NH₃)₃Cl₃] showed T/C values of 160% and 190%, respectively, although the latter was only poorly water soluble. The families (HB) *trans*-[Ru^{III}Cl₄B₂] and (HB)₂ [Ru^{III}Cl₅B] displayed good water solubility and T/C = 130–200%. In other *in vivo* studies it was also shown that sodium *trans*-[RuCl₄(dmsO)(HIm)] (NAMI) was inactive with respect to primary tumour growth inhibition in MCa mammary carcinoma [67].

It seems that charged Ru^{III} coordination compounds are better water soluble, while the charge *per se* does not seem to

affect greatly the antitumour activity *in vivo*. Judging from these experiments, sulfur and oxygen donor ligands yielded compounds of low activity in the leukaemia model. On the other hand, amino and imino ligands seem to lead to a more pronounced anticancer activity. Increasing the number of chlorido ligands from two to four increased the activity, while five chlorido ligands displayed a slightly lower antitumour activity compared to four and the hexachlororuthenates was inactive. Moreover, the coordination compounds with Ru in the +II oxidation state were inactive and abandoned, although only a small number of dmsO derivatives were tested. The most promising compound in the P388 mouse model was KP418 (Table 2). At 10-fold higher doses, it showed a T/C = 194% comparable to the efficacy of cisplatin [31]. Substituting the *N*-coordinating imidazole by other *N*-heterocycles decreased the survival time significantly, *e.g.* pyrazole, triazole, 1-methylimidazole, dimethylpyrazole, benzimidazole, indazole, quinoline and aminothiazole all showed T/C values in the range 130–160%. The complexes KP418, KP1019 and (H₂BzIm)₂ [Ru^{III}(HBzIm)Cl₅], where HBzIm is benzimidazole, were selected for further investigation in a chemically-induced colorectal adenocarcinoma tumour model in rats, which features pathophysiological similarities with human colorectal tumours [48]. The compounds were administered twice weekly at doses of 0.022 mmol/kg. While cisplatin was completely inactive in this tumour model, [Ru^{III}(HBzIm)Cl₅]²⁻ showed an antitumour activity of T/C = 18%. KP418 and KP1019 showed an even more pronounced effect yielding T/C = 5% and 8%, respectively. However, KP418 led to a drastic reduction of body weight and resulted in 55% mortality, whereas 0% mortality and virtually no reduction of body weight were observed for KP1019, which was then selected for further preclinical and clinical development.

The mentality change with respect to *in vivo* testing manifested itself from 2000 onwards with the up-coming organometallic Ru^{II}-arene anticancer agents. In the first report by Aird *et al.* in 2002, an *in vitro* SAR study of a small number of Ru^{II}-arene organometallics in the ovarian cancer (A2780) cell line yielded RM175 as the most promising compound. At that time, it was the sole representative to be tested in the A2780 xenograft model *in vivo* [90]. At 2.5-fold higher doses compared to cisplatin, the mice treated with RM175 showed a tumour-growth of T/C = 46% compared to the control group. RM175 is approximately half as active as cisplatin, which displayed a T/C = 23%. Interestingly, RM175 was equally tumour-inhibiting in the cisplatin-resistant A2780cis xenograft model, but inactive in the multi-drug resistant A2780^{AD} xenograft model.

In additional *in vivo* studies, RM175 was compared to its 1,4,9,10-tetraanthracene (HC11) [91] and osmium (AFAP51) [92] analogues. RM175 and HC11 were compared for their antitumour activity *in vivo* in two non-small lung cancer xenografts (LXFL529 and A549). Both compounds were administered *i.p.* at weekly doses of 25 mg/kg. Both compounds were inactive in the LXFL529 model, while they caused a significant tumour growth delay in the A549 xenograft and T/C = 54% and 48% were observed for RM175 and HC11, respectively. The more lipophilic HC11 was slightly more active *in vivo*, which is also paralleled by a higher cytotoxicity. However, the higher activity of HC11 is also accompanied by increased hepatotoxicity, probably due to cleavage of the polyaromatic arene from the metal (see section 2.3.6.). Consequently, carcinogenic or toxic arenes are

preferably to be omitted. Secondly, the tumour-inhibiting effect of RM175 was also compared to AFAP51 in the MCa mammary carcinoma model *in vivo* [92]. The compounds were administered at doses of 7.5 mg/kg i.p. for five consecutive days. RM175 caused a T/C = 53% after the administration period. AFAP51 was largely inactive displaying a T/C = 83%, although being more potent in the *in vitro* assay [92]. The pta complexes RAPTA-C and RAPTA-B were also investigated in the MCa mammary carcinoma model, showing no activity against the primary tumour [79].

Finally, FY026 was investigated in the colon adenocarcinoma xenograft model (HCT-116) *in vivo* [120]. While showing good tolerability [121], single dose administration of 40 mg/kg i.v. of the compound resulted in a T/C ≈ 50% [120].

In summary, several points can be derived from the limited data obtained with organometallic anticancer agents against primary tumours *in vivo*. It seems that inert bidentate ligands are crucial for activity against primary tumour models. An increase of the ring system of the η^6 -arene slightly increases the antitumor activity, but also increases the toxicity and decreases water solubility. Moreover, the use of non-toxic η^6 -arenes is advised due to potential arene cleavage in hepatocytes, *e.g.* hexamethylbenzene or *p*-cymene should be preferred. Finally, predictions on the effect of metal or leaving group are not yet possible.

In vitro SARs. Although *in vivo* and *in vitro* data do not necessarily correlate [5,31], it is worthwhile developing *in vitro* SARs for organometallic Ru^{II} and Os^{II} anticancer agents with respect to primary tumours. Due to the present lack of abundant *in vivo* data, potential correlations of molecular and physicochemical properties of this substance class with *in vitro* cytotoxicity are of great interest, *i.e.* the arene, the leaving group, the charge, hydrolysis and the pK_a of resulting aqua complexes, the coordination mode and the ligand system may greatly influence the antiproliferative activity of

organometallic anticancer agents (Table 3). In contrast to the commonly used *in vivo* P388 leukaemia model in the past [31], research groups are currently using many different cell lines to evaluate the antiproliferative effect of their compounds *in vitro* thus complicating the deduction of a general SAR. The following *in vitro* SAR is consequently based on two reasonably often employed cell lines, namely CH1 and A2780, which are both human ovarian adenocarcinoma cell lines. Note that in spite of their similar histology, data cannot be directly compared with each other and will be treated separately.

Organometallic Ru^{II} and Os^{II} metallodrugs share the half-sandwich “piano-stool” geometry [75,118]. The face-capping η^6 -arene occupies three binding sites while the three remaining sites are occupied by inert mono- or bidentate ligands and one or two labile leaving groups. As in the case of the Ru^{III} metallopharmaceuticals, the compounds of this substance class are prodrugs, which are activated by hydrolysis of the leaving group, *i.e.* the aquation step yields the reactive aqua complex. Therefore, the arene represents a common motif of virtually any organometallic Ru^{II} and Os^{II} anticancer agent and the choice of the arene influences the cytotoxic activity. Several studies indicated that the cytotoxicity of a metallodrug increases with increasing lipophilicity of the arene [90,129,130,132,133,142] and usually follows the order: benzene < toluene < *p*-cymene ≈ tetrahydronaphthalene < biphenyl < tetrahydroanthracene. This may be caused by increased uptake into cells by passive diffusion [129,202]. However, an increased lipophilicity comes at the cost of reduced water solubility, which is a crucial parameter for *in vivo* testing and further drug development [203]. There are also several examples, where arene variation did not affect the cytotoxicity [131,142,153], which might be indicating a catalytic mode of action of metallodrugs such as [Ru(arene)(azpy)] derivatives [131,204]. Attempts of substituting the η^6 -arene by η^3 -trithiocydonane ([9]aneS₃)

Table 2 Selected examples from the Ru^{III}-compound families of Table 1 are shown. Their anticancer activity was evaluated in the P388 leukaemia mouse model *in vivo*. The dose, the treatment scheme and the survival time with respect to the control group (T/C, %) are given. Cisplatin is listed as a reference. B denotes an *N*-donor and R an organic group. Adapted from Ref. [31].

Compound	Dose (mmol/kg)	Dose (mg/kg)	Treatment schedule (days)	T/C (%)
cisplatin	0.01	3	1, 5, 9	175
[Ru ^{II} Ru ^{III} Cl(MeCOO) ₄]	0.21	100	1	125
[Ru ^{II} Ru ^{III} Cl(EtCOO) ₄]	0.16	85	1	125
<i>fac</i> -[Ru ^{III} (4-Me-pyridine) ₃ Cl ₃]	0.16	78	1	83
<i>fac</i> -[Ru ^{III} (4- ^t Bu-pyridine) ₃ Cl ₃]	0.16	110	1	110
<i>fac</i> -[Ru ^{III} (4-dimethylamino-pyridine) ₃ Cl ₃]	0.16	92	1	125
<i>fac</i> -[Ru ^{III} (pyridazine) ₃ Cl ₃]	0.06	27	1, 5, 9	127
<i>fac</i> -[Ru ^{III} (phenylmethylsulfide) ₃ Cl ₃]	0.16	93	1	130
<i>fac</i> -[Ru ^{III} (phenylethylsulfide) ₃ Cl ₃]	0.16	100	1	134
<i>fac</i> -[Ru ^{III} (NH ₃) ₃ Cl ₃]	0.19	50	1, 5, 9	189
<i>trans</i> -[Ru ^{III} (indazole) ₂ Cl ₄](indazolium) KP1019	0.15	91.1	1, 5, 9	133
<i>trans</i> -[Ru ^{III} (benzimidazole) ₂ Cl ₄](benzimidazolium)	0.1	60.7	1, 2, 3	155
<i>trans</i> -[Ru ^{III} (quinoline) ₂ Cl ₄](quinolinium)	0.1	64.0	1, 2, 3	160
<i>trans</i> -[Ru ^{III} (imidazole) ₂ Cl ₄](imidazolium) KP418	0.15	69.8	1, 5, 9	194
[Ru ^{III} (benzimidazole)Cl ₅](benzimidazolium) ₂	0.15	100.7	1, 5, 9	133
[Ru ^{III} (1-Me-imidazole)Cl ₅](1-Me-imidazolium) ₂	0.1	52.4	1, 5, 9	144
[Ru ^{III} (imidazole)Cl ₅](imidazolium) ₂	0.15	72.8	1, 5, 9	163

tend to reduce the cytotoxic activity probably due to the decreased lipophilicity [205], while the antiproliferative activity profile of η^5 -cyclopentadiene derived metallodrugs seems to parallel that of η^6 -arene compounds [206]. Already in the mid-1980s, Ford *et al.* found that η^6 -arenes may be photo-cleaved from the Ru^{II} metal centre [207]. Arene cleavage seems to be particularly prominent for electron-withdrawing substituents at the η^6 -arene and when the coordinated bidentate ligand is a strong π -acceptor due to competition for electron density from the metal [130,182,208].

The effect of the metal centre on cytotoxicity is highly ligand dependent. It seems that the Os metallodrugs are less active compared to their Ru analogues when considering *P*-monodentate [102,170] or *O,O*-bidentate [138,153] ligands, while they are usually equally or more potent using *N,O*- [127] or *N,N*-bidentate [104,132,162,163,165,166] ligands. The choice of the metal additionally affects hydrolysis rates. Since Os^{II} is more inert towards ligand substitution than Ru^{II}, hydrolysis of the Os analogues is generally decreased or even completely inhibited [104,127,131,132,168,170]. However, the hydrolysis rate itself does not seem to correlate with the

antiproliferative activity [78,104,130-132,138,139]. The coordination mode substantially influences the cytotoxic activity of organometallic anticancer agents. Organometallics containing monodentate *P*- or *N*-ligands [78,79,102,104,168,170,171], *O,O*-bidentate ligands [126,138-143,155] or *N,O*-bidentate ligands [111,126,127] were largely inactive in CH1 and/or A2780 cells. However, there are notable exceptions where active metallodrugs were reported containing *O,O*- [152,176] or *N,O*-bidentate [127,129] ligands. On the other hand, *S,O*- [140,142] and *N,N*-bidentate [78,90,111,162,163,165,166,174] donor systems generally yielded highly antiproliferative metallodrugs, except for bipyridines [126] and bipyrimidines [208], which were inactive *in vitro*.

The leaving group exerts only subtle effects on the antiproliferative activity. Chlorido and iodido complexes are about equally potent, while the bromido analogues usually yielded the least active compounds *in vitro*. However, an activity increase using iodide compared to the chlorido analogue was reported in some cases [131,133,142]. Similarly to hydrolysis rates, neither the choice of the leaving group nor

Table 3 The different inert ligand systems of organometallic Ru^{II} and Os^{II} metallodrugs are compared with respect to their antiproliferative activity *in vitro*, which is expressed as the concentration at which 50% of the cells die (IC₅₀). Additionally, the coordination mode (Coord. Mode), the metal centre, the leaving group, the charge, the half-life (t_{1/2}) of hydrolysis in water and the pK_a of the hydrolyzed aqua-complexes are given where available.

Inert Ligand System	Coord. Mode	Metal	Leaving Group	Charge	Hydrolysis (t _{1/2})	pK _a	IC ₅₀ (μM)	Cell Line	Refs
pta	P	Ru/Os	Cl	0			>100	HT29	[79,102]
carbohydrate-based phosphites	P	Ru	Cl, Br, I	0	1 h		>100	A2780	[168,171]
	P	Os	Cl	0	>24 h		>100 – 29	CH1	[168]
amines/nitrile	N	Ru	Cl, Br	0, +1			>100	A2780	[78,90]
	N	Os	Cl	0, +1			>100	A2780	[104]
amino acids	N,O	Ru	Cl	0	partial	8.6	>100	A2780	[126]
picolinates	N,O	Os	Cl	0	12 min	6.7	5	A2780	[127-129]
<i>N</i> -phenylpicolinamides	N,O	Ru/Os	Cl	+1	0.4 – 4.3 h	7.0	>50	A2780	[111]
	N,N	Os	Cl	0	< 10 min	7.3	12 – 25	A2780	[111]
ethylenediamines	N,N	Ru	Cl, I	+1	10 – 24 min	8.2	0.5 – 56	A2780	[78]
	N,N	Os	Cl	+1	6.4 h	6.3	7	A2780	[104]
bipyridines	N,N	Ru	Cl	+1		5.8	>100	A2780	[126]
bipyrimidines	N,N	Ru	Cl, Br, I	+1	14 min – 24 h	7	>100	A2780	[208]
<i>N</i> -phenylazopyridines	N,N	Ru	Cl	+1	2.1 h	4.5	>100 – 18	A2780	[130]
	N,N		I	+1	>24 h		2 – 6	A2780	[131]
	N,N	Os	Cl	+1	>24 h		>50 – 0.8	A2780	[132]
	N,N		I	+1	>24 h		0.14 – 10	A2780	[132]
<i>N</i> -phenyliminopyridines	N,N	Os	Cl	+1	<24 h	5.2	1.5 – 33	A2780	[133]
	N,N		I	+1	24 h		0.8 – 36	A2780	[133]
6-paullones	N,N	Ru/Os	Cl	+1			0.5 – 5.5	CH1	[162,163]
9-paullones	N,N	Ru/Os	Cl	+1			8 – 10	CH1	[162]
2-indoloquinolines	N,N	Ru/Os	Cl	+1			1.3 – 20	CH1	[123]
6-indoloquinolines	N,N	Ru/Os	Cl	+1			0.4 – 0.5	CH1	[165]
6-indoloquinolines (2-sub.)	N,N	Ru/Os	Cl	+1			0.2 – 4	CH1	[166]
quinoxalinones	N,N	Ru	Cl	+1	partial		0.3 – 6	CH1	[174]
	N,N	Os	Cl	+1			0.4 – 3	CH1	[174]
acetylacetonates	O,O	Ru	Cl	0		9.4	>100 – 11	A2780	[126]
pyrones	O,O	Ru	Cl	0	<10 min	~9	>50	A2780	[138]
	O,O	Os	Cl	0	<10 min	7.6	>100 – 81	CH1	[139-142]
pyridones	O,O	Ru/Os	Cl	0	<10 min		>50	A2780	[138]
	O,O	Ru/Os	Cl	0	<10 min		>100	A2780	[155]
bis-pyridones	(O,O) ₂	2Ru	Cl	0	<10 min	9.5	>100 – 1	A2780	[152,153]
	(O,O) ₂	2Os	Cl	0			29	A2780	[153]
flavonoids	O,O	Ru	Cl	0			0.9 – 8	CH1	[176,177]
thiopyrones	S,O	Ru	Cl	0	<10 min	12.8	13 – 35	CH1	[139,141,142]

the charge of the complex seems to greatly influence the cytotoxic activity [153]. Increasing the charge of the complex from neutral to +1 seems to decrease hydrolysis rates [111,139] as well as the pK_a of the aqua complex, which is consistent with the reduced electron density at the metal centre [95,111]. Although the pK_a values of the aqua complex greatly vary across this substance class, it does not seem to correlate with the *in vitro* anticancer activity. The Os analogues generally give more acidic aqua complexes compared to Ru [95], while the bidentate ligands show the following order in the Ru^{II}(cym) scaffold: $pK_a(N,N) = 4.5 - 8.2$, $pK_a(N,O) = 7 - 8.6$, $pK_a(O,O) = \sim 9$, $pK_a(S,O) = \sim 12$ [95,111,126,140,142]. Furthermore, the choice of the arene can also slightly affect the pK_a of the aqua complex depending on its π -acceptor capability [95]. Electron-withdrawing substituents on the arene tend to decrease the pK_a , while electron-donating substituents have the opposite effect.

In summary, the *in vitro* cytotoxicity of organometallic anticancer agents seems to be influenced by the arene, the metal and the ligand system, while it is largely independent of the leaving group, the charge, the hydrolysis rate and the pK_a .

2.3.6. Pharmacokinetics and Toxicology of Ruthenium and Osmium Anticancer Agents

Most Ru/Os metallodrugs under development were designed for intravenous administration and would directly reach the blood stream of a potential patient. This simplifies pharmacokinetic aspects since bioavailability and first-pass effects must not be considered and the focus lies on distribution, metabolism, excretion and toxicity. Pharmacokinetic data are only available for a limited number of Ru/Os anticancer agents in hand with the previously mentioned low number of *in vivo* investigations. In the following section, the pharmacokinetics and toxicity of potential Ru/Os anticancer agents by intravenous (i.v.) or intraperitoneal (i.p.) administration will be delineated. Oral administration (p.o.) is discussed thereafter.

Distribution. KP1019 was shown to bind to a high percentage to serum proteins, in particular to HSA (> 90%) [210-212]. Furthermore, KP1339 showed approximately 3-fold higher Ru concentrations in plasma than in the blood cell fraction in non-tumour bearing mice, with peak concentrations in the plasma of $40 \pm 5 \mu\text{g Ru/g blood}$ 3 h after administering a single dose 40 mg/kg i.v. [213]. In the same study, the tissue distribution of KP1339 was determined in mouse models showing highest Ru concentrations in the colon, kidney, liver, lung and thymus, whereas the latter probably stems from the immune-suppression of the mice. The detected Ru concentrations ranged from 15–40 $\mu\text{g/g}$ after 1 h and merged at $\sim 20 \mu\text{g/g}$ after 24 h. Low Ru concentrations in the brain indicated low blood-brain barrier penetration for this compound [213]. *In vivo* studies of NAMI-A showed a similar biodistribution compared to KP1019 and comparable Ru concentrations in the brain, kidney, liver and lung even at daily doses of 50 mg/kg for 5 consecutive days [214]. It was also demonstrated that NAMI-A favourably binds to collagen with relevance to its antimetastatic activity [215]. The extensive binding to serum proteins of KP1019 and NAMI-A was also reflected by their low volume of distribution in their phase I evaluations [70,209], table 4.

Pharmacokinetic properties of single- and repeated-dose administration of the organometallic antimetastatic agent RAPTA-C were also determined *in vivo* [79]. RAPTA-C seems to exhibit similar pharmacokinetics in the mouse

Table 4 Non-compartmental pharmacokinetics determined in phase I studies with KP1019 and NAMI-A. The parameters are based on the first administration after 24 h. Adapted from refs. [70,209].

	KP1019	NAMI-A
Dose	600 mg	300 mg/m ²
CL (mL/min)	0.94	0.13 \pm 0.3
V _{ss} (L)	5.43	7.9 \pm 1.6
terminal t _{1/2} (h)	68.1	49 \pm 23.9
C _{max} (mg/L)	29.0	72.3 \pm 22.3

compared to the Ru^{III} complexes, although a slightly increased volume of distribution indicated better tissue penetration. The Ru content in the kidney, liver, spleen and lung was determined at doses of 100 or 200 mg/kg i.p. up to 4 days after administration and the final Ru concentrations in liver, lung and kidney were approximately 5-fold larger compared to treatment with KP1339 at a single dose of 40 mg/kg [79,213], *i.e.* the Ru concentrations ranged from 50–250 $\mu\text{g/g}$ and the lowest concentrations were found in the lung and spleen. Finally, pharmacokinetic results for the Os phenylazopyridine compound FY026 [120,121], which resists hydrolysis. Immediately after single-dose administration of 10 mg/kg i.v., high Os concentrations were detected particularly in the kidney, but also in the liver, while low concentrations were observed in plasma and the tumour (colon) [120]. It must be noted that the quantification of Os *via* ICP-MS is error-prone, presumably due to the formation of volatile OsO₄ during mineralization with HNO₃ [123]. Therefore, caution must be applied when interpreting such data sets.

Excretion. During preliminary phase I studies with KP1019, it was suggested that biliary excretion is important for the overall elimination of KP1019 in humans since renal excretion was low [209]. The clearance (CL) of KP1019 was low as was the volume of distribution at steady state (V_{ss}), probably caused by the coordinative binding to serum proteins, which in turn caused long half-lives (Table 4) [209]. Similarly to KP1019, NAMI-A showed also low clearance [70]. The accumulation of FY026 in the kidneys immediately after administration indicates low serum protein binding capacity and rapid renal elimination [120].

Toxicity. While the preclinical toxicity of KP418 was associated with nephro- and hepatotoxicity, increase in creatinine levels and also chronic toxicity, KP1019 was largely non-toxic in mouse and in rat models [31,48]. Nephrotoxicity of KP418 could be drastically reduced by pre- and post-administration of physiological saline [31]. Importantly, these preclinical findings correlated well with the preliminary phase I clinical study of KP1019 in humans, where only mild toxicities were reported at high doses, *i.e.*, > 600 mg/m² [60,61,209]. Currently, the dose-limiting toxicity of KP1339 in phase I of clinical trials was characterized by nausea, vomiting, fatigue and increased creatinine levels at weekly doses of 780 mg/m² [60,61]. The MTD was defined at 625 mg/m², leading to grade 1 fever and chills. Low toxicity in mouse models were also observed with NAMI-A at doses up to 600 mg/kg [216]. The clinical phase I study showed blister formation as the dose-limiting toxicity in humans at daily doses of > 400 mg/m² for 5 days [70]. Furthermore, nausea, vomiting and increased creatinine levels were diagnosed upon treatment of patients during the same treatment scheme.

Toxicological data is also available for RM175 and HC11, which allows comparison of the influence of the arene ring,

i.e., biphenyl vs. tetrahydroanthracene [91]. RM175 did not result in a significant reduction of body weight at doses up to 25 mg/kg *i.v.*, suggesting lower toxicity compared to cisplatin [90]. Even single doses of 40 mg/kg administered *i.p.* caused no changes in urea or creatinine levels *in vivo* and only minor changes in the histopathology caused by inflammation [91]. On the other hand, administration of HC11 *i.p.* led to increased levels of alanine transaminase in the blood indicating hepatotoxicity. Investigations on the cytotoxicity of HC11 on hepatocytes revealed an IC_{50} of 0.6 μ M, being slightly more potent than the positive control. It was suggested that arene cleavage and hydroxylation of the polyaromatic system in the hepatocytes by cytochrome P450 may be responsible for generating potentially toxic species [91]. Nephro- and bone marrow toxicity was not evidenced during these studies.

Finally, (preliminary) studies with the Os^{II} -arene phenylazopyridine compound FY026 revealed that single-dose administration of 40 mg/kg *i.v.* did not result in a significant reduction of body weight in mice indicating good tolerability [120,121]. The *in vivo* toxicity of RAPTA compounds was not reported [79].

Oral administration. Oral administration is desirable for patient compliance. However, orally active Ru/Os anticancer agents are currently not in the focus of investigation. To the best of my knowledge, only two investigations were reported to date [123,216]. NAMI-A was reported to be orally active against lung metastases and non-toxic to the gut *in vivo* at doses up to 600 mg/kg [216]. [MCI(cym)(IQ)], where M is Ru^{II} or Os^{II} and IQ is an indoloquinoline derivative, were also administered *p.o.* and especially the Os-analogue showed a tumour-inhibiting effect in the murine colon carcinoma model (CT-26) [123]. As mentioned in section 2.1.2., orally active compounds must cope with additional hurdles compared to drugs, which are administered intravenously.

Oral bioavailability can be estimated by a concept called drug-likeness, which is a rampant qualitative concept in drug discovery [217,218] and originates from a study on a large number of approved orally active drugs by Lipinski *et al.* [219]. From this data set, they deduced several physicochemical criteria, which, if met, might increase the probability of a drug to display favourable ADME profiles, *i.e.* oral bioavailability. In particular cut-off properties such as molecular weight (≤ 500 Da), lipophilicity/solubility ($ClogP \leq 5$, $MlogP \leq 4.15$), number of hydrogen bond acceptors (HBA)/donors (HBD) [≤ 5 HBD, ≤ 10 HBA] were summed up to the so-called "Lipinski's rule of five" since the numbers are multiples of five. However, such empirically derived rules necessarily allow for deviations and a significant percentage of "drug-unlike" entities (Lipinski fails) passed clinical trials as well [220].

It was the aim of several recent publications to improve the qualitative concept of drug-likeness in order to incorporate potential rule-breakers by extending the rule of five. For example, Veber *et al.* allowed for masses > 500 Da and introduced molecular flexibility (≤ 10 rotatable bonds) and the polar surface area ($\leq 140 \text{ \AA}^2$) as further decisive criteria on oral bioavailability [221]. Furthermore, structural factors such as the fraction of the molecular framework (f_{MF}) and fraction of the sp^3 -hybridized carbon atoms (F_{sp^3}) were shown to influence ADME properties of a drug [222]. The latter two seem to be independent of the criteria developed by Lipinski. Large f_{MF} (≥ 0.65) tend to decrease the solubility, while the inverse is observed for the permeability. Contrary, large F_{sp^3}

(≥ 0.35) seem to increase the solubility, but reduce the permeability. Intriguingly, the trends for f_{MF} and F_{sp^3} seem to be independent of the ionization state, which potentially makes them suitable for predicting the oral bioavailability of metal-based drugs. Additionally, large F_{sp^3} values also tend to increase plasma protein binding. While these approaches are based on 'yes-or-no' cut-off criteria and were initially suggested as guidelines, a more holistic estimate of drug-likeness was just recently reported called the quantitative estimate of drug-likeness (QED) [220]. The empirical QED is basically a percentage representing drug-likeness, *i.e.* 0 = very drug-unlike to 1 = ideally drug-like. The percentage is calculated by a weighted combination of molecular weight, lipophilicity, polar surface area (PSA), HBAs, HBDs, number of rotatable bonds, aromatic rings and reactive groups. It must be noted that the weightings of HBA and PSA are 0.05 and 0.06, respectively, while reactive groups are weighted with 0.95. Consequently, HBA and PSA have only a marginal effect on the QED and on oral bioavailability. The notion of drug-likeness was exclusively developed for organic drugs and analogous predictive tools do not exist for metal-based pharmaceuticals due to the lack of orally active metallodrugs approved for clinical use [223].

2.4. Mass Spectrometry for Investigating Metal-Based Anticancer Agents

The primary bioassay for determining the antiproliferative activity of metal-based anticancer agents is the colourimetric MTT experiment in cell cultures (MTT = (3-(4,5-dimethyl-2-thiazolyl)-2,5-diphenyl-2H-tetrazolium bromide). If this assay shows promising results, several analytical and biochemical investigations may then be envisioned with the aim of underlining the antitumour activity and of deducing a potential mode of action. Mass spectrometry (MS) has been extensively employed for the latter reason and emerged as one of the major bioanalytical tools in the preclinical evaluation of metal-based anticancer agents. The popularity of MS in the field of metallodrug research is partly due to the unique features of the (transition) metals. The classical metal-based anticancer agents contain non-physiological elements (Pt, Ru), which display high atomic masses and characteristic isotopic distributions. Additionally, these metallodrugs often carry a positive charge in their activated (hydrolyzed) state. These three points facilitate their selective detection in a biological environment using a mass spectrometer [224]. Here, the emphasis will be put on the discussion of the components of a mass spectrometer before giving a concise overview of the application of MS in the design and development of metal-based anticancer agents.

2.4.1. Instrumental Setup of a Mass Spectrometer

Typically, analytes have to be ionized and freed from their matrix prior to entering the mass spectrometer, *i.e.* the analyte must be transferred from liquid or solid phase into the gas phase and must entirely desolvate. Once in the gas phase, the analyte ions are separated by their mass-to-charge ratio (m/z ratio) and the abundance of analyte ions with a given m/z ratio is subsequently detected. Since ions travel in the gas phase, MS analysis requires high vacuum to reduce ion dispersion caused by collisions with residual gas particles. Therefore, a mass spectrometer consists of four main instrumental components, namely ion source, mass analyzer, ion detector and vacuum system [225-228]. Moreover, hyphenation to

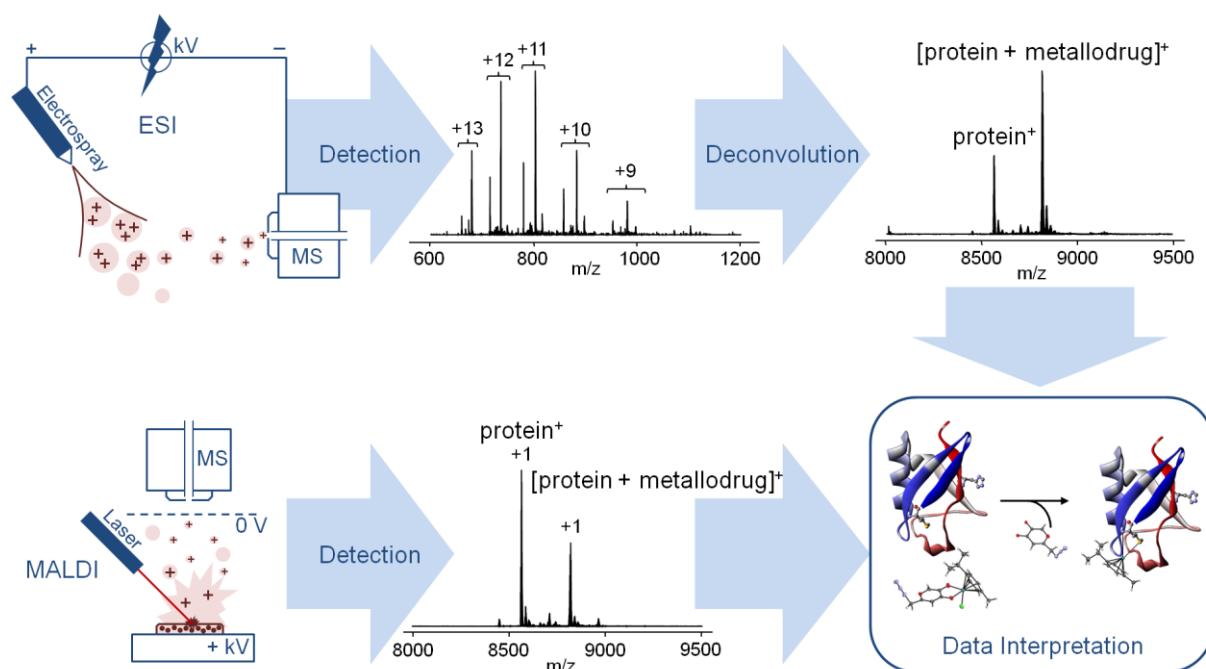


Fig. 18 The steps from sample ionization to detection and data interpretation are illustrated for ESI- and MALDI-MS. Both ionization methods are extensively used in metallodrug research in combination with various mass analyzers. ESI yields multiply-charged sample ions, while MALDI tends to yield singly-charged ions. ESI requires a deconvolution step to obtain a spectrum of (pseudo-)molecular ions. MALDI ionization suffers from a lower sensitivity with respect to the metallodrug-biomolecule adduct.

separation techniques and isolation/fragmentation, *i.e.*, multistage MS, are related topics that will also be covered [229,230].

Ion Source. Several ion sources are available for ionizing analytes, but only three of them are widely applied in the field of metallodrug research. The first representative is inductively coupled plasma (ICP) ionization for element-specific analysis and involves atomization of a sample in an induced argon plasma at 8'000 K. Therefore, single positively-charged elemental ions corresponding to a metal isotope are measured. This in turn allows the analysis of metal contents in complex biological systems such as tissues or cells *in vivo* and *in vitro*. This approach is partially limited by the occurrence of (polyatomic) interferences resulting from reactions in the plasma that may show non-resolvable m/z ratios as the metal isotope under investigation. Also, structural information may not be obtained using ICP due to the sample atomization.

Analysis of interactions between intact metallodrugs and biomolecules calls for soft ionization techniques that do not result in fragmentation of the biomolecule, the metallodrug or the interaction product (adduct). Electrospray ionization (ESI) as well as matrix-assisted laser desorption ionization (MALDI) are ideally suited for this purpose. The development of these two techniques had a tremendous impact on the characterization of high-molecular weight compounds (“flying elephants”) and the inventors of ESI (John Fenn) and MALDI (Koichi Tanaka) were awarded the Nobel Prize in Chemistry in 2002. Because of the different ionization processes, ESI and MALDI yield characteristic mass spectra: MALDI shows predominately singly-charged pseudomolecular ions in a mass spectrum, while multiply-charged pseudomolecular ions and also alkaline metal adducts are frequently observed in ESI experiments (Figure 18). Due to the high number of protonation/adduct formation sites, ESI yields a characteristic charge envelope for proteins (often in the positive ion mode) or oligonucleotides (usually analysed in negative ion mode).

The main advantage of ESI over MALDI is that ions are generated directly from solution instead of being embedded in a matrix. ESI is better suited for online hyphenation. Additionally, it was found that MALDI-MS of metallodrug-protein adducts results in a higher degree of adduct fragmentation and therefore, suffers from lower adduct sensitivity compared to ESI [231].

Mass Analyzer. Mass analyzers are responsible for separating ions according to their m/z ratio. This can be achieved in an electric field, a magnetic field or under field-free conditions (and often combinations of mass analyzers are used): The time-of-flight (TOF) is a typical field-free mass analyzer; quadrupole, quadrupole traps (linear and 3D ion traps) and the Fourier transform (FT) orbitrap are electric field mass analyzers; FT ion cyclotron resonance (ICR) is a magnetic field mass analyzer; and sector field instruments, which combine electric and magnetic fields in a mass analyzer are nowadays mainly used as high resolution mass analyzers in combination with ICP [232].

In the case of TOF mass analyzers, ion separation is achieved by acceleration of ions into a field-free drift zone of a given length. Ions with different m/z ratios are accelerated with different kinetic energies resulting in characteristic drift times. The precise measurement of the flight time allows calculating the m/z ratio of the ions. In principle, the mass resolving power improves with increasing length of the field-free region. This concept is exploited in the reflectron TOF, where the ions are reflected by an ion mirror by means of an electric field thereby virtually doubling the distance from acceleration to detection. Additionally, ion reflection reduces the initial energy dispersion from acceleration resulting in a higher resolving power. The wide mass range is the major advantage of TOFs over other mass analyzers as is the relatively constant mass resolving power even at large m/z ratios.

Quadrupole mass analyzers consist of four rods (round,

edged or hyperbolic), which are aligned in parallel pairs to the ion path. Each pair of opposite rods represents one pole and an electric field is created by applying a direct or alternating voltage between the perpendicular rod-pair, which allows passage of ions with certain m/z ratios at a time. When three quadrupoles are combined in series, they form a linear ion trap, also termed 2D ion trap (IT) or linear triple quadrupole (LTQ). In such a 2D IT, the quadrupoles 1 and 3 form a potential barrier for quadrupole 2, which allows accumulation and isolation of selected analytes in the mass spectrum. The 3D IT is a related technology, where a hyperbolic ring electrode is used in combination with a direct voltage and an oscillating radiofrequency to trap and accumulate ions. In order to confine the kinetically excited ions in the 3D trap, helium gas is used as a cooling gas. Generally, a 2D IT shows better ion storage and injection efficiency compared to the 3D IT. ITs show high measurement speed, but display only moderate resolving power and mass accuracy.

The FT orbitrap is also an electric field mass analyzer, where ion packets with identical m/z ratios oscillate around a central electrode. The frequencies of these oscillations can be measured by the current, which is induced by all the ion packets and subsequent Fourier transformation allows the conversion into a mass spectrum similarly to NMR spectroscopy with its FID. FT orbitraps show high mass resolution and accuracy but the high resolution comes at the cost of low measurement speed.

The FT ICR functions similarly but instead of an electric field, a magnetic field stemming from a superconducting magnet is responsible for ion oscillation. The FT ICR shows unsurpassed mass resolving power and accuracy.

Mass spectrometers may contain more than one mass analyzer. Such instruments are termed hybrid mass spectrometers and the most common ones are QqQs, qTOFs, LIT-FT orbitraps and LIT-FT-ICRs.

Ion Detector. Different ion detectors are used to work with the selected mass analyzers: conversion dynodes in combination with electron multipliers are employed in ITs, microchannel plates in TOFs and the measurement of induced currents in FT mass spectrometers. The purpose of conversion dynodes and microchannel plates is to intensify the signal from an analyte with a given m/z ratio in order to obtain a digital signal. On the other hand, the oscillating ion clouds in FT instruments allow the simultaneous measurement of all ions by the induced current, which is then Fourier-transformed into a mass spectrum.

Vacuum system. A mass spectrometer consists of several vacuum stages for reducing ion dispersion and fragmentation due to collisions with residual gas, but also for protecting the ion detectors from moisture and oxidation. In a MALDI-MS, the sample is introduced in the matrix directly in high vacuum, where it is ablated with the laser beam. On the other hand, ESI ionization occurs at atmospheric pressure and introduction of the analyte ions into the MS involves a pressure drop to ~ 1 mbar. The pressure is consecutively reduced when the ions travel deeper into the MS and reach high vacuum when they arrive at the mass analyzer and ion detector. ITs are operated typically at a pressure of $\sim 10^{-6}$ mbar, while high resolution TOF or FT mass spectrometers rather require $\sim 10^{-10}$ mbar. Since the entry into ESI mass spectrometer is always open, the vacuum stages are at an equilibrium state. This setup is also called atmospheric pressure ionization (API) MS. However, this requires enormously efficient pre-vacuum and turbomolecular pumps.

Hyphenation. Depending on the sample complexity, chromatographic or electrophoretic separation techniques may be coupled to the mass spectrometer prior to injection. This is also termed hyphenation and may be carried out on- or offline. For the analysis of metallodrugs in a (pseudo-)biological environment, the most widespread setups are liquid chromatography (HPLC – high performance liquid chromatography or SEC – size exclusion chromatography) and capillary electrophoresis- (CE) coupled online to a mass spectrometer. Additionally, laser ablation (LA) coupled to ICP-MS has attracted the attention of researchers in recent years also with respect to the analysis of the spatial distribution of metallodrugs [233,234], while MALDI tissue imaging has not yet been extensively used for the same purpose [235]. Furthermore, ion mobility spectrometry (IM) can be coupled with mass spectrometry yielding information on ion sizes, which are not available with classical MS setups, *i.e.* analyte cross-sections [236].

Fragmentation Techniques. Quadrupoles are extensively used in hybrid mass spectrometers due to the possibility of gas-phase fragmentation in combination with a high resolution mass analyzer. Fragmentation techniques are widely applied in mass spectrometry yielding structural or conformational data on analytes and are summarized under the term of tandem (MS/MS or MS^2) and multi-stage (MS^n) mass spectrometry. In metallodrug research, fragmentation of metallodrug–biomolecule adducts can be performed to gain insight into the metal binding site on a biomolecular target, *i.e.* on an oligonucleotide or a protein. Several fragmentation techniques have been established in commercially available instruments, including collision-induced dissociation (CID), higher energy C-trap dissociation (HCD), electron capture/transfer dissociation (ECD, ETD), and infrared multiphoton dissociation (IRMPD).

Fragmentation by CID and HCD relies on the collision of an ion with gas-phase atoms such as helium or argon. While a selected precursor ion is fragmented using CID, all ions are simultaneously fragmented using HCD in a similar manner. ECD and ETD rely on electron donation to the analyte ion in the gas phase, prior to fragmentation. Finally, IRMPD uses multiphoton excitation of ions with an infrared light beam. These fragmentation techniques yield characteristic fragment ions with proteins and oligonucleotides.

Collisionally-induced and electron-mediated dissociation

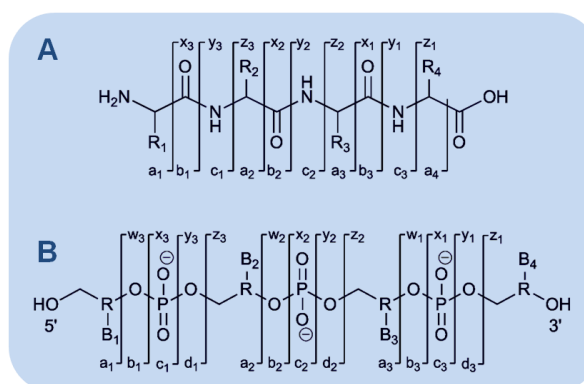


Fig. 19 The fragmentation nomenclature of proteins (A, where R_{1–4} denote an amino acid side chain) and DNA/RNA (B, where R denotes 2-deoxyribose and B_{1–4} the nucleobase). The fragments a–d are obtained with an intact N- or 5'-terminus, while the fragments w–z are obtained with an intact C- or 3'-terminus, respectively. Internal fragments may be formed in both cases.

techniques follow different mechanisms of fragmentation. Therefore, they may yield complementary information and improve specificity and sequence coverage [230]. When analyzing protein samples, CID, HCD and IRMPD give rise to a/x and b/y fragment ions, while ECD and ETD yield mainly c/z ions (Figure 19). When analyzing oligonucleotides, CID and IRMPD usually yield a/w ions accompanied by base loss while ECD generates a/w and d/z ions. ETD is not suitable for fragmenting oligonucleotides since charge reduction is frequently observed without fragmentation.

It must be noted that fragmentation experiments can be used in three different approaches to protein characterization, *i.e.* by bottom-up, middle-down or top-down [237,238]. Bottom-up describes enzymatic digestion of protein samples prior to fragmentation. Top-down involves fragmentation of intact proteins and middle-down employs enzymes that cleave only at sequence specific sites giving protein digests with oligopeptide fragments of ~30 kDa, which are subject to top-down analysis. By means of the bottom-up approach, one can analyze very large proteins, but post-translational modifications (PTMs) are largely lost during the digestion step. In contrast, the PTMs are retained following the top-down approach, which is limited however to proteins <100 kDa. The middle-down approach tries to combine the advantages of both bottom-up and top-down strategies. When investigating the interaction of metallodrugs with proteins, the top-down approach turned out to yield more information on metal binding sites since metallation can be considered a special type of PTM.

2.4.2. Application of Mass Spectrometry in Metallodrug Research

Mass spectrometry evolved into one of the major analytical techniques for studying metal-based anticancer agents in biological relevant settings (Figure 20). In particular, the availability of versatile ion sources, mass analyzers and separation techniques allows the investigation of metallodrugs not only in complex biological systems such as tissues, but intracellular and molecular analyses are also feasible. MS experiments provide crucial insight into pharmacokinetics, -dynamics and toxicological aspects of metallodrug modes-of-action. Since these topics are discussed in detail elsewhere [224], the focus of this section will be centred on providing examples for the wide application range of MS-based

techniques in metallodrug research.

ICP-MS has been widely applied for probing the *in vivo* pharmacokinetics of platinum- [239], but also of ruthenium-based [213] anticancer agents due to its high element specificity (see also section 2.3.6.). The total metal content of whole tissues and/or the blood can be determined, which may provide evidence of serum protein binding, tumour uptake or a preferred route of elimination. The spatial intra-tissue distribution of metallodrugs is probed by LA-ICP-MS [233] and MALDI tissue imaging [235], which are both emerging fields of metallodrug research. For example, LA-ICP-MS allowed to map the platinum distribution of cisplatin in mouse kidneys *in vivo* and to draw conclusions on nephrotoxicity [234]. While the metal was predominately found in the cortex, the Pt-concentration could be drastically reduced by co-administration of cilastatin, a nephroprotective agent. Similarly, MALDI tissue imaging was used to determine the intra-tissue distribution of oxaliplatin in mouse kidneys [240]. In this case, the mass signals of the Pt(chxn)-Met and -Cys adducts, where chxn is 1,2-cyclohexandiamine, were employed to determine the Pt content. However, a limit of detection (LOD) in the low mg/g region seems to hamper somewhat this approach for clinically relevant studies. Furthermore, due to the lack of a robust quantification method both LA-ICP-MS and MALDI imaging yet allow for semi-quantitative analysis only [233,235]. Since Pt-based metallopharmaceuticals seem to target DNA, the direct characterization of Pt-DNA adducts from patient samples is desirable. This was achieved by whole DNA extraction, followed by extensive digestion and subsequent LC-ESI-MS² analysis and allowed to detect as few as 23 intrastrand crosslinked Pt(chxn)-dGdG adducts, where dG is deoxyguanosine, per 10 billion nucleotides [241].

The analysis of the intracellular spatial distribution of metallodrugs is performed mainly *via* three approaches: 1) Subcellular fractionation prior to SEC-ICP-MS [242,243]; 2) non-reducing gel-electrophoresis of protein extracts followed by LA-ICP-MS of the gel bands and bottom-up ESI-MS² of the metal-containing gel band [244]; 3) multidimensional protein identification technology (MudPIT) [245,246]. The former allowed determining the preference of KP1019 for the cytosol of ovarian carcinoma cells while the second allowed characterizing the outer membrane protein A as a possible target for cisplatin in *E. coli* bacteria. MudPIT is a method

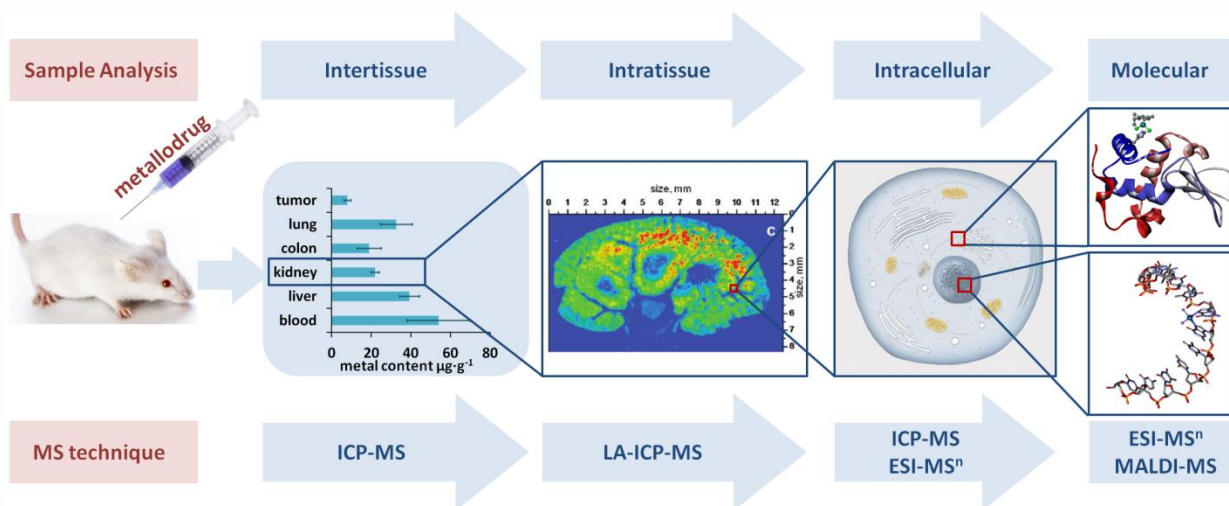


Fig. 20 The application of MS techniques in metallodrug research ranges from the analysis of inter- and intra-tissue distribution (ICP-MS) to molecular characterization (ESI-MS) of metallodrug-biomolecule interactions.

involving reversed-phase and strong cation exchange chromatography prior to ESI-MS² for peptide identification of cell lysates. Using this method, cisplatin was detected on 31 proteins in *E. coli* involving DNA mismatch repair proteins, DNA helicase II, topoisomerase I, thioredoxin I *etc.* [247,248]. In a further study, MudPIT and metallomic studies were combined to orthogonally analyze the effect of RAPTA-T on ovarian cancer cells in combination with subcellular fractionation and SEC-ICP-MS analysis [243]. It was shown that RAPTA-T was mainly found in the particulate fraction, but the down-regulated histone and cytoskeletal proteins indicate also DNA-targeting ability underlying the previously mentioned mode-of-action following multiple pathways.

Furthermore, the analysis of blood, serum and serum proteins upon administration of a metal-based anticancer agent is crucial since the classical metallodrugs were developed for intravenous administration. It was found that the majority of the metallodrug binds to serum proteins such as HSA or Tf [210]. Importantly, extensive serum protein binding was also partly associated with the occurrence of adverse effects during chemotherapy with cisplatin [249]. However, it is believed that the main role of HSA and Tf is to store metallodrugs and act as delivery systems to the tumour in particular for ruthenium metallopharmaceuticals [210]. The most frequently used methods in this respect are SEC- and capillary zone electrophoresis (CZE) ICP-MS [211,212]. Either CZE or a 2D separation involving SEC and ion exchange chromatography (IEC) are required in order to separate HSA and Tf [250] and revealed preferential KP1339 binding to HSA. Tf binding of KP1339 was below the LOD. Interestingly, administration of KP1339 led to an increase of high molecular weight proteins in the serum (>100 kDa) probably due to a HSA-crosslinking effect of the metallodrug. Direct ESI-MSⁿ analysis of single serum proteins or simple protein mixtures is a further approach and may deliver also molecular information on the metallodrug-protein interaction. One of the few studies reported the interaction of the trinuclear Pt^{II} anticancer agents BBR3464 with HSA [251] and indicated pre-associative interactions probably resulting from electrostatic interactions or hydrogen bonding between the metallodrug and the protein. On the other hand, several studies characterized metallodrug binding to Tf by ESI-MS [109,168,252,253]. A bottom-up approach was carried out in order to determine the metal binding site of cisplatin on Tf and the metallodrug seems to metallate mainly threonine-457, which is located in the C-terminal iron-binding site [252].

Classic organic drugs exert their therapeutic effect by electrostatic or non-covalent interactions with a molecular target. In contrast, hydrolyzed metal-based anticancer agents form coordinative bonds with a target. The binding behaviour of aquated metallodrugs is governed by the principle of hard and soft acids and bases (HSAB principle). It states that soft metals such as Pt^{II} or Ru^{II} form stable products with soft biological nucleophiles, for example thiols, thioethers or imines. A coordinative bond is at best kinetically very inert, but in principle allows for ligand substitution. This is a crucial point in the mode of action of metallopharmaceuticals since hydrolysable Pt and Ru metallodrugs seem to coordinatively bind to serum proteins, but must also be able to interact with their final target(s). Consequently, the MS-assisted analysis of metallodrug-biomolecule interactions on a molecular level may help optimizing their properties with respect to pharmacokinetics and -dynamics as well as improving their toxicological profile. The first studies in this direction

involved the investigation of the reactivity of Pt^{II} anticancer agents with DNA models, since DNA is believed to be the crucial target. For example, CE-ESI-MS studies were carried out to test the reactivity of cisplatin towards 5'-dGMP and an *O6,N7*-bidentate binding mode was suggested besides the classical *N7*-binding mode [254]. Furthermore, binding studies with oligonucleotides yielded a deeper insight into the reactivity of anticancer metallodrugs towards DNA models by taking into account the effects of the secondary structure. Cisplatin was exposed to a 13-mer double-stranded oligonucleotide and the mono-adducts were analyzed by a top-down approach using CID and IRMPD on an FT ICR mass spectrometer [255]. The data obtained suggest the formation of intrastrand cross-linked Pt-dGdG and Pt-dGdTdG adducts, where dT is thymidine. Moreover, RAPTA-C and its osmium analogue were reacted with a 14-mer single-stranded oligonucleotide [101]. The former underwent arene cleavage and formed mono-adducts, whereas the latter retained the arene and formed also bis-adducts. The binding of representative Pt^{II}, Ru^{III} and Ru^{II} metallodrugs was investigated towards double-stranded 13-mer and 16-mer oligonucleotides and deoxyguanosine seems to be the major binding partner in all cases [256]. Interestingly, the extents of adduct formation increased in the following order: KP1019 < carboplatin < RAPTA-T < NAMI-A < oxaliplatin < cisplatin.

Besides DNA interactions, the molecular characterization of metallodrugs reacting with proteins is highly relevant, because the adverse effects of platinum chemotherapy were in part associated with extensive serum protein binding [249], but also because many ruthenium metallodrugs do not seem to target primarily DNA. Around 2000, the first studies investigated the interaction of cisplatin and transplatin with ubiquitin (ub) by ESI-MS [257-259]. Ub was selected as a model protein and exhibits ideal characteristics for analysis by ESI-MS, *i.e.* it is a relatively small, non-glycosylated protein with only two potential binding sites corresponding to the *N*-terminal methionine (Met1) and histidine at position 68 (His68). The direct analysis of the reaction mixture revealed ub-Pt(NH₃)₂ as the most abundant adduct while additional adducts correspond to ub-Pt(NH₃)₂Cl and ub-Pt(NH₃)₂OH. Incubating ub with an excess of cisplatin resulted in the formation of up to tris-adducts, which seem to affect the tertiary structure of the protein as revealed by non-denaturing MS experiments. On the other hand, transplatin mainly forms ub-Pt(NH₃)₂Cl adducts with ub [257]. Additionally, the adducts formed between cisplatin and ub reacted with GSH and formed ternary adducts, which eventually resulted in the cleavage of the Pt moiety from the protein because of the *trans*-effect induced by the glutathione-thiol [259]. Ternary adducts were also observed with 5'-dGMP but did not cause Pt cleavage. Oxidation of the thioether of Met1 reduced the extent of platination indicating that it may be a binding partner for cisplatin, while it had no effect on transplatin binding. Moreover, Met1 was characterized as the primary binding site for cisplatin in both a bottom-up [260] and a top-down approach [261], while the top-down experiment additionally yielded the platinated sequence ¹⁹Pro-Ser-Asp-Thr-Ile-Glu²⁴ indicating the Asp23-Thr22 pair as possible binding partners for transplatin. Direct proof of His68 binding could not be obtained in these studies. Also it was found that cisplatin reacts faster with ub than transplatin, while oxaliplatin reacts at a much lower rate compared to the latter [258,261].

These early ESI-MS studies provided information on the nature of adduct formation, the binding sites, competitive

reactions, adduct reversibility and pseudo-kinetics of binding. Many studies then reported a similar approach involving many different model proteins, but also potential protein targets, e.g. calmodulin [262], cytochrome c [263-266], glutathione-S-transferase [267], haemoglobin [268], insulin [269], lysozyme [270], metallothioneins [271,272], myoglobin [258], superoxide dismutase [273] or thioredoxin reductase [274]. Of interest is also the measurement of the conformational change of the protein upon metallation because the protein tertiary structure dictates its function and two recently published strategies seem ideally suited for this purpose. The first involves ion mobility MS [236], which allows the separation of ions in a drift region according to their collisional cross section. In the case of adducts formed from cisplatin and ub, three different conformational states were determined [260]. Secondly, hydrogen-deuterium exchange (HDX) is also suited for determining small conformational changes upon metallation [275]. Although direct correlations between metaldrug-protein interactions and pharmacological effects are hard to establish, small variations in the reactivity of metaldrugs towards proteins or DNA may give valuable insight into their modes-of-action.

2.5. Research Justification

The family of (thio)pyri(id)onato Ru^{II}(arene) anticancer agents show a contrasting activity profile. The thiopyronato compounds are active in the low μM range [136,139,141], while the pyronato analogues show only low activity [140,143]. Therefore, it was aimed within this PhD project to improve the *in vitro* cytotoxicity of the pyronato analogues. Appropriate derivatization of the pyronato ligand was expected to yield metaldrugs with increased aqueous stability and lower reactivity towards biomolecules and a promising ligand precursor was found in 2-(azidomethyl)-5-hydroxy-4H-pyran-4-one (azido kojic acid) [276].

Secondly, the role of *S,N*-donor ligands had not been investigated in the pursuit of novel metal-based anticancer agents. Therefore, *N*-substituted carbothioamides were selected as easily accessible building blocks [277,278] for *S,N*-bidentate Ru^{II}- and Os^{II}(arene) complexes with potential anticancer activity and the aqueous chemistry and biological activity of the resulting organometallics were investigated. Notably, an early study reported *N*-substituted carbothioamides as gastric mucosal protectants, which showed negligible acute toxicities up to >1000 mg/kg [277]. This makes these ligands ideally suited for medical applications as they do not display significant systemic toxicity.

Finally, since conventional Ru^{II}- and Os^{II}(arene) metaldrugs are increasingly recognized not to solely target DNA, but also to interact strongly with proteins [109,155,264], a profound understanding of their molecular interactions is crucial for optimizing future organometallic anticancer agents [279]. ESI-MS serves as an ideal analytical technique for this purpose [264,279] and was employed to characterize the extent, the nature and the location of (non)platinum metaldrug binding on proteins. It was also aimed at relating the reactivity of metaldrugs towards proteins to their antiproliferative activity *in vitro* and to rationalize thereby their anticancer activity.

2.6. References

[1] G.L. Patrick, *An Introduction to Medicinal Chemistry*, Fourth Edition, Oxford University Press, **2009**.

[2] W.E. Stumpf, *Drug Discov. Today*, **2006**, *11*, 550-555.
 [3] B. Alberts, D. Bray, K. Hopkin, A. Johnson, J. Lewis, M. Raff, K. Roberts, P. Walter, *Essential Cell Biology*, Second Edition, Garland Science, Taylor & Francis Group, **2003**.
 [4] R.J. Ellis, *Trends Biochem. Sci.*, **2001**, *26*, 597-604.
 [5] J.G. Lombardino, J.A. Lowe, *Nat. Rev. Drug Discovery*, **2004**, *3*, 853-862.
 [6] International Conference on Harmonisation (ICH), *Quality Guidelines Q3A - Q3D*, ich.org/products/guidelines/, **2012**, 11-09-2012.
 [7] M.D. Rawlins, *Nat. Rev. Drug Discovery*, **2004**, *3*, 360-364.
 [8] K.H. Bleicher, H.J. Bohm, K. Muller, A.I. Alanine, *Nat. Rev. Drug Discovery*, **2003**, *2*, 369-378.
 [9] L.J. Gershell, J.H. Atkins, *Nat. Rev. Drug Discovery*, **2003**, *2*, 321-327.
 [10] T. Kodadek, *Chem. Commun.*, **2011**, *47*, 9757-9763.
 [11] G. Schneider, U. Fechner, *Nat. Rev. Drug Discovery*, **2005**, *4*, 649-663.
 [12] P. Morgan, P.H. Van der Graaf, J. Arrowsmith, D.E. Feltnier, K.S. Drummond, C.D. Wegner, S.D.A. Street, *Drug Discov. Today*, **2012**, *17*, 419-424.
 [13] World Health Organization (WHO), *Cancer Mortality Database*, www-dep.iarc.fr/WHOdb/WHOdb.htm, **2011**, 11-09-2012.
 [14] Statistik Austria, *Sterbefälle*, statistik.at/web_de/statistiken/, **2012**, 11-09-2012.
 [15] World Health Organization (WHO), *Cancer, Fact Sheet N°310*, who.int/mediacentre/factsheets/fs310/en/index.html, **2011**, 11-09-2012.
 [16] S.S. Hecht, F. Kassie, D.K. Hatsukami, *Nat. Rev. Cancer*, **2009**, *9*, 476-488.
 [17] O.M. Sieber, K. Heinimann, I.P.M. Tomlinson, *Nat. Rev. Cancer*, **2003**, *3*, 701-708.
 [18] M.J. Bissell, D. Radisky, *Nat. Rev. Cancer*, **2001**, *1*, 46-54.
 [19] D. Hanahan, R.A. Weinberg, *Cell*, **2011**, *144*, 646-674.
 [20] D. Hanahan, R.A. Weinberg, *Cell*, **2000**, *100*, 57-70.
 [21] W.E. Powers, L.J. Tolmach, *Nature*, **1964**, *201*, 272-273.
 [22] M.H. Barcellos-Hoff, C. Park, E.G. Wright, *Nat. Rev. Cancer*, **2005**, *5*, 867-875.
 [23] S.H.E. Kaufmann, *Nat. Rev. Drug Discovery*, **2008**, *7*, 373-373.
 [24] M.H. Andersen, J.C. Becker, P.T. Straten, *Nat. Rev. Drug Discovery*, **2005**, *4*, 399-409.
 [25] J.M. Reichert, E. Dhimolea, *Drug Discov. Today*, **2012**, *17*, 954-963.
 [26] B.C. Baguley, D.J. Kerr, *Anticancer Drug Development*, Academic Press, **2002**.
 [27] S. Neidle, *Cancer Drug Design and Discovery*, Academic Press, **2008**.
 [28] A.W. Prestayko, J.C. Daoust, B.F. Issell, S.T. Crooke, *Cancer Treat. Rev.*, **1979**, *6*, 17-39.
 [29] L. Fallowfield, *Nat. Rev. Cancer*, **2002**, *2*, 873-879.
 [30] M.A. Jakupec, M. Galanski, V.B. Arion, C.G. Hartinger, B.K. Keppler, *Dalton Trans.*, **2008**, 183-194.
 [31] B.K. Keppler, M. Henn, U.M. Juhl, M.R. Berger, R. Niebl, F.E. Wagner, *Prog. Clin. Biochem. Med.*, **1989**, *10*, 41-69.
 [32] C.G. Hartinger, P.J. Dyson, *Chem. Soc. Rev.*, **2009**, *38*, 391-401.
 [33] W.A. Collier, F. Krauss, *Z. Krebsforsch.*, **1931**, *34*, 526-530.
 [34] B. Rosenberg, L. Vancamp, T. Krigas, *Nature*, **1965**, *205*, 698-699.
 [35] B. Rosenberg, L. Vancamp, J.E. Trosko, V.H. Mansour, *Nature*, **1969**, *222*, 385-386.
 [36] Today, Ru-metalldrugs are often described as the alternative to Pt-based chemotherapeutics, although this is historically incorrect. Since Collier reported their anticancer activity in 1931, Rosenberg claimed the Pt-metalldrugs to be the alternative to Ru. However, Pt-chemotherapeutics are the only marketed metalldrugs and Ru-metallopharmaceuticals are consequently the alternative to Pt only from a clinical point of view.
 [37] J.M. Pascoe, J.J. Roberts, *Biochem. Pharmacol.*, **1974**, *23*, 1345-1357.
 [38] J.R. Durig, J. Danneman, W.D. Behnke, E.E. Mercer, *Chem.-Biol. Interact.*, **1976**, *13*, 287-294.
 [39] M.J. Clarke, H. Taube, *J. Am. Chem. Soc.*, **1974**, *96*, 5413-5419.
 [40] M.J. Clarke, *J. Am. Chem. Soc.*, **1978**, *100*, 5068-5075.
 [41] A.D. Kelman, M.J. Clarke, S.E. Edmonds, H.J. Peresie, *J. Clin. Hematol. Oncol.*, **1977**, *7*, 274-288.
 [42] M.J. Clarke, *Coord. Chem. Rev.*, **2003**, *236*, 209-233.

- [43] M.J. Clarke, S. Bitler, D. Rennert, M. Buchbinder, A.D. Kelman, *J. Inorg. Biochem.*, **1980**, *12*, 79-87.
- [44] M.J. Clarke, *Inorg. Chem.*, **1980**, *19*, 1103-1104.
- [45] World Health Organization (WHO), *Cancer, Fact Sheet N°297*, who.int/mediacentre/factsheets/fs297/en/index.html, **2012**, 09-25-2012.
- [46] B.K. Keppler, W. Rupp, *J. Cancer Res. Clin. Oncol.*, **1986**, *111*, 166-168.
- [47] B.K. Keppler, W. Rupp, U.M. Juhl, H. Endres, R. Niebl, W. Balzer, *Inorg. Chem.*, **1987**, *26*, 4366-4370.
- [48] M.R. Berger, F.T. Garzon, B.K. Keppler, D. Schmahl, *Anticancer Res.*, **1989**, *9*, 761-765.
- [49] O.M.N. Dhuhbhail, W.R. Hagen, B.K. Keppler, K.G. Lipponer, P.J. Sadler, *J. Chem. Soc., Dalton Trans.*, **1994**, 3305-3310.
- [50] J. Chatlas, R. Vaneldik, B.K. Keppler, *Inorg. Chim. Acta*, **1995**, *233*, 59-63.
- [51] C.A. Smith, A.J. SutherlandSmith, B.K. Keppler, F. Kratz, E.N. Baker, *J. Biol. Inorg. Chem.*, **1996**, *1*, 424-431.
- [52] L. Trynda-Lemiesz, B.K. Keppler, H. Kozlowski, *J. Inorg. Biochem.*, **1999**, *73*, 123-128.
- [53] H. Depenbrock, S. Schmelcher, R. Peter, B.K. Keppler, G. Weirich, T. Block, J. Rastetter, A.R. Hanauske, *Eur. J. Cancer*, **1997**, *33*, 2404-2410.
- [54] N. Cetinbas, M.I. Webb, J.A. Dubland, C.J. Walsby, *J. Biol. Inorg. Chem.*, **2010**, *15*, 131-145.
- [55] T. Pieper, B.K. Keppler, *Analisis*, **1998**, *26*, M84-M87.
- [56] S. Kapitzka, M. Pongratz, M.A. Jakupec, P. Heffeter, W. Berger, L. Lackinger, B.K. Keppler, B. Marian, *J. Cancer Res. Clin. Oncol.*, **2005**, *131*, 101-110.
- [57] C.G. Hartinger, M.A. Jakupec, S. Zorbas-Seifried, M. Groessl, A. Egger, W. Berger, H. Zorbas, P.J. Dyson, B.K. Keppler, *Chem. Biodivers.*, **2008**, *5*, 2140-2155.
- [58] M. Pongratz, P. Schluga, M.A. Jakupec, V.B. Arion, C.G. Hartinger, G. Allmaier, B.K. Keppler, *J. Anal. At. Spectrom.*, **2004**, *19*, 46-51.
- [59] U.S. National Institutes of Health, *Dose Escalation Study of NKP-1339 to Treat Advanced Solid Tumors*, clinicaltrials.gov, **2012**, 2012-10-01.
- [60] N.R. Dickson, S.F. Jones, H.A. Burris, R.K. Ramanathan, G.J. Weiss, J.R. Infante, J.C. Bendell, W. McCulloch, D.D. Von Hoff, *J. Clin. Oncol.*, **2011**, *29*, suppl; abstr 2607.
- [61] D.S. Thompson, G.J. Weiss, S.F. Jones, H.A. Burris, R.K. Ramanathan, J.R. Infante, J.C. Bendell, A. Ogden, D.D. Von Hoff, *J. Clin. Oncol.*, **2012**, *30*, suppl; abstr 3033.
- [62] C. Monti-Bragadin, L. Ramani, L. Samer, G. Mestroni, G. Zassinovich, *Antimicrob. Agents Chemother.*, **1975**, *7*, 825-827.
- [63] E. Alessio, G. Mestroni, G. Nardin, W.M. Attia, M. Calligaris, G. Sava, S. Zorzat, *Inorg. Chem.*, **1988**, *27*, 4099-4106.
- [64] G. Sava, S. Pacor, S. Zorzat, E. Alessio, G. Mestroni, *Pharmacol. Res.*, **1989**, *21*, 617-628.
- [65] E. Alessio, G. Balducci, M. Calligaris, G. Costa, W.M. Attia, G. Mestroni, *Inorg. Chem.*, **1991**, *30*, 609-618.
- [66] G. Sava, S. Pacor, G. Mestroni, E. Alessio, *Anti-Cancer Drug.*, **1992**, *3*, 25-31.
- [67] G. Sava, S. Pacor, M. Coluccia, M. Mariggio, M. Cocchietto, E. Alessio, G. Mestroni, *Drug Investig.*, **1994**, *8*, 150-161.
- [68] G. Mestroni, E. Alessio, G. Sava, S. Pacor, M. Coluccia, A. Boccarelli, *Met. Based Drugs*, **1994**, *1*, 41-63.
- [69] G. Sava, R. Gagliardi, M. Cocchietto, K. Clerici, I. Capozzi, M. Marrella, E. Alessio, G. Mestroni, R. Milanino, *Pathol. Oncol. Res.*, **1998**, *4*, 30-36.
- [70] J.M. Rademaker-Lakhai, D. van den Bongard, D. Pluim, J.H. Beijnen, J.H. Schellens, *Clin. Cancer Res.*, **2004**, *10*, 3717-3727.
- [71] A. Bergamo, C. Gaidon, J.H.M. Schellens, J.H. Beijnen, G. Sava, *J. Inorg. Biochem.*, **2012**, *106*, 90-99.
- [72] Y.N.V. Gopal, D. Jayaraju, A.K. Kondapi, *Biochemistry*, **1999**, *38*, 4382-4388.
- [73] A.H. Velders, H. Kooijman, A.L. Spek, J.G. Haasnoot, D. de Vos, J. Reedijk, *Inorg. Chem.*, **2000**, *39*, 2966-2967.
- [74] A.C.G. Hotze, A.H. Velders, F. Ugozzoli, M. Biagini-Cingi, A.M. Manotti-Lanfredi, J.G. Haasnoot, J. Reedijk, *Inorg. Chem.*, **2000**, *39*, 3838-3844.
- [75] Y.K. Yan, M. Melchart, A. Habtemariam, P.J. Sadler, *Chem. Commun.*, **2005**, 4764-4776.
- [76] C.S. Allardyce, P.J. Dyson, *Platinum Met. Rev.*, **2001**, *45*, 62-69.
- [77] C.S. Allardyce, P.J. Dyson, D.J. Ellis, S.L. Heath, *Chem. Commun.*, **2001**, 1396-1397.
- [78] R.E. Morris, R.E. Aird, P.D. Murdoch, H.M. Chen, J. Cummings, N.D. Hughes, S. Parsons, A. Parkin, G. Boyd, D.I. Jodrell, P.J. Sadler, *J. Med. Chem.*, **2001**, *44*, 3616-3621.
- [79] C. Scolaro, A. Bergamo, L. Brescacin, R. Delfino, M. Cocchietto, G. Laurenczy, T.J. Geldbach, G. Sava, P.J. Dyson, *J. Med. Chem.*, **2005**, *48*, 4161-4171.
- [80] W.H. Ang, E. Daldini, C. Scolaro, R. Scopelliti, L. Juillerat-Jeannerat, P.J. Dyson, *Inorg. Chem.*, **2006**, *45*, 9006-9013.
- [81] S. Chatterjee, S. Kundu, A. Bhattacharyya, C.G. Hartinger, P.J. Dyson, *J. Biol. Inorg. Chem.*, **2008**, *13*, 1149-1155.
- [82] M. Ozaslan, I.D. Karagoz, I.H. Kilic, M.E. Guldur, *Afr. J. Biotechnol.*, **2011**, *10*, 2375-2378.
- [83] A. Bergamo, A. Masi, P.J. Dyson, G. Sava, *Int. J. Oncol.*, **2008**, *33*, 1281-1289.
- [84] P. Nowak-Sliwinska, J.R. van Beijnum, A. Casini, A.A. Nazarov, G. Wagnieres, H. van den Bergh, P.J. Dyson, A.W. Griffioen, *J. Med. Chem.*, **2011**, *54*, 3895-3902.
- [85] B. Wu, M.S. Ong, M. Groessl, Z. Adhikreksan, C.G. Hartinger, P.J. Dyson, C.A. Davey, *Chem. Eur. J.*, **2011**, *17*, 3562-3566.
- [86] B. Wu, P. Droge, C.A. Davey, *Nat. Chem. Biol.*, **2008**, *4*, 110-112.
- [87] W.H. Ang, A. Casini, G. Sava, P.J. Dyson, *J. Organomet. Chem.*, **2011**, *696*, 989-998.
- [88] R.E. Aird, J. Cummings, R. Morris, A.A. Ritchie, P.J. Sadler, D.I. Jodrell, *Br. J. Cancer*, **2001**, *85*, 101.
- [89] J. Cummings, R.E. Aird, R. Morris, H. Chen, P.D. Murdoch, P.J. Sadler, J.F. Smyth, D.I. Jodrell, *Clin. Cancer Res.*, **2000**, *6*, 4494s.
- [90] R.E. Aird, J. Cummings, A.A. Ritchie, M. Muir, R.E. Morris, H. Chen, P.J. Sadler, D.I. Jodrell, *Br. J. Cancer*, **2002**, *86*, 1652-1657.
- [91] S.M. Guichard, R. Else, E. Reid, B. Zeitlin, R. Aird, M. Muir, M. Dodds, H. Fiebig, P.J. Sadler, D.I. Jodrell, *Biochem. Pharmacol.*, **2006**, *71*, 408-415.
- [92] A. Bergamo, A. Masi, A.F.A. Peacock, A. Habtemariam, P.J. Sadler, G. Sava, *J. Inorg. Biochem.*, **2010**, *104*, 79-86.
- [93] H.M. Chen, J.A. Parkinson, S. Parsons, R.A. Coxall, R.O. Gould, P.J. Sadler, *J. Am. Chem. Soc.*, **2002**, *124*, 3064-3082.
- [94] H.M. Chen, J.A. Parkinson, R.E. Morris, P.J. Sadler, *J. Am. Chem. Soc.*, **2003**, *125*, 173-186.
- [95] A.M. Pizarro, A. Habtemariam, P.J. Sadler, in: G. Jaouen, N. Metzler-Nolte (Eds.), *Medicinal Organometallic Chemistry, Topics in Organometallic Chemistry 32*, Springer, *Heidelberg*, **2010**, 21-56.
- [96] F. Wang, H.M. Chen, S. Parsons, L.D.H. Oswald, J.E. Davidson, P.J. Sadler, *Chem. Eur. J.*, **2003**, *9*, 5810-5820.
- [97] F.Y. Wang, H.M. Chen, J.A. Parkinson, P.D. Murdoch, P.J. Sadler, *Inorg. Chem.*, **2002**, *41*, 4509-4523.
- [98] F.Y. Wang, J. Bella, J.A. Parkinson, P.J. Sadler, *J. Biol. Inorg. Chem.*, **2005**, *10*, 147-155.
- [99] F.Y. Wang, J.J. Xu, A. Habtemariam, J. Bella, P.J. Sadler, *J. Am. Chem. Soc.*, **2005**, *127*, 17734-17743.
- [100] S.H. van Rijt, A.F.A. Peacock, P.J. Sadler, in: A. Bonetti, R. Leone, F.M. Muggia, S.B. Howell (Eds.), *Platinum and Other Heavy Metal Compounds in Cancer Chemotherapy - Molecular Mechanisms and Clinical Applications*, Cancer Drug Discovery and Development, Humana Press, *New York*, **2009**, 73-79.
- [101] A. Dorcier, P.J. Dyson, C. Gossens, U. Rothlisberger, R. Scopelliti, I. Tavernelli, *Organometallics*, **2005**, *24*, 2114-2123.
- [102] A. Dorcier, W.H. Ang, S. Bolano, L. Gonsalvi, L. Juillerat-Jeannerat, G. Laurenczy, M. Peruzzini, A.D. Phillips, F. Zanobini, P.J. Dyson, *Organometallics*, **2006**, *25*, 4090-4096.
- [103] A.F.A. Peacock, A. Habtemariam, R. Fernandez, V. Walland, F.P.A. Fabbiani, S. Parsons, R.E. Aird, D.I. Jodrell, P.J. Sadler, *J. Am. Chem. Soc.*, **2006**, *128*, 1739-1748.
- [104] A.F.A. Peacock, A. Habtemariam, S.A. Moggach, A. Prescimone, S. Parsons, P.J. Sadler, *Inorg. Chem.*, **2007**, *46*, 4049-4059.
- [105] B. Cebrian-Losantos, A.A. Krokhin, I.N. Stepanenko, R. Eichinger, M.A. Jakupec, V.B. Arion, B.K. Keppler, *Inorg. Chem.*, **2007**, *46*, 5023-5033.
- [106] G.E. Buchel, I.N. Stepanenko, M. Hejl, M.A. Jakupec, B.K. Keppler, V.B. Arion, *Inorg. Chem.*, **2011**, *50*, 7690-7697.
- [107] Y. Hung, W.J. Kung, H. Taube, *Inorg. Chem.*, **1981**, *20*, 457-463.
- [108] M. Steblerothlisberger, W. Hummel, P.A. Pittet, H.B. Burgi, A. Ludi, A.E. Merbach, *Inorg. Chem.*, **1988**, *27*, 1358-1363.
- [109] M. Groessl, E. Reisner, C.G. Hartinger, R. Eichinger, O. Semenova, A.R. Timerbaev, M.A. Jakupec, V.B. Arion, B.K. Keppler, *J. Med. Chem.*, **2007**, *50*, 2185-2193.

- [110] H. Kostrhunova, J. Florian, O. Novakova, A.F.A. Peacock, P.J. Sadler, V. Brabec, *J. Med. Chem.*, **2008**, *51*, 3635-3643.
- [111] S.H. van Rijt, A.J. Hebden, T. Amaresekera, R.J. Deeth, G.J. Clarkson, S. Parsons, P.C. McGowan, P.J. Sadler, *J. Med. Chem.*, **2009**, *52*, 7753-7764.
- [112] P.J. Dyson, G. Sava, *Dalton Trans.*, **2006**, 1929-1933.
- [113] S.J. Dougan, P.J. Sadler, *Chimia*, **2007**, *61*, 704-715.
- [114] A.M. Pizarro, P.J. Sadler, *Biochimie*, **2009**, *91*, 1198-1211.
- [115] G. Gasser, I. Ott, N. Metzler-Nolte, *J. Med. Chem.*, **2011**, *54*, 3-25.
- [116] G. Suss-Fink, *Dalton Trans.*, **2010**, *39*, 1673-1688.
- [117] G.S. Smith, B. Therrien, *Dalton Trans.*, **2011**, *40*, 10793-10800.
- [118] C.G. Hartinger, N. Metzler-Nolte, P.J. Dyson, *Organometallics*, **2012**, *31*, 5677-5685.
- [119] T. Gianferrara, I. Bratsos, E. Alessio, *Dalton Trans.*, **2009**, 7588-7598.
- [120] S.D. Shnyder, Y. Fu, A. Habtemariam, S.H. van Rijt, P.A. Cooper, P.M. Loadman, P.J. Sadler, *MedChemComm*, **2011**, *2*, 666-668.
- [121] Y. Fu, A. Habtemariam, A.M. Pizarro, S.H. van Rijt, D.J. Healey, P.A. Cooper, S.D. Shnyder, G.J. Clarkson, P.J. Sadler, *J. Med. Chem.*, **2010**, *53*, 8192-8196.
- [122] X. Meng, M.L. Leyva, M. Jenny, I. Gross, S. Benosman, B. Fricker, S. Harlepp, P. Hebraud, A. Boos, P. Wlosik, P. Bischoff, C. Sirlin, M. Pfeffer, J.P. Loeffler, C. Gaiddon, *Cancer Res.*, **2009**, *69*, 5458-5466.
- [123] L.K. Filak, S. Göschl, P. Heffeter, K. Ghannadzadeh Samper, A.E. Egger, M.A. Jakupec, B.K. Keppler, W. Berger, V.B. Arion, *Organometallics*, **2013**, *32*, 903-914.
- [124] M. Pernet, T. Bastogne, N.P.E. Barry, B. Therrien, G. Koellensperger, S. Hann, V. Reshetov, M. Barberi-Heyob, *J. Photochem. Photobiol. B*, **2012**, *117*, 80-89.
- [125] A search in the SciFinder® database on "ruthenium anticancer agents", "ruthenium drug" and "ruthenium arene" yields 628, 694 and 1178 references, respectively, while "osmium anticancer agent" yields 66 references., 2012-10-04.
- [126] A. Habtemariam, M. Melchart, R. Fernandez, S. Parsons, I.D.H. Oswald, A. Parkin, F.P.A. Fabbiani, J.E. Davidson, A. Dawson, R.E. Aird, D.I. Jodrell, P.J. Sadler, *J. Med. Chem.*, **2006**, *49*, 6858-6868.
- [127] A.F.A. Peacock, S. Parsons, P.J. Sadler, *J. Am. Chem. Soc.*, **2007**, *129*, 3348-3357.
- [128] S.H. van Rijt, A.F.A. Peacock, R.D.L. Johnstone, S. Parsons, P.J. Sadler, *Inorg. Chem.*, **2009**, *48*, 1753-1762.
- [129] S.H. van Rijt, A. Mukherjee, A.M. Pizarro, P.J. Sadler, *J. Med. Chem.*, **2010**, *53*, 840-849.
- [130] S.J. Dougan, M. Melchart, A. Habtemariam, S. Parsons, P.J. Sadler, *Inorg. Chem.*, **2006**, *45*, 10882-10894.
- [131] S.J. Dougan, A. Habtemariam, S.E. McHale, S. Parsons, P.J. Sadler, *Proc. Natl. Acad. Sci.*, **2008**, *105*, 11628-11633.
- [132] Y. Fu, A. Habtemariam, A.M.B.H. Basri, D. Braddick, G.J. Clarkson, P.J. Sadler, *Dalton Trans.*, **2011**, *40*, 10553-10562.
- [133] Y. Fu, M.J. Romero, A. Habtemariam, M.E. Snowden, L.J. Song, G.J. Clarkson, B. Qamar, A.M. Pizarro, P.R. Unwin, P.J. Sadler, *Chem. Sci.*, **2012**, *3*, 2485-2494.
- [134] R. Fernandez, M. Melchart, A. Habtemariam, S. Parsons, P.J. Sadler, *Chem. Eur. J.*, **2004**, *10*, 5173-5179.
- [135] M.A. Santos, S.M. Marques, S. Chaves, *Coord. Chem. Rev.*, **2012**, *256*, 240-259.
- [136] W. Kandioller, A. Kurzwernhart, M. Hanif, S.M. Meier, H. Henke, B.K. Keppler, C.G. Hartinger, *J. Organomet. Chem.*, **2011**, *696*, 999-1010.
- [137] M. Rouffet, S.M. Cohen, *Dalton Trans.*, **2011**, *40*, 3445-3454.
- [138] A.F. Peacock, M. Melchart, R.J. Deeth, A. Habtemariam, S. Parsons, P.J. Sadler, *Chem. Eur. J.*, **2007**, *13*, 2601-2613.
- [139] W. Kandioller, C.G. Hartinger, A.A. Nazarov, C. Bartel, M. Skocic, M.A. Jakupec, V.B. Arion, B.K. Keppler, *Chem. Eur. J.*, **2009**, *15*, 12283-12291.
- [140] W. Kandioller, C.G. Hartinger, A.A. Nazarov, J.H. Kasser, R.O. John, M. Jakupec, V. Arion, P.J. Dyson, B.K. Keppler, *J. Organomet. Chem.*, **2009**, *694*, 922-929.
- [141] W. Kandioller, C.G. Hartinger, A.A. Nazarov, M.L. Kuznetsov, R.O. John, C. Bartel, M.A. Jakupec, V.B. Arion, B.K. Keppler, *Organometallics*, **2009**, *28*, 4249-4251.
- [142] M. Hanif, P. Schaaf, W. Kandioller, M. Hejl, M.A. Jakupec, A. Roller, B.K. Keppler, C.G. Hartinger, *Aust. J. Chem.*, **2010**, *63*, 1521-1528.
- [143] J.H. Kasser, W. Kandioller, C.G. Hartinger, A.A. Nazarov, V.B. Arion, P.J. Dyson, B.K. Keppler, *J. Organomet. Chem.*, **2010**, *695*, 875-881.
- [144] V. Brabec, J. Kasparkova, O. Vrana, O. Novakova, J.W. Cox, Y. Qu, N. Farrell, *Biochemistry*, **1999**, *38*, 6781-6790.
- [145] C. Manzotti, G. Pratesi, E. Menta, R. Di Domenico, E. Cavalletti, H.H. Fiebig, L.R. Kelland, N. Farrell, D. Polizzi, R. Supino, G. Pezzoni, F. Zunino, *Clin. Cancer Res.*, **2000**, *6*, 2626-2634.
- [146] D.I. Jodrell, T.R.J. Evans, W. Steward, D. Cameron, J. Prendiville, C. Aschele, C. Noberasco, M. Lind, J. Carmichael, N. Dobbs, G. Camboni, B. Gatti, F. De Braud, *Eur. J. Cancer*, **2004**, *40*, 1872-1877.
- [147] T.A. Hensing, N.H. Hanna, H.H. Gillenwater, M.G. Camboni, C. Allievi, M.A. Socinski, *Anti-Cancer Drug.*, **2006**, *17*, 697-704.
- [148] H. Piotrowski, G. Hilt, A. Schulz, P. Mayer, K. Polborn, K. Severin, *Chem. Eur. J.*, **2001**, *7*, 3196-3208.
- [149] H. Piotrowski, K. Polborn, G. Hilt, K. Severin, *J. Am. Chem. Soc.*, **2001**, *123*, 2699-2700.
- [150] M.G. Mendoza-Ferri, C.G. Hartinger, R.E. Eichinger, N. Stolyarova, K. Severin, M.A. Jakupec, A.A. Nazarov, B.K. Keppler, *Organometallics*, **2008**, *27*, 2405-2407.
- [151] M.G. Mendoza-Ferri, C.G. Hartinger, A.A. Nazarov, W. Kandioller, K. Severin, B.K. Keppler, *Appl. Organomet. Chem.*, **2008**, *22*, 326-332.
- [152] M.G. Mendoza-Ferri, C.G. Hartinger, M.A. Mendoza, M. Groessl, A.E. Egger, R.E. Eichinger, J.B. Mangrum, N.P. Farrell, M. Maruszak, P.J. Bednarski, F. Klein, M.A. Jakupec, A.A. Nazarov, K. Severin, B.K. Keppler, *J. Med. Chem.*, **2009**, *52*, 916-925.
- [153] M.G. Mendoza-Ferri, C.G. Hartinger, A.A. Nazarov, R.E. Eichinger, M.A. Jakupec, K. Severin, B.K. Keppler, *Organometallics*, **2009**, *28*, 6260-6265.
- [154] O. Novakova, A.A. Nazarov, C.G. Hartinger, B.K. Keppler, V. Brabec, *Biochem. Pharmacol.*, **2009**, *77*, 364-374.
- [155] M. Hanif, H. Henke, S.M. Meier, S. Martic, M. Labib, W. Kandioller, M.A. Jakupec, V.B. Arion, H.B. Kraatz, B.K. Keppler, C.G. Hartinger, *Inorg. Chem.*, **2010**, *49*, 7953-7963.
- [156] D.S. Williams, G.E. Atilla, H. Bregman, A. Arzoumanian, P.S. Klein, E. Meggers, *Angew. Chem., Int. Ed. Engl.*, **2005**, *44*, 1984-1987.
- [157] H. Bregman, P.J. Carroll, E. Meggers, *J. Am. Chem. Soc.*, **2006**, *128*, 877-884.
- [158] R. Anand, J. Maksimoska, N. Pagano, E.Y. Wong, P.A. Gimotty, S.L. Diamond, E. Meggers, R. Marmorstein, *J. Med. Chem.*, **2009**, *52*, 1602-1611.
- [159] W.H. Ang, L.J. Parker, A. De Luca, L. Juillerat-Jeanneret, C.J. Morton, M. Lo Bello, M.W. Parker, P.J. Dyson, *Angew. Chem., Int. Ed. Engl.*, **2009**, *48*, 3854-3857.
- [160] D.W. Zaharevitz, R. Gussio, M. Leost, A.M. Senderowicz, T. Lahusen, C. Kunick, L. Meijer, E.A. Sausville, *Cancer Res.*, **1999**, *59*, 2566-2569.
- [161] W.F. Schmid, S. Zorbas-Seifried, R.O. John, V.B. Arion, M.A. Jakupec, A. Roller, M. Galanski, I. Chiorescu, H. Zorbas, B.K. Keppler, *Inorg. Chem.*, **2007**, *46*, 3645-3656.
- [162] W.F. Schmid, R.O. John, G. Muhlgassner, P. Heffeter, M.A. Jakupec, M. Galanski, W. Berger, V.B. Arion, B.K. Keppler, *J. Med. Chem.*, **2007**, *50*, 6343-6355.
- [163] W.F. Schmid, R.O. John, V.B. Arion, M.A. Jakupec, B.K. Keppler, *Organometallics*, **2007**, *26*, 6643-6652.
- [164] V.B. Arion, A. Dobrov, S. Goschl, M.A. Jakupec, B.K. Keppler, P. Rapta, *Chem. Commun.*, **2012**, *48*, 8559-8561.
- [165] L.K. Filak, G. Muhlgassner, M.A. Jakupec, P. Heffeter, W. Berger, V.B. Arion, B.K. Keppler, *J. Biol. Inorg. Chem.*, **2010**, *15*, 903-918.
- [166] L.K. Filak, G. Muhlgassner, F. Bacher, A. Roller, M. Galanski, M.A. Jakupec, B.K. Keppler, V.B. Arion, *Organometallics*, **2011**, *30*, 273-283.
- [167] G. Muhlgassner, C. Bartel, W.F. Schmid, M.A. Jakupec, V.B. Arion, B.K. Keppler, *J. Inorg. Biochem.*, **2012**, *116*, 180-187.
- [168] I. Berger, M. Hanif, A.A. Nazarov, C.G. Hartinger, R.O. John, M.L. Kuznetsov, M. Groessl, F. Schmitt, O. Zava, F. Biba, V.B. Arion, M. Galanski, M.A. Jakupec, L. Juillerat-Jeanneret, P.J. Dyson, B.K. Keppler, *Chem. Eur. J.*, **2008**, *14*, 9046-9057.
- [169] R.A. Gatenby, R.J. Gillies, *Nat. Rev. Cancer*, **2004**, *4*, 891-899.
- [170] M. Hanif, A.A. Nazarov, C.G. Hartinger, W. Kandioller, M.A. Jakupec, V.B. Arion, P.J. Dyson, B.K. Keppler, *Dalton Trans.*, **2010**, *39*, 7345-7352.

- [171] M. Hanif, S.M. Meier, W. Kandioller, A. Bytzeck, M. Hejl, C.G. Hartinger, A.A. Nazarov, V.B. Arion, M.A. Jakupec, P.J. Dyson, B.K. Keppler, *J. Inorg. Biochem.*, **2011**, *105*, 224-231.
- [172] M. Hanif, A.A. Nazarov, C.G. Hartinger, *Inorg. Chim. Acta*, **2012**, *380*, 211-215.
- [173] R. Hoessel, S. Leclerc, J.A. Endicott, M.E.M. Nobel, A. Lawrie, P. Tunnah, M. Leost, E. Damiens, D. Marie, D. Marko, E. Niederberger, W.C. Tang, G. Eisenbrand, L. Meijer, *Nat. Cell Biol.*, **1999**, *1*, 60-67.
- [174] W. Ginzinger, G. Muhlgassner, V.B. Arion, M.A. Jakupec, A. Roller, M. Galanski, M. Reithofer, W. Berger, B.K. Keppler, *J. Med. Chem.*, **2012**, *55*, 3398-3413.
- [175] R.J. Nijveldt, E. van Nood, D.E.C. van Hoorn, P.G. Boelens, K. van Norren, P.A.M. van Leeuwen, *Am. J. Clin. Nutr.*, **2001**, *74*, 418-425.
- [176] A. Kurzwernhart, W. Kandioller, C. Bartel, S. Bachler, R. Trondl, G. Muhlgassner, M.A. Jakupec, V.B. Arion, D. Marko, B.K. Keppler, C.G. Hartinger, *Chem. Commun.*, **2012**, *48*, 4839-4841.
- [177] A. Kurzwernhart, W. Kandioller, S. Bachler, C. Bartel, S. Martic, M. Buczkowska, G. Muhlgassner, M.A. Jakupec, H.B. Kraatz, P.J. Bednarski, V.B. Arion, D. Marko, B.K. Keppler, C.G. Hartinger, *J. Med. Chem.*, **2012**, *55*, 10512-10522.
- [178] A. Kurzwernhart, W. Kandioller, E.A. Enyedy, M. Novak, M.A. Jakupec, B.K. Keppler, C.G. Hartinger, *Dalton Trans.*, **2012**.
- [179] D.E. Dolmans, D. Fukumura, R.K. Jain, *Nat. Rev. Cancer*, **2003**, *3*, 380-387.
- [180] K. Szacilowski, W. Macyk, A. Drzewiecka-Matuszek, M. Brindell, G. Stochel, *Chem. Rev.*, **2005**, *105*, 2647-2694.
- [181] M. Brindell, E. Kulis, S.K.C. Elmroth, K. Urbanska, G. Stochel, *J. Med. Chem.*, **2005**, *48*, 7298-7304.
- [182] S.W. Magennis, A. Habtemariam, O. Novakova, J.B. Henry, S. Meier, S. Parsons, I.D.H. Oswald, V. Brabec, P.J. Sadler, *Inorg. Chem.*, **2007**, *46*, 5059-5068.
- [183] S. Betanzos-Lara, L. Salassa, A. Habtemariam, P.J. Sadler, *Chem. Commun.*, **2009**, 6622-6624.
- [184] S. Betanzos-Lara, L. Salassa, A. Habtemariam, O. Novakova, A.M. Pizarro, G.J. Clarkson, B. Liskova, V. Brabec, P.J. Sadler, *Organometallics*, **2012**, *31*, 3466-3479.
- [185] T. Gianferrara, A. Bergamo, I. Bratsos, B. Milani, C. Spagnul, G. Sava, E. Alessio, *J. Med. Chem.*, **2010**, *53*, 4678-4690.
- [186] T. Gianferrara, I. Bratsos, E. Iengo, B. Milani, A. Ostric, C. Spagnul, E. Zangrando, E. Alessio, *Dalton Trans.*, **2009**, 10742-10756.
- [187] F. Schmitt, J. Freudenreich, N.P. Barry, L. Juillerat-Jeanneret, G. Suss-Fink, B. Therrien, *J. Am. Chem. Soc.*, **2012**, *134*, 754-757.
- [188] N. Metzler-Nolte, *Angew. Chem., Int. Ed. Engl.*, **2001**, *40*, 1040-1043.
- [189] N. Metzler-Nolte, in: G. Jaouen, N. Metzler-Nolte (Eds.), *Medicinal Organometallic Chemistry*, Topics in Organometallic Chemistry 32, Springer, Heidelberg, **2010**, 195-217.
- [190] E. Garcia-Garayoa, R. Schibli, P.A. Schubiger, *Nucl. Sci. Tech.*, **2007**, *18*, 88-100.
- [191] H. Struthers, B. Spingler, T.L. Mindt, R. Schibli, *Chem. Eur. J.*, **2008**, *14*, 6173-6183.
- [192] J. Lemke, N. Metzler-Nolte, *Eur. J. Inorg. Chem.*, **2008**, 3359-3366.
- [193] J. Lemke, N. Metzler-Nolte, *J. Organomet. Chem.*, **2011**, *696*, 1018-1022.
- [194] S.H. van Rijt, H. Kostrhunova, V. Brabec, P.J. Sadler, *Bioconjug. Chem.*, **2011**, *22*, 218-226.
- [195] F. Barragan, P. Lopez-Senin, L. Salassa, S. Betanzos-Lara, A. Habtemariam, V. Moreno, P.J. Sadler, V. Marchan, *J. Am. Chem. Soc.*, **2011**, *133*, 14098-14108.
- [196] F. Barragan, D. Carrion-Salip, I. Gomez-Pinto, A. Gonzalez-Canto, P.J. Sadler, R. de Llorens, V. Moreno, C. Gonzalez, A. Massaguer, V. Marchan, *Bioconjug. Chem.*, **2012**, *23*, 1838-1855.
- [197] W.H. Ang, E. Daldini, L. Juillerat-Jeanneret, P.J. Dyson, *Inorg. Chem.*, **2007**, *46*, 9048-9050.
- [198] M. Hanif, A.A. Nazarov, A. Legin, M. Groessl, V.B. Arion, M.A. Jakupec, Y.O. Tsybin, P.J. Dyson, B.K. Keppler, C.G. Hartinger, *Chem. Commun.*, **2012**, *48*, 1475-1477.
- [199] Council of Europe Treaty Office, *European Convention for the Protection of Vertebrate Animals used for Experimental and Other Scientific Purposes*, *European Treaty Series (ETS) No. 123*, **1991**, Strasbourg.
- [200] Parliament of the Republic of Austria, *Bundesgesetz vom 27. September 1989 über Versuche an lebenden Tieren (Tierversuchsgesetz - TVG)*, **1989**, Wien.
- [201] T. Mosmann, *J. Immunol. Methods*, **1983**, *65*, 55-63.
- [202] M.J. McKeage, S.J. Berners-Price, P. Galetti, R.J. Bowen, W. Brouwer, L. Ding, L. Zhuang, B.C. Baguley, *Cancer Chemother. Pharmacol.*, **2000**, *46*, 343-350.
- [203] L. Di, P.V. Fish, T. Mano, *Drug Discov. Today*, **2012**, *17*, 486-495.
- [204] A.L. Noffke, A. Habtemariam, A.M. Pizarro, P.J. Sadler, *Chem. Commun.*, **2012**, *48*, 5219-5246.
- [205] B. Serli, E. Zangrando, T. Gianferrara, C. Sclaro, P.J. Dyson, A. Bergamo, E. Alessio, *Eur. J. Inorg. Chem.*, **2005**, 3423-3434.
- [206] D.N. Akbayeva, L. Gonsalvi, W. Oberhauser, M. Peruzzini, F. Vizza, P. Bruggeller, A. Romerosa, G. Sava, A. Bergamo, *Chem. Commun.*, **2003**, 264-265.
- [207] W. Weber, P.C. Ford, *Inorg. Chem.*, **1986**, *25*, 1088-1092.
- [208] S. Betanzos-Lara, O. Novakova, R.J. Deeth, A.M. Pizarro, G.J. Clarkson, B. Liskova, V. Brabec, P.J. Sadler, A. Habtemariam, *J. Biol. Inorg. Chem.*, **2012**, *17*, 1033-1051.
- [209] F. Lentz, A. Drescher, A. Lindauer, M. Henke, R.A. Hilger, C.G. Hartinger, M.E. Scheulen, C. Dittich, B.K. Keppler, U. Jaehde, *Anti-Cancer Drug.*, **2009**, *20*, 97-103.
- [210] A.R. Timerbaev, C.G. Hartinger, S.S. Aleksenko, B.K. Keppler, *Chem. Rev.*, **2006**, *106*, 2224-2248.
- [211] A.K. Bytzeck, K. Boeck, G. Hermann, S. Hann, B.K. Keppler, C.G. Hartinger, G. Koellensperger, *Metallomics*, **2011**, *3*, 1049-1055.
- [212] M. Groessl, C.G. Hartinger, K. Polec-Pawlak, M. Jarosz, B.K. Keppler, *Electrophoresis*, **2008**, *29*, 2224-2232.
- [213] A. Bytzeck, *Dissertation*, Institute of Inorganic Chemistry, University of Vienna, **2011**.
- [214] M. Cocchietto, G. Sava, *Pharmacol. Toxicol.*, **2000**, *87*, 193-197.
- [215] G. Sava, S. Zorzet, C. Turrin, F. Vita, M. Soranzo, G. Zabucchi, M. Cocchietto, A. Bergamo, S. DiGiovine, G. Pezzoni, L. Sartor, S. Garbisa, *Clin. Cancer Res.*, **2003**, *9*, 1898-1905.
- [216] S. Zorzet, A. Sorc, C. Casarsa, M. Cocchietto, G. Sava, *Met. Based Drugs*, **2001**, *8*, 1-7.
- [217] P. Leeson, *Nature*, **2012**, *481*, 455-456.
- [218] P.D. Leeson, B. Springthorpe, *Nat. Rev. Drug Discovery*, **2007**, *6*, 881-890.
- [219] C.A. Lipinski, F. Lombardo, B.W. Dominy, P.J. Feeney, *Adv. Drug Delivery Rev.*, **1997**, *23*, 3-25.
- [220] G.R. Bickerton, G.V. Paolini, J. Besnard, S. Muresan, A.L. Hopkins, *Nat. Chem.*, **2012**, *4*, 90-98.
- [221] D.F. Veber, S.R. Johnson, H.Y. Cheng, B.R. Smith, K.W. Ward, K.D. Kopple, *J. Med. Chem.*, **2002**, *45*, 2615-2623.
- [222] Y.D. Yang, O. Engkvist, A. Llinas, H.M. Chen, *J. Med. Chem.*, **2012**, *55*, 3667-3677.
- [223] M. Galanski, V.B. Arion, M.A. Jakupec, B.K. Keppler, *Curr. Pharm. Des.*, **2003**, *9*, 2078-2089.
- [224] C.G. Hartinger, M. Groessl, S.M. Meier, A. Casini, P.J. Dyson, *Chem. Soc. Rev.*, **2013**, under review.
- [225] R.B. Cole (Ed.), *Electrospray Ionization Mass Spectrometry: Fundamentals, Instrumentation & Applications*, John Wiley & Sons, Inc., New York, **1997**.
- [226] H. Zorbas, F. Lottspeich (Eds.), *Bioanalytik*, Spektrum Akademischer Verlag, Heidelberg, **1998**.
- [227] G.L. Glish, R.W. Vachet, *Nat. Rev. Drug Discovery*, **2003**, *2*, 140-150.
- [228] R. Lobinski, D. Schaumlöffel, J. Szpunar, *Mass Spectrom. Rev.*, **2006**, *25*, 255-289.
- [229] X. Sun, C.-N. Tsang, H. Sun, *Metallomics*, **2009**, *1*, 25-31.
- [230] M.L. Nielsen, M.M. Savitski, R.A. Zubarev, *Mol. Cell. Proteomics*, **2005**, *4*, 835-845.
- [231] C.G. Hartinger, W.H. Ang, A. Casini, L. Messori, B.K. Keppler, P.J. Dyson, *J. Anal. At. Spectrom.*, **2007**, *22*, 960-967.
- [232] M. Moldovan, E.M. Krupp, A.E. Holliday, O.F.X. Donard, *J. Anal. At. Spectrom.*, **2004**, *19*, 815-822.
- [233] I. Konz, B. Fernandez, M.L. Fernandez, R. Pereiro, A. Sanz-Medel, *Anal. Bioanal. Chem.*, **2012**, *403*, 2113-2125.
- [234] E. Moreno-Gordaliza, C. Giesen, A. Lazaro, D. Esteban-Fernandez, B. Humanes, B. Canas, U. Panne, A. Tejedor, N. Jakubowski, M.M. Gomez-Gomez, *Anal. Chem.*, **2011**, *83*, 7933-7940.
- [235] K. Schwamborn, R.M. Caprioli, *Nat. Rev. Cancer*, **2010**, *10*, 639-646.

- [236] A.B. Kanu, P. Dwivedi, M. Tam, L. Matz, H.H. Hill, *J. Mass Spectrom.*, **2008**, *43*, 1-22.
- [237] N.L. Kelleher, *Anal. Chem.*, **2004**, *76*, 196a-203a.
- [238] C. Wu, J.C. Tran, L. Zamborg, K.R. Durbin, M.X. Li, D.R. Ahlf, B.P. Early, P.M. Thomas, J.V. Sweedler, N.L. Kelleher, *Nat. Methods*, **2012**, *9*, 822-826.
- [239] E.E.M. Brouwers, M. Tibben, H. Rosing, J.H.M. Schellens, J.H. Beijnen, *Mass Spectrom. Rev.*, **2008**, *27*, 67-100.
- [240] A. Bouslimani, N. Bec, M. Glueckmann, C. Hirtz, C. Larroque, *Rapid Commun. Mass Spectrom.*, **2010**, *24*, 415-421.
- [241] R.C. Le Pla, K.J. Ritchie, C.J. Henderson, C.R. Wolf, C.F. Harrington, P.B. Farmer, *Chem. Res. Toxicol.*, **2007**, *20*, 1177-1182.
- [242] P. Heffeter, K. Bock, B. Atil, M.A. Reza Hoda, W. Korner, C. Bartel, U. Jungwirth, B.K. Keppler, M. Micksche, W. Berger, G. Koellensperger, *J. Biol. Inorg. Chem.*, **2010**, *15*, 737-748.
- [243] D.A. Wolters, M. Stefanopoulou, P.J. Dyson, M. Groessl, *Metallomics*, **2012**, *4*, 1185-1196.
- [244] C.S. Allardyce, P.J. Dyson, F.R. Abou-Shakra, H. Birtwistle, J. Coffey, *Chem. Commun.*, **2001**, 2708-2709.
- [245] M.P. Washburn, D. Wolters, J.R. Yates, *Nat. Biotechnol.*, **2001**, *19*, 242-247.
- [246] D.A. Wolters, M.P. Washburn, J.R. Yates, *Anal. Chem.*, **2001**, *73*, 5683-5690.
- [247] J. Will, W.S. Sheldrick, D. Wolters, *J. Biol. Inorg. Chem.*, **2008**, *13*, 421-434.
- [248] J. Will, A. Kyas, W.S. Sheldrick, D. Wolters, *J. Biol. Inorg. Chem.*, **2007**, *12*, 883-894.
- [249] J. Lokich, N. Anderson, *Ann. Oncol.*, **1998**, *9*, 13-21.
- [250] M. Sulyok, S. Hann, C.G. Hartinger, B.K. Keppler, G. Stingeder, G. Koellensperger, *J. Anal. At. Spectrom.*, **2005**, *20*, 856-863.
- [251] E.I. Montero, B.T. Benedetti, J.B. Mangrum, M.J. Oehlsen, Y. Qu, N.P. Farrell, *Dalton Trans.*, **2007**, 4938-4942.
- [252] C.S. Allardyce, P.J. Dyson, J. Coffey, N. Johnson, *Rapid Commun. Mass Spectrom.*, **2002**, *16*, 933-935.
- [253] I. Khalaila, C.S. Allardyce, C.S. Verma, P.J. Dyson, *ChemBioChem*, **2005**, *6*, 1788-1795.
- [254] U. Warnke, C. Rappel, H. Meier, C. Kloft, M. Galanski, C.G. Hartinger, B.K. Keppler, U. Jaehde, *ChemBioChem*, **2004**, *5*, 1543-1549.
- [255] A.E. Egger, C.G. Hartinger, H. Ben Hamidane, Y.O. Tsybin, B.K. Keppler, P.J. Dyson, *Inorg. Chem.*, **2008**, *47*, 10626-10633.
- [256] M. Groessl, Y.O. Tsybin, C.G. Hartinger, B.K. Keppler, P.J. Dyson, *J. Biol. Inorg. Chem.*, **2010**, *15*, 677-688.
- [257] D. Gibson, C.E. Costello, *Eur. Mass Spectrom.*, **1999**, *5*, 501-510.
- [258] T. Peleg-Shulman, Y. Najajreh, D. Gibson, *J. Inorg. Biochem.*, **2002**, *91*, 306-311.
- [259] T. Peleg-Shulman, D. Gibson, *J. Am. Chem. Soc.*, **2001**, *123*, 3171-3172.
- [260] J.P. Williams, H.I.A. Phillips, I. Campuzano, P.J. Sadler, *J. Am. Soc. Mass Spectrom.*, **2010**, *21*, 1097-1106.
- [261] C.G. Hartinger, Y.O. Tsybin, J. Fuchser, P.J. Dyson, *Inorg. Chem.*, **2008**, *47*, 17-19.
- [262] H.L. Li, T.Y. Lin, S.L. Van Orden, Y. Zhao, M.P. Barrow, A.M. Pizarro, Y.L. Qi, P.J. Sadler, P.B. O'Connor, *Anal. Chem.*, **2011**, *83*, 9507-9515.
- [263] G.S. Yang, R. Miao, C. Jin, Y.H. Mei, H.W. Tang, J. Hong, Z.J. Guo, L.G. Zhu, *J. Mass Spectrom.*, **2005**, *40*, 1005-1016.
- [264] A. Casini, G. Mastrobuoni, W.H. Ang, C. Gabbiani, G. Pieraccini, G. Moneti, P.J. Dyson, L. Messori, *ChemMedChem*, **2007**, *2*, 631-635.
- [265] A. Casini, C. Gabbiani, G. Mastrobuoni, R.Z. Pellicani, F.P. Intini, F. Arnesano, G. Natile, G. Moneti, S. Francese, L. Messori, *Biochemistry*, **2007**, *46*, 12220-12230.
- [266] C. Gabbiani, A. Casini, G. Mastrobuoni, N. Kirshenbaum, O. Moshel, G. Pieraccini, G. Moneti, L. Messori, D. Gibson, *J. Biol. Inorg. Chem.*, **2008**, *13*, 755-764.
- [267] W.H. Ang, I. Khalaila, C.S. Allardyce, L. Juillerat-Jeanneret, P.J. Dyson, *J. Am. Chem. Soc.*, **2005**, *127*, 1382-1383.
- [268] R. Mandal, R. Kalke, X.F. Li, *Rapid Commun. Mass Spectrom.*, **2003**, *17*, 2748-2754.
- [269] E. Moreno-Gordaliza, B. Canas, M.A. Palacios, M.M. Gomez-Gomez, *Analyst*, **2010**, *135*, 1288-1298.
- [270] A. Casini, G. Mastrobuoni, C. Temperini, C. Gabbiani, S. Francese, G. Moneti, C.T. Supuran, A. Scozzafava, L. Messori, *Chem. Commun.*, **2007**, 156-158.
- [271] A. Casini, A. Karotki, C. Gabbiani, F. Rugi, M. Vasak, L. Messori, P.J. Dyson, *Metallomics*, **2009**, *1*, 434-441.
- [272] M. Knipp, A.V. Karotki, S. Chesnov, G. Natile, P.J. Sadler, V. Brabec, M. Vasak, *J. Med. Chem.*, **2007**, *50*, 4075-4086.
- [273] S.K. Weidt, C.L. Mackay, P.R.R. Langridge-Smith, P.J. Sadler, *Chem. Commun.*, **2007**, 1719-1721.
- [274] A. Casini, C. Gabbiani, F. Sorrentino, M.P. Rigobello, A. Bindoli, T.J. Geldbach, A. Marrone, N. Re, C.G. Hartinger, P.J. Dyson, L. Messori, *J. Med. Chem.*, **2008**, *51*, 6773-6781.
- [275] N.B. Zhang, Y.G. Du, M. Cui, J.P. King, Z.Q. Liu, S.Y. Liu, *Anal. Chem.*, **2012**, *84*, 6206-6212.
- [276] J.A. Durden, H.A. Stansbury, W.H. Catlette, *J. Chem. Eng. Data*, **1964**, *9*, 228-232.
- [277] W.A. Kinney, N.E. Lee, R.M. Blank, C.A. Demerson, C.S. Sarnella, N.T. Scherer, G.N. Mir, L.E. Borella, J.F. Dijoseph, C. Wells, *J. Med. Chem.*, **1990**, *33*, 327-336.
- [278] J.A. Kitchen, N.G. White, M. Boyd, B. Moubaraki, K.S. Murray, P.D.W. Boyd, S. Brooker, *Inorg. Chem.*, **2009**, *48*, 6670-6679.
- [279] A. Casini, A. Guerri, C. Gabbiani, L. Messori, *J. Inorg. Biochem.*, **2008**, *102*, 995-1006.

3. Results and Discussion

3.1. Novel Metal(II) Arene 2-Pyridinecarbothioamides: A Rationale to Orally Active Organometallic Anticancer Agents

Samuel M. Meier,^{a,b} Muhammad Hanif,^{a,c} Zenita Adhireksan,^d Verena Pichler,^a Maria Novak,^a Elisabeth Jirkovsky,^a Michael A. Jakupec,^{a,b} Vladimir B. Arion,^a Curt A. Davey,^d Bernhard K. Keppler,^{a,b} Christian G. Hartinger^{a,b,e}

Chemical Science, 2013, 4, 1837-1846.

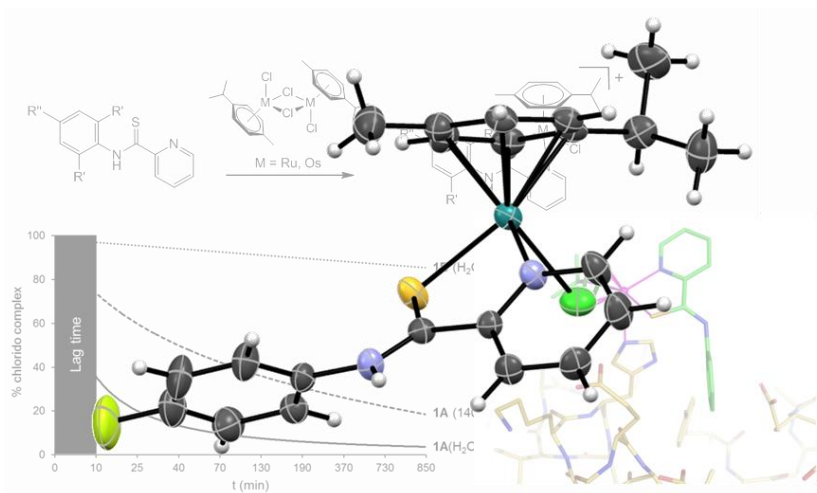
^a University of Vienna, Institute of Inorganic Chemistry, Waehring Str. 42, A-1090 Vienna, Austria.

^b University of Vienna, Research Platform "Translational Cancer Therapy Research", Waehring Str. 42, A-1090 Vienna, Austria.

^c COMSATS Institute of Information Technology, Department of Chemistry, Abbottabad-22060, Pakistan.

^d Nanyang Technological University, School of Biological Sciences, Division of Structural Biology and Biochemistry, 60 Nanyang Drive, Singapore 637551, Singapore.

^e University of Auckland, School of Chemical Sciences, Private Bag 92019, 1142 Auckland, New Zealand.



Novel metal(II) arene 2-pyridinecarbothioamides: a rationale to orally active organometallic anticancer agents†

Cite this: *Chem. Sci.*, 2013, 4, 1837

Samuel M. Meier,^{ab} Muhammad Hanif,^{ac} Zenita Adhireksan,^d Verena Pichler,^a Maria Novak,^a Elisabeth Jirkovsky,^a Michael A. Jakupec,^{ab} Vladimir B. Arion,^a Curt A. Davey,^d Bernhard K. Keppler^{ab} and Christian G. Hartinger^{*abe}

A novel series of organometallic antitumour agents based on Ru^{II} and Os^{II} complexes containing *N*-substituted 2-pyridinecarbothioamides (PCAs) has been synthesized and characterized. To the best of our knowledge, this is the first report of organometallic anticancer compounds with an *S,N*-bidentate ligand system. While the ligands showed activity as gastric mucosal protectants and low acute toxicity *in vivo* (*J. Med. Chem.*, 1990, **33**, 327–336), coordination leads to highly antiproliferative metallodrugs, depending on lipophilicity and steric demand, in colon carcinoma and non-small lung cancer cell lines with intrinsic chemoresistances. The most lipophilic and smallest congeners are the most effective with IC₅₀ values in the low micromolar range. This new family of potential metallodrugs features exceptional stability in hydrochloric acid (60 mM), characterized by complete suppression of hydrolysis and low reactivity towards biological nucleophiles. Therefore, their unexpected aqueous chemistry renders this family of antiproliferative agents suitable for oral administration. An unprecedented feature is their ability to form transient thioketone-bridged dimers in aqueous solution upon hydrolysis, which is believed to minimize deactivation by biological nucleophiles. However, the biological effect seems to be caused by the monomer as observed with crystallographic studies of the nucleosome core particle (NCP), which revealed that [chlorido(η^6 -*p*-cymene)(*N*-phenyl-2-pyridinecarbothioamide)osmium(II)] chloride and [chlorido(η^6 -*p*-cymene)(*N*-fluorophenyl-2-pyridinecarbothioamide)osmium(II)] chloride react at two types of binding sites on the histone proteins. The adducts form at histidine side chains located on the nucleosome surface and the inner cleft of the nucleosome in the midst of an extensive histone–histone interface, suggesting interference with chromatin activity as a possible mode of action of these compounds. Additionally, ligand-based S → O exchange allows for a potential dual-mode of action by targeting DNA (*J. Med. Chem.*, 2009, **52**, 7753–7764). The quantitative estimates of drug-likeness (QED) for this family of compounds revealed a similar drug-likeness compared to erlotinib, tamoxifen, imatinib and sorafenib.

Received 21st December 2012
Accepted 12th February 2013

DOI: 10.1039/c3sc22294b

www.rsc.org/chemicalscience

Introduction

Orally active anticancer agents are desirable for patient compliance and ease of administration. However, organometallic Ru^{II} and Os^{II} anticancer metallodrugs with various ligand systems and nuclearities were mostly developed for intravenous administration so far.^{1–12} Inert platinum(IV) coordination compounds are currently the only orally active anticancer metallodrugs with satraplatin as the most prominent example.^{13–16} The reason for the low research efforts devoted to the development of orally active organometallics is probably related to concerns about the stability of the compound in the acidic and proteolytic environment of the stomach, the uptake into the blood stream and the associated first-pass effect.¹⁷ The existing rules that relate molecular properties to oral bioavailability formulated by Lipinski *et al.*¹⁸ and extended by Veber *et al.*¹⁹ list

^aUniversity of Vienna, Institute of Inorganic Chemistry, Waehringer Str. 42, A-1090 Vienna, Austria

^bUniversity of Vienna, Research Platform “Translational Cancer Therapy Research”, Waehringer Str. 42, A-1090 Vienna, Austria

^cCOMSATS Institute of Information Technology, Department of Chemistry, Abbottabad-22060, Pakistan

^dNanyang Technological University, School of Biological Sciences, Division of Structural Biology and Biochemistry, 60 Nanyang Drive, Singapore 637551, Singapore

^eUniversity of Auckland, School of Chemical Sciences, Private Bag 92019, 1142 Auckland, New Zealand. E-mail: c.hartinger@auckland.ac.nz

† Electronic supplementary information (ESI) available. PDB ID codes: **1A** – 4J8V, **3A** – 4J8X, **1B** – 4J8U, **3B** – 4J8W. CCDC 902334, 902335. For ESI and crystallographic data in CIF or other electronic format see DOI: 10.1039/c3sc22294b

several criteria which might increase the probability of a drug to display favourable oral bioavailability. Importantly, the original molecular mass constraint postulated by Lipinski was extended to molecular masses $>500 \text{ g mol}^{-1}$ by Veber. According to their reports, a calculated partition coefficient of $<+5$, the presence of a total of ≤ 12 hydrogen bond donors and acceptors and ≤ 10 rotatable bonds seem ideal molecular properties for this purpose. The fact that these criteria work by cut-off values has entailed critical voices, and a more holistic treatment of an extended set of these criteria was recently reported termed the quantitative estimate of drug-likeness (QED).²⁰ It must be noted though that these empirical rules were derived from purely organic drug candidates and are not necessarily valid for metallodrugs, which remain largely unexplored so far. The lack of orally active metal-based drugs in clinical studies further hinders the establishment of analogous criteria. However, organometallic or coordination compounds may offer access to unused chemical space for applications in medicinal chemistry with potentially novel modes of action, which cannot be obtained by organic molecules.²¹ Yang *et al.* pointed out that the molecular topology directly influences absorption, distribution, metabolism, excretion and toxicity (ADMET).²² In fact, even ADMET data for organometallic anticancer agents are still sparse.^{10,23–26}

Most of the organometallic Ru^{II} and Os^{II} arene complexes share the “half-sandwich piano-stool” motif, where the low oxidation state is stabilized by a η^6 -coordinating arene, such as biphenyl (bip) or *p*-cymene (cym).^{2,3,27} Adopting a pseudo-tetrahedral structure, there are three remaining binding sites available, which are occupied by inert and/or labile ligands. In the pursuit of orally active organometallic anticancer agents, the choice of the ligands is crucial for obtaining effective and stable metallodrugs. Additionally, the nature of the inert ligand and the inner sphere coordination mode seem to strongly influence the cytotoxic activity of potential organometallic anticancer compounds as well as their biological targets. For example, thiopyronato complexes showed higher cytotoxicity *in vitro* than the corresponding pyr(id)onato complexes,⁷ although otherwise isostructural. Furthermore, [(bip)Ru(en)Cl]PF₆ (RM175), exhibiting high antiproliferative activity *in vitro* and promising *in vivo* properties, seems to target DNA by mono-functionally binding to N7 of guanine,^{2,26} although protein interactions^{28,29} were also demonstrated along with considerable antimetastatic activity.³⁰ On the other hand, RAPTA-C, containing a mono-dentate 1,3,5-triaza-7-phosphaadamantane (pta) and two labile chlorido ligands, was found non-cytotoxic in the cell lines TS/A or HBL-100 but showed pronounced antimetastatic activity and also inhibits angiogenesis.^{11,23,31} In contrast to RM175, the primary target of RAPTA-C seems to involve proteins as evidenced by crystallographic experiments of this compound with the nucleosome core,³² although modified compounds designed to inhibit specific proteins have also been described.^{33,34} In fact, the nucleosome, as the basic repeating unit of cellular DNA packaged by the histone protein octamer, is an important model system for comparing the reactivity of metallodrugs towards proteins and DNA.³⁵ Besides modifying the ligands, it is also possible to fine-tune the chemical and biological properties

of metallodrugs by changing the metal centre. Therefore, osmium, the heavier congener of ruthenium, has attracted the attention of researchers in recent years.³⁶ Organometallic ruthenium and osmium complexes adopt similar pseudo-octahedral geometries and can be considered as metallo-bioisosters.³⁷ Osmium shows increased inertness toward ligand substitution, which often results in a lower rate of aquation.^{38,39} In fact, correlations between these metals and cytotoxic activities are still controversially discussed, and the dependence of cytotoxic activity on ligand exchange rates is not always given.⁵

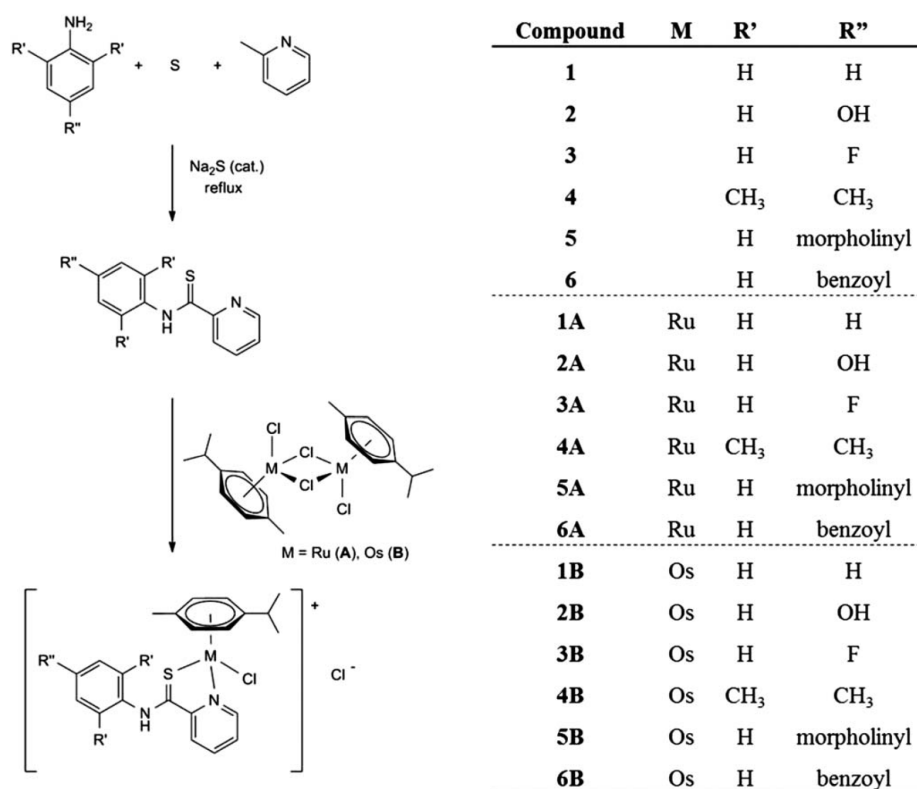
It is the aim of this work to introduce a novel family of organometallic Ru^{II} and Os^{II} anticancer compounds based on *N*-substituted 2-pyridinecarbothioamides (PCA). The unexpected aqueous chemistry involving the unprecedented *S,N*-donor system makes these highly active compounds promising anticancer agents for oral administration.

Results and discussion

Synthesis and characterization

N-Substituted 2-pyridinecarbothioamides (PCAs) are versatile and easily accessible building blocks for the synthesis of *S,N*-bidentate ligands for organometallic and coordination compounds. They are considered bioactive substances in particular as gastric mucosal protectants and exhibit low acute toxicity, *i.e.* the acute toxicity of **1** (Scheme 1) was determined as $>1000 \text{ mg kg}^{-1}$ in an *in vivo* model.⁴⁰ These characteristics appear ideal for ligands of orally active metallodrugs, since ligand cleavage from the metal was observed for some donor atom systems.^{7,41} In a one pot synthesis to obtain PCAs, the substituted aniline and elemental sulfur were refluxed for 48 h in 2-picoline and catalytic amounts of sodium sulfide were employed to initiate the reaction (Scheme 1). After work-up and recrystallization, the PCAs were generally obtained in moderate to high yields (77–88%), which are comparable to the ones obtained by Klingele and Brooker.⁴² The ligands were characterized by 1D and 2D NMR spectroscopy and ESI-MS, as well as elemental analysis in the case of the newly synthesized ligands **5** and **6**. ¹H and ¹³C{¹H} NMR spectra of PCAs show some characteristic features, *i.e.* in aprotic deuterated solvents, the thioamide proton was detected at *ca.* 12 ppm. This accounts for a down-field shift of *ca.* 2.5 ppm compared to the amide proton of a related picolinamido ligand.⁹

For the complexation reactions, a methanolic suspension of the dimeric Ru(cym) (**A**) or Os(cym) (**B**) precursor was added to a methanolic solution containing 2 eq. of the respective ligand. A change in color from brown to dark red was observed immediately after addition of the precursor, and reaction times were found to be in the order of 4–18 hours. The solvent was subsequently removed, and the solid residue was re-dissolved in dichloromethane and filtered. Precipitation and subsequent drying *in vacuo* yielded analytically pure products. The Ru^{II} and Os^{II} PCA complexes were synthesized from RuCl₃·*x*H₂O and OsO₄ starting materials with average overall yields of 60% for ruthenium complexes and 25% for the respective osmium analogues. The lower yields of the osmium analogues are mainly due to lower yields during preparation of precursor **B**.^{43,44} The



Scheme 1 Synthesis and numbering scheme of the organometallic Ru^{II} (A) and Os^{II} (B) complexes of *N*-substituted 2-pyridinecarbothioamides.

complexes were isolated with a chloride counter ion, which improves the solubility in aqueous solvent systems. All organometallic compounds were characterized by 1D and 2D NMR spectroscopy, ESI MS and elemental analysis. Complexation of the PCA to the metal is characterized by a down-field shift of the $-NH$ proton signal to *ca.* 14 ppm in aprotic solvents. The H-1 and H-4 proton signals of the pyridine ring also shift down-field by *ca.* 1 ppm, consistent with electron donation of the thioamide moiety and the pyridine nitrogen to the metal, *i.e.* bidentate S,N -coordination. The metal centre had only a marginal effect on the chemical shifts of the PCA proton and carbon NMR signals. A

clear difference was only observed for the carbon atoms which are directly coordinated to the metal centre, *i.e.* the η^6 -arene carbons coordinated to ruthenium were observed with a 10 ppm down-field shift compared to their osmium analogues. In ESI mass spectra, the $[M - Cl - H]^+$ ion was characteristically detected for all complexes in methanolic solution.

The molecular structures of **3A** and **2B** were determined by X-ray crystallography (Fig. 1). Compound **3A** was crystallized by slow diffusion of pentane into acetone and **2B** by diffusion of diethyl ether into a methanol solution (see Tables S1 and S2[†] for crystallographic parameters). The 3D structures of the metal

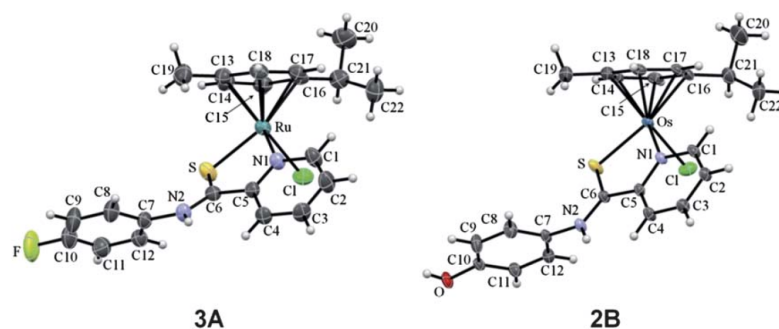


Fig. 1 The crystal structures of **3A** (left) and **2B** (right) are shown with thermal ellipsoids at 50% probability level. The *R*-enantiomers are displayed including the numbering scheme. Counter ions and co-crystallized solvent molecules were omitted for clarity. The crystal structures of **3A** and **2B** contain a 1 : 1 ratio of *R*- and *S*-enantiomers.

complexes are very similar adopting the characteristic “piano-stool” configuration. Surprisingly, both compounds feature a 1 : 1 ratio of monometallic *R*- and *S*-enantiomers in their crystal structures (Fig. S1 and S2†). In contrast to organometallic *N*-phenyl-picolinamido complexes⁹ where amido-switching was detected, only the *N,S*-coordination mode was observed using PCAs, probably due to the increased stability of the metal–sulfur bond, as suggested by the HSAB principle. The torsion angle N1–C5–C6–S for **2B** is 4.1(4)° and implies that the carbothioamide and the pyridine ring form a delocalized system, whereas a reduced tendency is observed for **3A** with a torsion angle of 15.9(4)°. The large torsion angles C6–N2–C7–C8 for both compounds (>52°) suggest that the delocalized system does not extend to the *N*_{amide}-substituted ring. Finally, the *R*- and *S*-enantiomers of **2B** form intermolecular hydrogen bonding and π -stacking networks. The independent *R*- and *S*-enantiomers are connected by two chloride counter ions (Fig. S1†). They form on one molecule Cl \cdots H–O and on the other Cl \cdots H–N hydrogen bonds at distances of 3.011(2) and 3.129(3) Å, respectively, between the donor and acceptor atoms. In addition, the neighboring phenol rings are aligned in parallel offset manner,⁴⁵ with H-11 pointing toward the centroid of the neighboring ring and *vice versa* at a distance of 3.390 Å and an angle of 109.3°.

Hydrolysis studies

Organometallic Ru^{II} and Os^{II} anticancer agents are usually designed as prodrugs containing a labile metal–halido bond. Therefore, they need to be activated in order to exert their biological effect. In an aqueous environment, the mechanism of activation involves hydrolysis of the metal–halido bond and formation of the respective aqua complex, which exhibits

increased reactivity towards potential nucleophilic targets in biological environments.⁴⁶ On the other hand, hydrolysis can also lead to cleavage of ligands from the metal and result in hydroxido-bridged dimeric Ru^{II} species, which are thermodynamically stable and biologically inactive.⁷ The rate of hydrolysis is therefore an important parameter, which provides insights into the activation profile of an investigational metal–drug,³⁹ and requires careful control by appropriate ligand selection. For this purpose, **1A** and **1B** were analyzed for their hydrolysis behaviour in aqueous and 104 mM NaCl solution, the latter representing the sodium chloride concentration in the blood stream. Complexes **1A** and **1B** were chosen due to their increased solubility compared to the other compounds in the series. It was found that **1A** hydrolyzes rapidly in aqueous solution and only 29% of the chlorido complex was observed in the ¹H NMR spectrum after 10 min. Experiments in a 104 mM NaCl solution revealed that elevated chloride concentrations slow down the hydrolysis of the chlorido complex, and a half-life of $t_{1/2} = 49$ min was determined (Fig. S3†). The findings for **1A** parallel earlier results with the cationic metallodrug [(bip)Ru(en)Cl]⁺, where the half-life of the chlorido complex increased with higher ionic strength of the solution.⁴⁷ Osmium compounds generally exhibit slower ligand exchange kinetics than their ruthenium analogues, and indeed **1B** did not hydrolyze significantly within 14 h in aqueous solution. Similar results were obtained for organometallic Os^{II} compounds containing phenylazopyridine ligands.⁴⁸ Once hydrolyzed, both compounds are stable over a pH range of 1.74–11.62 as indicated by NMR titrations. Unexpectedly, ESI-MS studies in aqueous solution revealed that hydrolysis of the M–Cl bond does not yield the aquated monomeric complexes but rather dimers (Fig. 2 and Scheme 2). The ESI IT mass spectra feature doubly-charged peaks at m/z 448.9 \pm 0.1 and 537.9 \pm 0.1, and

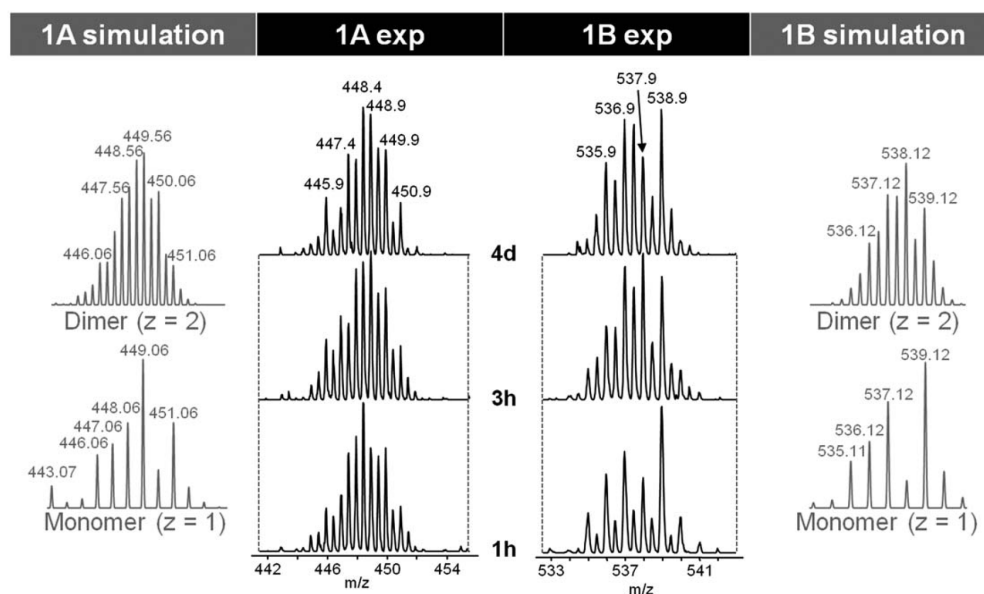
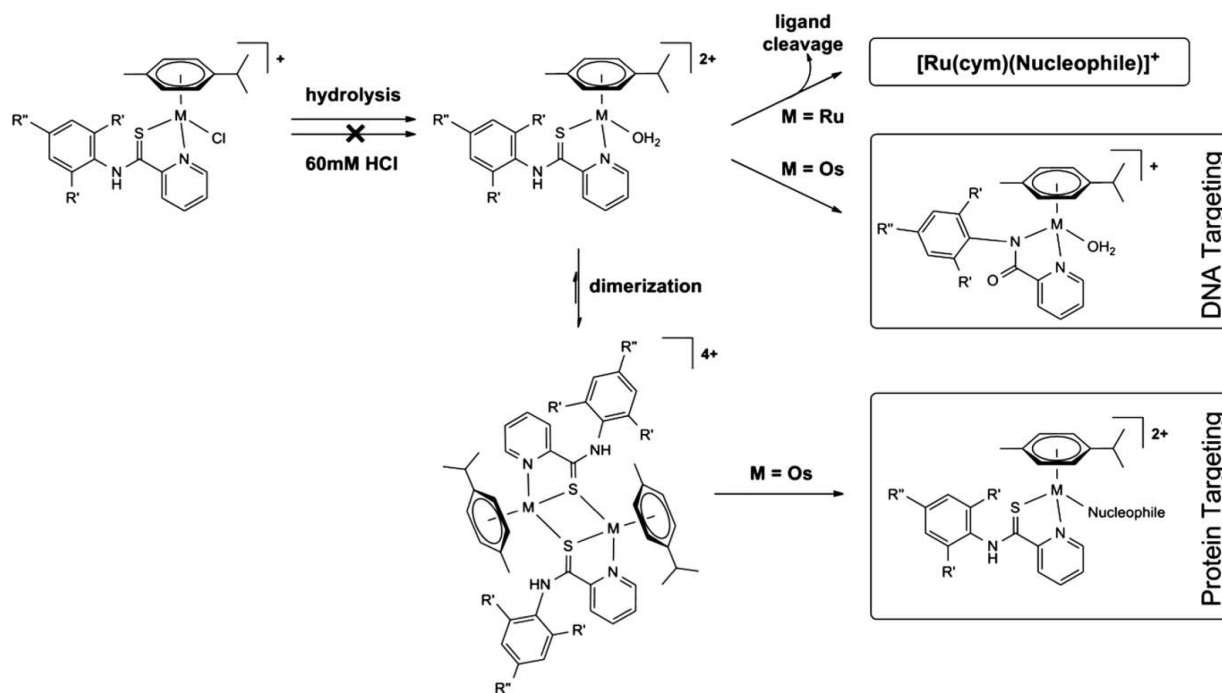


Fig. 2 Time-dependent dimer formation of **1A** and **1B** in aqueous solution assessed by ESI IT-MS. The experimental measurements are given in black and the theoretical peak pattern in grey. All experimental measurements include a standard deviation of $m/z \pm 0.1$.



Scheme 2 Reaction pathways of organometallic Ru^{II} and Os^{II} PCA complexes in aqueous solution and in the presence of biological nucleophiles. The osmium analogues can undergo ligand-based S → O substitution, which leads to *N,N*-coordinated cytotoxic agents at pH > 7 with electron-withdrawing substituents at the phenyl ring.⁹ This potentially offers a dual targeting mode.

their associated isotopic distribution indicates $[(M - Cl - H)_2]^{2+}$ dimers $[M = Ru (m_{ex} = 449.06) \text{ or } Os (m_{ex} = 538.12)]$. Dimers are formed in significant extents for **1A** after 1 h, and for **1B** after 3 h, although an equilibrium between monomer and dimer seems to exist as suggested by the steady presence of a few percent of monomers (Fig. 2). Both dimers are stable for at least 4 days in aqueous solution. Surprisingly, dimerization is even observed when the compounds are directly dissolved in *L*-methionine- or *L*-cysteine-containing aqueous solutions, while no adduct formation was detected with the amino acids. Further proof of dimer formation was obtained from X-ray diffraction analysis of single crystals of **1A** from basic aqueous solution. Although the data set was of low quality, it allowed concluding that these dimeric species feature a 2Ru–2S core, where each PCA thioketone bridges two ruthenium centres leading to a 4+ charged dimeric compound (Fig. S4†). It turned out that dimer formation can be inhibited when using DMSO for stock solutions or when employing non-aqueous solvents such as methanol.

Stability in hydrochloric acid

The stability of **1A** and **1B** (each 400 μM) in HCl_{aq} (pH 1.2, ~60 mM) was investigated by mass spectrometric methods, and they were found to be stable for at least 7 days under these conditions (Fig. S5†). The sole detected signals were assigned to $[M]^+$ species, corresponding to $[1A]^+$ ($m/z 484.80 \pm 0.1$, $m_{ex} = 485.04$) and $[1B]^+$ ($m/z 574.83 \pm 0.1$, $m_{ex} = 575.09$). Hydrolysis is completely suppressed by 60 mM hydrochloric acid, while a

104 mM chloride-containing aqueous solution slows down the process. The compounds are therefore expected to tolerate the acidic environment of the stomach. Importantly, this pH-dependent suppression of hydrolysis in an acidic environment inhibits activation of the prodrug till it reaches the slightly basic environment of the cytosol or blood stream.

Interaction with biomolecules

Mass spectrometry is a powerful tool for probing metallodrug–biomolecule interactions.⁴⁹ Compounds **1A** and **1B** were further investigated by ESI mass spectrometric methods with respect to their reactivity towards small biological nucleophiles. Compound **1A** was incubated with *L*-cysteine (Cys), *L*-histidine (His), *L*-methionine (Met), ubiquitin (ub), cytochrome-C (cyt) and 5'-deoxyguanosine monophosphate (5'-dGMP) at a 1 : 1 molar ratio at 37 °C up to 7 days. Compound **1B** was similarly incubated with Cys, Met, ub and cyt. It turned out that both compounds do not form detectable adducts with these biomolecules. Interestingly, compound **1B** underwent partial ligand-based sulfur to oxygen substitution clearly detectable after 19 h. Using high resolution ESI TOF mass spectrometry, the peak detected at $m/z 523.140$ ($m_{ex} = 523.142$, 4 ppm, 42% relative to **1B**) was assigned to this **1B_{oxo}** species (Fig. S6†), which in contrast to **1B** forms adducts with ub (Fig. 3) corresponding to $[ub + 1B_{oxo} - Cl]^+$ ($m_{acc} = 9085.742$ Da, $m_{ex} = 9085.764$, 3 ppm, 9%), but not with cyt. Van Rijt *et al.* reported the pH-dependent *N,O*- vs. *N,N*-coordination switching for related complexes.⁹ At slightly basic pH, the *N,N*-coordination

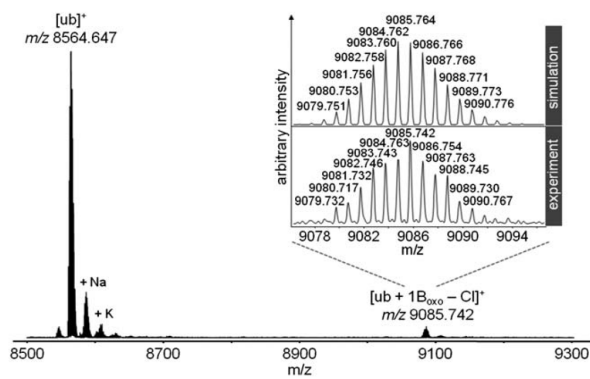


Fig. 3 Deconvoluted ESI TOF mass spectrum of the reaction between **1B** and ubiquitin (ub) after 24 h. Adduct formation with ub is only detected with the **1B_{oxo}** species.

mode is favoured, leading to highly cytotoxic agents, whereas the *N,O*-bidentate donor system showed only modest activity *in vitro*. The reactivity towards Cys and Met was further evaluated with **2A** and **2B**. As in the case of **1B**, no reaction occurred with **2B**. However, **2A** was stable in the presence of Met, but not in the presence of Cys, which yielded adducts corresponding to $[(\text{cym})\text{Ru}(\text{Cys})]^+$ ($m/z\ 355.9 \pm 0.1$, $m_{\text{ex}} = 356.0$, 9%) and $[(2\text{A} - \text{Cl}) + (\text{cym})\text{Ru}(\text{Cys})]^{2+}$ ($m/z\ 410.4 \pm 0.1$, $m_{\text{ex}} = 410.5$, 14%) after 24 h (Fig. S7†). Reactions with biomolecules such as peptides or proteins may constitute a possible pathway for deactivation of metallodrugs in the cell, and a mass spectrometric study of (thio)pyr(id)onato Ru^{II} complexes with ubiquitin showed that increased biomolecule binding accompanied by ligand cleavage from the metal may correlate with reduced *in vitro* cytotoxicity.⁴¹ Our results show that this inverse correlation is also valid for Ru^{II} and Os^{II} complexes based on *N*-substituted 2-pyridinecarbothioamides, where only the least potent **2A** is partially deactivated by Cys (*vide infra*).

The nucleosome as a potential target for organometallic metallodrugs

Mass spectrometric methods could not provide proof of any interaction between **1A** or **1B** and biomolecules probably due to their ability to form dimers in aqueous solution, but a clear cytotoxic effect was demonstrated in *in vitro* models. In order to elucidate a potential mode of action of these compounds, crystallographic studies were conducted with the nucleosome core particle (NCP), which entails a complex of 145 base pairs of double-stranded DNA with the histone protein octamer. In previous work, a clear difference between the binding modes of cisplatin/oxaliplatin³⁵ and RAPTA-C³² with the NCP was shown. The established mechanism of action of cisplatin is believed to involve binding to cellular DNA,⁵⁰ and accordingly cisplatin showed multiple binding sites to the DNA of the nucleosome core, in particular at solvent-accessible guanine nucleotides.⁵¹ In addition, histone protein binding sites were observed involving exclusively Met, and it was suggested that these Met adducts may serve as a reservoir for DNA platination.³⁵ In

contrast, the interaction of RAPTA-C, a ruthenium(II) anti-metastatic drug, with the NCP was largely devoid of DNA binding.³² RAPTA-C showed three distinct binding sites on the histone surface, where it formed adducts with His, L-lysine and L-glutamate side chains. It was hypothesized that this preference for proteins may be responsible for the antimetastatic effect of RAPTA-C.⁵²

In the present crystallographic study, the binding of **1A**, **3A**, **1B** and **3B** to the NCP was investigated (see Table S3† for data collection and refinement). The Os^{II} compounds **1B** and **3B** show identical binding sites exclusively with the histone octamer and involving His residues. Although dimer formation is fast relative to binding to biomolecules, the equilibrium between monomers and dimers slowly releases the biologically active monomer, which finally forms adducts at binding sites 1, 2 and 2' (Fig. 4). The first binding site is located on H2B His-106 on the histone surface and corresponds to one of the sites observed for RAPTA-C binding to the NCP.³² H2B His-79 comprises the second type of binding site and is situated within a cleft between the two halves of the nucleosome. The fact that this second binding site, encompassing a substantial number of hydrophobic histone groups, is favoured may be explained by the increased lipophilicity of **1B** and **3B** compared to RAPTA-C and suggests a mode of action different from this compound. Site 2/2' is situated at the histone dimer-dimer and dimer-tetramer interfaces composing the octamer and may therefore affect chromatin dynamics. The reduced cytotoxic activity of the sterically more demanding complexes may be explained by the inability of these compounds to efficiently bind within small crevices or channel passages of proteins, such as sites 2 and 2'. The two Ru^{II} compounds **1A** and **3A** form adducts exclusively on the histone proteins at sites 2 and 2' but are subject to cleavage of the carbothioamide ligand from the metal, resulting in the coordination of the Ru(cym) moiety to the NCP. Such behaviour is usually associated with a reduction of cytotoxic activity.⁷ However, in the present study, the Ru^{II} analogues also display high antiproliferative activity.

Evaluation of *in vitro* anticancer activity and lipophilicity

Kinney *et al.* characterized various carbothioamides for their activity as gastric mucosal protectants.⁴⁰ For **1** and the related *N*-(3,4-difluorophenyl)-2-pyridinecarbothioamide, they determined very low acute toxicities in the mouse in the range of >1 and >1.5 g kg⁻¹, respectively, indicating high tolerability *in vivo*. The cytotoxicity of **1A–6B** (from DMSO stocks diluted with medium) was determined in human colon carcinoma (SW480), ovarian cancer (CH1) and non-small cell lung cancer (A549) cell lines by means of the colorimetric MTT assay (Table 1). CH1 cells are the most chemosensitive in this panel, and the compounds were most active in this cell line. Importantly, this novel family of metallodrugs is about equally potent in the intrinsically cisplatin-resistant, P-glycoprotein-overexpressing colon carcinoma cell line as in the ovarian cancer cell line. Within both the Ru^{II} and Os^{II} series, the *N*-phenyl, *N*-4-fluorophenyl and *N*-mesityl containing complexes showed the highest antiproliferative activity with IC₅₀ values in the low

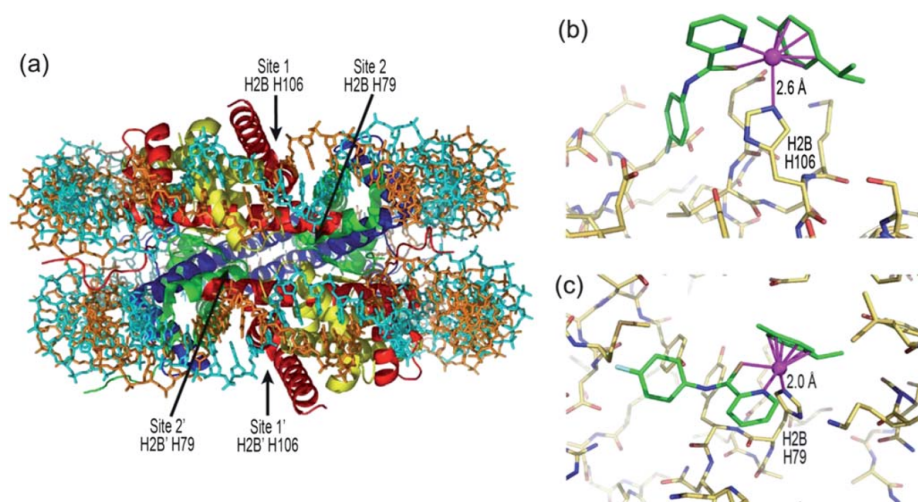


Fig. 4 Adduct formation by **1A**, **3A**, **1B** and **3B** on the nucleosome core particle. (a) Summary of binding sites on the NCP viewed down the pseudo two-fold axis (the two DNA strands are cyan and orange, and histone proteins are colored yellow, red, blue and green for H2A, H2B, H3 and H4, respectively). Compounds **1A** and **3A** formed adducts only at sites 2 and 2', whereas **1B** and **3B** formed adducts at sites 1, 2 and 2'. Binding at the symmetry-related site 1' is sterically blocked by nucleosome–nucleosome crystal contacts.³² (b) and (c) Adduct structures from reaction of **3B** at sites 1 (b) and 2 (c).

Table 1 *In vitro* anticancer activity of compounds **1A–6B** in human ovarian cancer (CH1), colon carcinoma (SW480) and non-small cell lung cancer (A549) cell lines after 96 h exposure,^a their chromatographic lipophilicity indices (ϕ_0) and weighted quantitative estimates of drug-likeness based on maximum information content (QED_w^{mo})

Compound	IC ₅₀ (μM)			ϕ_0	QED _w ^{mo}
	CH1	SW480	A549		
1A	5.4 ± 0.7	5.2 ± 1.1	29 ± 2	38.3	0.54
2A	66 ± 5	70 ± 15	403 ± 80	34.0	0.48
3A	3.8 ± 0.6	4.3 ± 1.2	14 ± 2	39.3	0.53
4A	4.7 ± 0.7	5.3 ± 0.6	19 ± 4	62.5	0.56
5A	17 ± 1	15 ± 2	100 ± 1	41.1	0.47
6A	9.4 ± 1.2	12 ± 1	43 ± 4	— ^b	— ^b
1B	6.5 ± 1.0	8.4 ± 1.4	25 ± 3	39.5	0.46
2B	26 ± 4	60 ± 8	175 ± 20	34.7	0.41
3B	6.0 ± 1.1	10 ± 2	29 ± 5	40.5	0.45
4B	7.2 ± 2.2	12 ± 1	29 ± 3	64.3	0.49
5B	13 ± 1	13 ± 2	61 ± 18	41.6	0.43
6B	12 ± 2	20 ± 3	45 ± 8	— ^b	— ^b

^a Values include standard deviations obtained from at least three independent experiments. ^b ϕ_0 was not determined due to uncertainty in peak assignment and consequently QED_w^{mo} calculation was not possible.

micromolar range in CH1 and SW480 cell lines. Interestingly, these compounds also exhibit some cytotoxic activity in the multidrug-resistant non-small cell lung cancer cell line A549, where fluorinated **3A** shows the highest activity with an IC₅₀ value of 14 ± 2 μM, implying that the compound is only four-fold less potent than in CH1 cells. Therefore, complexation of these ligands to an organometallic Ru^{II} or Os^{II} moiety yields highly antiproliferative agents *in vitro*, but neither of the two metals is consistently more favourable than the other with regard to inhibition of tumor cell growth.

In order to explore possible reasons for these structure–activity relationships, the lipophilicity of these compounds was determined. The lipophilicity of (metallo)drugs influences both pharmacokinetics and -dynamics,⁵³ and it is often associated with increased cellular uptake and therefore increased cytotoxic activity.⁵⁴ Several methods for determining the lipophilicity are available, with the shake flask method in combination with ICP-MS metal detection being the most frequently used.⁵⁵ However, the determination of the lipophilicity by the shake flask method may entail several uncertainties when dealing with organometallic ruthenium or osmium complexes, especially with regard to stability, hydrolytic activity and charge. The clear advantage of chromatographically determining the lipophilic character of such compounds lies in the fact that the lipophilicity of a single compound can be accurately determined even when traces of other species are present in solution, *e.g.* caused by formation of aqua or hydroxido species. Chromatographic lipophilicity indices ϕ_0 were therefore determined for the investigated compounds, which additionally show a better correlation with the more common partition coefficient than the related log k_w .⁵⁶ Potassium iodide was used as an internal standard for measuring the dead-volume and its addition slowed down the hydrolysis of the chlorido complex. The index ϕ_0 thus corresponds to the chlorido complex of each compound, *i.e.* the prodrug state. As expected, ruthenium and osmium series show similar ϕ_0 . The osmium analogues have slightly larger ϕ_0 indices, suggesting a slight increase in lipophilicity probably due to the longer Os–ligand coordination bonds (Table S2†). The following trend was observed within each series in terms of lipophilicity: *N*-4-hydroxyphenyl < *N*-phenyl < *N*-4-fluorophenyl ≅ *N*-4-morpholinophenyl < *N*-mesityl. Consequently, complexes **2A** and **2B** containing the *N*-(4-hydroxyphenyl)-2-pyridinecarbothioamide are most hydrophilic with ϕ_0 values corresponding to **34**, showed only very modest cytotoxic activity

in CH1 and SW480 cells and are virtually inactive in the A549 cell line with corresponding IC_{50} values of 403 ± 80 and 175 ± 20 μM , respectively. This correlates also with the observation that compounds which easily undergo ligand cleavage in the presence of biomolecules are less active in *in vitro* anticancer assays (compare the reaction of **2A** with Cys).⁴¹ The more lipophilic compounds **1A/B**, **3A/B** and **4A/B** display a $\varphi_0 > 38$ and exhibit more potent cytotoxic activities in all three cancer cell lines. The φ_0 values could not be determined for **6A** and **6B** due to uncertainties in peak assignment. They are expectedly the most lipophilic but also sterically demanding and show slightly reduced antiproliferative effect. In addition to lipophilicity, it seems that the anticancer activity is also dependent on the size of the metallodrug. Compounds **3B** and **5B** possess a very similar φ_0 , but the sterically less demanding **3B** is about twice as active as **5B** in two of the three cell lines *in vitro*.

The ligand-based S \rightarrow O exchange of the Os^{II} congeners offers a potentially dual mode of action (Scheme 2). While the Os^{II} PCA compounds rather target proteins as suggested by the crystallographic studies with the NCP, the Os picolinamido complexes are believed to target DNA.⁹ These ligands can reversibly form *N,O*-bidentate or *N,N*-bidentate complexes dependent on the pH. The *N,O*-coordination mode was found to yield inactive complexes, whereas the *N,N*-coordination mode yielded highly cytotoxic agents. Since *in vitro* assays are performed at pH ~ 7.4 over 96 h, the S \rightarrow O exchanged complexes are believed to be present in an *N,N*-coordination mode and should therefore retain their cytotoxicity, consistent with the results of the MTT assay.

Implications for oral bioavailability

The investigated series of compounds fail the Lipinski rules with respect to their molecular weights and only **1A** displays a molecular mass of <500 g mol^{-1} .¹⁸ However, since a significant amount of Lipinski-fails were approved for clinical use, we use here the weighted quantitative estimate of drug-likeness based on maximum information content (QED_w^{mo}) to assess the drug-likeness of this series of compounds.²⁰ Instead of using cut-off rules as in the Lipinski rule-of-five, QED is based on a weighted desirability function to integrate physico-chemical properties of a drug candidate. QED ranges from 0 to 1 and represents the percentage of drug-likeness. It must be noted that QED was calculated for the chlorido complexes, *i.e.* the prodrug state. The Ru- and Os-series show QED_w^{mo} of 0.47–0.56 and 0.41–0.49, respectively (see Table S4† for pre-calculated molecular properties). Overall, the Os compounds are slightly less drug-like due to the higher chromatographic lipophilicity index. Interestingly, the QED_w^{mo} reflects largely the findings of the *in vitro* assays: **1A/B**, **3A/B** and **4A/B** were found to be the most active and also show a higher drug-likeness compared to **2A/B** and **5A/B**, which were found to be least active and similarly possess the lowest QED_w^{mo} . The QED_w^{mo} of the approved anticancer agents erlotinib (0.41), imatinib (0.41), tamoxifen (0.43), dasatinib (0.46) and sorafenib (0.51) are found in a similar QED range.

Furthermore, the fraction of the sp^3 -hybridized carbon atoms (F_{sp^3}) represents an additional parameter for predicting

the permeability of a drug candidate and seems of particular relevance to organometallic anticancer agents, since it is largely independent of the ionization state.²² In the present study, F_{sp^3} varies between 0.18 (0.22) and 0.31 (0.33) indicating good permeability. The values in the brackets are obtained by including the metal centre in the sp^3 -count due to its pseudo-tetrahedral geometry. Therefore, the obtained complexes are lipophilic and rigid structures, possessing ideal molecular properties for the development as orally active organometallic anticancer agents. Additionally, hydrolysis is suppressed in an acidic environment and the prodrugs are stable for $>7\text{d}$ under these conditions. As a consequence, the prodrug may stay intact when encountering the harsh conditions in the stomach and hydrolysis only occurs in the slightly basic environment of the lower intestine, blood stream or cytosol. Even if some decomposition should occur, the liberated ligands show gastric mucosal protective properties. Dimerization upon hydrolysis is believed to minimize deactivation by biomolecules (Scheme 2). However, the intrinsic charge of the prodrug state remains an uncertain factor with respect to oral bioavailability, which has yet to be evaluated experimentally in *in vivo* studies.

Conclusions

A series of organometallic Ru^{II} and Os^{II} *N*-substituted 2-pyridinecarbothioamides was synthesized and characterized. The complexes were efficiently obtained in a concise three-step synthesis and are easily derivatized. While the carbothioamide ligands are non-toxic (especially **1** showed a tolerability of >1 g kg^{-1} after oral administration *in vivo*),⁴⁰ complexation to organometallic ruthenium(II) and osmium(II) complexes yields highly cytotoxic agents, also in the intrinsically more chemoresistant SW480 and A549 cell lines. Increased lipophilicity and reduced steric demand of the complexes were determined as crucial parameters for elevated antiproliferative activity. The ruthenium compound **1A** shows a hydrolytic half-life of $t_{1/2} = 49$ min, whereas the osmium analogue **1B** is practically inert with respect to hydrolysis under cytoplasmic salt concentrations. ESI-MS experiments indicated that neither type of metal complexes forms adducts with small nucleophilic biomolecules probably due to their tendency to dimerize. Crystallographic studies with the nucleosome core revealed that **1A/B** and **3A/B** form exclusively histidine-adducts, while being devoid of DNA binding. The location and character of the binding sites on the histone octamer suggests interference with chromatin dynamics as a possible mode of action of these compounds and may explain the reduced cytotoxic activity of the sterically more demanding congeners. Importantly, the osmium compounds **1B** and **3B** stay intact under the applied conditions, while the ruthenium analogues **1A** and **3A** undergo ligand cleavage from the metal centre upon binding to histone proteins. Furthermore, ligand-based S \rightarrow O coordination exchange potentially allows for dual targeting, since the resulting *N,N*-bidentate complexes, which form at pH > 7 , seem to target DNA.⁹ Finally, these compounds are stable in hydrochloric acid for more than 7 days and seem to obey the rules for oral bioavailability.^{18–20,22} In view of the slower ligand exchange kinetics, the high *in vitro*

cytotoxicity and favourable QEDs, the small congeners of the osmium series, e.g. **3B**, seem therefore particularly promising for the development as the first orally active organometallic anticancer agents.

Acknowledgements

The authors gratefully acknowledge COST D39, CM1105, CM0902 and the "Johanna Mahlke née Obermann Foundation" for financial support. Alexander Roller is thanked for collection X-Ray diffraction data. Additionally, S. M. M. would like to thank Dr A. Egger for helpful discussions and the Mass Spectrometry Center, University of Vienna, for providing access to the Maxis UHR ESI TOF-MS instrument. X-ray data for the nucleosomal structures were collected at the Swiss Light Source (Paul Scherrer Institute, Villigen, Switzerland). C. A. D. and Z. A. are grateful to the National Medical Research Council, Ministry of Health, Singapore, for funding (grant NMRC/1312/2011).

Notes and references

- 1 C. S. Allardyce, P. J. Dyson, D. J. Ellis and S. L. Heath, *Chem. Commun.*, 2001, 1396–1397.
- 2 R. E. Morris, R. E. Aird, P. D. Murdoch, H. M. Chen, J. Cummings, N. D. Hughes, S. Parsons, A. Parkin, G. Boyd, D. I. Jodrell and P. J. Sadler, *J. Med. Chem.*, 2001, **44**, 3616–3621.
- 3 M. J. Clarke, *Coord. Chem. Rev.*, 2003, **236**, 209–233.
- 4 A. Habtemariam, M. Melchart, R. Fernandez, S. Parsons, I. D. H. Oswald, A. Parkin, F. P. A. Fabbiani, J. E. Davidson, A. Dawson, R. E. Aird, D. I. Jodrell and P. J. Sadler, *J. Med. Chem.*, 2006, **49**, 6858–6868.
- 5 C. G. Hartinger and P. J. Dyson, *Chem. Soc. Rev.*, 2009, **38**, 391–401.
- 6 W. Kandioller, C. G. Hartinger, A. A. Nazarov, C. Bartel, M. Skocic, M. A. Jakupec, V. B. Arion and B. K. Keppler, *Chem.–Eur. J.*, 2009, **15**, 12283–12291.
- 7 W. Kandioller, C. G. Hartinger, A. A. Nazarov, M. L. Kuznetsov, R. O. John, C. Bartel, M. A. Jakupec, V. B. Arion and B. K. Keppler, *Organometallics*, 2009, **28**, 4249–4251.
- 8 M. G. Mendoza-Ferri, C. G. Hartinger, M. A. Mendoza, M. Groessel, A. E. Egger, R. E. Eichinger, J. B. Mangrum, N. P. Farrell, M. Maruszak, P. J. Bednarski, F. Klein, M. A. Jakupec, A. A. Nazarov, K. Severin and B. K. Keppler, *J. Med. Chem.*, 2009, **52**, 916–925.
- 9 S. H. van Rijt, A. J. Hebden, T. Amaresekera, R. J. Deeth, G. J. Clarkson, S. Parsons, P. C. McGowan and P. J. Sadler, *J. Med. Chem.*, 2009, **52**, 7753–7764.
- 10 S. D. Shnyder, Y. Fu, A. Habtemariam, S. H. van Rijt, P. A. Cooper, P. M. Loadman and P. J. Sadler, *Med. Chem. Commun.*, 2011, **2**, 666–668.
- 11 P. Nowak-Sliwiska, J. R. van Beijnum, A. Casini, A. A. Nazarov, G. Wagnieres, H. van den Bergh, P. J. Dyson and A. W. Griffioen, *J. Med. Chem.*, 2011, **54**, 3895–3902.
- 12 F. Schmitt, J. Freudenreich, N. P. E. Barry, L. Juillerat-Jeanneret, G. Suss-Fink and B. Therrien, *J. Am. Chem. Soc.*, 2012, **134**, 754–757.
- 13 V. Pichler, P. Heffeter, S. M. Valiahdi, C. R. Kowol, A. Egger, W. Berger, M. A. Jakupec, M. Galanski and B. K. Keppler, *J. Med. Chem.*, 2012, **55**, 11052–11061.
- 14 M. Galanski, V. B. Arion, M. A. Jakupec and B. K. Keppler, *Curr. Pharm. Des.*, 2003, **9**, 2078–2089.
- 15 M. D. Hall and T. W. Hambley, *Coord. Chem. Rev.*, 2002, **232**, 49–67.
- 16 H. Choy, C. Park and M. Yao, *Clin. Cancer Res.*, 2008, **14**, 1633–1638.
- 17 S. M. Pond and T. N. Tozer, *Clin. Pharmacokinet.*, 1984, **9**, 1–25.
- 18 C. A. Lipinski, F. Lombardo, B. W. Dominy and P. J. Feeney, *Adv. Drug Delivery Rev.*, 1997, **23**, 3–25.
- 19 D. F. Veber, S. R. Johnson, H. Y. Cheng, B. R. Smith, K. W. Ward and K. D. Kopple, *J. Med. Chem.*, 2002, **45**, 2615–2623.
- 20 G. R. Bickerton, G. V. Paolini, J. Besnard, S. Muresan and A. L. Hopkins, *Nat. Chem.*, 2012, **4**, 90–98.
- 21 H. Bregman, P. J. Carroll and E. Meggers, *J. Am. Chem. Soc.*, 2006, **128**, 877–884.
- 22 Y. Yang, O. Engkvist, A. Llinas and H. Chen, *J. Med. Chem.*, 2012, **55**, 3667–3677.
- 23 C. Scolaro, A. Bergamo, L. Brescacin, R. Delfino, M. Cocchietto, G. Laurenczy, T. J. Geldbach, G. Sava and P. J. Dyson, *J. Med. Chem.*, 2005, **48**, 4161–4171.
- 24 Y. Fu, A. Habtemariam, A. M. Pizarro, S. H. van Rijt, D. J. Healey, P. A. Cooper, S. D. Shnyder, G. J. Clarkson and P. J. Sadler, *J. Med. Chem.*, 2010, **53**, 8192–8196.
- 25 S. M. Guichard, R. Else, E. Reid, B. Zeitlin, R. Aird, M. Muir, M. Dodds, H. Fiebig, P. J. Sadler and D. I. Jodrell, *Biochem. Pharmacol.*, 2006, **71**, 408–415.
- 26 R. E. Aird, J. Cummings, A. A. Ritchie, M. Muir, R. E. Morris, H. Chen, P. J. Sadler and D. I. Jodrell, *Br. J. Cancer*, 2002, **86**, 1652–1657.
- 27 P. J. Dyson, *Chimia*, 2007, **61**, 698–703.
- 28 J. P. Williams, J. M. Brown, I. Campuzano and P. J. Sadler, *Chem. Commun.*, 2010, **46**, 5458–5460.
- 29 F. Y. Wang, J. Bella, J. A. Parkinson and P. J. Sadler, *JBIC, J. Biol. Inorg. Chem.*, 2005, **10**, 147–155.
- 30 A. Bergamo, A. Masi, A. F. A. Peacock, A. Habtemariam, P. J. Sadler and G. Sava, *J. Inorg. Biochem.*, 2010, **104**, 79–86.
- 31 S. Chatterjee, S. Kundu, A. Bhattacharyya, C. G. Hartinger and P. J. Dyson, *JBIC, J. Biol. Inorg. Chem.*, 2008, **13**, 1149–1155.
- 32 B. Wu, M. S. Ong, M. Groessel, Z. Adhireksan, C. G. Hartinger, P. J. Dyson and C. A. Davey, *Chem.–Eur. J.*, 2011, **17**, 3562–3566.
- 33 C. A. Vock, W. H. Ang, C. Scolaro, A. D. Phillips, L. Lagopoulos, L. Juillerat-Jeanneret, G. Sava, R. Scopelliti and P. J. Dyson, *J. Med. Chem.*, 2007, **50**, 2166–2175.
- 34 W. H. Ang, L. J. Parker, A. De Luca, L. Juillerat-Jeanneret, C. J. Morton, M. Lo Bello, M. W. Parker and P. J. Dyson, *Angew. Chem., Int. Ed.*, 2009, **48**, 3854–3857.

- 35 B. Wu, P. Droge and C. A. Davey, *Nat. Chem. Biol.*, 2008, **4**, 110–112.
- 36 A. Dorcier, P. J. Dyson, C. Gossens, U. Rothlisberger, R. Scopelliti and I. Tavernelli, *Organometallics*, 2005, **24**, 2114–2123.
- 37 N. A. Meanwell, *J. Med. Chem.*, 2011, **54**, 2529–2591.
- 38 A. L. Noffke, A. Habtemariam, A. M. Pizarro and P. J. Sadler, *Chem. Commun.*, 2012, **48**, 5219–5246.
- 39 A. M. Pizarro, A. Habtemariam and P. J. Sadler, Activation Mechanisms for Organometallic Anticancer Complexes, in *Topics in Organometallic Chemistry*, ed. G. Jaouen and N. Metzler-Nolte, Springer, Heidelberg, 2010, vol. 32, pp. 21–56.
- 40 W. A. Kinney, N. E. Lee, R. M. Blank, C. A. Demerson, C. S. Sarnella, N. T. Scherer, G. N. Mir, L. E. Borella, J. F. Dijoseph and C. Wells, *J. Med. Chem.*, 1990, **33**, 327–336.
- 41 S. M. Meier, M. Hanif, W. Kandioller, B. K. Keppler and C. G. Hartinger, *J. Inorg. Biochem.*, 2012, **108**, 91–95.
- 42 M. H. Klingele and S. Brooker, *Eur. J. Org. Chem.*, 2004, 3422–3434.
- 43 M. A. Bennett and A. K. Smith, *J. Chem. Soc., Dalton Trans.*, 1974, 233–241.
- 44 W. A. Kiel, R. G. Ball and W. A. G. Graham, *J. Organomet. Chem.*, 1990, **383**, 481–496.
- 45 C. R. Martinez and B. L. Iverson, *Chem. Sci.*, 2012, **3**, 2191–2201.
- 46 W. H. Ang, E. Daldini, C. Scolaro, R. Scopelliti, L. Juillerat-Jeannerat and P. J. Dyson, *Inorg. Chem.*, 2006, **45**, 9006–9013.
- 47 F. Wang, H. M. Chen, S. Parsons, L. D. H. Oswald, J. E. Davidson and P. J. Sadler, *Chem.–Eur. J.*, 2003, **9**, 5810–5820.
- 48 Y. Fu, A. Habtemariam, A. M. B. H. Basri, D. Braddick, G. J. Clarkson and P. J. Sadler, *Dalton Trans.*, 2011, **40**, 10553–10562.
- 49 M. Groessl and P. J. Dyson, *Curr. Top. Med. Chem.*, 2011, **11**, 2632–2646.
- 50 M. A. Barry, C. A. Behnke and A. Eastman, *Biochem. Pharmacol.*, 1990, **40**, 2353–2362.
- 51 B. Wu, G. E. Davey, A. A. Nazarov, P. J. Dyson and C. A. Davey, *Nucleic Acids Res.*, 2011, **39**, 8200–8212.
- 52 D. A. Wolters, M. Stefanopoulou, P. J. Dyson and M. Groessl, *Metallomics*, 2012, **4**, 1185–1196.
- 53 M. J. McKeage, S. J. Berners-Price, P. Galettis, R. J. Bowen, W. Brouwer, L. Ding, L. Zhuang and B. C. Baguley, *Cancer Chemother. Pharmacol.*, 2000, **46**, 343–350.
- 54 M. R. Reithofer, A. K. Bytzek, S. M. Valiahdhi, C. R. Kowol, M. Groessl, C. G. Hartinger, M. A. Jakupcic, M. Galanski and B. K. Keppler, *J. Inorg. Biochem.*, 2011, **105**, 46–51.
- 55 A. K. Bytzek and C. G. Hartinger, *Electrophoresis*, 2012, **33**, 622–634.
- 56 K. Valko and P. Slegel, *J. Chromatogr., A*, 1993, **631**, 49–61.

3.2. Identification of the Structural Determinants for Anticancer Activity of an Organometallic Ru^{II}(Arene)-Peptide Conjugate

Samuel M. Meier,^{a,b} Maria Novak,^a Wolfgang Kandioller,^{a,b} Michael A. Jakupec,^{a,b} Vladimir B. Arion,^a Nils Metzler-Nolte,^c Bernhard K. Keppler,^{a,b} Christian G. Hartinger^{a,b,d}

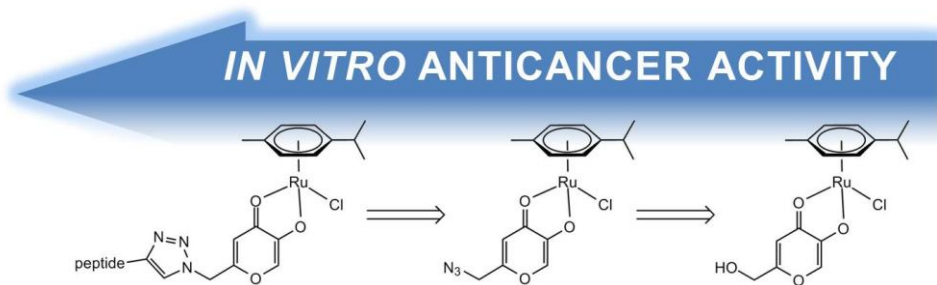
Chemistry – A European Journal, submitted.

^a University of Vienna, Institute of Inorganic Chemistry, Waehringer Str. 42, A-1090 Vienna, Austria.

^b University of Vienna, Research Platform “Translational Cancer Therapy Research”, Waehringer Str. 42, A-1090 Vienna, Austria.

^c Ruhr-University Bochum, Inorganic Chemistry I-Bioinorganic Chemistry, Faculty of Chemistry and Biochemistry, Universitaetstr. 150, D-44801 Bochum, Germany.

^d University of Auckland, School of Chemical Sciences, Private Bag 92019, Auckland 1142, New Zealand.



Identification of the Structural Determinants for Anticancer Activity of an Organometallic Ru^{II}(Arene)–Peptide Conjugate

Samuel M. Meier,^[a,b] Maria Novak,^[a] Wolfgang Kandioller,^[a,b] Michael A. Jakupec,^[a,b] Vladimir B. Arion,^[a] Nils Metzler-Nolte,^[c] Bernhard K. Keppler,^[a,b] Christian G. Hartinger*^[a,b,d]

Abstract: Organometallic Ru^{II}(arene)–peptide bioconjugates with potent *in vitro* anticancer activity are rare. In this project, we have prepared a conjugate of a Ru^{II}(arene) complex with the neuropeptide [Leu⁵]-enkephalin by Cu-catalyzed azide-alkyne coupling (CuAAC, "click" chemistry). [Chlorido(η^6 -p-cymene)(5-oxo- κ O-2-((4-[(*N*-tyrosinyl-glycinyll-glycinyll-phenylallanyl-leucinyll-NH₂)propanamido]-1*H*-1,2,3-triazol-1-yl)methyl)-4*H*-pyronato- κ O)ruthenium(II)] (**8**) shows antiproliferative activity in human ovarian carcinoma cells with an IC₅₀ value as low as 13 μ M, whereas the peptide or the Ru moiety alone are hardly cytotoxic. The conjugation

strategy for linking the Ru^{II}(cym) (cym = η^6 -p-cymene) moiety to the peptide involved *N*-terminal modification of an alkyne-[Leu⁵]-enkephalin with a 2-(azidomethyl)-5-hydroxy-4*H*-pyran-4-one linker, using a Cu^I azide-alkyne cycloaddition reaction, and subsequent metallation with the Ru^{II}(cym) moiety. The Ru^{II}–bioconjugate was characterized by high resolution top-down electrospray ionization mass spectrometry (ESI-MS) with regard to peptide sequence, linker modification and metallation site. Notably, complete sequence coverage was obtained and the Ru^{II}(cym) moiety was confirmed to be coordinated to the pyronato linker.

The Ru^{II}–bioconjugate was analyzed with respect to cytotoxicity-determining constituents, and through the bioconjugate models [{2-(azidomethyl)-5-oxo- κ O-4*H*-pyronato- κ O}chlorido(η^6 -p-cymene)ruthenium(II)] (**5**) and [chlorido(η^6 -p-cymene){5-oxo- κ O-2-((4-(phenoxymethyl)-1*H*-1,2,3-triazol-1-yl)methyl)-4*H*-pyronato- κ O)ruthenium(II)] (**6**) the Ru^{II}(cym) fragment with a triazole-carrying pyronato ligand was identified as the minimal unit required to achieve *in vitro* anticancer activity.

Keywords: anticancer activity • bioorganometallic chemistry • mass spectrometry • ruthenium complexes • peptide bioconjugate

- [a] S.M. Meier, M. Novak, Dr. W. Kandioller, Dr. Dr. M.A. Jakupec, Prof. Dr. V.B. Arion, Prof. Dr. Dr. B.K. Keppler, Prof. Dr. C.G. Hartinger
Institute of Inorganic Chemistry
University of Vienna
Währinger Strasse 42, 1090 Vienna (Austria)
- [b] S.M. Meier, Dr. W. Kandioller, Dr. M.A. Jakupec, Prof. Dr. Dr. B.K. Keppler, Prof. Dr. C.G. Hartinger
Research Platform "Translational Cancer Therapy Research"
University of Vienna
Währinger Strasse 42, 1090 Vienna (Austria)
- [c] Prof. Dr. N. Metzler-Nolte
Inorganic Chemistry I-Bioinorganic Chemistry, Faculty of Chemistry and Biochemistry
Ruhr-University Bochum
Universitätsstrasse 150, 48801 Bochum (Germany)
- [d] Prof. Dr. C.G. Hartinger
School of Chemical Sciences
University of Auckland
Private Bag 92019, Auckland 1142 (New Zealand)
Fax: (+64) 9-3737-599 ext 87422
E-mail: c.hartinger@auckland.ac.nz
Supporting information for this article is available on the WWW under <http://www.chemeurj.org/> or from the author.

Introduction

Peptides are useful carriers for the specific accumulation of drugs in desired tissues and/or cell compartments.^[1-5] In diagnostic and therapeutic metallodrug research,^[6] the approach of tagging metal fragments to peptides is an emerging targeting strategy and several recent investigations were dedicated to organometal–peptide conjugation strategies.^[7-17] The peptide carrier is typically obtained by solid phase synthesis, and the metallodrug is conjugated to the peptide either on solid support or in solution after peptide cleavage from the resin. The metal can be conjugated directly *via* a suitable amino acid, or a linker with metal-chelating properties can be incorporated into the peptide sequence.^[14,18] When pursuing the latter strategy, *N*-terminal and intra-sequence derivatizations are most commonly used for metal-tagging. Moreover, most of the reported metal–peptide bioconjugates are synthesized with inert linkers.^[14] Based on these strategies, encouraging

but rare examples of anticancer active metal-peptide bioconjugates were reported with different metal systems including ferrocenoyl-dipeptides,^[19] dicobalt hexacarbonyl tagged to alkyne-modified enkephalin,^[16] [Mn(Cp)(CO)₃] tagged to the cell-penetrating peptides sC18 or hCT(18-32)-k7,^[12,15,20] Rh^{III}(Cp*)-sandwich bioconjugates,^[7] gold(I) bioconjugates^[21] or platinum(IV) bioconjugates of TAT, pseudo-neurotensin or octreotate.^[8,22]

Surprisingly, only little is known about bioconjugates of anticancer half-sandwich Ru^{II} and Os^{II} organometallics with peptide carriers. This is probably related to synthetic difficulties arising from hydrolysis of the metal-halido bond in aqueous solution, which is a crucial activation parameter for these classes of anticancer metallodrugs in a biological setting.^[23] The few existing investigations show that loading of the metallodrug on a peptide carrier is associated with a decrease in antiproliferative activity compared to the non-conjugated small metallodrug.^[8,9] In particular, conjugation of an Os^{II}(arene) picolinate moiety to an octaarginine sequence led to a substantial activity decrease and moderate cytotoxicity was only obtained in protein depleted fetal calf serum.^[9] Moreover, conjugation of an imidazole-modified dicarba analogue of octreotide to a Ru^{II}(arene)(triphenylphosphine) moiety also resulted in modest cytotoxic activity, which was approximately 4-fold lower than of the analogous small anticancer metallodrug.^[24]

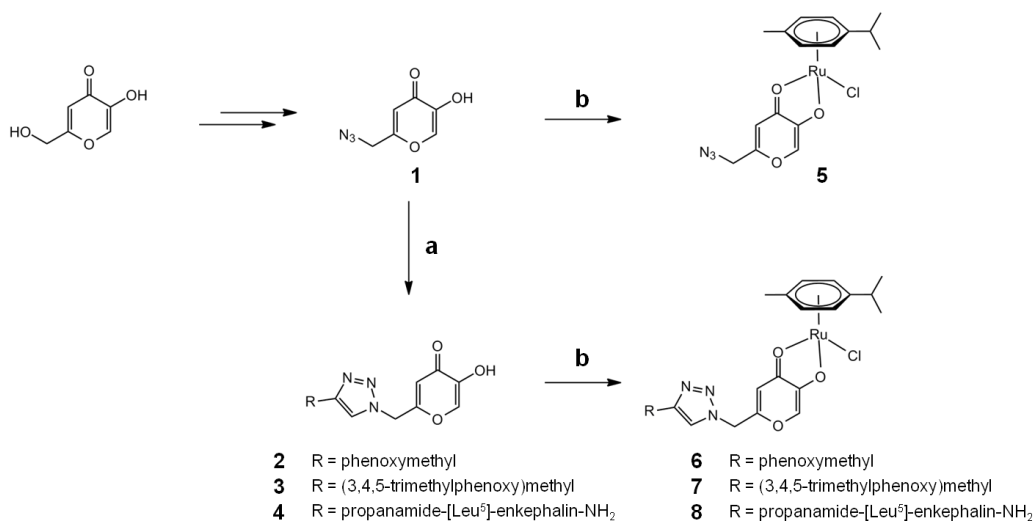
The apparent lack of anticancer active organometallic Ru^{II}-peptide conjugates from potent metallodrugs prompted us to investigate an appropriate model system with the aim of identifying its cytotoxicity-determining building block(s). The neuropeptide [Leu⁵]-enkephalin was chosen for this purpose, and an *N*-terminal alkyne derivative thereof was further modified by a Cu^I assisted alkyne-azide cyclization (CuAAC) using 2-(azidomethyl)-5-hydroxy-4*H*-pyran-4-one as a linker to the organometallic Ru^{II} moiety. Hydroxypyrones are well known metal chelators offering *O,O*-bidentate coordination,^[25] and recent developments involving hydroxypyrones as ligands for organometallic Ru^{II} and Os^{II} arene compounds with anticancer properties showed intriguing results with respect to *in vitro* antitumor activity.^[26-32] For example, dinuclear ruthenium bis-pyridonato complexes display cytotoxic activity in cell culture assays in dependence of the spacer length

separating the two Ru-chelating pyridone moieties. In contrast, several mononuclear organometallic Ru^{II} compounds based on *O,O*-bidentate pyrones were found to exhibit anticancer activity only in the high micromolar range whereas a substantial increase in activity was observed with *S,O*-bidentate thiopyrones, which have been less investigated so far, however.^[29,30,32-34] Based on the mentioned components, *i.e.*, Ru^{II}(arene), hydroxypyronone, triazole linker and peptide, we aimed to elucidate the structural determinants for anticancer activity in human tumor cells.

Results and Discussion

Synthesis and Characterization. Peptide carrier systems are an attractive means for obtaining specificity with respect to accumulation in a certain (cancer) tissue or even a specific cell compartment, and they are being studied as promising vectors in the discovery and design of metal-based anticancer agents with targeting properties.^[2,14] Most often, the cytotoxic moiety is conjugated to the peptide using an inert linker with the aim of generating a cytotoxic metal-peptide bioconjugate. In the case of organometallic Ru^{II}- and Os^{II}(arene) compounds, conjugation to peptides often results in a significant reduction of the antiproliferative activity of the metal-peptide bioconjugate compared to the small molecule metallodrug.^[8,9] Therefore, it was aimed to investigate a Ru^{II}(arene)-based bioconjugate exhibiting antiproliferative activity *in vitro* and to identify the cytotoxicity-determining building block by comparing the antiproliferative activity of the bioconjugate with lower molecular weight fragments of related structural components.

The linker for the conjugation of the Ru^{II}-arene fragment to the peptide, *i.e.*, 2-(azidomethyl)-5-hydroxy-4*H*-pyran-4-one (**1**), was obtained in two steps starting from kojic acid by adapting a published procedure.^[35] Compound **1** contains two functional moieties of interest: The pyrone scaffold permits anionic *O,O*-bidentate metal coordination, and the azide allows facile and selective modification of the ligand. Importantly, the azide was modified in a single step by a Cu^I-catalyzed Huisgen 1,3-dipolar cycloaddition (Cu-AAC, "click" chemistry, see Scheme 1).^[36-38] The cycloaddition involves the reaction of an azide and a terminal alkyne and allows derivatization of **1** with virtually any molecule containing a terminal alkyne. Cu^I catalysis yields regioselectively 1,4-substituted triazoles *via*



Scheme 1. Synthetic pathway to neutral pyronato complexes, starting from kojic acid. Step (a) features a Cu^I-catalyzed 1,3-dipolar cycloaddition with a terminal alkyne. The complexation step (b) involves deprotonation of the hydroxypyronone prior to coordination leading to neutral [Ru^{II}(η⁶-p-cymene)(Pyr)Cl] complexes, where Pyr is the pyronato ligand.

transient formation of a Cu-acetylide species and represents a powerful tool for extending SARs of the pyronato class of metallodrugs. In metal-based anticancer research, the 1,2,3-triazole pharmacophore is not yet well established in the therapeutic context, although its value in diagnostics is well appreciated.^[11,39] Cu^I was prepared *in situ* from Cu^{II} sulfate and sodium ascorbate, and the cycloaddition reaction products **2** and **3** were isolated in moderate yields. The molecular structure of **2** was obtained by single crystal X-ray diffraction analysis confirming the formation of the 1,4-substituted triazole (Figure S1). The alkyne-modified [Leu⁵]-enkephalin was prepared adapting a literature procedure.^[16] The cycloaddition reaction with **1** was carried out on solid support, *i.e.*, a suspension of the Rink amide resin was treated with 2 equiv CuI and an excess of nitrogen base. Diethyldithiocarbamate (Cupral) proved to be suitable for efficiently removing Cu from the suspension after the reaction. The desired hydroxypyrono-modified [Leu⁵]-enkephalin **4** was obtained in 58% overall yield after cleavage from the Rink amide resin.

Complexation of the hydroxypyrones to the Ru^{II}(cym) moiety was achieved by deprotonation of the ligand and subsequent addition of 0.5 equiv bis[dichlorido(η^6 -p-cymene)ruthenium(II)] in dry methanol under an inert atmosphere, similarly to earlier studies.^[31] Salt impurities were removed by dissolving the reaction product in DCM, followed by filtration. In general, subsequent precipitation yielded analytically pure products of **5**, **6** and **7** in moderate to high yields (63–82%). The peptide conjugate **8** was treated similarly, since an attempt of performing the cycloaddition reaction with **5** and the alkyne-modified [Leu⁵]-enkephalin on solid support was unsuccessful, probably due to the harsh conditions used during work-up and the pyronato organometallics being known to be acid labile.^[32] Complexes **5**, **6** and **7** were characterized by 1D/2D NMR, UHR ESI-TOF MS and elemental analysis. The peptide conjugate **8** was characterized by 1D/2D NMR, UHR ESI-TOF MS and HPLC-MS (see Figure S3 for the analytical HPLC-MS experiment).

The modification at the azide moiety is directly detectable in the ¹H-NMR spectrum (recorded in *d*₆-DMSO), by comparing in particular the H-7 (CH₂) signals (see Figure S1 in the Supporting Information for the NMR numbering scheme). The H-7 signal of **1** displays a singlet with a chemical shift of 4.42 ppm. Conversion of the azide into a 1,4-substituted triazole is characterized by a down-field shift of the H-7 singlet (CH₂) to 5.61 ppm. The detection of an additional singlet at ~8.3 ppm in **6**, **7** and **8** is indicative of H-8 (H_{Triaz}), the proton in the 1,4-substituted triazole ring. Upon complexation, the ¹H-NMR signals corresponding to H-7 and H-8 did not shift significantly. However, the H-2 signal underwent an up-field shift by ~0.2 ppm. This indicates that the pyronato moiety but not the triazole nitrogen is involved in coordination to the metal, corresponding to a pendant design of triazole complexes, in contrast to the “click-to-chelate” strategy, where the triazole is directly involved in metal-binding.^[11,40] *O,O,N*-Chelation is sterically improbable as can be deduced from Figure 1 and S1. Finally, the chemical shifts of the coordinated cym and pyrone moieties are generally in good agreement with those of the close analogue [chlorido(η^6 -p-cymene)(2-hydroxymethyl-5-oxo-4*H*-pyronato)ruthenium(II)].^[31]

X-ray Diffraction Analysis. Single crystals suitable for X-ray diffraction analysis were obtained for **5** by slow diffusion of *n*-pentane into dichloromethane and the complex displays the characteristic half-sandwich “piano-stool” configuration. The crystal structure confirms anionic *O,O*-bidentate chelation of the pyronato moiety to the metal center yielding a neutral monochlorido complex (Figure 1). Details on crystal cell parameters and selected bond lengths, angles and torsion angles are listed in the Supporting Information (Tables S1 and S2). Interestingly, both enantiomers were observed at a 1:1

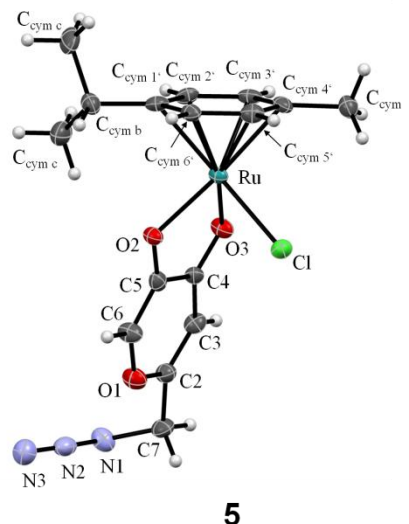


Figure 1. The molecular structure of the *R*-enantiomer of **5** is shown including the general numbering scheme. The ellipsoids are drawn at 50% probability level.

ratio in the crystal lattice of **5**. The asymmetric unit of **5** additionally contains two stereo-isomers, which feature varying bond lengths in the first coordination sphere (Figure S2). The isoform **5B** shows shorter Ru–O3 and Ru–Cl bond lengths, but longer Ru–O2 and Ru–centroid bond lengths compared to **5A**. In general, the bond lengths and angles are on the same order as observed for related Ru^{II}-pyronato and –pyridonato complexes.^[27,31] It is noteworthy, that the azide does not degrade in the presence of Ru^{II}.

Top-Down ESI-MS Characterization of the Half-Sandwich Ru^{II} Peptide Bioconjugate. In addition to NMR and UHR ESI-TOF MS analysis, the peptide bioconjugate **8** was characterized by tandem mass spectrometric methods in a top-down approach using both ESI-IT and UHR ESI-TOF MS. In principle, top-down MS allows the determination of the sequence of amino acids and of the site of pyrone modification and metal coordination. Investigations were performed using collision-induced dissociation (CID) and electron transfer dissociation (ETD, only for IT), which often deliver complementary information due to underlying differences in the fragmentation mechanisms.^[41,42] In general, ESI-IT- and ESI-TOF-MS of **8** yields singly- and doubly-charged species corresponding to **8**_{hydr}, [**8**_{hydr} + H]²⁺ and [**8**_{hydr} + Na]²⁺ (all experimental and theoretical signals are listed in Table S3). The notation **8**_{hydr} describes the mass signal corresponding to [**8** – Cl]⁺.

ETD relies on the transfer of electrons from a radical anion to the analyte and leads to specific fragmentations of the peptide backbone.^[42] ETD of the doubly-charged ion [**8**_{hydr} + H]²⁺ yields primarily three species; a charge-reduced species [**8**_{hydr} + H]⁺, a [(cym)Ru(C₆H₄O₃)]⁺ radical cation and the most abundant mass signal corresponding to [**8**_{hydr} – (cym)]⁺. Therefore, it seems that ETD fragmentation leads primarily to arene cleavage, probably induced by a one-electron reduction of the metal during the electron transfer process (Figure S4). This result was underlined by additional CID investigation of the isolated charge-reduced species (CRCID)^[43] corresponding to [**8**_{hydr} – (cym)]⁺. The most abundant signal in the mass spectrum corresponds to [**8**_{hydr} – (cym) – GGFL]⁺. This species was found at *m/z* 512.02 suggesting a Ru^I species, since Ru^{II} would have led to the detection of a signal at *m/z* 511.02. The mass signal of [(cym)Ru(C₆H₄O₃)]⁺ in the ETD spectrum proves that the pyrone-modified [Leu⁵]-enkephalin coordinates *via* the pyronato moiety to the metal center, however, no information on the peptide sequence was obtained. On the other hand, CID of the **8**_{hydr} parent signal with 75 eV yielded a

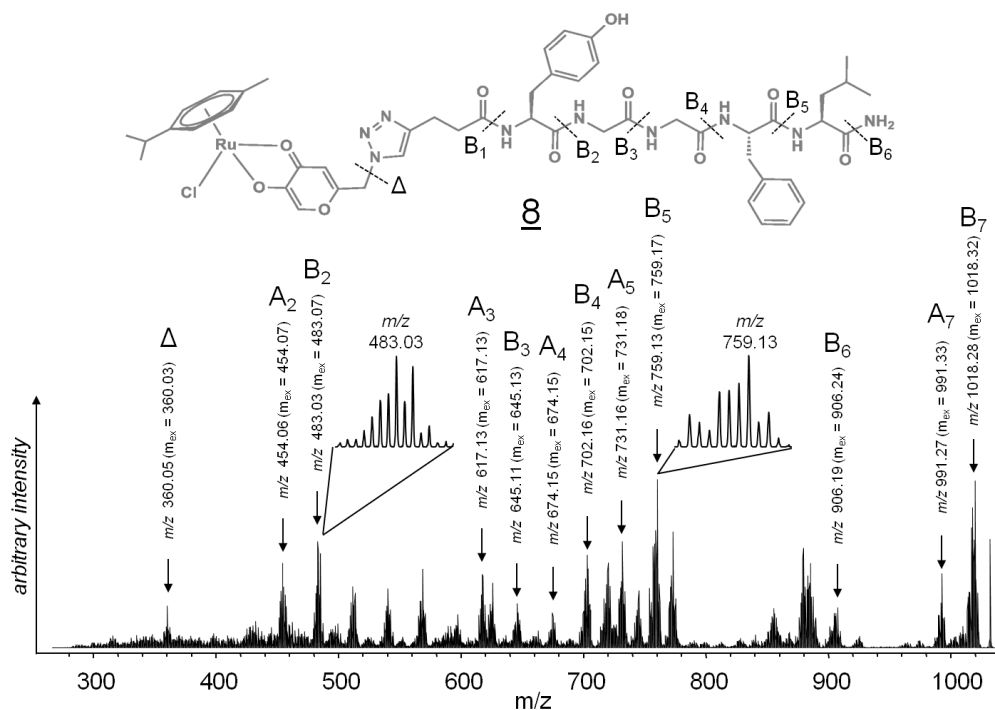


Figure 2. CID-tandem mass spectrum of **8**_{hydr} measured on an ESI-IT MS using a collision energy of 75 eV. The identified fragments were labeled according to classical peptide fragment nomenclature. β denotes the radical cation, whereas capital letters denote metallated fragments.

more detailed fragmentation picture (Figure 2). The IT and TOF instruments yielded similar fragmentation patterns in the CID spectra, but the IT instrument allowed higher fragmentation efficiency. In fact, complete sequence coverage was obtained confirming the amino acid sequence of the modified [Leu⁵]-enkephalin. CID leads to strand brakes of the peptide backbone at the amide CO–N bond, which generates predominately positively charged acylium ions corresponding to b-fragments and the complementary amine y-fragments.^[41] In the context of metallated peptides, capital letters are used to denote metallated peptide fragments.^[44] The occurrence of a complete set of B-fragments indicates that the charged metal must be near the N-terminus, where [Leu⁵]-enkephalin was modified with the pyrone. Again, the radical β -fragment corresponding to [(cym)Ru(C₆H₄O₃)]⁺ (m/z 360.0292, m_{ex} = 360.0298, 2 ppm) underlines that the metal–peptide conjugate is formed *via* metal coordination to the pyronato moiety. Additional secondary fragmentation products (A-fragments) were observed, which were assigned to aldimine ions.

Stability in Aqueous Solution. Aqueous stability of metallodrugs destined for clinical applications is a crucial prerequisite for drug development. In addition, when considering the class of (thio)pyr(id)onato metallodrugs the ability to resist ligand cleavage from the metal was determined as a second key parameter for obtaining cytotoxic compounds.^[29,45] Therefore, the stability of the organometallic complexes **5**, **6** and the bioconjugate **8** was investigated in aqueous solution by ESI-IT mass spectrometry over a period of 48 h. The stability of **7** was not determined because the solubility in aqueous solution is insufficient for performing cytotoxicity assays. Compounds **5** and **8** proved to be stable over the entire incubation period. For each compound the characteristic **M**_{hydr} mass signal was detected corresponding to [M–Cl]⁺, where **M** = **5**, **6**, **8**. An additional signal at m/z 373.94 ± 0.02 (m_{ex} = 374.03, < 5%) was detected in the mass spectrum of **5**, which can be assigned to a species formed through loss of N₂ from the azide during the spraying process. Compound **6** turned out to be somewhat less stable in aqueous solution. After 24 h, ligand cleavage led to the formation of the dinuclear species [Ru₂(cym)₂(μ -OCH₃)₃]⁺ (6%), which increased to 15% relative to the **6**_{hydr} mass signal after 48 h

(Figures 3 and S5). The μ -methoxide probably stems from the sample preparation, which involved dilution with H₂O : MeOH (1 : 1). Aliquots of the same incubation solutions were additionally measured on the MaXis UHR ESI-TOF, and the identities of the **M**_{hydr} complexes were confirmed with an accuracy of ≤ 5ppm as listed in the experimental part.

In vitro Anticancer Activity. Organometallic Ru^{II} arene anticancer agents containing bidentate (thio)pyronato ligands exhibit an intriguing anticancer activity profile. The *in vitro* cytotoxicity of these metallodrugs as expressed by the IC₅₀ value covers a wide range from inactive to active representatives. The anticancer activity of these compounds depends specifically on the ligand choice, and notably hydroxypyrono derivatives are generally non-cytotoxic.^[30,31,34] Altering the inner coordination sphere from *O,O*- to *S,O*-chelates leads to a dramatic activity increase and IC₅₀ values in the low μ M range.^[31] Furthermore, the stability of the complexes in the presence of biomolecules is the second parameter determining anticancer activity.^[29,45] When peptide carrier systems are employed, organometallic Ru^{II} and also Os^{II} conjugation often results in a decrease of the antiproliferative activity compared to the structurally related small molecule metallodrugs.^[8,9] In the present study, the antiproliferative activity was evaluated in ovarian (CH1), colon (SW480) and

Table 1. IC₅₀ (50% inhibitory concentration) values in three human cancer cell lines after 96 h.

Compound	IC ₅₀ (μ M)		
	CH1	SW480	A549
Ru-kojic acid [a]	234 ± 21	429 ± 10	n.d. [b]
1	264 ± 2	> 640	> 640
2	194 ± 11	> 640	> 640
4	> 640	> 640	> 640
5	168 ± 35	224 ± 24	520 ± 46
6	7.6 ± 2.7	170 ± 32	159 ± 52
8	13 ± 5	> 320	> 320

[a] taken from ref. [31], [b] not determined.

non-small lung (A549) cancer cell lines by means of the colorimetric MTT assay.

The bioconjugate precursor **4** is anticancer inactive *in vitro*, as are the ligands **1** and **2** and the hydrolysis product of the Ru^{II}(cym) moiety, *i.e.*, [Ru₂(cym)₂(μ-OH)₃]⁺.^[29,32] In contrast, tagging the Ru^{II}(cym) moiety onto **4** resulted in the highly antiproliferative bioconjugate **8** with an IC₅₀ value of 13 ± 5 μM in chemo-sensitive CH1 cells. This represents, to the best of our knowledge, the first example of a half-sandwich Ru^{II} bioconjugate with antiproliferative activity in the low μM range. The selective activity in the CH1 cell line parallels the findings with previously reported pyronato complexes.^[29-31] It must be noted that pyronato metallodrugs display modest anticancer activity *in vitro*, while the cytotoxicity of the pyronato-based bioconjugate **8** is of the same order of magnitude as that of *S,O*-bidentate thiopyronato complexes.^[29,31] Roughly comparable to the cytotoxicity of **8** in CH1 cells is that of the bioconjugate model **6**, displaying an IC₅₀ value of 7.6 ± 2.7 μM. On the other hand, compound **5** featuring the free azide is hardly active *in vitro*. Within this series, the relation between lipophilicity, solubility and *in vitro* activity seems quite subtle, as **7** was found to be too poorly soluble in aqueous media for performing cytotoxicity assays. In our approach, triazole formation in a pendant design seems to be an important parameter with respect to antiproliferative of the Ru^{II} bioconjugate based on non-bioactive pyrones. In fact, the antiproliferative activity seems to be independent of the peptide carrier, as **6** and **8** show similar anticancer activity *in vitro*. Consequently, it is suggested that Ru^{II}(cym) in combination with the triazolyl-pyronato linker represents the anticancer-determining building block, which is also supported by the fact that **4** and **5** are inactive *in vitro*. In principle, this might offer a promising bioconjugation strategy to other cell-penetrating peptides with potential retention of the biological activity.

Reactivity towards Biomolecules. Encouraged by the promising results obtained in the *in vitro* assay, the interaction of the bioconjugate **8** and the model complexes **5** and **6** with small biomolecules and proteins was studied. Since metallodrugs would usually be administered intravenously, they may react with a broad range of biomolecules in the blood stream, in particular plasma proteins, before reaching the drug target. In order to estimate the reactivity of **5**, **6** and **8** toward biological nucleophiles, they were incubated with the amino acids glycine (Gly), l-cysteine (Cys) and l-histidine (His) and the DNA model 9-ethylguanine (EtG) as well as the proteins ubiquitin (ub) and cytochrome-c (cyt). Mass spectrometry has emerged in recent years as a powerful technique for the analysis of such interactions between metallodrugs and biomolecules, both with respect to the nature of binding as well as location of binding sites.^[44-50] The experiments were performed with ESI-ion trap (IT) and UHR ESI-time-of-flight

(TOF) mass spectrometry. ESI-IT MS was employed for analyzing small molecules, whereas high resolution ESI-TOF MS was used for protein interaction studies.

Similarly to **5** and **6**, the reactions of the bioconjugate **8** with amino acids are characterized by ligand cleavage from the metal and formation of [Ru(aa)(cym)]⁺ (aa = amino acid) adducts similarly to related Ru^{II}-pyr(id)onato metallodrugs.^[27,45] Such a behavior was observed in the presence of Cys and His, but also to some extent in the presence of Gly (Figure S6 and Table S3). Cys turned out to be the most potent amino acid for inducing quantitative ligand cleavage, which may be related to the *trans* effect of the thiol group. Initially, several Cys adducts were detected in the mass spectra, which convert after 48 h, however, to the thermodynamically most stable adduct corresponding to [Ru(cym)(Cys)]⁺. His with its imidazole side chain was also able to form metal adducts *via* ligand cleavage, although the kinetics of this reaction were slightly slower than for Cys. His leads to quantitative depletion of the signals assignable to **5**_{hydr}, **6**_{hydr} and **8**_{hydr} in the mass spectra within 6 h. The conjugate model **6**_{hydr} was slightly more resistant to ligand cleavage, which was reflected in a lower percentage of [Ru(cym)(His)]⁺ adduct formation (68%) compared to **5**_{hydr} and **8**_{hydr} (> 85%) after 1 h. In contrast to previous reports, the reaction with Gly was also characterized by adduct formation and ligand cleavage from the metal, albeit to a low extent. Interestingly, mono- and bis-adducts were formed during the reaction corresponding to [Ru(cym)(Gly)]⁺ and [Ru(cym)(Gly)₂]⁺. The occurrence of bis-adducts is probably related to the reduced steric demand of the amino acid. However, Gly was not able to completely consume the free complexes over an incubation period of 48 h (Figure S6). Binding of Gly was least pronounced for the bioconjugate **8** possibly due to steric reasons. Furthermore, the reaction with EtG, used as a DNA model, resulted in the formation of [M_{hydr} + EtG]⁺ adducts (M = **5**, **6** and **8**) and was characterized by ligand retention, which can be explained by the mono-dentate character EtG. Despite the increased molar ratio (2 : 1 EtG to Ru^{II}), EtG adducts did not exceed a relative abundance of 36% (relative to M_{hydr}) and only mono-adducts were observed within 48 h. EtG adduct formation seems to depend again on the steric demand of the ligand, with **5** forming 36% of adducts after 48 h and the bioconjugate **8** forming only 6% adducts with EtG. The following trend for the reactivity toward EtG was observed: **5** > **6** > **8**. The stability of the [6_{hydr} + EtG]⁺ adduct in the presence of His and Gly was additionally investigated (Figure S7). For this purpose, **6** was incubated with EtG for 5 d prior to the addition of 2 equiv of either Gly or His. Addition of His led to quantitative conversion of **6**_{hydr} and [6_{hydr} + EtG]⁺ to the [Ru(cym)(His)]⁺ adduct within 3 h. Addition of Gly did not entirely deplete the [6_{hydr} + EtG]⁺ adduct within 24 h. However, Gly seems to react with **6**_{hydr} forming a mixed ligand adduct

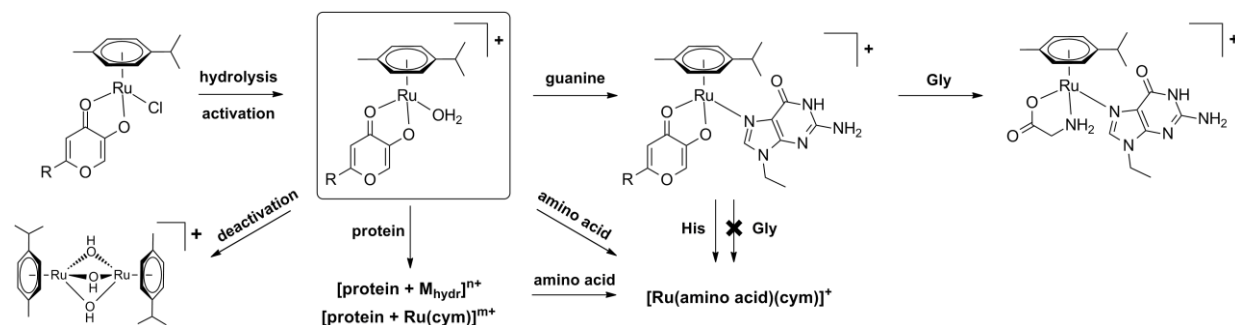


Figure 3. The investigated metabolic pathways of pyronato complexes are illustrated. Organometallic Ru^{II} pyronato complexes have to be considered as anticancer prodrugs, which are activated by hydrolysis. For details regarding the stability of the [ub + Ru(cym)]⁺ adduct in the presence of amino acids and other biological nucleophiles, see ref. [45].

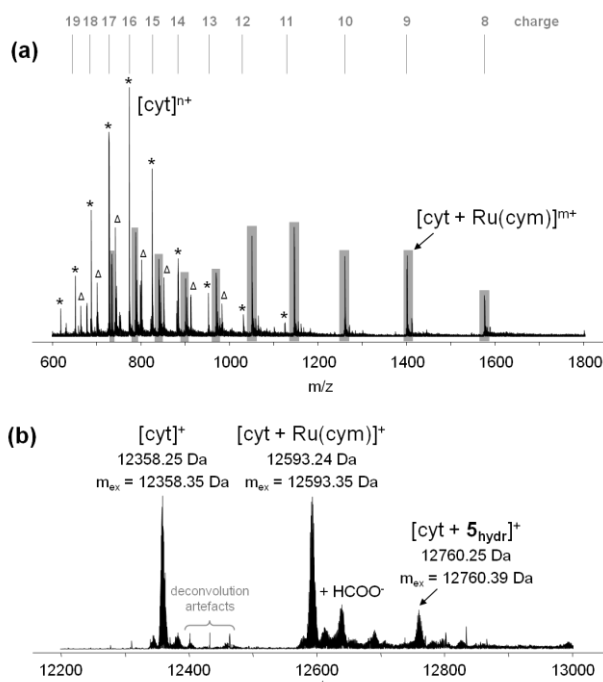


Figure 4. (a) Charge state distributions observed in the broadband ESI mass spectrum of the incubation mixture containing **5** and cyt at a 3 : 1 metal-to-protein ratio. Free cyt is detected at high charge states (*) indicating complete loss of the tertiary structure, similarly to $[\text{cyt} + 5_{\text{hydr}}]^+$ (Δ), which can only bind in a mono-dentate coordination mode. On the other hand, the lower charge state distribution of the $[\text{cyt} + \text{Ru}(\text{cym})]^+$ adduct (grey) indicates the cross-linking ability of the $\text{Ru}^{\text{II}}(\text{cym})$ moiety. The spectrum was recorded under denaturing conditions. (b) The deconvoluted UHR ESI-TOF mass spectrum of the same experiment is shown. A cyt adduct with intact 5_{hydr} was detected at m/z 12760.25.

with free EtG corresponding to $[\text{Ru}(\text{cym})(\text{EtG})(\text{Gly})]^+$, which becomes the most abundant species after 24 h. The absence of an analogous adduct upon addition of His indicates a possible tridentate binding mode of His to the metal.

The subtle differences in reactivity of the bioconjugate **8** (and its cytotoxic model **6**) on the one hand and **5** on the other hand with small biomolecules suggest that slower kinetics of adduct formation and ligand cleavage from the metal are associated with increased *in vitro* cytotoxic activity, which is also in accordance with an earlier study on pyronato metallodrugs.^[45]

Moreover, it seems that the compounds in this study interact preferentially with amino acids rather than with nucleobases, suggesting that Ru^{II} metallodrugs containing the pyronato scaffold probably have a cellular target different from DNA and more likely related to proteins (Figure 3). Consequently, **5**, **6** and **8** were additionally analyzed with respect to their reactivity toward the proteins ubiquitin (ub) and cytochrome-c (cyt) by using UHR ESI-TOF mass spectrometry. Ub and cyt were chosen in order to elucidate the general reactivity of the investigated metallodrugs toward proteins.

Binding to ub was found to be accompanied by ligand cleavage from the metal, giving rise to the characteristic $[\text{ub} + \text{Ru}(\text{cym})]^+$ adducts when incubating ub with the bioconjugate **8** or its models **5** or **6** (Table S3). Ub features two probable binding partners for a Ru^{II} metal, namely the N-terminal methionine (Met1) and histidine at position 68 (His68). It was suggested that Met1 may act as a bidentate binding partner to a metallodrug,^[48,51] which may increase reaction kinetics and also adduct stability. Mono-adducts are most probably formed by metallation of Met1, as recently determined in a top-down ESI-MS analysis of the $[\text{ub} + \text{Ru}(\text{cym})]^+$ adduct.^[52] The ESI-TOF MS experiments yielded detailed information on the adduct types, *i.e.* bis-adducts corresponding to $[\text{ub} + 2\text{Ru}(\text{cym})]^+$ were also detected in small amounts indicating metallation of His68 to a minor degree. Interestingly, bis-

adducts with ub were detected only at 1% and 6% relative abundance for **8** and **6**, respectively, whereas they were present at 12% relative abundance for **5**.

The incubation with cyt at a molar ratio of 3 : 1 was characterized by two types of mono-adducts. Similarly to the experiments with ub, the most abundant adduct corresponds to $[\text{cyt} + \text{Ru}(\text{cym})]^+$. Despite the addition of a molar excess of the metallodrug, bis-adducts were not observed. Additional M_{hydr} -cyt adducts were observed in all three cases and were characterized by ligand retention, *e.g.*, $[\text{cyt} + 5_{\text{hydr}}]^+$ (13%, Figure 4a). After 48 h, the relative abundance of the combined mono-adducts formed with the bioconjugate **8** and the model **6** corresponds to $41 \pm 4\%$, compared to 64% for the inactive model **5**. The kinetics of adduct formation are significantly lower for cyt than for ub, which is attributed to the presence of different binding partners in these proteins. Cyt contains three solvent accessible metal binding sites, *i.e.*, His26, His33 and Met65 that are mono-dentate binding partners similar to His68 in ub. It is therefore assumed that the ability of bidentate Met1 binding in ub is responsible for the kinetic differences of adduct formation observed for ub and cyt. Furthermore, the lack of potential bidentate binding partners in cyt may be responsible for the observation of M_{hydr} -cyt adducts. Again, the slightly slower kinetics of adduct formation with proteins for **6** and **8** compared to **5** are reflected in their increased antiproliferative activity *in vitro*.

When comparing the charge state distributions of free cyt and the mono-adduct under denaturing conditions (50% MeOH, 0.2% formic acid) in the broadband mass spectrum, most of the charge states for free cyt are found between +12 and +19 referring to entirely denatured protein (labeled with *, Figure 4b).^[53] The adduct $[\text{cyt} + 5_{\text{hydr}}]^+$ displays roughly the same charge distribution, indicating that mono-dentate binding of the organometallic fragment to the protein does not influence its tertiary structure (labeled with Δ , Figure 4b). Interestingly, the $[\text{cyt} + \text{Ru}(\text{cym})]^+$ adduct shows two charge state populations, with the first population showing charge states of +13 to +17 indicative of a completely unfolded protein (Figure 4b, grey) similar to free cyt. In contrast, the second population with charge states from +8 to +13 refers to a partially folded protein and suggests a cross-linking of the protein backbone by the $\text{Ru}^{\text{II}}(\text{cym})$ fragment. The first population may correspond to $\text{Ru}^{\text{II}}(\text{cym})$ binding to His26 and/or His33, which does not affect the protein tertiary structure. On the other hand, the second population may correspond to $\text{Ru}^{\text{II}}(\text{cym})$ binding to His33 and Met65, leading to the observed crosslinking effect in MS experiments. This behavior was observed exclusively for **5**, **6** and **8** incubated with cyt but not with ub. This is an intriguing aspect, since the function of proteins highly depends on their tertiary structure and consequently, cross-linking might play a role in the mode of action of the investigated metallodrugs.

Conclusion

Attaching a cytotoxic moiety to peptide carrier systems has attracted much interest, for example because this opens up new possibilities for drug targeting with cell-penetrating peptides. However, conjugation of organometallic Ru^{II} and also Os^{II} anticancer agents to a peptide carrier usually resulted in a reduction of the antiproliferative activity compared to the small metallodrug alone. Here, a metal bio-conjugation strategy is pursued where the opposite effect was observed and to the best of our knowledge, the first organometallic half-sandwich Ru^{II} bioconjugate displaying antiproliferative activity in the low micromolar range (in CH1 ovarian cancer cells) is reported,

while the non-metallated peptide **4** is completely inactive. The comparison of the Ru^{II}-bioconjugate **8** with the smaller bioconjugate models **5** and **6**, which can be considered building blocks of **8**, revealed that the anticancer potency seems to be independent of the peptide carrier, while the triazole moiety is essential, suggesting the Ru^{II}(cym) species with the triazolyl-pyronato linker as the minimal structural requirement for activity *in vitro*. The identification of this cytotoxic moiety may open an approach to a wider range of anticancer active Ru^{II}-bioconjugates. High resolution top-down ESI-MS was performed confirming the expected amino acid sequence, linker modification and metallation site in **8** and providing a useful approach for characterizing organometal-peptide bioconjugates. Finally, ESI-MS studies provided insights into their molecular reactivity toward biomolecules and proteins, and a delayed reactivity of the bioconjugate toward the biomolecules seems to be reflected in an increased *in vitro* cytotoxicity.

Experimental Section

Materials and methods: All reactions were carried out in dry solvents and under inert atmosphere. Chemicals obtained from commercial suppliers were used as received and were of analytical grade. Methanol and dichloromethane were dried using standard procedures. RuCl₃·3H₂O (40.4%) was purchased from Johnson Matthey; ubiquitin (bovine erythrocytes), horse heart cytochrome c, dimethyl sulfoxide (DMSO) and 9-ethylguanidine from Sigma; *N,N*-dimethylformamide (extra dry), 2-propanol, propargylbromide (80%, stabilized in toluene), α -terpinene and tetrahydrofuran from Acros; copper(II) sulfate pentahydrate, phenol and 3,4,5-trimethylphenol from Fisher; l-histidine and potassium carbonate from Merck; l-methionine, sodium ascorbate, sodium azide, sodium methoxide, thionyl chloride and triphenylphosphite from Sigma-Aldrich and kojic acid from TCI Europe. Methanol (VWR Int., HiPerSolv CHROMANORM), formic acid (Fluka) and MilliQ H₂O (18.2 M Ω , Advantage A10, 185 UV Ultrapure Water System, Millipore, France) were used in ESI-MS studies. The dimer bis[dichlorido(η^6 -p-cymene)ruthenium(II)]^[54,55] and the ligand 2-(azidomethyl)-5-hydroxy-4*H*-pyran-4-one^[55] were synthesized as previously described.

NMR spectra were recorded at 25 °C on a Bruker FT NMR spectrometer Avance IIITM 500 MHz at 500.10 (¹H), 202.63 MHz (³¹P{¹H}) and 125.75 MHz (¹³C{¹H}) and 2D NMR data were collected in a gradient-enhanced mode. Hydrogen and carbon atoms were numbered according to crystal structure numbering. Elemental analysis was carried out on a Perkin-Elmer 2400 CHN Elemental Analyzer by the Laboratory for Elemental Analysis, Faculty of Chemistry, University of Vienna. An analytical HPLC system (TM100, Dionex) was equipped with a reversed-phased column (Zorbax Eclipse Plus C18, Agilent, 5 μ m pore size, 4.6 μ m inner diameter and 250 mm column length), that was thermostatted at 25 °C, and a UV-detector (UVD 170U, Dionex). The flow rate was 1 mL/min using a H₂O : MeOH (95 : 5) eluent ratio for the first 3 min. Afterwards, a linear gradient was employed starting with H₂O:MeOH (95 : 5) and ending with H₂O:MeOH (5 : 95) for 15 min, which was then kept for 5 min. 0.1% TFA was added to all eluents. The HPLC was coupled to an AmaZon ESI-ion trap mass spectrometer (Bruker Daltonics GmbH, Bremen, Germany) and controlled by Chromeleon 6.8 software (Thermo Scientific, Bremen, Germany). Electrospray ionization mass spectra were recorded on a Bruker AmaZon SL, a Bruker AmaZon Speed ETD ion trap (IT) and on a UHR MaXis time-of-flight (TOF) mass spectrometer (Bruker Daltonics GmbH, Bremen, Germany). Collision-induced dissociation (CID) was performed using 50–75 eV collision energy, whereas 100–300 ms reaction times were employed for electron transfer dissociation (ETD) experiments on the AmaZon Speed ETD. Data was acquired and processed using Compass 1.3 and Data Analysis 4.0 (Bruker Daltonics GmbH, Bremen, Germany). Deconvolution was obtained by applying the maximum entropy algorithm with a 0.1 *m/z* mass step and 0.5 *m/z* instrument peak width for the IT and automatic data point spacing and 30'000 instrument resolving power for the TOF. X-ray diffraction measurements of single crystals were performed on a Bruker X8 APEX II CCD diffractometer at 100 K. The single crystals of **2** and **5** (CCDC N^o 902337 and 902338, respectively) were positioned at 35 mm from the detector. A total of 1141 frames for 60 sec over 1° were measured for **2** and 2039 frames for 20 sec over 1° for **5**. The data was processed using the SAINT Plus software package.^[56] Crystal data, data

collection parameters, and structure refinement details are given in Table S1. The structure was solved by direct methods and refined by full-matrix least-squares techniques. Non-hydrogen atoms were refined with anisotropic displacement parameters. H atoms were inserted at calculated positions and refined with a riding model. The following software programs and tables were used: structure solution SHELXS-97,^[57] refinement SHELXL-97,^[57] molecular diagrams Mercury CSD 3.0.^[58]

Interaction with biomolecules: Samples for ESI-MS were analyzed by direct infusion at a flow rate of 3 μ L/min and at typical concentrations of 1–5 μ M. Protein samples were analyzed under denaturing conditions by diluting them with water : methanol : formic acid (50 : 50 : 0.2), while the reference complexes and small molecule samples were diluted with water : methanol (50 : 50). Stock solutions of compound **5** and **8** were prepared in H₂O, whereas **6** was dissolved in aqueous solution containing 1% DMSO. The following molar ratios were used for interaction studies at 37 °C and pH 5.5: ub : **M** (1 : 2), cyt : **M** (1 : 3), amino acid : **M** (1 : 1) and EtG : **M** (2 : 1), where **M** is the respective Ru^{II} metallodrug. Mass spectra were recorded after 1, 3, 6, 24 and 48 h. In general, relative intensities correspond to percentages of the area under peaks of the sum of all assignable metal signals in the spectrum.

Cell lines and culture conditions: CH1 cells (ovarian adenocarcinoma, human) were provided by Lloyd R. Kelland (CRC Centre for Cancer Therapeutics, Institute of Cancer Research, Sutton, U.K), SW480 (adenocarcinoma of the colon, human) and A549 (non-small cell lung cancer, human) cells were provided by Brigitte Marian (Institute of Cancer Research, Department of Medicine I, Medical University of Vienna, Austria). All cell culture reagents were purchased from Sigma-Aldrich. Cells were grown in 75 cm² culture flasks (Starlab) as adherent monolayer cultures in Eagle's minimal essential medium (MEM) supplemented with 10% heat-inactivated fetal calf serum, 1 mM sodium pyruvate, 4 mM l-glutamine and 1% v/v non-essential amino acids (from 100 \times ready-to-use stock). Cultures were maintained at 37 °C in a humidified atmosphere containing 95% air and 5% CO₂.

Cytotoxicity in cancer cell lines: Cytotoxicity was determined by the colorimetric MTT (3-(4,5-dimethyl-2-thiazolyl)-2,5-diphenyl-2*H*-tetrazolium bromide; purchased from Sigma-Aldrich) microculture assay. For this purpose, cells were harvested from culture flasks by trypsinization and seeded in 100 μ L aliquots of complete MEM (see above) into 96-well microculture plates (Starlab). Cell densities of 1.0 \times 10³ cells/well (CH1), 2.0 \times 10³ cells/well (SW480) and 3.0 \times 10³ cells/well (A549) were chosen in order to ensure exponential growth of untreated controls throughout the experiment. Cells were allowed to settle and resume exponential growth for 24 h. Compound **1** was dissolved directly in complete MEM, whereas all other test compounds were dissolved in DMSO first and then serially diluted in complete MEM such that the effective DMSO content did not exceed 0.5% v/v. Dilutions were added in 100 μ L aliquots to the microcultures, and cells were exposed to the test compounds for 96 h. At the end of the exposure period, all media were replaced with 100 μ L/well of a 6 : 1 mixture of RPMI1640 medium (supplemented with 10% heat-inactivated fetal calf serum and 2 mM l-glutamine) and MTT solution (5 mg/ml phosphate-buffered saline). After incubation for 4 h, the supernatants were removed, and the formazan product formed by viable cells was dissolved in 150 μ L DMSO per well. Optical densities at 550 nm were measured with a microplate reader (BioTek ELx808), by using a reference wavelength of 690 nm to correct for unspecific absorption. The quantity of viable cells was expressed in terms of T/C values by comparison to untreated control microcultures, and 50% inhibitory concentrations (IC₅₀) were calculated from concentration-effect curves by interpolation. Evaluation is based on means from at least three independent experiments, each comprising three replicates per concentration level.

Synthesis

(*Prop-2-yn-1-yloxy*)benzene. Phenol (3.00 g, 32 mmol) and propargyl bromide (3.56 mL, 32 mmol) were added in a 100 mL round flask containing dry DMF (30 mL) and potassium carbonate (6.62 g, 48 mmol). The reaction mixture was stirred for 18 h under argon atmosphere at room temperature. The product was extracted with dichloromethane (3 \times 50 mL), the combined extracts were washed with H₂O (50 mL) and dried over anhydrous Na₂SO₄. The solution was concentrated yielding the crude product as a yellow oil, which was purified by flash-column chromatography using *n*-hexane/dichloromethane as eluent (1:1.1). Yield: 2.20 g (52%). ¹H NMR (500.10 MHz, *d*₆-DMSO): δ = 7.31 (dd, ³*J*(H,H) = 7 Hz, ³*J*(H,H) = 7 Hz, 2H, *H*_{Ar 3',5'}), 6.99–6.94 (m, 3H, *H*_{Ar 2',4',6'}), 4.78 (d, ⁴*J*(H,H) = 2 Hz, 2H, $-\underline{\text{CH}}_2$), 3.55 (t, ⁴*J*(H,H) = 2 Hz, 1H, $-\text{C}\equiv\text{CH}$) ppm. ¹³C{¹H} NMR (125.75 MHz, *d*₆-DMSO): δ = 157.1 (*C*_{Ar 1'}), 129.4 (*C*_{Ar 2',6'}), 121.09 (*C*_{Ar 4'}), 114.7 (*C*_{Ar 3',5'}), 78.0 ($-\underline{\text{C}}\equiv\text{CH}$), 55.2 ($-\underline{\text{CH}}_2$) ppm.

1,2,3-Trimethyl-5-(prop-2-yn-1-yloxy)benzene. In a 100 mL round flask, 3,4,5-trimethylphenol (1.36 g, 10 mmol) was dissolved in acetone (50 mL). Propargyl bromide (0.90 mL, 11 mmol) and potassium carbonate (1.52 g, 11 mmol) were added. The reaction mixture was refluxed at 65 °C for 24 h. Water (20 mL) was added and the pH adjusted to 12 with NaOH. The product was quickly extracted with dichloromethane (3 × 20 mL). The combined organic phase was dried over anhydrous Na₂SO₄ and subsequently filtered. The solvent was removed yielding the product as a yellow oil. Yield: 1.61 g (89%). MS (ESI⁺): *m/z* 175.13 [M + H]⁺ (*m*_{ex} = 175.11). ¹H NMR (500.10 MHz, *d*₆-DMSO): δ = 6.62 (s, 2H, H_{Ar}), 4.69 (d, ³*J*(H,H) = 3 Hz, 2H, -CH₂), 3.49 (t, ⁴*J*(H,H) = 3 Hz, 1H, -C≡CH), 2.20 (s, 6H, C_{Ar} 3',5'-CH₃), 2.03 (s, 3H, C_{Ar} 4'-CH₃) ppm. ¹³C{¹H} NMR (125.75 MHz, *d*₆-DMSO): δ = 154.3 (C_{Ar} 1'), 136.9 (C_{Ar} 3',5'), 126.7 (C_{Ar} 4'), 113.8 (C_{Ar} 2',6'), 77.7 (-C≡CH), 55.1 (-CH₂), 20.4 (C_{Ar} 3',5'-CH₃), 14.2 (C_{Ar} 4'-CH₃) ppm.

2-(Azidomethyl)-5-hydroxy-4H-pyran-4-one (1). The procedure of Atkinson *et al.* was used with minor modifications.^[35] Step 1: Thionyl chloride (19.5 mL, 271 mmol) was added to kojic acid (7.00 g, 50 mmol) under vigorous stirring at 0 °C. After complete addition, the reaction was stirred for 4 h and the remaining thionyl chloride was removed under reduced pressure using a cooling trap. The dry yellowish reaction product was suspended in *n*-hexane and filtered. Recrystallization from ³PrOH yielded colorless crystals of 2-(chloromethyl)-5-hydroxy-pyran-4H-one which were dried *in vacuo*. Yield: 6.60 g (84%). ¹H NMR (500.10 MHz, *d*₆-DMSO): δ = 9.29 (s, 1H, -OH), 8.12 (s, 1H, H-2), 6.56 (s, 1H, H-5), 4.66 (s, 2H, H-7) ppm. Step 2: In a round-bottom flask, sodium azide (1.22 g, 19 mmol) was suspended in dry DMF (12.3 mL) under argon atmosphere at 0 °C. Then 2-(chloromethyl)-5-hydroxy-pyran-4H-one (3.00 g, 19 mmol) was slowly added and the reaction mixture became turbid after several minutes. The suspension was allowed to warm to room temperature and was stirred in the absence of light for 24 h, before it was slowly poured into H₂O (7.5 mL, 0 °C). A colorless solid precipitated, which was separated by filtration and dried *in vacuo*. Yield: 2.71 g (87%). Elemental analysis calculated for C₆H₅N₃O₃: C, 43.12; H, 3.02; N, 25.14; found: C, 43.11; H, 2.76; N, 24.97. MS (ESI⁺): *m/z* 168.11 [M + H]⁺ (*m*_{ex} = 168.04). ¹H NMR (500.10 MHz, *d*₆-DMSO): δ = 9.24 (s, 1H, -OH), 8.11 (s, 1H, H-2), 6.45 (s, 1H, H-5), 4.42 (s, 2H, H-7) ppm. ¹³C{¹H} NMR (125.75 MHz, *d*₆-DMSO, 25 °C): δ = 174.1 (C-4), 162.3 (C-2), 146.4 (C-5), 140.5 (C-6), 113.0 (C-3), 50.6 (C-7) ppm.

5-Hydroxy-2-((4-(phenoxymethyl)-1H-1,2,3-triazol-1-yl)methyl)-4H-pyran-4-one (2). Copper sulfate pentahydrate (30 mg, 10 mol%) and sodium ascorbate (95.1 mg, 40 mol%) were suspended in deoxygenated H₂O (2.5 mL) and stirred until the reaction mixture turned yellow. This reaction mixture was added to a suspension of **1** (200 mg, 1.2 mmol) and (prop-2-yn-1-yloxy)benzene (237 mg, 1.8 mmol) in deoxygenated argon-flushed H₂O : THF (7.5 mL, 1 : 2 ratio). The reaction mixture was stirred for 24 h at room temperature under argon atmosphere and then the solvent was removed. The residue was dissolved in ethyl acetate, dried over anhydrous Na₂SO₄ and filtered. After removal of the solvent and recrystallization from ³PrOH, the yellowish product was obtained after filtration and dried *in vacuo*. Yield: 165 mg (46%). Elemental analysis calculated for C₁₅H₁₃N₃O₄·0.4H₂O: C, 58.78; H, 4.54; N, 13.71; found: C, 59.05; H, 4.14; N, 13.32. MS (ESI⁺): *m/z* 298.15 [M - H]⁻ (*m*_{ex} = 298.08). ¹H NMR (500.10 MHz, *d*₆-DMSO): δ = 9.28 (s, 1H, -OH), 8.33 (s, 1H, H-8), 8.06 (s, 1H, H-2), 7.30 (t, ³*J*(H,H) = 8 Hz, 2H, H_{Ar} 3',5'), 7.03 (d, ³*J*(H,H) = 8 Hz, 2H, H_{Ar} 2',6'), 6.95 (t, ³*J*(H,H) = 8 Hz, 1H, H_{Ar} 4'), 6.40 (s, 1H, H-5), 5.61 (s, 2H, H-7), 5.16 (s, 2H, H-10) ppm. ¹³C{¹H} NMR (125.75 MHz, *d*₆-DMSO): δ = 173.5 (C-4), 160.5 (C-2), 157.9 (C_{Ar} 1'), 145.9 (C-5), 143.1 (C-9), 139.9 (C-6), 129.4 (C_{Ar} 3',5'), 125.3 (C-8), 120.8 (C_{Ar} 4'), 114.6 (C_{Ar} 2',6'), 113.0 (C-3), 60.8 (C-10), 49.9 (C-7) ppm.

5-Hydroxy-2-((4-((3,4,5-trimethylphenoxy)methyl)-1H-1,2,3-triazol-1-yl)methyl)-4H-pyran-4-one (3). Copper sulfate pentahydrate (30 mg, 10 mol%) and sodium ascorbate (95 mg, 40 mol%) were suspended in deoxygenated H₂O (2.5 mL) and stirred until the mixture turned yellow. This reaction mixture was then added to the suspension of **1** (200 mg, 1.2 mmol) and 1,2,3-trimethyl-5-(prop-2-yn-1-yloxy)benzene (314 mg, 1.8 mmol) in deoxygenated, argon-flushed H₂O : THF (7.5 mL, 1 : 2 ratio). The reaction mixture was stirred for 24 h at room temperature after which the solvent was evaporated. The residue was dissolved in ethyl acetate, dried over anhydrous Na₂SO₄ and filtered. After removal of the solvent and recrystallization from ³PrOH, the yellowish product was obtained after filtration and dried *in vacuo*. Yield: 260 mg (64%). MS (ESI⁺): *m/z* 342.10 [M + H]⁺ (*m*_{ex} = 342.15). ¹H NMR (500.10 MHz, *d*₆-DMSO): δ = 9.28 (s, 1H, -OH), 8.29 (s, 1H, H-8), 8.05 (s, 1H, H-2), 6.67 (s, 2H, H_{Ar} 2',6'), 6.38 (s, 1H, H-5), 5.60 (s, 2H, H-7), 5.08 (s, 2H, H-10), 2.19 (s, 6H, C_{Ar} 3',5'-CH₃), 2.03 (s, 3H, C_{Ar} 4'-CH₃) ppm. ¹³C{¹H} NMR (125.75 MHz, *d*₆-DMSO): δ = 173.5 (C-4), 160.5 (C-2), 155.2 (C_{Ar} 1'), 145.9 (C-5), 143.4 (C-9), 139.9 (C-6), 136.9 (C_{Ar} 3',5'), 126.7 (C_{Ar} 4'), 125.1 (C-8), 113.7 (C_{Ar} 2',6'), 112.9 (C-3), 60.7 (C-10), 49.8 (C-7), 20.3 (C_{Ar} 4'-CH₃), 14.2 (C_{Ar} 3',5'-CH₃) ppm.

5-Hydroxy-2-((4-(*N*-tyrosinyl-glycyl-phenylalanyl-leucinylnh₂)propanamido)-1H-1,2,3-triazol-1-yl)methyl)-4H-pyran-4-one (4). The

Fmoc-protected [Leu⁵]-enkephalin was manually prepared on Rink amide resins (500 mg, 0.36 mmol) according to standard solid-phase synthesis procedures^[16,39] using a four-fold excess of the Fmoc-protected amino acid. Each coupling was performed in the presence of TBTU (433 mg, 1.35 mmol), HOBt (192 mg, 1.35 mmol) and DIPEA (618 μL, 0.36 mmol) and 4-pentynoic acid was coupled in the same manner. The solid-phase Huisgen 1,3-dipolar cycloaddition was performed adapting a procedure by Tornøe *et al.*^[37] and Koester *et al.*^[60] Compound **1** (119 mg, 0.71 mmol) was dissolved in ACN : DCM (2 : 1, 6 mL) and purged with N₂. CuI (135 mg, 0.71 mmol) was dissolved in ACN : DCM (2 : 1, 8 mL) and both compounds were transferred into the syringe containing the resin (500 mg, 0.36 mmol). Finally, DIPEA (2.98 mL, 18 mmol, 50 equiv) was taken up in the syringe and the mixture was shaken at room temperature in the absence of light for 18 h under N₂. After washing with DMF (5 × 4 mL, 2 min), Cu impurities were removed with a 0.14 M solution of cupral (0.71 mmol) in DMF and again washed with DMF (5 × 4 mL, 2 min) and DCM (5 × 4 mL, 2 min). The modified peptide was cleaved from the resin by treatment with 7 mL of TFA : TIS : H₂O (95 : 2.5 : 2.5) for 2 h and then precipitated by addition of cold diethyl ether. After centrifugation, the solution was decanted and the product was washed twice with cold diethyl ether and finally dried *in vacuo*. After purification by preparative HPLC and lyophilization, the product was obtained as a colorless solid. Yield: 166 mg (58%). MS (ESI⁺): *m/z* 802.23 [M + H]⁺ (*m*_{ex} = 802.35), MS (ESI⁺): *m/z* 914.44 [M - H + TFA]⁺ (*m*_{ex} = 914.33), anal. HPLC: 11.26 min. ¹H NMR (500.10 MHz, *d*₆-DMSO): δ = 9.18 (br s, 1H, -OH_{Tyr}), 8.26 (t, ³*J*(H,H) = 6 Hz, 1H, -NH_{Gly}), 8.14 (d, ³*J*(H,H) = 8 Hz, 1H, -NH_{Leu}), 8.06 (t, ³*J*(H,H) = 8 Hz, 1H, -NH_{Tyr}), 8.03 (s, 1H, H-8), 7.99 (t, ³*J*(H,H) = 6 Hz, 1H, -NH_{Phe}), 7.96 (d, ³*J*(H,H) = 8 Hz, 1H, -NH_{Gly}), 7.81 (s, 1H, H-2), 7.24 (d, ³*J*(H,H) = 5 Hz, 4H, H_{Ar,Phe}), 7.17-7.14 (m, 1H, H_{Ar,Phe}), 7.09 (s, 1H, -NH₂), 7.00 (d, ³*J*(H,H) = 9 Hz, 2, H_{Ar,Tyr}), 6.97 (s, 1H, -NH₂), 6.62 (d, ³*J*(H,H) = 9 Hz, 2, H_{Ar,Tyr}), 6.36 (s, 1H, H-5), 5.49 (s, 2H, H-7), 4.53-4.48 (m, 1H, H_{α,Leu}), 4.42-4.39 (m, 1H, H_{α,Tyr}), 4.22-4.17 (m, 1H, H_{α,Leu}), 3.72-3.69 (m, 4H, H_{α,Gly}), 3.03 (dd, ²*J*(H,H) = 14 Hz, ³*J*(H,H) = 5 Hz, 2H, H_{β,Tyr}), 2.92 (dd, ²*J*(H,H) = 14 Hz, ³*J*(H,H) = 5 Hz, 2H, H_{β,Phe}), 2.76 (t, ³*J*(H,H) = 9 Hz, 2H, H_{α,pen}), 2.64 (t, ³*J*(H,H) = 9 Hz, 2H, H_{β,pen}), 1.60-1.52 (m, 1H, H_{γ,Leu}), 1.48-1.45 (m, 2H, H_{β,Leu}), 0.84 (dd, ²*J*(H,H) = 26 Hz, ³*J*(H,H) = 7 Hz, 6H, H_{δ,Leu}) ppm.

General Procedure for the synthesis of [chlorido(η⁶-p-cymene)(pyronato)ruthenium(II)] complexes. The pyrone ligand (1–1.1 equiv) and sodium methoxide (1–1.1 equiv) were suspended in dry methanol under argon atmosphere at room temperature and stirred for 15 min. Then bis[dichlorido(η⁶-p-cymene)ruthenium(II)] (0.5 equiv) was added and the clear, orange-red colored solution was stirred for further 6–18 h. The solvent was removed under reduced pressure, the residue was dissolved in dichloromethane, filtered and the filtrate was concentrated to a final volume of ca. 2–3 mL. The product was precipitated by addition of *n*-hexane, filtered and dried *in vacuo*.

[2-(Azidomethyl)-5-oxo-κO-4H-pyronato-κO]chlorido(η⁶-p-cymene)ruthenium(II) (5). The reaction was performed according to the general procedure using pyrone **1** (40 mg, 0.23 mmol), sodium methoxide (13 mg, 0.23 mmol), bis[dichlorido(η⁶-p-cymene)ruthenium(II)] (70 mg, 0.16 mmol) and methanol (8 mL). The product was isolated as brownish crystals. Reaction time: 18 h. Yield: 65 mg (65%). Elemental analysis calculated for C₁₆H₁₈ClN₃O₃Ru·½H₂O: C, 43.39; H, 4.25; N, 9.48; found: C, 43.79; H, 3.97; N, 9.09. MS (ESI⁺): *m/z* 402.0377 [M - Cl]⁺ (*m*_{ex} = 402.0391, 4 ppm), 374.0311 [M - Cl - N₂]⁺ (*m*_{ex} = 374.0329, 5 ppm). ¹H NMR (500.10 MHz, *d*₆-DMSO): δ = 7.93 (s, 1H, H-2), 6.68 (s, 1H, H-5), 5.70-5.68 (m, 2H, H_{Cym} 3',5'), 5.42-5.40 (m, 2H, H_{Cym} 2',6'), 4.43 (s, 2H, H-7), 2.76 (sept, ³*J*(H,H) = 7 Hz, 1H, H_{Cym} b), 2.14 (s, 3H, H_{Cym} a), 1.25 (dd, ³*J*(H,H) = 7 Hz, ⁴*J*(H,H) = 2 Hz, 6H, H_{Cym} c) ppm. ¹³C{¹H} NMR (125.75 MHz, *d*₆-DMSO): δ = 185.2 (C-4), 161.5 (C-2), 159.9 (C-5), 140.8 (C-6), 108.8 (C-3), 97.9 (C_{Cym} 1'), 94.9 (C_{Cym} 4'), 79.9 (C_{Cym} 3',5'), 76.9 (C_{Cym} 2',6'), 49.8 (C-7), 30.5 (C_{Cym} b), 22.0 (C_{Cym} c), 17.9 (C_{Cym} a) ppm.

[Chlorido(η⁶-p-cymene)[5-oxo-κO-2-((4-(phenoxymethyl)-1H-1,2,3-triazol-1-yl)methyl)-4H-pyronato-κO]ruthenium(II) (6). The reaction was performed according to the general procedure using pyrone **2** (100 mg, 0.33 mmol), sodium methoxide (18 mg, 0.34 mmol), bis[dichlorido(η⁶-p-cymene)ruthenium(II)] (99 mg, 0.16 mmol) and methanol (10 mL). The product was isolated as yellow microcrystals. Reaction time: 18 h. Yield: 115 mg (63%). Elemental analysis calculated for C₂₅H₂₆ClN₃O₃Ru·0.5H₂O: C, 51.95; H, 4.71; N, 7.27; found: C, 52.14; H, 4.36; N, 7.30. MS (ESI⁺): *m/z* 534.0947 [M - Cl]⁺ (*m*_{ex} = 534.0968, 4 ppm). ¹H NMR (500.10 MHz, *d*₆-DMSO): δ = 8.30 (s, 1H, H-8), 7.87 (s, 1H, H-2), 7.30 (t, ³*J*(H,H) = 8 Hz, 2H, H_{Ar} 3',5'), 7.02 (d, ³*J*(H,H) = 8 Hz, 2H, H_{Ar} 2',6'), 6.95 (t, ³*J*(H,H) = 8 Hz, 1H, H_{Ar} 4'), 6.61 (s, 1H, H-5), 5.69-5.67 (m, 2H, H_{Cym} 3',5'), 5.62 (s, 2H, H-7), 5.41-5.39 (m, 2H, H_{Cym} 2',6'), 5.14 (s, 2H, H-10), 2.76 (sept, ³*J*(H,H) = 7 Hz, 1H, H_{Cym} b), 2.13 (s, 3H, H_{Cym} a), 1.25 (d, ³*J*(H,H) = 7 Hz, 6H, H_{Cym} c) ppm. ¹³C{¹H} NMR (125.75 MHz, *d*₆-DMSO, 25 °C): δ = 185.2 (C-4), 160.1 (C-2), 160.0 (C-5), 157.9 (C_{Ar} 1'), 143.2 (C-9), 140.8 (C-6), 129.4 (C_{Ar} 3',5'), 126.0 (C-8), 120.8 (C_{Ar} 4'), 114.6 (C_{Ar} 2',6'), 109.1 (C-3), 97.9 (C_{Cym} 1'),

94.9 (C_{Cym 4'}), 79.9 (C_{Cym 3',5'}), 77.0 (C_{Cym 2',6'}), 60.7 (C-10), 49.6 (C-7), 30.6 (C_{Cym b}), 22.0 (C_{Cym c}), 17.9 (C_{Cym a}) ppm.

[Chlorido(η^6 -p-cymene)[5-oxo- κ O-2-[(4-((3,4,5-trimethylphenoxy)methyl)-1H-1,2,3-triazol-1-yl)methyl]-4H-pyridonato- κ O]ruthenium(II)] (7). The reaction was performed according to the general procedure using pyrone 3 (112 mg, 0.33 mmol), sodium methoxide (18 mg, 0.34 mmol), bis(dichlorido(η^6 -p-cymene)ruthenium(II)) (99 mg, 0.16 mmol) and methanol (10 mL). The product was isolated as yellow solid. Reaction time: 18 h. Yield: 160 mg (82%). Elemental analysis calculated for C₂₈H₃₂ClN₃O₄Ru·0.5H₂O: C, 54.23; H, 5.36; N, 6.78; found: C, 53.98; H, 4.97; N, 6.81. MS (ESI⁺): *m/z* 576.1406 [M - Cl]⁺ (*m*_{ex} = 576.1433, 5 ppm). ¹H NMR (500.10 MHz, *d*₆-DMSO): δ = 8.26 (s, 1H, H-8), 7.88 (s, 1H, H-2), 6.67 (s, 2H, H_{Ar 2',6'}), 6.59 (s, 1H, H-5), 5.69–5.67 (m, 2H, H_{Cym 3',5'}), 5.61 (s, 2H, H-7), 5.41–5.39 (m, 2H, H_{Cym 2',6'}), 5.06 (s, 2H, H-10), 2.76 (sept, ³J(H,H) = 7 Hz, 1H, H_{Cym b}), 2.19 (s, 6H, C_{Ar 3',5'}-CH₃), 2.13 (s, 3H, H_{Cym a}), 2.03 (s, 3H, C_{Ar 4'}-CH₃), 1.25 (d, ³J(H,H) = 7 Hz, 6H, H_{Cym c}) ppm. ¹³C{¹H} NMR (125.75 MHz, *d*₆-DMSO): δ = 185.2 (C-4), 160.2 (C-2), 160.0 (C-5), 155.2 (C_{Ar 1'}), 143.4 (C-9), 140.8 (C-6), 136.9 (C_{Ar 3',5'}), 126.7 (C_{Ar 4'}), 126.0 (C-8), 113.6 (C_{Ar 2',6'}), 109.0 (C-3), 97.9 (C_{Cym 1'}), 94.9 (C_{Cym 4'}), 79.9 (C_{Cym 3',5'}), 77.0 (C_{Cym 2',6'}), 60.7 (C-10), 49.6 (C-7), 30.6 (C_{Cym b}), 22.0 (C_{Cym c}), 20.3 (C_{Ar 3',5'}-CH₃), 17.9 (C_{Cym a}), 14.2 (C_{Ar 4'}-CH₃) ppm.

[Chlorido(η^6 -p-cymene)(5-oxo- κ O-2-[(4-[(N-tyrosinyl-glycyl-glycyl-phenylalanyl-leucyl)-NH₂propanamido]-1H-1,2,3-triazol-1-yl)methyl]-4H-pyridonato- κ O)ruthenium(II)] (8). The reaction was performed according to the general procedure using pyrone 4 (18.3 mg, 0.02 mmol), sodium methoxide (2.2 mg, 0.04 mmol), bis(dichlorido(η^6 -p-cymene)ruthenium(II)) (6.4 mg, 0.01 mmol) and methanol (4 mL). The reaction was stirred for 6 h in the absence of light at room temperature and under an inert atmosphere. A yellow solution was obtained, which was concentrated and the residue was dried *in vacuo*. Preparative HPLC and subsequent lyophilization yielded the desired product as a yellow powder. Yield: 11.7 mg (51%). MS (ESI⁺): *m/z* 518.6773 [M - Cl + H]²⁺ (*m*_{ex} = 518.6794, 4 ppm). anal. HPLC: 12.2 min. ¹H NMR (500.10 MHz, *d*₆-DMSO): δ = 9.15 (s, 1H, -OH_{Tyr}), 8.24 (t, ³J(H,H) = 7 Hz, 1H, -NH_{Gly}), 8.24 (s, 1H, H-8), 8.12 (d, ³J(H,H) = 8 Hz, 1H, -NH_{Leu}), 8.06 (d, ³J(H,H) = 8 Hz, 1H, -NH_{Tyr}), 7.99 (d, ³J(H,H) = 6 Hz, 1H, -NH_{Phe}), 7.95 (t, ³J(H,H) = 7 Hz, 1H, -NH_{Gly}), 7.80 (s, 1H, H-1), 7.24 (d, ³J(H,H) = 5 Hz, 4H, H_{Ar,Phe}), 7.19–7.15 (m, 1H, H_{Ar,Phe}), 7.09 (br s, 1H, -NH₂), 7.00 (d, ³J(H,H) = 9 Hz, 2H, H_{Ar,Tyr}), 6.96 (br s, 1H, -NH₂), 6.62 (d, ³J(H,H) = 9 Hz, 2H, H_{Ar,Tyr}), 6.35 (s, 1H, H-5), 5.69–5.66 (m, 2H, H_{Cym 3',5'}), 5.59 (s, 2H, H-7), 5.41–5.39 (m, 2H, H_{Cym 2',6'}), 4.51–4.49 (m, 1H, H_{u,Phe}), 4.44–4.40 (m, 1H, H_{u,Tyr}), 4.20 (q, ³J(H,H) = 7.5 Hz, H_{u,Leu}), 3.73–3.62 (m, 4H, H_{u,Gly}), 3.03 (dd, ²J(H,H) = 14 Hz, ³J(H,H) = 5 Hz, 1H, H_{β,Tyr}), 2.92 (dd, ²J = 14 Hz, ³J(H,H) = 5 Hz, 2H, H_{β,Phe}), 2.78–2.74 (m, 2H, H_{β,Leu}), 2.66–2.61 (m, 2H, H_{u,Phe}), 2.16 (s, 3H, H_{Cym a}), 1.60–1.52 (m, 1H, H_{β,Leu}), 1.46 (t, ³J(H,H) = 7 Hz, 2H, H_{β,Leu}), 1.27 (d, ³J(H,H) = 7 Hz, 6H, H_{Cym c}), 0.85 (dd, ³J(H,H) = 25 Hz, ³J(H,H) = 7 Hz, 6H, H_{δ,Leu}) ppm.

Acknowledgements

We would like to thank COST D39, CM1105 and the Johanna Mahlke née Obermann Foundation for financial support and the Mass Spectrometry Center (Faculty of Chemistry, University of Vienna) for access to the UHR ESI-TOF mass spectrometer. We gratefully acknowledge Alexander Roller for collecting the X-ray diffraction data. S.M.M. thanks in particular S. David Köster, H. Bauke Albada and Kathrin Klein for their support at RUB and Elisabeth Jirkovský for several ESI-MS measurements.

- [1] N. Yamamoto, N. S. Bryce, N. Metzler-Nolte, T. W. Hambley, *Bioconjug. Chem.* **2012**, *23*, 1110-1118.
- [2] F. Milletti, *Drug Discov. Today* **2012**, *17*, 850-860.
- [3] C. G. Hartinger, N. Metzler-Nolte, P. J. Dyson, *Organometallics* **2012**, *31*, 5677-5685.
- [4] Q. Geng, X. Sun, T. Gong, Z. R. Zhang, *Bioconjug. Chem.* **2012**, *23*, 1200-1210.
- [5] K. L. Horton, K. M. Stewart, S. B. Fonseca, Q. Guo, S. O. Kelley, *Chem. Biol.* **2008**, *15*, 375-382.
- [6] G. Gasser, N. Metzler-Nolte, *Curr. Opin. Chem. Biol.* **2012**, *16*, 84-91.
- [7] H. B. Albada, F. Wieberneit, I. Dijkgraaf, J. H. Harvey, J. L. Whistler, R. Stoll, N. Metzler-Nolte, R. H. Fish, *J. Am. Chem. Soc.* **2012**, *134*, 10321-10324.
- [8] S. Abramkin, S. M. Valiahd, M. A. Jakupec, M. Galanski, N. Metzler-Nolte, B. K. Keppler, *Dalton Trans.* **2012**, *41*, 3001-3005.
- [9] S. H. van Rij, H. Kostrhunova, V. Brabec, P. J. Sadler, *Bioconjug. Chem.* **2011**, *22*, 218-226.
- [10] A. Gross, M. Neukamm, N. Metzler-Nolte, *Dalton Trans.* **2011**, *40*, 1382-1386.
- [11] H. Struthers, T. L. Mindt, R. Schibli, *Dalton Trans.* **2010**, *39*, 675-696.
- [12] K. Splith, W. N. Hu, U. Schatzschneider, R. Gust, I. Ott, L. A. Onambele, A. Prokop, I. Neundorff, *Bioconjug. Chem.* **2010**, *21*, 1288-1296.

- [13] A. Pinto, U. Hoffmanns, M. Ott, G. Fricker, N. Metzler-Nolte, *ChemBioChem* **2009**, *10*, 1852-1860.
- [14] N. Metzler-Nolte, in *Top. Organomet. Chem.*, Vol. 32, (Eds: G. Jaouen, N. Metzler-Nolte), Springer, Heidelberg, **2009**, pp. 195-217.
- [15] I. Neundorff, J. Hoyer, K. Splith, R. Rennert, H. W. P. N'Dongo, U. Schatzschneider, *Chem. Commun.* **2008**, 5604-5606.
- [16] M. A. Neukamm, A. Pinto, N. Metzler-Nolte, *Chem. Commun.* **2008**, 232-234.
- [17] E. Garcia-Garayoa, R. Schibli, P. A. Schubiger, *Nucl. Sci. Tech.* **2007**, *18*, 88-100.
- [18] D. B. Grotjahn, *Coord. Chem. Rev.* **1999**, *192*, 1125-1141.
- [19] A. Mooney, A. J. Corry, D. O'Sullivan, K. R. Dilip, P. T. M. Kenny, *J. Organomet. Chem.* **2009**, *694*, 886-894.
- [20] H. W. P. N'Dongo, I. Ott, R. Gust, U. Schatzschneider, *J. Organomet. Chem.* **2009**, *694*, 823-827.
- [21] S. D. Koster, H. Alborzina, S. Z. Can, I. Kitanovic, S. Wolf, R. Rubbiani, I. Ott, P. Riesterer, A. Prokop, K. Merz, N. Metzler-Nolte, *Chem Sci* **2012**, *3*, 2062-2072.
- [22] L. Gaviglio, A. Gross, N. Metzler-Nolte, M. Ravera, *Metallomics* **2012**, *4*, 260-266.
- [23] A. M. Pizarro, A. Habtemariam, P. J. Sadler, in *Medicinal Organometallic Chemistry*, (Eds: G. Jaouen, N. Metzler-Nolte), Springer, Heidelberg, **2010**, pp. 21-56.
- [24] F. Barragan, D. Carrion-Salip, I. Gomez-Pinto, A. Gonzalez-Canto, P. J. Sadler, R. de Llorens, V. Moreno, C. Gonzalez, A. Massaguer, V. Marchan, *Bioconjug. Chem.* **2012**, *23*, 1838-1855.
- [25] M. A. Santos, *Coord. Chem. Rev.* **2008**, *252*, 1213-1224.
- [26] W. Kandioller, A. Kurzwehnart, M. Hanif, S. M. Meier, H. Henke, B. K. Keppler, C. G. Hartinger, *J. Organomet. Chem.* **2011**, *696*, 999-1010.
- [27] M. Hanif, H. Henke, S. M. Meier, S. Martic, M. Labib, W. Kandioller, M. A. Jakupec, V. B. Arion, H. B. Kraatz, B. K. Keppler, C. G. Hartinger, *Inorg. Chem.* **2010**, *49*, 7953-7963.
- [28] M. G. Mendoza-Ferri, C. G. Hartinger, M. A. Mendoza, M. Groessl, A. E. Egger, R. E. Eichinger, J. B. Mangrum, N. P. Farrell, M. Maruszak, P. J. Bednarski, F. Klein, M. A. Jakupec, A. A. Nazarov, K. Severin, B. K. Keppler, *J. Med. Chem.* **2009**, *52*, 916-925.
- [29] W. Kandioller, C. G. Hartinger, A. A. Nazarov, M. L. Kuznetsov, R. O. John, C. Bartel, M. A. Jakupec, V. B. Arion, B. K. Keppler, *Organometallics* **2009**, *28*, 4249-4251.
- [30] W. Kandioller, C. G. Hartinger, A. A. Nazarov, J. Kasser, R. John, M. A. Jakupec, V. B. Arion, P. J. Dyson, B. K. Keppler, *J. Organomet. Chem.* **2009**, *694*, 922-929.
- [31] W. Kandioller, C. G. Hartinger, A. A. Nazarov, C. Bartel, M. Skocic, M. A. Jakupec, V. B. Arion, B. K. Keppler, *Chem. Eur. J.* **2009**, *15*, 12283-12291.
- [32] A. F. A. Peacock, M. Melchart, R. J. Deeth, A. Habtemariam, S. Parsons, P. J. Sadler, *Chem. Eur. J.* **2007**, *13*, 2601-2613.
- [33] M. Hanif, P. Schaaf, W. Kandioller, M. Hejl, M. A. Jakupec, A. Roller, B. K. Keppler, C. G. Hartinger, *Aust. J. Chem.* **2010**, *63*, 1521-1528.
- [34] J. H. Kasser, W. Kandioller, C. G. Hartinger, A. A. Nazarov, V. B. Arion, P. J. Dyson, B. K. Keppler, *J. Organomet. Chem.* **2010**, *695*, 875-881.
- [35] J. G. Atkinson, Y. Girard, J. Rokach, C. S. Rooney, C. S. Mcfarlane, A. Rackhag, N. N. Share, *J. Med. Chem.* **1979**, *22*, 99-106.
- [36] V. V. Rostovtsev, L. G. Green, V. V. Fokin, K. B. Sharpless, *Angew. Chem., Int. Ed. Engl.* **2002**, *41*, 2596-2599.
- [37] C. W. Tornoe, C. Christensen, M. Meldal, *J. Org. Chem.* **2002**, *67*, 3057-3064.
- [38] C. F. C. Lam, A. C. Giddens, N. Chand, V. L. Webb, B. R. Copp, *Tetrahedron* **2012**, *68*, 3187-3194.
- [39] S. G. Agalave, S. R. Maujan, V. S. Pore, *Chem. Asian J.* **2011**, *6*, 2696-2718.
- [40] H. Struthers, B. Spingler, T. L. Mindt, R. Schibli, *Chem. Eur. J.* **2008**, *14*, 6173-6183.
- [41] I. A. Papayannopoulos, *Mass Spectrom. Rev.* **1995**, *14*, 49-73.
- [42] L. M. Mikes, B. Ueberheide, A. Chi, J. J. Coon, J. E. Syka, J. Shabanowitz, D. F. Hunt, *Biochim. Biophys. Acta* **2006**, *1764*, 1811-1822.
- [43] H. Ben Hamidane, D. Chiappe, R. Hartmer, A. Vorobyev, M. Moniatte, Y. O. Tsybin, *J. Am. Soc. Mass Spectrom.* **2009**, *20*, 567-575.
- [44] S. M. Meier, Y. O. Tsybin, P. J. Dyson, B. K. Keppler, C. G. Hartinger, *Anal. Bioanal. Chem.* **2012**, *402*, 2655-2662.
- [45] S. M. Meier, M. Hanif, W. Kandioller, B. K. Keppler, C. G. Hartinger, *J. Inorg. Biochem.* **2012**, *108*, 91-95.
- [46] N. Zhang, Y. Du, M. Cui, J. Xing, Z. Liu, S. Liu, *Anal. Chem.* **2012**, *84*, 6206-6212.
- [47] J. P. Williams, H. I. A. Phillips, I. Campuzano, P. J. Sadler, *J. Am. Soc. Mass Spectrom.* **2010**, *21*, 1097-1106.
- [48] J. P. Williams, J. M. Brown, I. Campuzano, P. J. Sadler, *Chem. Commun.* **2010**, *46*, 5458-5460.
- [49] A. Casini, C. Gabbiani, E. Michelucci, G. Pieraccini, G. Moneti, P. J. Dyson, L. Messori, *J. Biol. Inorg. Chem.* **2009**, *14*, 761-770.
- [50] A. Casini, A. Guerri, C. Gabbiani, L. Messori, *J. Inorg. Biochem.* **2008**, *102*, 995-1006.
- [51] D. Gibson, C. E. Costello, *Eur. Mass Spectrom.* **1999**, *5*, 501-510.
- [52] W. Kandioller, E. Balsano, S. M. Meier, U. Jungwirth, S. Göschl, A. Roller, M. A. Jakupec, W. Berger, B. K. Keppler, C. G. Hartinger, *Chem. Commun.* **2013**, submitted.
- [53] L. Konermann, D. J. Douglas, *Biochemistry* **1997**, *36*, 12296-12302.
- [54] M. A. Bennett, A. K. Smith, *J. Chem. Soc., Dalton Trans.* **1974**, 233-241.

-
- [55] M. A. Bennett, T. N. Huang, T. W. Matheson, A. K. Smith, *Inorg. Synth.* **1982**, *21*, 74-78.
- [56] M. R. Pressprich, J. Chambers, *SAINT + Integration Engine, Program for Crystal Structure Integration*, Bruker Analytical X-ray systems, Madison, **2004**.
- [57] G. M. Sheldrick, *SHELXL-97, Program for Crystal Structure Refinement*, University Göttingen (Germany), **1997**.
- [58] C. F. Macrae, I. J. Bruno, J. A. Chisholm, P. R. Edgington, P. McCabe, E. Pidcock, L. Rodriguez-Monge, R. Taylor, J. van de Streek, P. A. Wood, *J. Appl. Crystallogr.* **2008**, *41*, 466-470.
- [59] D. R. van Staveren, N. Metzler-Nolte, *Chem. Commun.* **2002**, 1406-1407.
- [60] S. D. Koster, J. Dittrich, G. Gasser, N. Husken, I. C. H. Castaneda, J. L. Jios, C. O. Della Vedova, N. Metzler-Nolte, *Organometallics* **2008**, *27*, 6326-6332.
-

Received: ((will be filled in by the editorial staff))
Revised: ((will be filled in by the editorial staff))
Published online: ((will be filled in by the editorial staff))

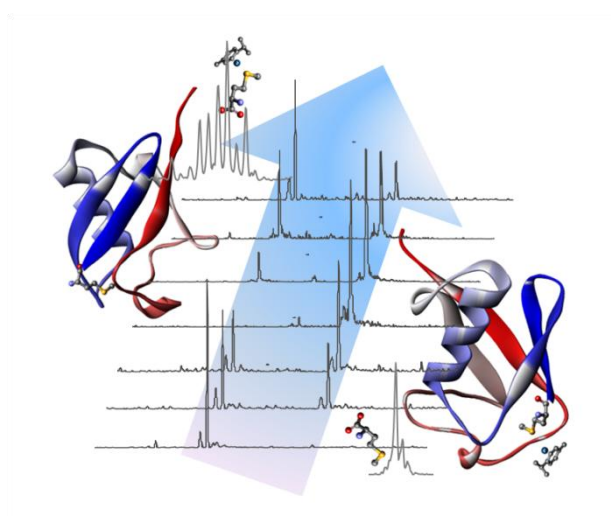
3.3. Biomolecule Binding vs. Anticancer Activity: Reactions of Ru(arene)[(thio)pyr(id)one] Compounds with Amino Acids and Proteins

Samuel M. Meier,^{a,b} Muhammad Hanif,^a Wolfgang Kandioller,^a Bernhard K. Keppler,^{a,b} Christian G. Hartinger^{a,b*}

Journal of Inorganic Biochemistry, **2012**, *108*, 91-95.

^a University of Vienna, Institute of Inorganic Chemistry, Waehringer Str. 42, A-1090 Vienna, Austria.

^b University of Vienna, Research Platform “Translational Cancer Therapy Research”, Waehringer Str. 42, A-1090 Vienna, Austria.





Biomolecule binding vs. anticancer activity: Reactions of Ru(arene)[(thio)pyr-(id)one] compounds with amino acids and proteins

Samuel M. Meier^{a,b}, Muhammad Hanif^{a,c}, Wolfgang Kandioller^a,
Bernhard K. Keppler^{a,b}, Christian G. Hartinger^{a,b,*}

^a University of Vienna, Institute of Inorganic Chemistry, Waehringer Str. 42, A-1090 Vienna, Austria

^b University of Vienna, Research Platform "Translational Cancer Therapy Research", Waehringer Str. 42, A-1090 Vienna, Austria

^c Department of Chemistry, COMSATS Institute of Information Technology Abbottabad, Tobe Camp, Abbottabad-22060, Pakistan

ARTICLE INFO

Article history:

Received 2 June 2011

Received in revised form 22 July 2011

Accepted 18 August 2011

Available online 26 August 2011

Keywords:

Adduct cleavage

Amino acids

Anticancer metalldrugs

Mass spectrometry

Ruthenium

Ubiquitin

ABSTRACT

The interactions of the ruthenium(arene) complexes [chlorido(η^6 -*p*-cymene)(2-methyl-3-(oxo- κ O)-4*H*-pyran-4-onato- κ O)ruthenium(II)] **1**, [chlorido(η^6 -*p*-cymene)(2-methyl-3-(oxo- κ O)-4*H*-thiopyran-4-onato- κ S)ruthenium(II)] **2** and [chlorido(η^6 -*p*-cymene){*N*-[(ethoxycarbonyl)methyl]-3-(oxo- κ O)-1*H*-pyrid-2-onato- κ O)ruthenium(II)] **3** with biomolecules such as L-methionine (Met) and ubiquitin (Ub) were investigated by electrospray ionization (ESI) ion trap mass spectrometry (MS). These Ru^{II} compounds were shown to exhibit anticancer activity which varies depending on the (thio)pyr(id)onato ligands. Compounds **1** and **3** reacted readily with the model protein Ub to yield stable [Ub + Ru(*p*-cym)] adducts (*p*-cym = η^6 -*p*-cymene), whereas **2** was converted only to a minor degree. The protein adduct formation is reversible by incubation with *N*- and *S*-donor systems, the latter being more efficient. From these studies, an inverse correlation between metalldrug–protein interaction and cytotoxicity against human tumor cell lines was derived, where low protein binding ability is indicative of increased cytotoxic activity.

© 2011 Elsevier Inc. All rights reserved.

1. Introduction

The appreciation of ruthenium-based compounds as a less toxic, but nonetheless potent alternative to established platinum(II) anticancer agents has prompted extensive research efforts in the area of inorganic medicinal chemistry. The success of the ruthenium(III) complexes KP1019 and NAMI-A, which are currently undergoing clinical trials [1,2], triggered further investigative focus in this direction. It is supposed that ruthenium(III) metalldrugs are prodrugs and that *in vivo* reduction yields an activated ruthenium(II) species [3]. Preparation of ruthenium(II) organometallics represents one of the latest trends in metalldrug research. Stabilization of the low oxidation state is achieved by formation of half-sandwich Ru^{II}(arene) compounds, where the arene occupies three ligand sites [4,5]. Based on this structural motif, a broad spectrum of organometallic anticancer agents has emerged, the best studied being RAPTA-C [6] and [η^6 -*p*-cymene)Ru(en)Cl]PF₆ (en = ethylenediamine) [7]. Recently, Ru^{II}(arene) organometallics bearing halide leaving groups and bidentate

pyrones were developed, which exhibit IC₅₀ values from low to high micromolar concentrations depending on the used ligand systems [8–15].

While platinum(II)-based chemotherapeutics exert their cytotoxic effect by binding to DNA [16–18], in particular to the *N7* atom of adjacent guanines, the exact mode of action of ruthenium-based metalldrugs is still unclear [19]. It was argued that genomic DNA may not represent the ultimate drug target, but that proteins involved in cellular signaling pathways play an important role [20]. Indeed, cellular and plasma proteins might constitute better binding partners than genomic DNA. This hypothesis was further strengthened by studies on the binding of RAPTA-C to nucleosome core particles [21]. The metal was found to have three distinct binding sites on the histone proteins, but none for DNA.

Besides X-ray diffraction analysis and NMR spectroscopy, electrospray ionization (ESI) mass spectrometry proved to be a valuable analytical technique for the direct investigation of metalldrug–protein interactions and was employed to elucidate the nature of metalldrug binding and for characterization of binding sites. The interactions of the approved platinum-based chemotherapeutics with proteins were extensively studied using mass spectrometric methods [22–31], whereas only a few investigations were carried out with ruthenium(II) compounds [28,32–35]. This paper reports on ESI-ion trap mass spectrometric studies for the characterization of metalldrug–protein interactions with the aim to correlate the

* Corresponding author at: University of Vienna, Institute of Inorganic Chemistry, Waehringer Str. 42, A-1090 Vienna, Austria. Tel.: +43 1 4277 52609; fax: +43 1 4277 52680.

E-mail address: christian.hartinger@univie.ac.at (C.G. Hartinger).

anticancer activity with the affinity of Ru^{II}(arene) compounds to biomolecular targets, their metabolization and release from proteins.

2. Experimental

2.1. Materials and methods

Ubiquitin (bovine erythrocytes) and human serum albumin were purchased from Sigma, L-methionine and reduced L-glutathione (GSH) from Sigma-Aldrich and L-cysteine, 2-deoxyguanosine 5'-monophosphate (dGMP), formic acid (99%) and ammonium bicarbonate from Fluka. All materials from chemical suppliers were used as received. The complexes [chlorido(η^6 -p-cymene)(2-methyl-3-(oxo- κ O)-4H-pyran-4-onato- κ O)ruthenium(II)] **1** [12], [chlorido(η^6 -p-cymene)(2-methyl-3-(oxo- κ O)-4H-thiopyran-4-onato- κ S)ruthenium(II)] **2** [12] and [chlorido(η^6 -p-cymene)[N-[(ethoxycarbonyl)methyl]-3-(oxo- κ O)-1H-pyrid-2-onato- κ O)ruthenium(II)] **3** [14] were prepared according to literature procedures.

MilliQ water (18.2 M Ω ; Millipore Synergy 185 UV Ultrapure Water System; Molsheim, France) and methanol (VWR Int., HiPerSolv, CHROMANORM) were used as solvents for ESI-MS studies. In a typical experiment, the respective metallodrug and Ub were incubated in aqueous solution (pH 5.5) at a molar ratio of 4:1 and 37 °C and with L-methionine at a molar ratio of 1:1, and spectra were recorded after 0, 3, 6, 24 and 72 h.

The [Ub + Ru(p-cym)] adduct properties were investigated by selective preparation according to the following procedure: Complex **3** was incubated with Ub at a 4:1 molar ratio and 37 °C for 72 h in the dark. After purification by consecutive centrifugation (three times at 14,000 rpm; Hettich MIKRO 120, Tuttlingen, Germany) with 3 kDa cut-off filters (Amicon Ultra, Millipore, Ireland), the concentrated mono-adduct was diluted to 200 μ M. For studies in buffered solution, the [Ub + Ru(p-cym)] adduct was prepared in aqueous solution, followed by centrifugation as described before. The formed adduct was redissolved in ammonium bicarbonate buffer (20 mM, pH 7.4) to yield a 200 μ M solution, which was used for hydrolysis and biomolecule cleavage studies. For the latter experiment, an excess of the respective nucleophile (Met, His, Cys, GSH, dGMP; 4 eq.) or equimolar amounts of HSA were added to the centrifuged reaction mixture and incubated at 37 °C. Samples were taken after 0, 48, 72 h and 7 d and analyzed by ESI-MS.

2.2. Instrumentation

Electrospray ionization mass spectra were recorded on a Bruker Esquire₃₀₀₀ ion trap instrument by direct infusion at typical concentrations of 5–10 μ M and a flow rate of 5 μ L/min. Protein samples were diluted with methanol:water:formic acid (50:50:0.2) while the reference complexes and L-methionine samples were diluted with methanol only. Typical acquisition conditions for ubiquitin measurements were as follows: positive ion mode, dry gas temperature 200 °C, dry gas 6 L/min, nebulizer 10 psi, trap drive 34.4, skim1 43.2 V, skim2 6.0 V, octopole 2.62 V, capillary exit 120.4 V, and capillary exit offset 77.2 V. The spectra were processed using ESI Compass 1.3 and DataAnalysis 4.0 software (Bruker Daltonics GmbH, Bremen, Germany). Deconvolution was obtained by applying the maximum entropy algorithm with a 0.1 m/z mass step and 0.5 m/z instrument peak width.

3. Results and discussion

3.1. Stability of the Ru(II) complexes **1–3** in aqueous solution

Ruthenium-based chemotherapeutics, which are currently undergoing clinical trials, are administered intravenously to the patient. These metallodrugs follow the prodrug concept and are activated by hydrolysis and/or reduction. This facilitates the interaction with biological nucleophiles in the blood stream and eventually

in cells. In particular serum proteins, such as human serum albumin (HSA) and transferrin (TF), but also intracellular components like glutathione or DNA represent well-suited binding partners for the activated metallodrug. Binding to biomolecules is considered important for both transport and deactivation, as well as causing adverse side effects observed during treatment [36]. Investigating biological interactions is thus crucial for understanding the behavior and mode of action of these metallodrugs in biological environment.

In the present study, three arene-capped ruthenium(II) complexes with ligands belonging to the pyrone class, i.e. 2-methyl-3-oxo-4H-pyran-4-onato **1**, 2-methyl-3-oxo-4H-thiopyran-4-onato **2** and N-[(ethoxycarbonyl)methyl]-3-oxo-1H-pyrid-2-onato **3** were investigated (Fig. 1). Their IC₅₀ values depend significantly on the chelating ligands; O,O-bidentate systems, as present in **1** and **3** yield low cytotoxic activity of the complexes toward CH1 and SW480 cell lines (>100 μ M), whereas compounds based on S,O-chelating ligands were proven to be one to two orders of magnitude more active [12,14]. In addition, the behavior in aqueous solution is significantly different for the three compounds. Compound **1** is fairly stable but ligand cleavage occurred to some extent over time. This process results in the formation of an inactive dinuclear product after 72 h [9,12], whereas pyridone-based **3** is known to be stable for more than 3 days [14]. In addition, transesterification to the methyl ester and hydrolysis to the carboxylic acid in small amounts in the presence of methanol was observed for **3**. In general, pyridonato ligands form complexes which are more stable than their pyronato analogs [8].

Complexes **1–3** predominately form in ESI-MS positively charged ions by abstraction of the chlorido ligand in methanolic solution. In accordance to NMR spectroscopic studies, ESI-MS of **1** showed a peak assignable to the parent ion [**1** – Cl]⁺ accompanied by the formation of dimeric species (10% relative to the parent ion signal intensity after 72 h; Scheme 1). Thiopyronato-based **2** is stable in aqueous solution during the first 6 h. However, the [**2** – Cl]⁺ parent signal vanished completely within 24 h yielding a set of ligand-containing homodimetallic species, e.g. [(p-cym)₂Ru₂(tpn)₂ + H₂O]²⁺ (m/z 385.02, m_{ex} = 385.28; tpn = 2-methyl-3-oxo-4H-thiopyran-4-onato) and [(p-cym)₂Ru₂(tpn) + 2OH + MeOH]⁺ (m/z 677.70, m_{ex} = 678.06), which might be related to the cross-linking capacity of the S-containing ligand. Similarly to **1**, methoxido/hydroxido dimeric species (m/z 535.72) were detected after 24 h. Interestingly, the signal at m/z 360.8 \pm 0.1 (8%) indicates conversion of the sulfur-containing thiopyronato into an oxygen-containing pyronato ligand.

3.2. Reaction toward biomolecules

In a next step, the organometallic compounds were investigated for their reactivity toward biological nucleophiles, i.e., Ub and amino acids. Preliminary studies were conducted with the amino acid Met at a molar ratio of 1:1 and both pyrone- and pyridone-based complexes **1** and **3** reacted similarly by cleavage of the O,O-bidentate ligands within several hours. The respective coordinated ligand was replaced by methionine, which generated selectively a methionine adduct [(p-cym)Ru(Met) – H]⁺ (m/z 383.8 \pm 0.1, m_{ex} = 384.06) as

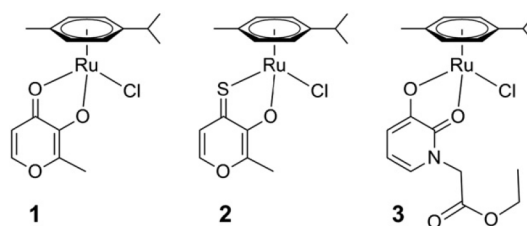
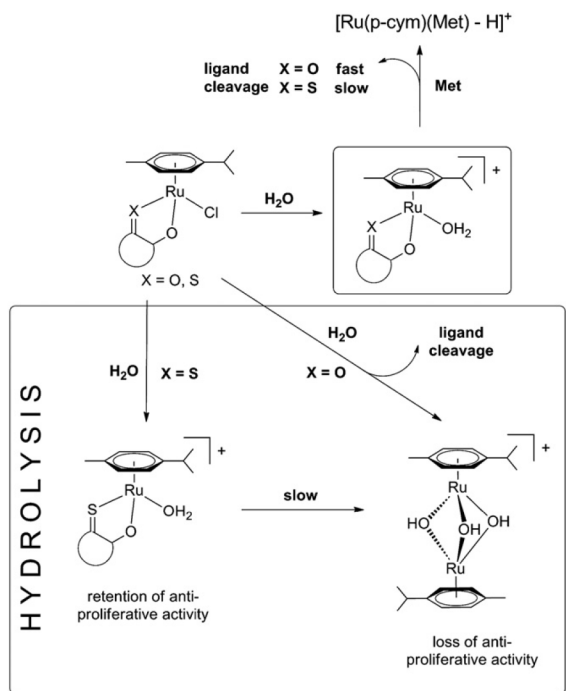


Fig. 1. Chemical structures of ruthenium(II) compounds bearing pyronato (**1**), thiopyronato (**2**) and pyridonato (**3**) ligands.



Scheme 1. Hydrolysis and biomolecular reaction pathways for the ruthenium(II) metallodrugs used in this study. After aquation, pyridonate and pyridonate ligands are cleaved in the presence of biological nucleophiles, whereas thiopyridonate-based complexes are more stable in the presence of biological nucleophiles.

the most abundant species and no further side products were observed. The thiopyridonate complex **2** displays enhanced stability toward Met. The recorded spectra revealed the presence of intact **2** within the first 6 h followed by the formation of identical ligand-containing dimeric products as observed in the hydrolysis experiments. After 24 h, the detection of a signal at m/z 383.9 indicates the formation of the methionine adduct and thus cleavage of the *S,O*-thiopyridonate ligand. However, considering the overall intensity, thiopyridonate ligand cleavage by methionine accounts for a significantly lower amount compared to *O,O*-ligand systems.

Ubiquitin represents a suitable model for metallodrug–protein interaction studies and contains two major binding sites involved in metallodrug binding, *i.e.* Met1 and His68 [22,23]. *N*-terminal Met1 can act as a potential bidentate ligand *via* coordination of the thioether and amino moieties [30,37], whereas His68 features a monodentate *N*-binding site at the imidazole residue. In a typical protein binding experiment the respective complex was incubated with Ub at a molar ratio of 4:1 at 37 °C in aqueous solution (pH 5.5). The protein samples were injected into the mass spectrometer by direct infusion under denaturing conditions, *i.e.* 50% methanol and 0.2% formic acid to achieve efficient protonation of the protein. Similarly to the reaction with Met, complex **1** reacted rapidly with Ub. After 3 h, mono- and bis-adducts had quantitatively formed and no unreacted Ub was observed. The adducts were identified to contain $[\text{Ru}(\text{p-cym})]^{2+}$ moieties attached to the protein, forming $[\text{Ub} + \text{Ru}(\text{p-cym})]^{+}$ and $[\text{Ub} + 2\text{Ru}(\text{p-cym})]^{+}$ -type adducts, and were detected at 8786.9 ± 0.6 Da and 9032.1 ± 1.0 Da, respectively. However, one of the binding sites does not seem to constitute a thermodynamically stable interaction and within 24 h, the $[\text{Ub} + 2\text{Ru}(\text{p-cym})]^{+}$ bis-adduct vanished. After 72 h, the final products between **1** and Ub were identified as the $[\text{Ub} + \text{Ru}(\text{p-cym})]^{+}$ mono-adduct and a bis-adduct in minor amounts. The mass difference of 153.0 ± 1.0 Da between the latter mono- and bis-adduct indicates cleavage of the cymene ring and

replacement by aqua/hydroxido ligands (Fig. 2). This behavior largely parallels the findings for the pyridonate complex **3**, where mono- and bis-adducts were also observed within the first hours of incubation, again accompanied by ligand cleavage. Ultimately, the higher order adducts vanished and the $[\text{Ub} + \text{Ru}(\text{p-cym})]^{+}$ mono-adduct is formed as the primary interaction product after 72 h (Fig. 2). In contrast, complex **2** containing a thiopyridonate ligand reacted with Ub at a considerably lower rate. Incubating the reaction mixture for 72 h yielded only minor amounts of the $[\text{Ub} + \text{Ru}(\text{p-cym})]^{+}$ mono-adduct. The intensities of the mono-adduct relative to free Ub increased from 8% after 6 h to 20% after 3 days and no further adduct types were observed (Fig. 2). The reason for the different behaviors is related to the increased binding strength of the thiopyridonate ligand to the transition metal compared to the pyr(id)onate ligands [11]. Consequently, *O,O*-chelating ligands are more readily cleaved and replaced by nitrogen- or sulfur-containing biological nucleophiles than *S,O*-ligands.

3.3. Investigations on the stability of the $[\text{Ub} + \text{Ru}(\text{p-cym})]^{+}$ adduct

Since the mode of action of ruthenium(II)-based metallodrugs is still a subject of debate, the investigation and characterization of metabolism products is essential for a better understanding of their pharmacological profile. Of particular interest is thereby the interaction between metallodrugs, which are administered intravenously, and proteins. In the present study, Ub was employed as a model protein to investigate metallodrug–protein adduct formation. The observation of the identical protein adduct, *i.e.* $[\text{Ub} + \text{Ru}(\text{p-cym})]^{+}$, for complexes **1–3** directed our interest to further investigate the properties of this mono-adduct, which was specifically obtained by incubating complex **3** with Ub for 72 h at a molar ratio of 4:1 in the dark and subsequent quenching of the reaction by centrifugation with 3 kDa cut-off filters. Being stable for more than 7 days in aqueous solution, the adduct was treated with different biological nucleophiles containing soft *N*- and/or *S*-donors ranging from small molecules to proteins, *i.e.* dGMP, Met, Cys, GSH and HSA.

dGMP with its nucleophilic N7 interacts weakly with the $[\text{Ub} + \text{Ru}(\text{p-cym})]^{+}$ adduct. Following the reaction at a four-fold excess, the adduct half-life was >7 d. Within this time period, about 30% free Ub formed and no evidence was detected of direct ruthenium-dGMP interaction products. In contrast, upon addition of 4 eq. of Met

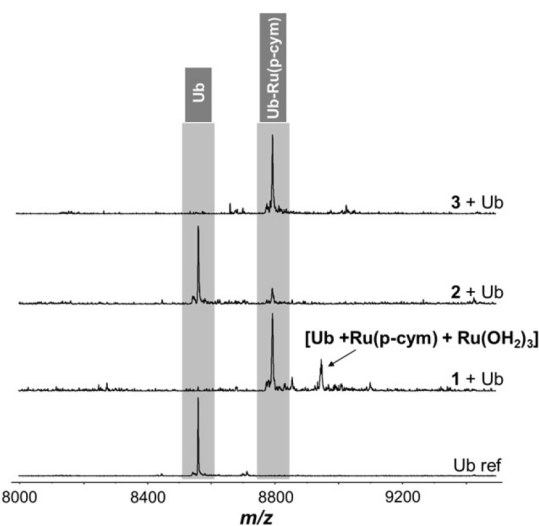


Fig. 2. Deconvoluted mass spectra of reaction mixtures recorded after 72 h containing Ub and complexes **1–3** at a molar ratio of 1:4. The Ub spectrum is given as a reference (Ub ref).

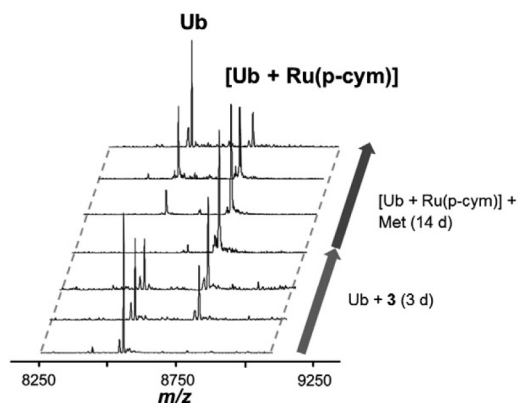


Fig. 3. Deconvoluted mass spectra demonstrating [Ub + Ru(p-cym)] adduct formation. Ub was incubated for 72 h with **3** to form the [Ub + Ru(p-cym)] adduct, which was then treated with Met for further 14 d at a molar ratio of 1:4.

the half-life of the adduct decreased to about 7 d (Fig. 3). In this case, the MS approach allows simultaneous determination of both kinetics of adduct depletion and characterization of the interaction products (Fig. 4). Besides the [Ub + Ru(p-cym)] adduct and free Ub, a ruthenium–methionine adduct with identical m/z values as in the interaction studies between **3** and methionine corresponding to [(p-cym)Ru(Met) – H]⁺ (m/z 383.8 ± 0.1) was observed.

The reaction between the [Ub + Ru(p-cym)] adduct and Cys showed similar kinetics as for Met. As observed earlier [14], the interaction of ruthenium complexes with Cys leads to partial decomposition of the (thio)pyr(id)onato complexes, due to the strong trans-effect of the thiol group, and thus no specific small molecule interaction products were observed. Both Met and Cys cleave the [Ub + Ru(p-cym)] adduct faster than *N*-chelating biological nucleophiles such as dGMP. Similar observations were made for incubation mixtures containing redox-active GSH. It displayed even faster kinetics ($\tau_{1/2} \approx 5.5$ d) than Met and Cys, resulting in 55% free Ub after 7 d. The oxidized form of glutathione, glutathione disulfide was detected in the negative mode ESI-mass spectrum (m/z 610.7 ± 0.1). The involvement of possible redox processes was further underlined by the appearance of a signal in the deconvoluted spectrum assignable to [Ub + Ru(OH)]⁺ (8682.5 ± 0.5 Da) after cleavage of the arene.

In addition to experiments on the stability of the [Ub + Ru(p-cym)] adduct in presence of small biomolecules, the influence of the serum protein HSA (1:1) was studied. HSA contains a total of 23

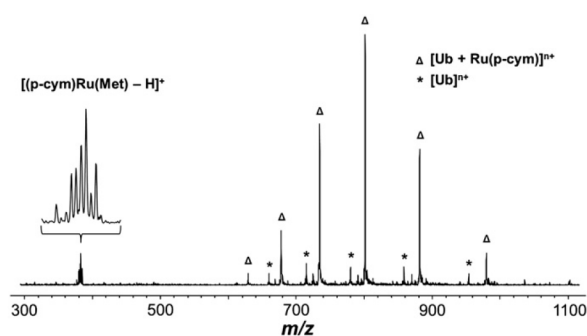


Fig. 4. The spectrum shows the interaction of the [Ub + Ru(p-cym)] adduct with Met after 48 h incubation. Simultaneous detection of protein cleavage kinetics and small molecule–ruthenium adduct formation is possible. Triangles (Δ) refer to the [Ub + Ru(p-cym)]ⁿ⁺ adduct ($n=9-14$) and asterisks (*) to regenerated free Ubⁿ⁺. The methionine–ruthenium adduct is visible in the low m/z mass range (the inset shows the isotope distribution of the [(p-cym)Ru(Met) – H]⁺ adduct (m/z 383.8 ± 0.1)).

accessible *S*- and *N*-donors (1 Cys, 6 Met and 16 His) and therefore the concentration of biological nucleophiles is approximately 5-times higher under the applied conditions than for the amino acid reactions. After 7 d, 62% of the [Ub + Ru(p-cym)] adduct was still present in the deconvoluted spectrum. The lower kinetics of adduct cleavage for the [Ub + Ru(p-cym)]/HSA incubations can be explained by the reduced efficiency of the biological nucleophile (HSA) to approach the metal-binding site of the [Ub + Ru(p-cym)] adduct, due to their respective macromolecular sizes.

According to these experiments, the following trend for the ability to cleave ruthenium from Ub in aqueous solution was observed: GSH > Cys ≈ Met > HSA > dGMP. This trend suggests that *S*-containing chelators, associated with the cellular redox system [38], are most potent in cleaving the Ru^{II} moiety from Ub though long half-lives were observed under the applied conditions. In addition, high molecular weight molecules, such as HSA, lack in approachability of the respective nucleophilic parts. Furthermore, amino acids seem to constitute better binding partners than nucleobases and that once the metallodrug binds to a protein, it is unlikely to be transferred to DNA. This is a further indication that the cytotoxic activity of Ru^{II}-based anticancer agents is associated with the proteome rather than with the genome. Similar experiments were carried out with cisplatin by Peleg-Shulman and Gibson [22]. In both cases, GSH was more efficient in cleaving the metallodrug–Ub adduct than dGMP, which is related to the increased trans-effect of the thiol group in GSH. On the other hand, differences between the two metal systems were observed when comparing the cleavage mechanisms. In the case of cisplatin ternary adducts were detected where GSH is directly bound to yield a Ub–Pt–GSH intermediate. The formation of such ternary adducts is facilitated in square planar platinum(II) complexes via a five-coordinate associative ligand exchange. However, signals assignable to comparable intermediates were not observed for cymene-capped pseudo-octahedral ruthenium(II) derivatives.

To determine the influence of the incubation conditions on the reactivity of the [Ub + Ru(p-cym)] system, the same set of reactions were performed in buffered solution (20 mM ammonium bicarbonate, pH 7.4). Since the adduct does not form in carbonate buffer in a quantitative manner, the [Ub + Ru(p-cym)] adduct was prepared in aqueous solution, followed by extensive ultracentrifugation and redissolving in buffer. Under these conditions, the [Ub + Ru(p-cym)] adduct is less stable and [Ub + Ru(p-cym)] is cleaved to yield approximately 30% of free Ub after 3 days. If the [Ub + Ru(p-cym)] adduct is incubated in buffer with biological nucleophiles at a molar ratio of 1:4, the ruthenium moiety is quantitatively cleaved from the adduct within 3 days, irrespective of the biological nucleophile. In the case of Met, the small molecule interaction product was again detected corresponding to [(p-cym)Ru-(Met) – H]⁺ (m/z 383.8 ± 0.1). A change to more physiologically relevant conditions therefore decreased the stability of the [Ub + Ru(p-cym)] adduct and cleavage rates increased. Although accelerated in buffered solution, the mechanism of adduct cleavage seems to be largely identical to non-buffered conditions.

3.4. Impact of protein binding on antitumor activity

The *in vitro* anticancer activity of **2** in the human tumor cell lines SW480 and CH1 is in the low μ M range and therefore the IC₅₀ values are at least one order of magnitude higher than of **1** and **3** [11,12,14]. When comparing the reactions of (thio)pyr(id)onato-Ru derivatives with biological nucleophiles, *i.e.*, amino acids and proteins, the *S,O*-complexes are much more stable in the presence of biological nucleophiles with respect to ligand cleavage. Furthermore, the concentration of free, unmetabolized drug in systemic circulation is often considered important for a drug's efficacy. For example, in case of cisplatin binding to serum proteins is not only thought to be a deactivation mechanism but even related to the drug's adverse effects [36]. Compounds **1** and **3** exhibit IC₅₀ values of >100 μ M and bind quantitatively to Ub within

3 h, forming mono- and bis-adducts. It is therefore assumed that extensive protein binding, accompanied by ligand cleavage, accounts for a possible deactivation pathway of these Ru^{II}-type metalodrugs. In contrast, **2** shows only a small percentage of adduct formation after 3 days of incubation and displays therefore increased stability toward biological nucleophiles, such as thiol-containing molecules, which in turn results in an increased probability that the drug reaches unmetabolized the tumorigenic tissue. This is reflected in the low IC₅₀ value, e.g. 13 ± 4 for CH1 and 5.1 ± 0.5 for SW480 [11,12,14]. Therefore, the observation of abundant adduct formation of **1** and **3** with Ub but only minor reactivity of **2** suggests an inverse correlation between cytotoxic potency of the respective compounds and the extent of adduct formation. Accordingly, prior to time-consuming, laborious and expensive *in vitro* testing, studies on the different degrees of binding of the Ru organometallics accompanied by ligand cleavage might give important indications on the biological activity of structurally related compounds. Exceptions to this rule may apply, when hydrolytically stable species are considered which do not bind covalently to biological targets [15] or if a multi-target strategy is pursued where metalodrugs release bioactive ligands paralleled by the binding of a metal center to a target biomolecule [39,40].

4. Conclusions

The interactions of the ruthenium-based developmental anticancer agents **1–3** with ubiquitin (Ub) and methionine (Met) were investigated by ESI-ion trap mass spectrometry. Complexes **1** and **3**, which contain pyronato and pyridonato ligands, respectively, were found to react rapidly with Ub inducing the cleavage of the bidentate ligand. The most abundant product [Ub + Ru(p-cym)] was selectively obtained and is stable for more than 7 d in aqueous media, however, can in turn be cleaved with S-donor containing biomolecules such as Met, GSH or Cys. The fastest cleavage kinetics in aqueous solution was observed for redox-active glutathione, especially when working in buffered solutions. On the contrary, the thiopyronato-based complex **2** showed only a minor tendency to form [Ub + Ru(p-cym)]⁺ adducts. Therefore, an inverse correlation between metalodrugs–protein interaction and cytotoxicity against tumor cells can be derived from these studies, i.e., the lower the compounds' rate of adduct formation with biomolecules the more pronounced their cytotoxic activity. Note that exceptions may apply for hydrolytically stable species or compounds which release active ligands.

Abbreviations

CH1	ovarian cancer cell line
ESI-MS	electrospray ionization mass spectrometry
GSH	reduced glutathione
HSA	human serum albumin
p-cym	p-cymene
Ru	ruthenium
SW480	colon carcinoma cell line
tpn	2-methyl-3-oxo-4H-thiopyran-4-onato
Ub	ubiquitin

Acknowledgments

The authors are indebted to the Johanna Mahlke geb. Obermann Foundation, COST D39 and CM0902 and the Hochschuljubiläumstiftung Vienna.

References

- [1] C.G. Hartinger, M.A. Jakupec, S. Zorbas-Seifried, M. Groessl, A. Egger, W. Berger, H. Zorbas, P.J. Dyson, B.K. Keppler, *Chem. Biodiversity* 5 (2008) 2140–2155.
- [2] E. Alessio, G. Mestroni, A. Bergamo, G. Sava, *Curr. Top. Med. Chem.* 4 (2004) 1525–1535.
- [3] M.J. Clarke, S. Bitler, D. Rennert, M. Buchbinder, A.D. Kelman, *J. Inorg. Biochem.* 12 (1980) 79–87.
- [4] C.G. Hartinger, P.J. Dyson, *Chem. Soc. Rev.* 38 (2009) 391–401.
- [5] Y.K. Yan, M. Melchart, A. Habtemariam, P.J. Sadler, *Chem. Commun.* (2005) 4764–4776.
- [6] C. Scolaro, A. Bergamo, L. Brescacin, R. Delfino, M. Cocchietto, G. Laurency, T.J. Geldbach, G. Sava, P.J. Dyson, *J. Med. Chem.* 48 (2005) 4161–4171.
- [7] A. Habtemariam, M. Melchart, R. Fernandez, S. Parsons, I.D.H. Oswald, A. Parkin, F.P.A. Fabbiani, J.E. Davidson, A. Dawson, R.E. Aird, D.J. Jodrell, P.J. Sadler, *J. Med. Chem.* 49 (2006) 6858–6868.
- [8] W. Kandioller, A. Kurzwernhart, M. Hanif, S.M. Meier, H. Henke, B.K. Keppler, C.G. Hartinger, *J. Organomet. Chem.* 696 (2011) 999–1010.
- [9] A.F. Peacock, M. Melchart, R.J. Deeth, A. Habtemariam, S. Parsons, P.J. Sadler, *Chem. Eur. J.* 13 (2007) 2601–2613.
- [10] M.G. Mendoza-Ferri, C.G. Hartinger, M.A. Mendoza, M. Groessl, A.E. Egger, R.E. Eichinger, J.B. Mangrum, N.P. Farrell, M. Maruszak, P.J. Bednarski, F. Klein, M.A. Jakupec, A.A. Nazarov, K. Severin, B.K. Keppler, *J. Med. Chem.* 52 (2009) 916–925.
- [11] W. Kandioller, C.G. Hartinger, A.A. Nazarov, C. Bartel, M. Skocic, M.A. Jakupec, V.B. Arion, B.K. Keppler, *Chem. Eur. J.* 15 (2009) 12283–12291.
- [12] W. Kandioller, C.G. Hartinger, A.A. Nazarov, M.L. Kuznetsov, R.O. John, C. Bartel, M.A. Jakupec, V.B. Arion, B.K. Keppler, *Organometallics* 28 (2009) 4249–4251.
- [13] J.H. Kasser, W. Kandioller, C.G. Hartinger, A.A. Nazarov, V.B. Arion, P.J. Dyson, B.K. Keppler, *J. Organomet. Chem.* 695 (2010) 875–881.
- [14] M. Hanif, H. Henke, S.M. Meier, S. Martic, M. Labib, W. Kandioller, M.A. Jakupec, V.B. Arion, H.B. Kraatz, B.K. Keppler, C.G. Hartinger, *Inorg. Chem.* 49 (2010) 7953–7963.
- [15] M. Hanif, S.M. Meier, W. Kandioller, A. Bytzeck, M. Hejl, C.G. Hartinger, A.A. Nazarov, V.B. Arion, M.A. Jakupec, P.J. Dyson, B.K. Keppler, *J. Inorg. Biochem.* 105 (2011) 224–231.
- [16] S.E. Sherman, D. Gibson, A.H.J. Wang, S.J. Lippard, *J. Am. Chem. Soc.* 110 (1988) 7368–7381.
- [17] M.A. Jakupec, M. Galanski, V.B. Arion, C.G. Hartinger, B.K. Keppler, *Dalton Trans.* (2008) 183–194.
- [18] M.A. Barry, C.A. Behnke, A. Eastman, *Biochem. Pharmacol.* 40 (1990) 2353–2362.
- [19] P.J. Dyson, G. Sava, *Dalton Trans.* (2006) 1929–1933.
- [20] S. Chatterjee, S. Kundu, A. Bhattacharyya, C.G. Hartinger, P.J. Dyson, *J. Biol. Inorg. Chem.* 13 (2008) 1149–1155.
- [21] B. Wu, M.S. Ong, M. Groessl, Z. Adhikrekan, C.G. Hartinger, P.J. Dyson, C.A. Davey, *Chem. Eur. J.* 17 (2011) 3562–3566.
- [22] T. Peleg-Shulman, D. Gibson, *J. Am. Chem. Soc.* 123 (2001) 3171–3172.
- [23] C.G. Hartinger, Y.O. Tsybin, J. Fuchser, P.J. Dyson, *Inorg. Chem.* 47 (2008) 17–19.
- [24] J. Will, D.A. Wolters, W.S. Sheldrick, *Chem. Med. Chem.* 3 (2008) 1696–1707.
- [25] Y. Najajreh, T.P. Shulman, O. Moshel, N. Farrell, D. Gibson, *J. Biol. Inorg. Chem.* 8 (2003) 167–175.
- [26] C.S. Allardyce, P.J. Dyson, J. Coffey, N. Johnson, *Rapid Commun. Mass Spectrom.* 16 (2002) 933–935.
- [27] I. Khalaila, C.S. Allardyce, C.S. Verma, P.J. Dyson, *ChemBioChem* 6 (2005) 1788–1795.
- [28] J.P. Williams, J.M. Brown, I. Campuzano, P.J. Sadler, *Chem. Commun.* 46 (2010) 5458–5460.
- [29] C.G. Hartinger, W.H. Ang, A. Casini, L. Messori, B.K. Keppler, P.J. Dyson, *J. Anal. At. Spectrom.* 22 (2007) 960–967.
- [30] J.P. Williams, H.I.A. Phillips, I. Campuzano, P.J. Sadler, *J. Am. Soc. Mass Spectrom.* 21 (2010) 1097–1106.
- [31] A. Casini, C. Gabbiani, G. Mastrobuoni, L. Messori, G. Moneti, G. Pieraccini, *Chem. Med. Chem.* 1 (2006) 413–417.
- [32] A. Casini, C. Gabbiani, F. Sorrentino, M.P. Rigobello, A. Bindoli, T.J. Geldbach, A. Marrone, N. Re, C.G. Hartinger, P.J. Dyson, L. Messori, *J. Med. Chem.* 51 (2008) 6773–6781.
- [33] A. Casini, G. Mastrobuoni, W.H. Ang, C. Gabbiani, G. Pieraccini, G. Moneti, P.J. Dyson, L. Messori, *ChemMedChem* 2 (2007) 631–635.
- [34] A. Casini, G. Mastrobuoni, M. Terenghi, C. Gabbiani, E. Monzani, G. Moneti, L. Casella, L. Messori, *J. Biol. Inorg. Chem.* 12 (2007) 1107–1117.
- [35] C.G. Hartinger, A. Casini, C. Duhot, Y.O. Tsybin, L. Messori, P.J. Dyson, *J. Inorg. Biochem.* 102 (2008) 2136–2141.
- [36] J. Reedijk, *Chem. Rev.* 99 (1999) 2499–2510.
- [37] D. Gibson, C.E. Costello, *Eur. Mass Spectrom.* 5 (1999) 501–510.
- [38] U. Jungwirth, C.R. Kowol, B.K. Keppler, C.G. Hartinger, W. Berger, P. Heffeter, *Anti-oxid. Redox Signal* 15 (4) (2011) 1085–1127.
- [39] W.H. Ang, A. De Luca, C. Chapuis-Bernasconi, L. Juillerat-Jeanerret, M. Lo Bello, P.J. Dyson, *Chem. Med. Chem.* 2 (2007) 1799–1806.
- [40] W.H. Ang, L.J. Parker, A. De Luca, L. Juillerat-Jeanerret, C.J. Morton, M. Lo Bello, M.W. Parker, P.J. Dyson, *Angew. Chem., Int. Ed. Engl.* 48 (2009) 3854–3857.

3.4. Fragmentation Methods on the Balance: Unambiguous Top-Down Mass Spectrometric Characterization of Oxaliplatin-Ubiquitin Binding Sites

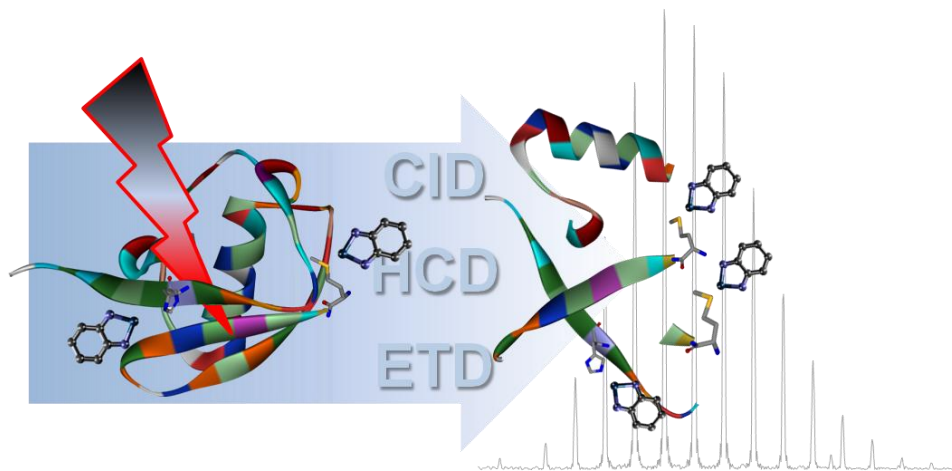
Samuel M. Meier,^{a,b} Yury O. Tsybin,^c Paul J. Dyson,^c Bernhard K. Keppler,^{a,b} Christian G. Hartinger^{a,b,c}

Analytical and Bioanalytical Chemistry, **2012**, *402*, 2655-2662.

^a University of Vienna, Institute of Inorganic Chemistry, Waehringer Str. 42, A-1090 Vienna, Austria.

^b University of Vienna, Research Platform “Translational Cancer Therapy Research”, Waehringer Str. 42, A-1090 Vienna, Austria.

^c Ecole Polytechnique Fédérale de Lausanne (EPFL), Institut des Sciences et Ingénierie Chimiques, CH-1015 Lausanne, Switzerland.



Fragmentation methods on the balance: unambiguous top–down mass spectrometric characterization of oxaliplatin–ubiquitin binding sites

Samuel M. Meier · Yury O. Tsybin · Paul J. Dyson ·
Bernhard K. Keppler · Christian G. Hartinger

Received: 31 July 2011 / Revised: 19 October 2011 / Accepted: 19 October 2011 / Published online: 8 November 2011
© Springer-Verlag 2011

Abstract The interaction between oxaliplatin and the model protein ubiquitin (Ub) was investigated in a top–down approach by means of high-resolution electrospray ionization mass spectrometry (ESI-MS) using diverse tandem mass spectrometric (MS/MS) techniques, including collision-induced dissociation (CID), higher-energy C-trap dissociation (HCD), and electron transfer dissociation (ETD). To the best of our knowledge, this is the first time that metallodrug–protein adducts were analyzed for the metal-binding site by ETD-MS/MS, which outperformed both CID and HCD in terms of number of identified metallated peptide fragments in the mass spectra and the localization of the binding sites. Only ETD allowed the simultaneous and exact determination of Met1 and His68 residues as binding partners for oxaliplatin. CID-MS/MS experiments were carried out on orbitrap and ion cyclotron

resonance (ICR)-FT mass spectrometers and both instruments yielded similar results with respect to number of metallated fragments and the localization of the binding sites. A comparison of the protein secondary structure with the intensities of peptide fragments generated by collisional activation of the [Ub+Pt-(chxn)] adduct [chxn=(1*R*,2*R*)-cyclohexanediamine] revealed a correlation with cleavages in solution phase random coil areas, indicating that the *N*-terminal β -hairpin and α -helix structures are retained in the gas phase.

Keywords Anticancer metallodrugs · Tandem mass spectrometry · Electron transfer dissociation · Oxaliplatin · Ubiquitin

Published in the *ANAKON* special issue with guest editors P. Dittrich, D. Günther, G. Hopfgartner, and R. Zenobi

Electronic supplementary material The online version of this article (doi:10.1007/s00216-011-5523-0) contains supplementary material, which is available to authorized users.

S. M. Meier · B. K. Keppler · C. G. Hartinger (✉)
Institute of Inorganic Chemistry, University of Vienna,
Währinger Str. 42,
1090 Vienna, Austria
e-mail: christian.hartinger@univie.ac.at

S. M. Meier · B. K. Keppler · C. G. Hartinger
Research Platform “Translational Cancer Therapy Research”,
University of Vienna,
Währinger Str. 42,
1090 Vienna, Austria

Y. O. Tsybin · P. J. Dyson · C. G. Hartinger
Institut des Sciences et Ingénierie Chimiques,
Ecole Polytechnique Fédérale de Lausanne (EPFL),
1015 Lausanne, Switzerland

Introduction

Platinum-based chemotherapeutics such as cisplatin, carboplatin, and oxaliplatin play an important role in cancer treatment. To exert their therapeutic effects, platinum-based anticancer drugs primarily target cellular DNA [1]. However, prior to entering the cell, plasma proteins also constitute excellent binding partners and it was found that Pt(II)-based metallodrugs bind to human serum albumin (HSA) and other plasma proteins upon administration [2, 3]. Furthermore, it is thought that the interaction with proteins accounts at least partially for the deactivation of these therapeutic agents and also for some adverse side effects observed during chemotherapy of cancer patients [4]. Understanding the binding to biomolecules is thus crucial for the development of novel metal-based anticancer drugs with enhanced selectivity and reduced side effects, however, the preferred binding sites of the Pt(II)-based anticancer drugs on proteins are still a matter of debate [5–8].

The identification of binding sites and of the nature of metallodrug–protein interactions both with clinically approved metal-based anticancer agents and also with developmental metallodrugs have been attempted using a wide range of bioanalytical and biophysical methods [9, 10]. Several off- and on-line mass spectrometric (MS) methods have proven to be powerful tools for the characterization of metallodrug–biomolecule interactions [11]. Electrospray ionization (ESI) and MALDI have been used to study various systems including *in vitro* binding studies to both DNA and proteins [8, 12–14], and even whole cells were treated with cisplatin, digested, and analyzed [15, 16]. The ability of metallodrugs to form adducts with plasma and cytoplasmic proteins such as HSA [8, 17, 18], myoglobin [19], transferrin [5, 20], model interactions with peptides [21, 22], and small model proteins such as ubiquitin (Ub) [11, 19, 23, 24], cytochrome-*c* (cyt-*c*) [25], lysozymes [7], and oligonucleotides [22, 26] have been subject of investigation by various MS methods.

In classical proteomics, bottom–up methodologies are widely used to characterize and identify protein sequences by analysis of enzymatic digests of proteins based on their mass fingerprints [27–29]. While bottom–up methods remain the best option for large proteins, they should cautiously be applied when investigating metallodrug–protein interactions since these may be prone to metallodrug cleavage during enzymatic digestion. More recently, top–down strategies were introduced [30], offering reduced experimental complexity and the ability to characterize entire protein sequences, whilst retaining post-translational modifications (PTMs) or even allowing the study of non-covalent interactions [31]. Considering metallation as a special type of PTM, top–down MS should be the method of choice for the detailed characterization of metallodrug–biomolecule conjugates [32]. Binding site localization can be achieved by tandem mass spectrometric methods, which include collision-induced dissociation (CID) [33], higher-energy C-trap dissociation (HCD) [34], infrared multiphoton dissociation [35], electron transfer dissociation (ETD) [36], or electron-capture dissociation (ECD) [37–39] and often deliver complementary information. CID and HCD are similar fragmentation methods relying on the collision of the molecules with inert gas molecules, which in turn leads to protein backbone cleavage, specifically at the amide C–N bond to produce predominantly *b*- and *y*-peptide fragments. Collisions with low-energy CID are less energetic than by HCD. Fragmentation by ECD and ETD is based on the transfer of electrons, which results in softer and more random protein backbone cleavages at N–C $_{\alpha}$ bonds and produces mainly *c*- and *z*-type peptide fragments. These methods have rarely been employed in studies on metal-based anticancer agents and therefore, we report here a comparative study on the binding site characteriza-

tion of oxaliplatin bound to Ub using different fragmentation methods in combination with high-resolution mass spectrometry. Oxaliplatin is the latest of the clinically approved platinum-based anticancer agents and compared with cisplatin, there are only a few investigations on binding interactions of this compound with biomolecules. The 76-amino acid protein Ub was established as a model in metallodrug binding studies [11, 19, 23, 24, 40] and Met1 has been characterized as a binding partner for cisplatin [24] and His68 being believed to represent the second binding site.

Experimental

Materials and methods

Ub (from bovine red blood cells, min 90%) was purchased from Sigma (Vienna, Austria), oxaliplatin from Sequoia Research Products (Pangbourne, UK), trifluoroacetic acid (98%) from Fluka (Vienna, Austria), and methanol (HiPer-Solv CHROMANORM) from VWR (Vienna, Austria). All materials from chemical suppliers were used as received. MilliQ water was obtained from a Millipore Synergy 185 UV Ultrapure apparatus (18.2 M Ω). Oxaliplatin and Ub were incubated in a molar ratio of 2:1 in water (pH 5.5) for 7 days at 37 °C. The reaction mixture was diluted with water/methanol/trifluoroacetic acid (50:50:0.1) to yield a final protein concentration of 1–5 μ M, i.e., measurements were performed under denaturing conditions.

Instrumentation

LTQ Velos Orbitrap MS Incubation mixtures of oxaliplatin and Ub were introduced by direct infusion into the ESI source of the mass spectrometer at a flow rate of 5 μ L/min. Survey and tandem mass spectra were recorded on a hybrid LTQ Velos Orbitrap mass spectrometer (Thermo Scientific, Bremen, Germany) employing CID-, HCD-, and ETD-MS/MS. Additional experimental settings were as follows: source voltage, +4 kV; source temperature, 40 °C; capillary temperature, 250 °C; sheath gas flow, 10 L/min; minimal signal required, 500; and isolation width, 10 Th. The normalized collision energies during MS/MS experiments were 30%, 40%, and 8% for CID, HCD, and ETD, respectively. Data were processed with Xcalibur 2.1 software (Thermo Scientific).

FT-ICR MS Incubation mixtures of oxaliplatin and Ub (ca. 3 μ M) were introduced by direct infusion *via* an ESI source into a 9.4-T mass spectrometer (Bruker Daltonics GmbH, Bremen, Germany) with a flow rate of 0.5 μ L/min. CID-MS/MS measurements were performed with 10 ms accu-

mulation time in the external quadrupole-based collisional cell. Additional instrument settings were as follows: capillary entrance voltage, -1.5 kV; capillary exit voltage, $+100$ V; dry gas flow rate, 35 L/min; dry gas temperature, 200 °C; scan width, m/z 400 – $3,000$; extraction voltage for ESI, -10 V; and nebulizing gas flow rate, 30 L/min. Spectra were acquired using Apex Control II. Data were analyzed and processed by ESI Compass 1.3 and Data Analysis 4.0 software (Bruker Daltonics).

Results and discussion

Characterization of oxaliplatin–Ub adducts by broadband ESI-MS

Oxaliplatin/Ub mixtures were incubated under non-denaturing conditions at pH 6, which reflect conditions that exist in hypoxic tumorigenic tissue [41, 42]. The incubation mixture was diluted to 1 – 5 μ M (protein) with $H_2O/MeOH/TFA$, causing denaturation of the protein to improve fragmentation efficiencies, and the samples were immediately injected into the ESI source of the mass spectrometer.

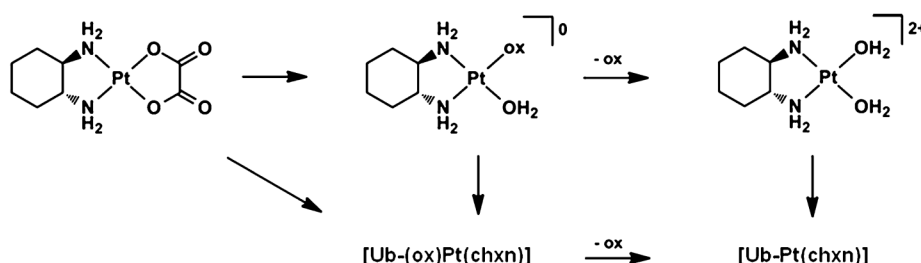
Platinum-based anticancer agents may interact with biomolecules at different stages of their activation process [43]. Oxaliplatin was designed to exhibit a very slow hydrolysis rate with a view to reduce unwanted side effects. Indeed, analysis of the reaction mixture containing a twofold excess of oxaliplatin by ESI-MS showed $\sim 50\%$ free Ub after incubation for 7 days. The activation mechanism of oxaliplatin rendering it capable of binding to biological molecules is thought to involve two successive steps. Initially, one bond between platinum and the oxalato chelating ligand is hydrolyzed forming a mono-aqua complex, after which cleavage of the remaining platinum-oxalato bond and ligand release from the platinum center occurs (Scheme 1). Therefore, several Pt–Ub derivatives were observed in the deconvoluted mass spectrum (Fig. 1) with the most prominent corresponding to an oxaliplatin–Ub adduct at m/z $8,871.704$ (84% relative intensity to free Ub;

all relative intensities refer to the most abundant peak in the respective mass spectrum). This signal can be assigned to a mono-adduct consisting of Ub and a Pt(chxn) moiety (chxn = (1*R*,2*R*)-cyclohexanediamine) having undergone cleavage of the oxalato ligand. Further identified species include the mono-adduct after the first activation step $[Ub+(ox)Pt(chxn)]^+$ (m/z $8,961.697$, 10%; oxalate (ox)), as well as higher adducts such as $[Ub+2Pt(chxn)]^+$ (m/z $9,177.582$, 24%) and $[Ub+Pt(chxn)+(ox)Pt(chxn)]^+$ (m/z $9,268.751$, 11%). The existence of platinum species stemming from the initial hydrolysis step was reported previously [43], and these findings provide further support for a two-step activation mechanism.

Comparative tandem mass spectrometry of oxaliplatin–Ub adducts

Top-down tandem mass spectrometric experiments on the incubation mixture were performed to directly identify binding sites of oxaliplatin on Ub using different fragmentation methods. These investigations were carried out with the most abundant adduct identified in the broadband mass spectrum, i.e., $[Ub+Pt(chxn)]$. The $12+$ charge state (m/z 740.313) was selected for binding site characterization in the orbitrap FT MS-based experiments and, for comparison, the $11+$ charge stage (m/z 807.515) in the FT-ICR MS-based experiments. The employment of charge states larger than $10+$ implies that Ub is entirely denatured and protonated to a large degree. CID-MS/MS was performed on both orbitrap- and ICR-FT MS instruments, whereas HCD- and ETD-MS/MS were performed on the orbitrap mass spectrometer only.

CID-MS/MS fragmentation profiles were comparable on both instruments and similar metallated peptide fragments were found. While the platinated peptide fragments were generally more abundant using FT-ICR MS, a higher number of such fragments was identified with the orbitrap MS approach. For the $[Ub+Pt(chxn)]$ adduct, CID led to the characterization of 23 different metallated peptide fragments for the orbitrap MS, compared to 15 with the FT-ICR MS. Assignable platinated peptide fragment ions



Scheme 1 Hydrolysis of oxaliplatin is responsible for activation of the prodrug and involves two successive steps (ox oxalate, chxn (1*R*,2*R*)-cyclohexanediamine). Upon hydrolysis, oxaliplatin may more readily react with suitable biological binding partners

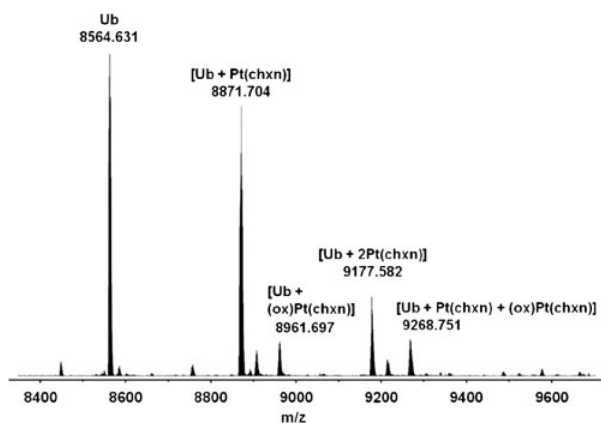


Fig. 1 Deconvoluted FT-ICR mass spectrum of the oxaliplatin/Ub incubation mixture after 7 days in the region m/z 8,400–9,600. Oxaliplatin and Ub were reacted in a molar ratio of 2:1. The most abundant adduct corresponds to [Ub+Pt(chxn)]

were found over a broad mass (especially m/z 700–1,000) and charge (1+ to 11+) range with a resolution of $R \approx 120,000$ at m/z 567.171 ($\text{Pt}(\text{chxn})\text{B}_2^+$) for both instrument types (Fig. 2). The mass accuracy of the metallated fragments was in general <1 ppm.

Since bis-platinated Ub adducts were observed in significant intensities in the survey mass spectra, at least two main binding sites are to be expected for the [Ub+Pt(chxn)] adducts. Indeed, the Pt(chxn)-containing peptide fragments detected by CID-MS/MS indicated two possible binding sites. The former was identified as N-terminal Met1 based on the $\text{Pt}(\text{chxn})\text{B}_2^+$ ion (the following annotation system was used throughout the text to describe platinated peptide fragments: capital letters indicate metallated frag-

ments, analogous to the conventional peptide ion type nomenclature. The nature of the bound metal species is given as preceding superscript; e.g., $\text{Pt}(\text{chxn})\text{B}_2^+$ stands for the Pt(chxn) moiety bound to the b_2 -fragment of Ub in charge state 1+) as the smallest metal-containing peptide fragment, identified on both instruments and also observed earlier [23]. In addition, high molecular weight fragments, such as the b_2 complementary metallated fragment $\text{Pt}(\text{chxn})\text{Y}_{74}^{10+/11+}$, indicate the presence of a second binding site. Several C-terminal metallated peptide fragments were detected with both instruments. They range from $\text{Pt}(\text{chxn})\text{Y}_{24}^{5+}$ to $\text{Pt}(\text{chxn})\text{Y}_{75}^{11+}$ on the orbitrap FT MS and from $\text{Pt}(\text{chxn})\text{Y}_{18}^{3+}$ to $\text{Pt}(\text{chxn})\text{Y}_{74}^{10+}$ on the FT-ICR MS. These fragments do not give the exact location of the second binding site, but they do reveal that it must be within the last 18 residues of the C-terminal protein sequence. Most of the B- and Y-fragments are centered around y_{58} , which was observed in all collisionally activated tandem mass spectra, i.e., $\text{Pt}(\text{chxn})\text{B}_{16}^{2+}$, and also the complementary peptide fragment y_{60}^{8+} (m/z 845.833, 1%) was detected.

HCD is a fragmentation technique that makes use of higher-energy collisions and generally results in increased fragmentation efficiency and sequence coverage. Indeed, 27 metallated fragments were unambiguously identified in the HCD-orbitrap MS/MS experiments. In addition, higher-energy collisions yielded a fragmentation profile where the metallated peptide fragments were generally smaller and of lower charge than with CID-orbitrap MS/MS. N- and C-terminal metallated fragments were essentially equal in intensity and number. HCD gave rise to metallodrug-peptide fragments with higher relative intensities compared with CID and with similar resolution and mass accuracies of <1 ppm (Fig. 3a).

Fig. 2 (a) CID-orbitrap- and (b) CID-ICR-FT tandem mass spectra of the [Ub+Pt(chxn)] adduct. Oxaliplatin and Ub were reacted in 2:1 molar ratio and incubated for 7 days. The two most probable binding partners, i.e., Met1 and His68, are underlined in the amino acid sequence of Ub. Bars between the sequence letters refer to metallated peptide fragments

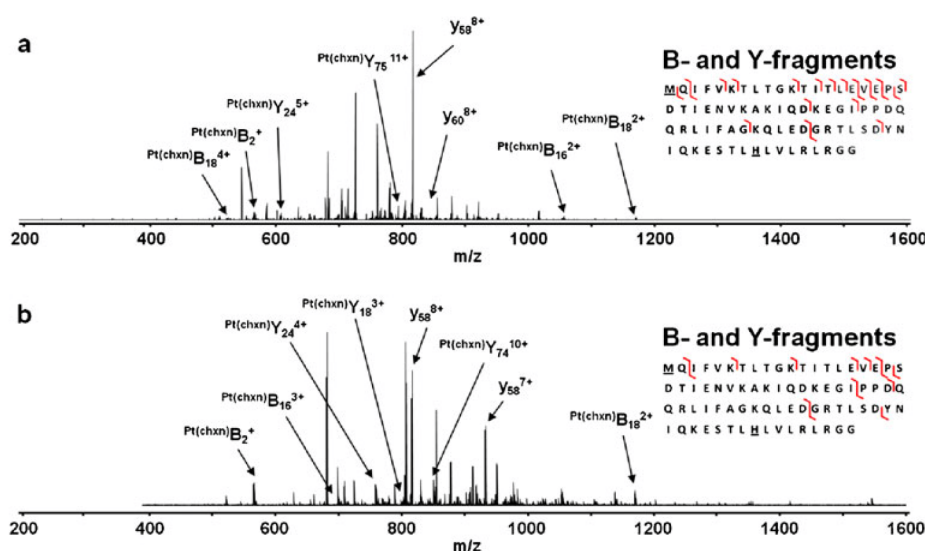
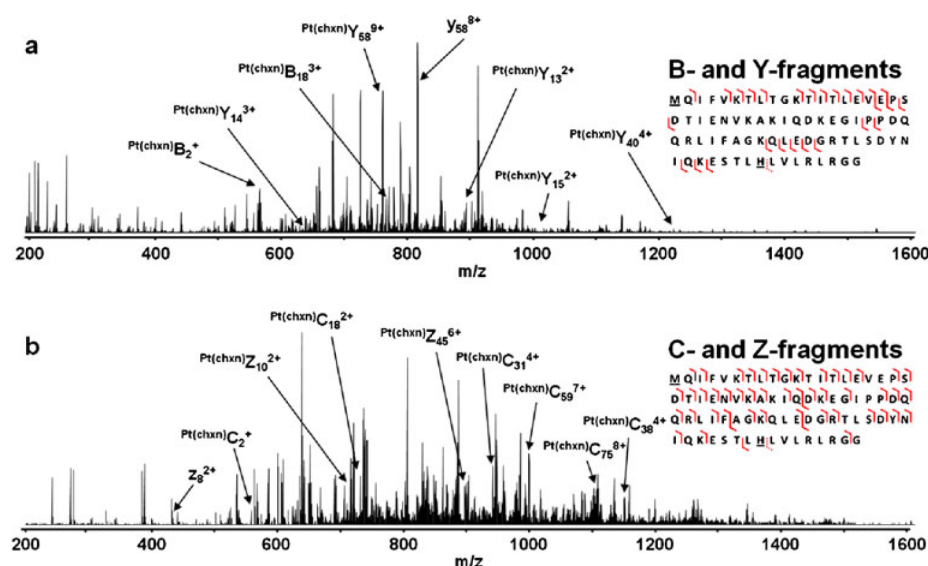


Fig. 3 (a) HCD-orbitrap- and (b) ETD-orbitrap tandem mass spectra of the [Ub+Pt(chxn)] adduct. Oxaliplatin and Ub were reacted in 2:1 molar ratio and incubated for 7 days. The two most probable binding partners, i.e., Met1 and His68, are underlined in the amino acid sequence of Ub. *Solid bars between the sequence letters* refer to detected metallated peptide fragments whereas the *dashed bars* refer to the y_8 and z_8 fragments



Many metallated *N*-terminal fragments were detected, ranging from $\text{Pt}(\text{chxn})\text{B}_2^+$ to $\text{Pt}(\text{chxn})\text{B}_{18}^{3+}$, also confirming Met1 as the primary binding site for oxaliplatin. With regard to the second binding site of oxaliplatin, small platinated and non-platinated C-terminal fragments were analyzed. Indeed, the HCD tandem mass spectrum contained signals assignable to non-metallated y_8^{2+} ions, as well as metallated $\text{Pt}(\text{chxn})\text{Y}_{13}^{2+}$, $\text{Pt}(\text{chxn})\text{Y}_{14}^{2+}$ and $\text{Pt}(\text{chxn})\text{Y}_{15}^{2+}$ fragments. This finding narrowed the number of possible binding sites to a 5-amino acid sequence containing Glu64 and His68 as most nucleophilic sites. In contrast to CID where complementary fragments were found at several points along the protein sequence, the only observable complementary pair was the $\text{Pt}(\text{chxn})\text{B}_{18}^{3+}/y_8^{8+}$ couple.

In parallel to collision-induced fragmentation techniques, the [Ub+Pt(chxn)] adduct was subjected to ETD. This fragmentation method, based on ion/ion reactions resulting in electron transfers, leads to N-C α bond breaks along the peptide backbone and specifically yields *c*- and *z*-fragment ions. The general advantage of ETD is that it retains PTMs to a large extent, making it a valuable tool for top-down protein sequencing in proteomics. In addition, electron transfer should result in a more random fragmentation pattern relative to collisionally induced fragmentation techniques.

ETD-MS/MS generated a very different fragmentation profile in comparison to collisionally activated fragmentation methods (Fig. 3b). Even though the relative intensities and the resolution ($R \approx 120,000$ at m/z 586.785 [$\text{Pt}(\text{chxn})\text{C}_7^{2+}$]) of the platinated peptide fragments were similar to those obtained by CID and HCD methods, ETD allowed identifying a higher number of metallated fragments, i.e., 50 in total, which represents the highest value among the different

fragmentation techniques. A total of 46 *N*-terminal platinated fragments were detected ranging from $\text{Pt}(\text{chxn})\text{C}_2^+$ to $\text{Pt}(\text{chxn})\text{C}_{75}^{8+}$, thus verifying Met1 as the first binding partner of oxaliplatin on Ub. The most abundant metal-containing fragment was identified as $\text{Pt}(\text{chxn})\text{C}_{59}^{7+}$ (21%), as opposed to $\text{Pt}(\text{chxn})\text{B}_{18}^{2+/3+}$ for collisionally activated methods, which may be related to the different fragmentation mechanisms. It is believed that positively charged amino acids act as electron scavengers during electron transfer [44]. In the case of Ub, Lys48 is in close proximity to the peptide bond between Tyr59 and Asn60. This may facilitate backbone cleavage and be responsible for the high abundance observed. In addition, collisionally induced fragmentation at Glu18 may also produce very stable products, i.e., in source generation of y_{58} is known. On the other hand, C-terminal metallated peptide fragments ranged from $\text{Pt}(\text{chxn})\text{Z}_{10}^{2+}$ to $\text{Pt}(\text{chxn})\text{Z}_{45}^{6+}$. The metallated $\text{Pt}(\text{chxn})\text{Z}_{10}^{2+}$ and non-metallated z_8^{2+} C-terminal fragments clearly identify the second binding site as His68 excluding Glu64 as a potential binding partner. ETD therefore emerges as a superior fragmentation technique to CID and HCD when investigating metallodrug-protein adducts via a top-down approach both in terms of fragment numbers and localization of binding sites. It is the only fragmentation technique that allowed the simultaneous identification of both Met1 and His68 as binding partners from a single precursor. The lower efficiency of CID- and HCD-MS/MS for detecting metallated peptides might be due to collision-induced gas phase demetallation, whereas ETD-MS/MS is a softer fragmentation technique and might retain coordinative Pt-protein bonds to a larger degree.

A striking observation is the large discrepancy between the number of C- and Z-fragments (46:4). One explanation

might involve favored binding of oxaliplatin to the N-terminal Met1 which causes a higher abundance of such fragments compared with C-terminal His68. In support of this hypothesis is the fact that the number of characterized *z*-fragments during ETD measurements on bare Ub is approximately three times higher than the respective *c*-fragments. Therefore, Met1 is considered the primary binding site of oxaliplatin on Ub.

Insights into the secondary structure of the [Ub+Pt(chxn)] adduct

ESI mass spectrometry is extensively used to gain information on the higher order structure of proteins, in particular in the elucidation of the tertiary structure. For this purpose, several approaches have proven effective, the most widespread being H/D-exchange [45, 46], covalent labeling [47], and ion mobility MS [24, 48]. The tertiary protein structure is affected by the solvent conditions employed during incubation and infusion into the mass spectrometer [49, 50]. Importantly, a correlation between charge state (i.e., unfolding), temperature and fragmentation efficiency has been established [51]. In contrast to tertiary structure, only a few experiments were conducted on protein secondary structures by means of ESI mass spectrometry. Secondary structures are supposed to remain, to some degree, intact under denaturing conditions but it is unknown if the same secondary structures are retained in the gas phase as present in solution [49, 51–54].

In the present study, MS/MS experiments were performed under denaturing conditions which led to breakdown of the protein tertiary structure. When the protein transfers from solution to the gas phase at the ESI interface, hydrophobic interactions are further diminished and electrostatic effects enhanced, resulting in the protein adopting a near-linear conformation [51]. Secondary structures are stabilized by H-bonding in the gas phase and presumably more energy is required in collisionally activated fragmentation experiments to cleave the protein backbone at these locations compared to random coil sequences. Interestingly,

plotting the MS/MS-fragment intensities from the combined CID and HCD data sets relative to the sequence revealed a strong correlation with solution random coil structures (Fig. 4) [55]. The backbone cleavages suggest that the N-terminal β -hairpin section stays intact. The random coil sequence Val17–Thr22 connects the β -hairpin with the only α -helix in Ub and from Glu16–Ile23, six out of eight peptide bond cleavages were observed. The section of the α -helix remained intact to a large degree. The next cleavage occurred prior to the successive prolines at positions 36/37, which initiate the α -turn. The subsequent β -strand is followed by an extended random coil sequence, which displays four consecutive cleavages from Gln49–Asp52. The remaining α -turn and β -strand sections are not sufficiently stabilized when the protein adopts a near-linear conformation and therefore, numerous cleavages occur between Asp58 and Glu64. These results suggest that solution secondary structures of the [Ub+Pt(chxn)] adduct are retained to a considerable extent in the gas phase. Contrary to CID and HCD methods, ETD did not yield such pronounced specificity because it generates more random cleavages on the protein backbone (Fig. 4).

Conclusions

This work highlights the application of high-resolution mass spectrometric methods for top-down characterization of metaldrug-protein adducts. The major adduct of oxaliplatin at Ub is formed with a Pt(chxn) moiety. In addition, the experimental setup yielded further adduct types, which were identified as [Ub+(ox)Pt(chxn)], [Ub+2Pt(chxn)], and [Ub+Pt(chxn)+(ox)Pt(chxn)] in support of a two-step activation mechanism of oxaliplatin. ESI Orbitrap- and ICR-FT MS combined with CID-, HCD-, and ETD-MS/MS data were used to locate the binding sites of oxaliplatin on Ub. All fragmentation experiments were carried out under denaturing conditions and analyzed in high charge states in order to maximize fragmentation efficiency. ETD yielded the highest number of metallated

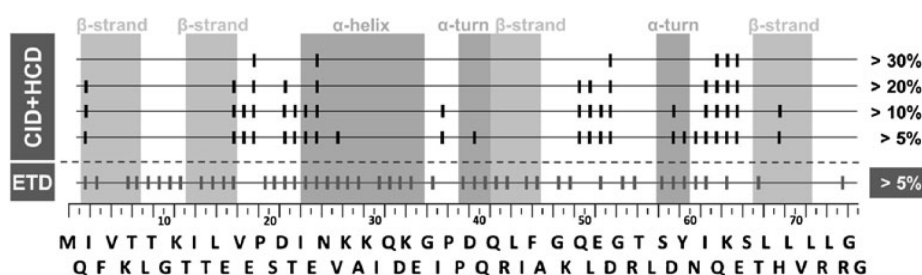


Fig. 4 A combined plot of backbone cleavage sites (*bars*) depending on decreasing relative intensities observed during CID- and HCD-MS/MS experiments with the [Ub+Pt(chxn)] adduct. The last row features

cleavages from the ETD-MS/MS experiment. The positions of the secondary structures were determined by the Kabsch–Sanders algorithm. *White background* refers to random coil sequence areas

fragments and was the only technique to unequivocally establish Met1 and His68 as the two binding sites for oxaliplatin on Ub. From this study, ETD has emerged as a powerful method for characterizing metallodrug–protein binding sites. On the other hand only collisionally activated methods yielded insights into the secondary structure of Ub. In particular, a correlation was found between peptide fragments and cleavage at random coil sequences, indicating that β -hairpin and α -helix structures of the [Ub+Pt(chxn)] adduct are retained in the gas phase.

Acknowledgment The authors are indebted to the Austrian Science Fund (FWF; I496-B11), the Hochschuljubiläumsstiftung Vienna and COST D39 and CM0902. We would like to thank Dr. Yue Xuan (Thermo Scientific) and Dr. Jens Fuchser (Bruker Daltonics) for assistance during measurements on the orbitrap FT MS and FT-ICR MS instruments, respectively.

References

1. Barry MA, Behnke CA, Eastman A (1990) Activation of programmed cell-death (apoptosis) by cisplatin, other anticancer drugs, toxins and hyperthermia. *Biochem Pharmacol* 40:2353–2362
2. Ivanov AI, Christodoulou J, Parkinson JA, Barnham KJ, Tucker A, Woodrow J, Sadler PJ (1998) Cisplatin binding sites on human albumin. *J Biol Chem* 273:14721–14730
3. Groessl M, Zava O, Dyson PJ (2011) Cellular uptake and subcellular distribution of ruthenium-based metallodrugs under clinical investigation versus cisplatin. *Metallomics* 3:591–599
4. Lokich J, Anderson N (1998) Carboplatin versus cisplatin in solid tumors: an analysis of the literature. *Ann Oncol* 9:13–21
5. Allardyce CS, Dyson PJ, Coffey J, Johnson N (2002) Determination of drug binding sites to proteins by electrospray ionisation mass spectrometry: the interaction of cisplatin with transferrin. *Rapid Commun Mass Spectrom* 16:933–935
6. Calderone V, Casini A, Mangani S, Messori L, Orioli PL (2006) Structural investigation of cisplatin–protein interactions: selective platinumation of His19 in a cuprozinc superoxide dismutase. *Angew Chem Int Ed Engl* 45:1267–1269
7. Casini A, Mastrobuoni G, Temperini C, Gabbiani C, Francese S, Moneti G, Supuran CT, Scozzafava A, Messori L (2007) ESI mass spectrometry and X-ray diffraction studies of adducts between anticancer platinum drugs and hen egg white lysozyme. *Chem Commun* (2):156–158.
8. Groessl M, Terenghi M, Casini A, Elvirri L, Lobinski R, Dyson PJ (2010) Reactivity of anticancer metallodrugs with serum proteins: new insights from size exclusion chromatography-ICP-MS and ESI-MS. *J Anal At Spectrom* 25:305–313
9. Timerbaev AR, Hartinger CG, Aleksenko SS, Keppler BK (2006) Interactions of antitumor metallodrugs with serum proteins: advances in characterization using modern analytical methodology. *Chem Rev* 106:2224–2248
10. Sun X, Tsang C-N, Sun H (2009) Identification and characterization of metallodrug binding proteins by (metallo)proteomics. *Metallomics* 1:25–31
11. Hartinger CG, Ang WH, Casini A, Messori L, Keppler BK, Dyson PJ (2007) Mass spectrometric analysis of ubiquitin–platinum interactions of leading anticancer drugs: MALDI versus ESI. *J Anal At Spectrom* 22:960–967
12. Hartinger CG, Casini A, Duhot C, Tsybin YO, Messori L, Dyson PJ (2008) Stability of an organometallic ruthenium-ubiquitin adduct in the presence of glutathione: relevance to antitumor activity. *J Inorg Biochem* 102:2136–2141
13. Ang WH, Parker LJ, De Luca A, Juillerat-Jeanneret L, Morton CJ, Lo Bello M, Parker MW, Dyson PJ (2009) Rational design of an organometallic glutathione transferase inhibitor. *Angew Chem Int Ed* 48:3854–3857
14. Egger AE, Hartinger CG, Renfrew AK, Dyson PJ (2010) Metabolization of [Ru(η^6 -C₆H₅CF₃)(pta)Cl₂]: a cytotoxic RAPTA-type complex with a strongly electron withdrawing arene ligand. *J Biol Inorg Chem* 15:919–927
15. Allardyce CS, Dyson PJ, Abou-Shakra FR, Birtwistle H, Coffey J (2001) Inductively coupled plasma mass spectrometry to identify protein drug targets from whole cell systems. *Chem Commun* 2708–2709.
16. Scharwitz MA, Ott I, Geldmacher Y, Gust R, Sheldrick WS (2008) Cytotoxic half-sandwich rhodium(III) complexes: polypyridyl ligand influence on their DNA binding properties and cellular uptake. *J Organomet Chem* 693:2299–2309
17. Timerbaev AR, Aleksenko KS, Polec-Pawlak K, Ruzik R, Semenova O, Hartinger CG, Oszwaldowski S, Galanski M, Jarosz M, Keppler BK (2004) Platinum metallodrug–protein binding studies by capillary electrophoresis-inductively coupled plasma-mass spectrometry: characterization of interactions between Pt(II) complexes and human serum albumin. *Electrophoresis* 25:1988–1995
18. Will J, Wolters DA, Sheldrick WS (2008) Characterisation of cisplatin binding sites in human serum proteins using hyphenated multidimensional liquid chromatography and ESI tandem mass spectrometry. *ChemMedChem* 3:1696–1707
19. Najajreh Y, Shulman TP, Moshel O, Farrell N, Gibson D (2003) Ligand effects on the binding of *cis*- and *trans*-[PtCl(2)Am1Am2] to proteins. *J Biol Inorg Chem* 8:167–175
20. Khalaila I, Allardyce CS, Verma CS, Dyson PJ (2005) A mass spectrometric and molecular modelling study of cisplatin binding to transferrin. *Chembiochem* 6:1788–1795
21. Williams JP, Brown JM, Campuzano I, Sadler PJ (2010) Identifying drug metallation sites on peptides using electron transfer dissociation (ETD), collision induced dissociation (CID) and ion mobility-mass spectrometry (IM-MS). *Chem Commun* 46:5458–5460
22. Groessl M, Tsybin YO, Hartinger CG, Keppler BK, Dyson PJ (2010) Ruthenium versus platinum: interactions of anticancer metallodrugs with duplex oligonucleotides characterised by electrospray ionisation mass spectrometry. *J Biol Inorg Chem* 15:677–688
23. Hartinger CG, Tsybin YO, Fuchser J, Dyson PJ (2008) Characterization of platinum anticancer drug protein-binding sites using a top-down mass spectrometric approach. *Inorg Chem* 47:17–19
24. Williams JP, Phillips HIA, Campuzano I, Sadler PJ (2010) Shape changes induced by N-terminal platinumation of ubiquitin by cisplatin. *J Am Soc Mass Spectrom* 21:1097–1106
25. Casini A, Guerri A, Gabbiani C, Messori L (2008) Biophysical characterisation of adducts formed between anticancer metallodrugs and selected proteins: new insights from X-ray diffraction and mass spectrometry studies. *J Inorg Biochem* 102:995–1006
26. Krivos KL, Limbach PA (2010) Sequence analysis of peptide: oligonucleotide heteroconjugates by electron capture dissociation and electron transfer dissociation. *J Am Soc Mass Spectrom* 21:1387–1397
27. van der Rest G, He F, Emmett MR, Marshall AG, Gaskell SJ (2001) Gas-phase cleavage of PTC-derivatized electrosprayed tryptic peptides in an FT-ICR trapped-ion cell: mass-based protein identification without liquid chromatographic separation. *J Am Soc Mass Spectrom* 12:288–295

28. Han XM, Aslanian A, Yates JR (2008) Mass spectrometry for proteomics. *Curr Opin Chem Biol* 12:483–490
29. Zhao T, King FL (2011) Mass-spectrometric characterization of cisplatin binding sites on native and denatured ubiquitin. *J Biol Inorg Chem* 16:633–639
30. Kelleher NL (2004) Top-down proteomics. *Anal Chem* 76:196a–203a
31. Yin S, Loo JA (2010) Elucidating the site of protein-ATP binding by top-down mass spectrometry. *J Am Soc Mass Spectrom* 21:899–907
32. Moreno-Gordaliza E, Canas B, Palacios MA, Gomez-Gomez MM (2009) Top-down mass spectrometric approach for the full characterization of insulin-cisplatin adducts. *Anal Chem* 81:3507–3516
33. Papayannopoulos IA (1995) The interpretation of collision-induced dissociation tandem mass-spectra of peptides. *Mass Spectrom Rev* 14:49–73
34. Olsen JV, Macek B, Lange O, Makarov A, Horning S, Mann M (2007) Higher-energy C-trap dissociation for peptide modification analysis. *Nat Methods* 4:709–712
35. Laskin J, Futrell JH (2005) Activation of large ions in FT-ICR mass spectrometry. *Mass Spectrom Rev* 24:135–167
36. Mikesh LM, Ueberheide B, Chi A, Coon JJ, Syka JE, Shabanowitz J, Hunt DF (2006) The utility of ETD mass spectrometry in proteomic analysis. *Biochim Biophys Acta* 1764:1811–1822
37. Nielsen ML, Savitski MM, Zubarev RA (2005) Improving protein identification using complementary fragmentation techniques in Fourier transform mass spectrometry. *Mol Cell Proteomics* 4:835–845
38. Syrstad EA, Turecek F (2005) Toward a general mechanism of electron capture dissociation. *J Am Soc Mass Spectrom* 16:208–224
39. Zubarev RA, Zubarev AR, Savitski MM (2008) Electron capture/transfer versus collisionally activated/induced dissociations: solo or duet? *J Am Soc Mass Spectrom* 19:753–761
40. Peleg-Shulman T, Gibson D (2001) Cisplatin-protein adducts are efficiently removed by glutathione but not by 5'-guanosine monophosphate. *J Am Chem Soc* 123:3171–3172
41. Hartinger CG, Schluga P, Galanski M, Baumgartner C, Timerbaev AR, Keppler BK (2003) Tumor-inhibiting platinum(II) complexes with aminoalcohol ligands: comparison of the mode of action by capillary electrophoresis and electrospray ionization-mass spectrometry. *Electrophoresis* 24:2038–2044
42. Galanski M, Baumgartner C, Meelich K, Arion VB, Fremuth M, Jakupec MA, Schluga P, Hartinger CG, Von Keyserlingk NG, Keppler BK (2004) Synthesis, crystal structure and pH dependent cytotoxicity of (SP-4-2)-bis(2-aminoethanolato- κ^2N, O)platinum(II)—a representative of novel pH sensitive anticancer platinum complexes. *Inorg Chim Acta* 357:3237–3244
43. Jerremalm E, Videhult P, Alvelius G, Griffiths WJ, Bergman T, Eksborg S, Ehrsson H (2002) Alkaline hydrolysis of oxaliplatin— isolation and identification of the oxalato monodentate intermediate. *J Pharm Sci* 91:2116–2121
44. Simons J (2010) Mechanisms for S-S and N-C-alpha bond cleavage in peptide ECD and ETD mass spectrometry. *Chem Phys Lett* 484:81–95
45. Briggs MS, Roder H (1992) Early hydrogen-bonding events in the folding reaction of ubiquitin. *Proc Natl Acad Sci* 89:2017–2021
46. Pan J, Han J, Borchers CH, Konermann L (2008) Electron capture dissociation of electrosprayed protein ions for spatially resolved hydrogen exchange measurements. *J Am Chem Soc* 130:11574–11575
47. Mendoza VL, Vachet RW (2009) Probing protein structure by amino acid-specific covalent labeling and mass spectrometry. *Mass Spectrom Rev* 28:785–815
48. Robinson EW, Leib RD, Williams ER (2006) The role of conformation on electron capture dissociation of ubiquitin. *J Am Soc Mass Spectrom* 17:1469–1479
49. Konermann L, Douglas DJ (1997) Acid-induced unfolding of cytochrome c at different methanol concentrations: electrospray ionization mass spectrometry specifically monitors changes in the tertiary structure. *Biochemistry* 36:12296–12302
50. Konermann L, Douglas DJ (1998) Equilibrium unfolding of proteins monitored by electrospray ionization mass spectrometry: Distinguishing two-state from multi-state transitions. *Rapid Commun Mass Spectrom* 12:435–442
51. Breuker K, Oh HB, Horn DM, Cerda BA, McLafferty FW (2002) Detailed unfolding and folding of gaseous ubiquitin ions characterized by electron capture dissociation. *J Am Chem Soc* 124:6407–6420
52. Oh H, Breuker K, Sze SK, Ge Y, Carpenter BK, McLafferty FW (2002) Secondary and tertiary structures of gaseous protein ions characterized by electron capture dissociation mass spectrometry and photofragment spectroscopy. *Proc Natl Acad Sci* 99:15863–15868
53. Ben Hamidane H, He H, Tsybin OY, Emmett MR, Hendrickson CL, Marshall AG, Tsybin YO (2009) Periodic sequence distribution of product ion abundances in electron capture dissociation of amphipathic peptides and proteins. *J Am Soc Mass Spectrom* 20:1182–1192
54. Breuker K, Bruschweiler S, Tollinger M (2011) Electrostatic stabilization of a native protein structure in the gas phase. *Angew Chem Int Ed Engl* 50:873–877
55. Zhang Z, Bordas-Nagy J (2006) Peptide conformation in gas phase probed by collision-induced dissociation and its correlation to conformation in condensed phases. *J Am Soc Mass Spectrom* 17:786–794

4. Conclusions

Some Ru^{III} complexes are promising anticancer drug candidates. In particular, clinical studies of the Ru^{III} complexes KP1339 and NAMI-A indicate milder adverse effects in humans compared to standard chemotherapy and antitumour activity in chemoresistant cancer types such as slowly growing adenotumours (*e.g.* colon or lung). Clarke coined the hypothesis that Ru^{III} complexes are activated by reduction to the corresponding Ru^{II} species. In this respect, the preparation of Ru^{II} and Os^{II} complexes, stabilized by a η^6 -coordinating arene, represents the latest strategy for obtaining potent anticancer metallodrugs. Besides the arene, the metallodrug features three remaining binding sites, which are occupied by inert and labile ligands. Overall, these organometallics exhibit a contrasting anticancer- and antiproliferative activity, which is critically influenced amongst others by the arene, the metal centre and most importantly, by the inert ligand.

It was also previously reported that inert bidentate ligands yield the most anticancer active metallodrugs against primary tumours *in vivo*. Consequently, several bidentate ligand systems were investigated for their antiproliferative activity, involving *O,O*-, *N,O*-, *S,O*- and *N,N*-coordinating ligands. Within this Ph.D. thesis, Ru^{II} and Os^{II} metallodrugs are reported containing *S,N*-bidentate ligands. The ligands are gastric mucosal protectants, based on the 2-pyridinecarbothioamide core, which are non-toxic *in vivo* (*J. Med. Chem.*, **1990**, *33*, 327–336). Complexation to the organometallic M^{II}-arene scaffold, where M is Ru or Os, yields highly antiproliferative anticancer agents not only in the ovarian cancer cell line CH1, but also in the intrinsically resistant colon carcinoma SW480 and non-small cell lung A549 cancer cell lines. These organometallics tend to dimerize upon hydrolysis of the M–Cl bond, which seems to protect the metallodrugs from deactivation even by thiol-containing biomolecules. Hydrolysis of the M–Cl bond is suppressed in a highly acidic environment (pH = 1.2) and the organometallics stay intact. For this family of metallodrugs, the lipophilicity (expressed as the chromatographic lipophilicity index) seems to correlate with the antiproliferative activity. Moreover, the evaluation of their quantitative estimates of drug-likeness reveals a similar drug-likeness compared to erlotinib, sorafenib or tamoxifen, while the structural parameter Fsp³ indicates good permeability. Consequently, these carbothioamide-based organometallic anticancer agents may be suitable for oral administration. Studies of representative Ru^{II} and Os^{II} carbothioamides with the nucleosome core particle showed that these metallodrugs bind exclusively to the histone proteins at histone dimer–dimer and dimer–tetramer interfaces and therefore, may interfere with chromatin dynamics as a possible mode of action. The lower cytotoxic activity of the sterically more demanding analogues may be explained by a reduced accessibility to these histone interfaces.

Furthermore, the first organometallic Ru^{II}-arene metallodrugs based on *O,O*-bidentate triazolyl-modified pyronato ligands are reported with previously unmet antiproliferative activity in ovarian cancer cell lines. The strategy of triazolyl modification was followed to prepare the first organometallic Ru–peptide bioconjugate where the peptide is a [Leu⁵]-enkephalin derivative exhibiting also a cytotoxic activity in the low μM range in the CH1 ovarian

cancer cell line. The metal–peptide bioconjugate was thoroughly characterized with respect to amino acid sequence, pyrone modification and metallation site by a top-down approach using electrospray ionization-mass spectrometry (ESI-MS). Enhanced stability of these pyronato metallodrugs in the presence of biomolecules seems to correlate with increased antitumour potency *in vitro*. These metallodrugs display the ability to cross-link cytochrome C as indicated by mass spectrometric methods.

In recent years, mass spectrometry has emerged as an invaluable tool for analyzing reactions between metallodrugs and biomolecules. MS-based techniques were used to characterize the nature and extent of metal-binding on proteins and DNA, but also to investigate metallodrug reactivity towards amino acids and nucleotides. Moreover, the metallation sites can also be characterized on biomolecules. Driving force of the progress in this field of research is the appreciation that the molecular reactivity of metallodrugs may give insight into their modes of action.

Within this frame, mass spectrometric techniques were used to characterize the reactivity of representative (thio)pyr(id)onato Ru^{II}-*p*-cymene metallodrugs towards amino acids, nucleotides and proteins and an inverse correlation was found between the extent of protein binding and antiproliferative activity, at least for these families of metallodrugs. Moreover, the formation of metallodrug–protein adducts was found to be reversible, which has relevance for the mode-of-action of a compound since plasma proteins are the major binding partners for metallodrugs upon potential intravenous administration.

The analysis of metallation sites of proteins by metallodrugs using mass spectrometric methods poses significant challenges in many cases due to low adduct detection efficiencies. A methodological approach in top-down mass spectrometric analysis is shown as a promising route to analyze oxaliplatin binding sites on ubiquitin (ub). Different fragmentation techniques were investigated for obtaining the metallation sites of the most abundant adduct, *i.e.*, [ub + Pt(chxn)]⁺, with the combination of higher energy C-trap dissociation (HCD) and electron transfer dissociation (ETD) tandem mass spectrometry yielding the highest information content. This approach on a high resolution orbitrap FT MS led to the confirmation of methionine-1 as the primary and histidine-68 as the secondary binding site, the latter being evidenced for the first time by direct analytical methods.

Further research effort will be directed into the *in vivo* evaluation of the carbothioamide M^{II}-arene metallodrugs, where M is Ru or Os, in order to estimate their oral bioavailability and tumour-inhibiting properties after oral administration in comparison to intraperitoneal administration.

The introduction of the triazole pharmacophore in *S,O*-bidentate thiopyronato organometallics would combine their structural determinants for a potentially even higher antiproliferative activity and should in principle also allow to obtain anticancer activity in chemoresistant tumour cell lines.

Lastly, the development of mass spectrometry-based methods for analyzing interactions between metallodrugs and plasma proteins on a molecular level would be highly relevant to pharmacokinetic evaluation of drugs in general and metallodrugs in particular.

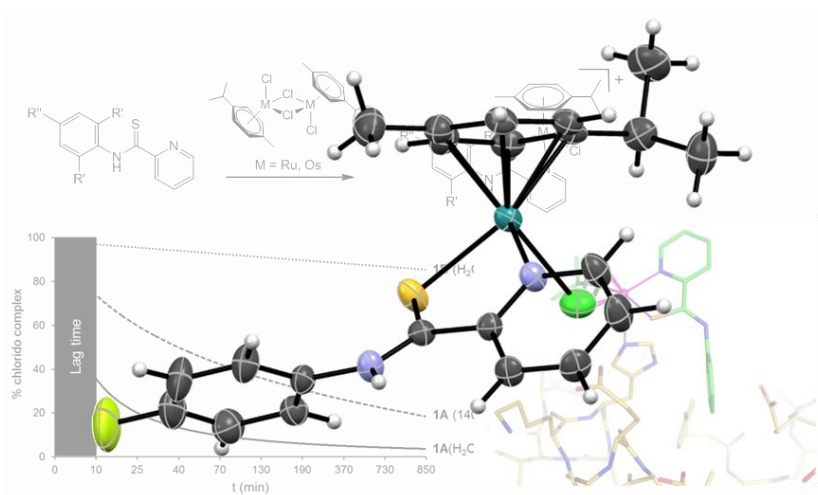
5. Supporting Information

5.1. Novel Metal(II) Arene 2-Pyridinecarbothioamides: A Rationale to Orally Active Organometallic Anticancer Agents

Electronic supplementary information available

Samuel M. Meier, Muhammad Hanif, Zenita Adhireksan, Verena Pichler, Maria Novak, Elisabeth Jirkovsky, Michael A. Jakupec, Vladimir B. Arion, Curt A. Davey, Bernhard K. Keppler, Christian G. Hartinger

Chemical Science, 2013, 4, 1837–1846.



Chemical Science

Supporting Information

**Novel Metal(II) Arene 2-Pyridinecarbothioamides: A Rationale
to Orally Active Organometallic Anticancer Agents**

Samuel M. Meier, Muhammad Hanif, Zenita Adhireksan, Verena Pichler, Maria
Novak, Elisabeth Jirkovsky, Michael A. Jakupec, Vladimir B. Arion, Curt A. Davey,
Bernhard K. Keppler, Christian G. Hartinger

Experimental

Materials

All reactions were carried out in dry solvents under an inert atmosphere. Chemicals obtained from commercial suppliers were used as received and were of analytical grade. Methanol and dichloromethane were dried using standard procedures. OsO₄ (99.8%) and RuCl₃·3H₂O (40.4%) were purchased from Johnson Matthey, ubiquitin (bovine erythrocytes) and cytochrome-C from Sigma, α -terpinene and 4-fluoroaniline from Acros, L-histidine (His), 2-picoline, aniline and sodium sulfide nonahydrate from Merck, N₂H₄·2HCl, 5'-deoxyguanosine monophosphate (5'-dGMP) and L-cysteine (Cys) from Fluka, 4-morpholinoaniline from Fisher and L-methionine (Met), 4-aminophenol, 2,4,6-trimethylaniline, 4-aminobenzophenone and sulfur from Sigma-Aldrich. The solvents for ESI-MS studies were methanol (VWR Int., HiPerSolv CHROMANORM), formic acid (Fluka) and milliQ water (18.2 M Ω , Synergy 185 UV Ultrapure Water System, Millipore, France). The dimers bis[dichlorido(η^6 -*p*-cymene)ruthenium(II)],^{1, 2} and bis[dichlorido(η^6 -*p*-cymene)osmium(II)],³ and the ligands *N*-phenyl- (**1**),⁴ *N*-(4-hydroxyphenyl)- (**2**),⁵ *N*-(4-fluorophenyl)- (**3**)⁶ and *N*-(2,4,6-trimethylphenyl)-2-pyridinecarbothioamide (**4**)⁷ were synthesized by adapting literature procedures.

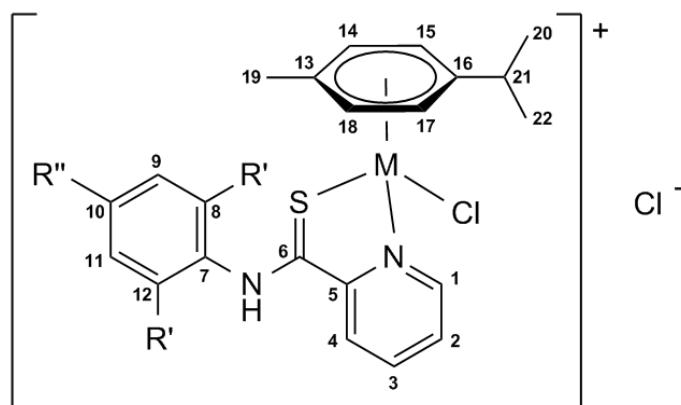
Instrumentation

¹H and ¹³C{¹H} NMR spectra were recorded at 25 °C on a Bruker FT NMR spectrometer Avance III 500 MHz at 500.10 (¹H) and 125.75 MHz (¹³C{¹H}) and 2D NMR data were collected in a gradient-enhanced mode. Protons were numbered according to crystal structure numbering (see Figure 1). Elemental analysis was carried out on a Perkin–Elmer 2400 CHN Elemental Analyzer by the Laboratory for Elemental Analysis, Faculty of Chemistry, University of Vienna. UV–vis experiments were performed on a temperature-controlled Perkin-Elmer Lambda 650 spectrophotometer using a Peltier element. ESI mass spectra were recorded on a Bruker AmaZon SL ion trap mass spectrometer (Bruker Daltonics GmbH, Bremen, Germany) by direct infusion at

a flow rate of 3–4 $\mu\text{L}/\text{min}$. The following parameters were employed: capillary –3.5 kV, gas flow 6 psi, dry gas 6 L/min, dry temperature 180–200 $^{\circ}\text{C}$, end plate offset –500 V and RF 69–71%. The spectra were recorded and processed using ESI Compass 1.3 and Data Analysis 4.0 software (both Bruker Daltonics GmbH, Bremen, Germany). Protein samples were additionally analyzed on a MaXis UHR ESI time-of-flight mass spectrometer (Bruker Daltonics, Bremen, Germany) employing the following parameters: capillary –4.5 kV, gas flow 8 psi, dry gas 6 L/min, dry temperature 150 $^{\circ}\text{C}$, 400 Vpp funnel RF, 4 eV quadrupole ion energy and 100 μs transfer time. Samples were diluted to 2 μM using water/methanol/formic acid (50 : 50 : 0.2) and injected by direct infusion into the mass spectrometer at a flow rate of 3 $\mu\text{L}/\text{min}$. Spectra were recorded in positive ion mode over 0.5 min and averaged. The Data Analysis 4.0 software package (Bruker Daltonics, Bremen, Germany) was used for processing and maximum entropy deconvolution (automatic data point spacing and 30000 instrument resolving power).

X-ray diffraction measurements of single crystals were carried out on a Bruker X8 APEX II CCD diffractometer at 100 K (**2B**) and 200 K (**3A**). The crystals were positioned at 35 mm from the detector and the following data collection parameters were used: 1236 frames for 30 sec over 1° for **2B** and 788 frames for 10 s over 1° for **3A**. The data was processed using the SAINT Plus software package.⁸ Crystal data, data collection parameters, and structure refinement details are given in Table S1, bond lengths and angles in Table S2. The structures were solved by direct methods and refined by full-matrix least-squares techniques. Non-hydrogen atoms were refined with anisotropic displacement parameters. H atoms were inserted at calculated positions and refined with a riding model. SHELX software programs were used for solving the structures and refinement.⁹

General procedure for the synthesis of *N*-substituted 2-pyridinecarbothioamides. The method of Klingele and Brooker⁷ was adapted. In brief, a mixture of *N*-substituted aniline (25 mmol), sulfur (75 mmol) and sodium sulfide (0.5 mol%) was refluxed in 2-picoline (15 mL) for 48 h at 135 °C. The reaction mixture was cooled to room temperature and the solvent was evaporated under high vacuum. The residue was dissolved in dichloromethane, filtered through a pad of silica gel and washed with additional dichloromethane (100 mL). The solvent was removed under reduced pressure. After recrystallization in hot methanol, the product was filtered and dried.



NMR numbering scheme used for the metal(II) arene 2-pyridinecarbothioamides.

***N*-(4-Morpholinophenyl)-2-pyridinecarbothioamide (5).** 4-Morpholinoaniline (4.46 g, 25 mmol), sulfur (2.41 g, 75 mmol) and sodium sulfite (0.13 g, 0.5 mol%) were refluxed in 2-picoline (15 mL). After work-up and recrystallization from hot methanol, the orange product was filtered and dried. Yield: 5.00 g (88%). Elemental analysis found: C, 63.89; H, 5.88; N, 14.03; S, 10.95, calculated for C₁₆H₁₇N₃OS: C, 64.19; H, 5.72; N, 14.04; S, 10.71. ¹H NMR (500.10 MHz, CDCl₃, 25 °C): δ = 11.97 (s, 1H, -NH), 8.80 (d, ³J_(H₃,H₄) = 8 Hz, 1H, H-4), 8.54 (d, ³J_(H₁,H₂) = 5 Hz, 1H, H-1), 8.00 (d, ³J_{(H₈,H₉)/(H₁₁,H₁₂)} = 9 Hz, 2H, H-9/H-11), 7.87 (td, ³J_{(H₂,H₃)/(H₃,H₄)} = 7.5 Hz, ⁴J_(H₁,H₃) = 2 Hz, 1H, H-3), 7.45 (ddd, ³J_(H₂,H₃) = 7.5 Hz, ³J_(H₁,H₂) = 5 Hz, ⁴J_{(H₁,H₂)/(H₂,H₃)} = 1 Hz, 1H, H-2), 7.00 (d, ³J_{(H₈,H₉)/(H₁₁,H₁₂)} = 7 Hz, 2H, H-8/H-12), 3.89 (t, ³J_{(H¹,H²)/(H³,H⁴)} = 5 Hz, 4H, H^c-2/H^c-3), 3.22 (t, ³J_{(H¹,H²)/(H³,H⁴)} = 5 Hz, 4H, H^c-1/H^c-4) ppm. ¹³C{¹H} NMR (125.75 MHz,

CDCl₃, 25 °C): δ = 186.56 (C-6), 151.59 (C-5), 148.38 (C-10), 146.50 (C-1), 137.43 (C-3), 125.83 (C-2), 124.76 (C-4), 123.86 (C-9/C-11), 115.71 (C-8/C-12), 66.64 (C'-2/C'-3), 49.39 (C'-1/C'-4) ppm. MS (ESI⁺): m/z 300.04 [M + H]⁺ (m_{ex} = 300.11).

***N*-(4-Benzoylphenyl)-2-pyridinecarbothioamide (6).** 4-Aminobenzoylphenone (4.93 g, 25 mmol), sulfur (2.41 g, 75 mmol) and sodium sulfite (0.13 g, 0.5 mol%) were refluxed in 2-picoline (15 mL). After work-up and recrystallization from hot methanol, the yellow crystals were filtered and dried. Yield: 3.50 g (77%). Elemental analysis found: C, 71.53; H, 4.77; N, 8.84, calculated for C₁₉H₁₄N₂OS: C, 71.67; H, 4.43; N, 8.80. ¹H NMR (500.10 MHz, CDCl₃, 25 °C): δ = 12.33 (s, 1H, -NH), 8.80 (d, ³ $J_{(H3,H4)}$ = 8 Hz, 1H, H-4), 8.58 (d, ³ $J_{(H1,H2)}$ = 5 Hz, 1H, H-1), 8.31 (d, ³ $J_{(H8,H9)/(H10,H11)}$ = 8.5 Hz, 2H, H-9/H-11), 7.94 (d, ³ $J_{(H8,H9)/(H10,H11)}$ = 8.5 Hz, 2H, H-8/H-12), 7.92 (t, ³ $J_{(H2,H3)/(H3,H4)}$ = 6.5 Hz, 1H, H-3), 7.82 (d, ³ $J_{(H'3,H'4)/(H'6,H'7)}$ = 7.5 Hz, 2H, H'-3/H'-7), 7.60 (t, ³ $J_{(H'4,H'5)/(H'5,H'6)}$ = 7.5 Hz, 1H, H'-5), 7.53 (t, ³ $J_{(H1,H2)/(H2,H3)}$ = 5 Hz, 1H, H-2), 7.50 (t, ³ $J_{(H'3,H'4)/(H'6,H'7)}$ = 7.5 Hz, 2H, H'-4/H'-6) ppm. ¹³C{¹H} NMR (125.75 MHz, CDCl₃, 25 °C): δ = 195.42 (C'-1), 188.05 (C-6), 151.10 (C-5), 146.18 (C-1), 142.28 (C-7), 138.04 (C-3), 137.65 (C-10), 135.04 (C'-2), 132.38 (C'-5), 131.21 (C-8/C-12), 129.95 (C'-3/C'-7), 128.33 (C'-4/C'-6), 126.34 (C-2), 125.12 (C-4), 121.61 (C-9/C-11) ppm. MS (ESI⁺): m/z 319.02 [M + H]⁺ (m_{ex} = 319.09).

General procedure for the synthesis of [chlorido(η^6 -p-cymene)(*N*-substituted 2-pyridinecarbothioamide)ruthenium(II)] chloride complexes. *N*-Substituted 2-pyridinecarbothioamide (2 eq.) was dissolved in dry methanol (20 mL) and heated to 40 °C under argon atmosphere. The ruthenium dimer [Ru(η^6 -p-cymene)Cl₂]₂ (1 eq.) was added under argon atmosphere and the reaction mixture was stirred for 4–18 h at 40 °C. The reaction mixture turned deep red upon addition of the dimer. The solvent was evaporated under reduced pressure and the solid residue was dissolved in dichloromethane and filtered. Hexane was added for precipitation. The pure product was obtained after filtration under suction and drying under vacuum at 40 °C.

[Chlorido(η^6 -p-cymene)(*N*-phenyl-2-pyridinecarbothioamide)ruthenium(II)] chloride (1A).

The compound was prepared following the general procedure using *N*-phenyl-2-pyridinecarbothioamide (70 mg, 0.326 mmol) and [Ru(η^6 -p-cymene)Cl₂]₂ (100 mg, 0.163 mmol). The reaction time was 4 h. After precipitation with hexane, the solvent was decanted and the product was dried under reduced pressure to give a red solid. Yield: 152 mg (90%). Elemental analysis found: C, 49.09; H, 4.94; N, 5.17; S, 5.61, calculated for C₂₂H₂₄Cl₂N₂SRu·H₂O: C, 49.07; H, 4.87; N, 5.20; S, 5.95. ¹H NMR (500.10 MHz, CDCl₃, 25 °C): δ = 14.57 (s, 1H, -NH), 9.73 (d, ³*J*_(H3,H4) = 8 Hz, 1H, H-4), 9.40 (d, ³*J*_(H1,H2) = 5 Hz, 1H, H-1), 8.15 (t, ³*J*_{(H2,H3)/(H3,H4)} = 7.5 Hz, 1H, H-3), 7.89 (d, ³*J*_{(H8,H9)/(H11,H12)} = 8 Hz, 2H, H-8/H-12), 7.60 (t, ³*J*_{(H1,H2)/(H2,H3)} = 6 Hz, 1H, H-2), 7.50 (t, ³*J*_{(H8,H9)/(H11,H12)} = 8 Hz, 2H, H-9/H-11), 7.40 (t, ³*J*_{(H9,H10)/(H10,H11)} = 8 Hz, 1H, H-10), 5.72 (d, ³*J*_(H14,H15) = 6 Hz, 1H, H-15), 5.62 (d, ³*J*_(H17,H18) = 6 Hz, 1H, H-18), 5.58 (d, ³*J*_(H17,H18) = 6 Hz, 1H, H-17), 5.42 d, ³*J*_(H14,H15) = 6 Hz, 1H, H-14), 2.78 (sept, ³*J*_{(H20,H21)/(H21,H22)} = 7 Hz, 1H, H-21), 2.22 (s, 3H, H-19), 1.23 (d, ³*J*_(H20,H21) = 7 Hz, 3H, H-20), 1.17 (d, ³*J*_(H21,H22) = 7 Hz, 3H, H-22) ppm. ¹³C{¹H} NMR (125.75 MHz, CDCl₃, 25 °C): δ = 190.83 (C-6), 157.43 (C-1), 153.82 (C-5), 140.16 (C-3), 137.64 (C-7), 129.25 (C-9/C-11), 129.06 (C-2), 128.80 (C-10), 127.80 (C-4), 125.48 (C-8/C-12), 106.61 (C-16), 102.90 (C-13), 87.58 (C-15), 87.13 (C-18), 84.76 (C-17), 84.06 (C-14), 31.04 (C-21), 22.63 (C-20), 21.90 (C-22), 18.73 (C-19) ppm. MS (ESI⁺): *m/z* 448.88 [M – Cl – H]⁺ (*m*_{ex} = 448.57).

[Chlorido(η^6 -p-cymene)(*N*-{4-hydroxyphenyl}-2-pyridinecarbothioamide)ruthenium(II)]

chloride (2A). The compound was prepared following the general procedure using *N*-(4-hydroxyphenyl)-2-pyridinecarbothioamide (76 mg, 0.326 mmol) and [Ru(η^6 -p-cymene)Cl₂]₂ (100 mg, 0.163 mmol). The reaction time was 18 h. A red microcrystalline product was obtained after filtration. Yield: 71 mg (41%). Elemental analysis found: C, 47.54; H, 4.80; N, 4.89; S, 5.44, calculated for C₂₂H₂₄Cl₂N₂OSRu·H₂O: C, 47.65; H, 4.73; N, 5.05; S, 5.78. ¹H NMR (500.10 MHz, *d*₄-MeOD, 25 °C): δ = 9.66 (d, ³*J*_(H1,H2) = 5.5 Hz, 1H, H-1), 8.40 (d, ³*J*_(H3,H4) = 8 Hz, 1H, H-

4), 8.28 (t, $^3J_{(H2,H3)/(H3,H4)} = 7.5$ Hz, 1H, H-3), 7.84 (t, $^3J_{(H1,H2)/(H2,H3)} = 6$ Hz, 1H, H-2), 7.46 (d, $^3J_{(H8,H9)/(H11,H12)} = 8.5$ Hz, 2H, H-9/H-11), 6.96 (d, $^3J_{(H8,H9)/(H11,H12)} = 8.5$ Hz, 2H, H-8/H-12), 6.04 (d, $^3J_{(H14,H15)} = 6$ Hz, 1H, H-15), 5.94 (d, $^3J_{(H17,H18)} = 6$ Hz, 1H, H-18), 5.90 (d, $^3J_{(H17,H18)} = 6$ Hz, 1H, H-17), 5.63 (d, $^3J_{(H14,H15)} = 6$ Hz, 1H, H-14), 2.75 (sept, $^3J_{(H20,H21)/(H21,H22)} = 7$ Hz, 1H, H-21), 2.21 (s, 3H, H-19), 1.21 (d, $^3J_{(H20,H21)} = 7$ Hz, 3H, H-20), 1.14 (d, $^3J_{(H21,H22)} = 7$ Hz, 3H, H-22) ppm. $^{13}\text{C}\{^1\text{H}\}$ NMR (125.75 MHz, d_4 -MeOD, 25 °C): $\delta = 192.92$ (C-6), 160.17 (C-1), 159.62 (C-10), 154.84 (C-5), 141.15 (C-3), 130.70 (C-2), 130.47 (C-7), 127.69 (C-9/C-11), 124.85 (C-4), 117.24 (C-8/C-12), 107.29 (C-16), 105.50 (C-13), 89.27 (C-15), 89.24 (C-18), 86.68 (C-17), 84.92 (C-14), 32.43 (C-21), 22.96 (C-20), 21.95 (C-22), 18.85 (C-19) ppm. MS (ESI⁺): m/z 464.86 [M – Cl – H]⁺ ($m_{\text{ex}} = 464.57$).

[Chlorido(η^6 -p-cymene)(*N*-{4-fluorophenyl}-2-pyridinecarbothioamide)ruthenium(II)]

chloride (3A). The compound was prepared following the general procedure using *N*-(4-fluorophenyl)-2-pyridinecarbothioamide (100 mg, 0.431 mmol) and [Ru(η^6 -p-cymene)Cl₂]₂ (132 mg, 0.215 mmol). The reaction time was 4 h. A dark red solid was obtained after filtration. Yield: 210 mg (90%). Elemental analysis found: C, 47.71; H, 4.38; N, 5.30; S, 6.10, calculated for C₂₂H₂₃Cl₂N₂FSRu·H₂O: C, 47.48; H, 4.53; N, 5.04; S, 5.75. ^1H NMR (500.10 MHz, d_4 -MeOD, 25 °C): $\delta = 9.68$ (d, $^3J_{(H1,H2)} = 5$ Hz, 1H, H-1), 8.47 (d, $^3J_{(H3,H4)} = 8$ Hz, 1H, H-4), 8.30 (t, $^3J_{(H2,H3)/(H3,H4)} = 7.5$ Hz, 1H, H-3), 7.86 (t, $^3J_{(H1,H2)/(H2,H3)} = 6.5$ Hz, 1H, H-2), 7.63 (m, 2H, H-9/H-11), 7.34 (t, $^3J_{(H7,H8)/(H11,H12)} = 8$ Hz, 2H, H-8/H-12), 6.05 (d, $^3J_{(H14,H15)} = 5.5$ Hz, 1H, H-15), 5.94 (d, $^3J_{(H17,H18)} = 5.5$ Hz, 1H, H-18), 5.92 (d, $^3J_{(H17,H18)} = 5.5$ Hz, 1H, H-17), 5.65 (d, $^3J_{(H14,H15)} = 5.5$ Hz, 1H, H-14), 2.75 (sept, $^3J_{(H20,H21)/(H21,H22)} = 6.5$ Hz, 1H, H-21), 2.21 (s, 3H, H-19), 1.21 (d, $^3J_{(H20,H21)} = 6.5$ Hz, 3H, H-20), 1.14 (d, $^3J_{(H21,H22)} = 6.5$ Hz, 3H, H-22) ppm. $^{13}\text{C}\{^1\text{H}\}$ NMR (125.75 MHz, d_4 -MeOD, 25 °C): $\delta = 194.06$ (C-6), 163.71 (C-10), 160.20 (C-1), 154.84 (C-5), 141.17 (C-3), 135.73 (C-7), 130.89 (C-2), 128.79 (C-9/C-11), 125.16 (C-4), 117.76 (C-8/C-12), 107.46 (C-16), 105.48 (C-13), 89.32 (C-15), 89.21 (C-18), 86.73 (C-17), 85.08 (C-14), 32.43 (C-

21), 22.96 (C-20), 21.97 (C-22), 18.86 (C-19) ppm. MS (ESI⁺): m/z 466.88 [M – Cl – H]⁺ ($m_{\text{ex}} = 466.57$).

[Chlorido(η^6 -p-cymene)(*N*-{2,4,6-trimethylphenyl}-2-pyridinecarbothioamide)ruthenium(II)] chloride (4A). The compound was prepared following the general procedure using *N*-(2,4,6-trimethylphenyl)-2-pyridinecarbothioamide (83 mg, 0.326 mmol) and [Ru(η^6 -p-cymene)Cl₂]₂ (100 mg, 0.163 mmol). The reaction time was 4 h. An intense red powder was obtained after filtration. Yield: 154 mg (84%). Elemental analysis found: C, 51.97; H, 5.25; N, 4.92; S, 5.59, calculated for C₂₅H₃₀Cl₂N₂SRu·H₂O: C, 51.72; H, 5.56; N, 4.83; S, 5.52. ¹H NMR (500.10 MHz, *d*₄-MeOD, 25 °C): $\delta = 9.71$ (d, ³ $J_{(H1,H2)} = 5.5$ Hz, 1H, H-1), 8.47 (d, ³ $J_{(H3,H4)} = 5.5$ Hz, 1H, H-4), 8.34 (t, ³ $J_{(H2,H3)/(H3,H4)} = 8$ Hz, 1H, H-3), 7.88 (t, ³ $J_{(H1,H2)/(H2,H3)} = 6$ Hz, 1H, H-2), 7.12 (s, 1H, H-9), 7.07 (s, 1H, H-11), 6.05 (d, ³ $J_{(H14,H15)} = 6$ Hz, 1H, H-15), 5.99 (d, ³ $J_{(H17,H18)} = 6$ Hz, 1H, H-18), 5.91 (d, ³ $J_{(H17,H18)} = 6$ Hz, 1H, H-17), 5.56 (d, ³ $J_{(H14,H15)} = 6$ Hz, 1H, H-14), 2.73 (sept, ³ $J_{(H20,H21)/(H21,H22)} = 7$ Hz, 1H, H-21), 2.36 (s, 3H, C_{ar}-CH₃), 2.23 (s, 3H, C_{ar}-CH₃), 2.23 (s, 3H, H-19), 2.14 (s, 3H, C_{ar}-CH₃), 1.19 (d, ³ $J_{(H20,H21)} = 7$ Hz, 3H, H-20), 1.11 (d, ³ $J_{(H21,H22)} = 7$ Hz, 3H, H-22) ppm. ¹³C{¹H} NMR (125.75 MHz, *d*₄-MeOD, 25 °C): $\delta = 193.76$ (C-6), 160.44 (C-1), 153.66 (C-5), 141.40 (C-3), 141.13 (C-7), 136.00 (C_{ar}-CH₃), 135.35 (C_{ar}-CH₃), 133.92 (C_{ar}-CH₃), 131.08 (C-2), 131.03 (C-9), 130.79 (C-11), 124.84 (C-4), 107.22 (C-16), 106.28 (C-13), 89.65 (C-18), 88.84 (C-15), 87.07 (C-17), 83.97 (C-14), 32.47 (C-21), 22.95 (C-20), 22.04 (C-22), 21.18 (C_{ar}-CH₃), 18.99 (C-19), 17.83 (C_{ar}-CH₃), 17.64 (C_{ar}-CH₃) ppm. MS (ESI⁺): m/z 490.91 [M – Cl – H]⁺ ($m_{\text{ex}} = 490.65$).

[Chlorido(η^6 -p-cymene)(*N*-{4-morpholinophenyl}-2-pyridinecarbothioamide)ruthenium(II)] chloride (5A). The compound was prepared following the general procedure using *N*-(4-morpholinoylphenyl)-2-pyridinecarbothioamide (98 mg, 0.326 mmol) and [Ru(η^6 -p-cymene)Cl₂]₂ (100 mg, 0.163 mmol). The reaction time was 18 h. A dark red solid was obtained after filtration. Yield: 145 mg (73%). Elemental analysis found: C,

49.90; H, 5.69; N, 6.69; S, 4.71, calculated for C₂₆H₃₁Cl₂N₃OSRu·1.25H₂O: C, 49.72; H, 5.38; N, 6.69; S, 5.09. ¹H NMR (500.10 MHz, CDCl₃, 25 °C): δ = 14.37 (s, 1H, -NH), 9.60 (brs, 1H, H-4), 9.38 (brs, 1H, H-1), 8.09 (brs, 1H, H-3), 7.93 (brs, 2H, H-9/H-11), 7.57 (brs, 1H, H-2), 7.05 (brs, 2H, H-8/H-11), 5.71 (d, ³J_(H14,H15) = 5.5 Hz, 1H, H-15), 5.60 (brs, 1H, H-17), 5.57 (brs, 1H, H-18), 5.41 (d, ³J_(H14,H15) = 5.5 Hz, 1H, H-14), 3.91 (brs, 4H, H'-2/H'-3), 3.27 (brs, 4H, H'-1/H'-4), 2.78 (sept, ³J_{(H20,H21)/(H21,H22)} = 6.5 Hz, 1H, H-21), 2.20 (s, 3H, H-19), 1.22 (d, ³J_(H20,H21) = 6.5 Hz, 3H, H-20), 1.15 (d, ³J_(H21,H22) = 6.5 Hz, 3H, H-22) ppm. ¹³C{¹H} NMR (125.75 MHz, CDCl₃, 25 °C): δ = 157.31 (C-1), 154.16 (C-5), 139.90 (C-3), 128.71 (C-2), 127.40 (C-4), 126.37 (C-9/C-11), 116.00 (C-8/C-12), 106.37 (C-16), 102.74 (C-13), 87.63 (C-15), 86.97 (C-17), 84.62 (C-18), 83.99 (C-14), 66.19 (C'-2/C'-3), 49.51 (C'-1/C'-4), 31.01 (C-21), 22.66 (C-20), 21.86 (C-22), 18.71 (C-19) ppm. MS (ESI⁺): *m/z* 533.97 [M – Cl – H]⁺ (*m*_{ex} = 533.67).

[Chlorido(*η*⁶-*p*-cymene)(*N*-{4-benzoylphenyl}-2-pyridinecarbothioamide)ruthenium(II)]

chloride (6A). The compound was prepared following the general procedure using *N*-(4-benzoylphenyl)-2-pyridinecarbothioamide (104 mg, 0.326 mmol) and [Ru(*η*⁶-*p*-cymene)Cl₂]₂ (100 mg, 0.163 mmol). The reaction time was 6 h. Violet-red crystals were obtained after filtration. Yield: 106 mg (50%). Elemental analysis found: C, 53.91; H, 4.48; N, 4.36; S, 4.81, calculated for C₂₉H₂₈Cl₂N₂OSRu·H₂O: C, 54.20; H, 4.71; N, 4.36; S, 4.99. ¹H NMR (500.10 MHz, *d*₄-MeOD, 25 °C): δ = 9.71 (d, ³J_(H1,H2) = 5 Hz, 1H, H-1), 8.54 (d, ³J_(H3,H4) = 8 Hz, 1H, H-4), 8.34 (t, ³J_{(H2,H3)/(H3,H4)} = 7.5 Hz, 1H, H-3), 7.99 (d, ³J_{(H8,H9)/(H11/H12)} = 8.5 Hz, 2H, H-9/H-11), 7.89 (t, ³J_{(H1,H2)/(H2,H3)} = 6.5 Hz, 1H, H-2), 7.86 (d, ³J_{(H8,H9)/(H11/H12)} = 8.5 Hz, 2H, H-8/H-12), 7.83 (d, ³J_{(H'3,H'4)/(H'6/H'7)} = 7.5 Hz, 2H, H'-3/H'-7), 7.70 (t, ³J_{(H'4,H'5)/(H'5,H'6)} = 7.5 Hz, 1H, H'-5), 7.58 (d, ³J_{(H'3,H'4)/(H'6/H'7)} = 7.5 Hz, 2H, H'-4/H'-6), 6.11 (d, ³J_(H14,H15) = 6 Hz, 1H, H-15), 5.99 (d, ³J_(H17,H18) = 6 Hz, 1H, H-18), 5.97 (d, ³J_(H17,H18) = 6 Hz, 1H, H-17), 5.70 (d, ³J_(H14,H15) = 6 Hz, 1H, H-14), 2.77 (sept, ³J_{(H20,H21)/(H21,H22)} = 7 Hz, 1H, H-21), 2.23 (s, 3H, H-19), 1.22 (d, ³J_(H20,H21) = 7 Hz, 3H, H-20), 1.15 (d, ³J_(H21,H22) = 7 Hz, 3H, H-22) ppm. ¹³C{¹H} NMR (125.75 MHz, *d*₄-MeOD, 25 °C): δ = 197.03 (C'-1), 194.39 (C-6), 160.31 (C-1), 154.85 (C-5), 142.76 (C-7), 141.24 (C-3), 138.94

(C-10), 138.44 (C'-2), 134.23 (C'-5), 132.50 (C-9/C-11), 131.06 (C-2, C'-3/C'-7), 129.76 (C'-4/C'-6), 126.27 (C-8/C-12), 125.43 (C-4), 107.80 (C-16), 105.76 (C-13), 89.41 (C-15/C-17), 86.99 (C-18), 85.27 (C-14), 32.48 (C-21), 22.98 (C-20), 22.00 (C-22), 18.89 (C-19) ppm. MS (ESI⁺): m/z 552.92 [M - Cl - H]⁺ ($m_{\text{ex}} = 552.67$).

General procedure for the synthesis of [chlorido(η^6 -p-cymene){*N*-substituted 2-pyridinecarbothioamide}osmium(II)]⁺ complexes. *N*-Substituted 2-pyridinecarbothioamide (2 eq.) was dissolved in dry methanol (20 mL) and heated to 40 °C under argon atmosphere. The osmium dimer [Os(η^6 -p-cymene)Cl₂]₂ (1 eq.) was added under argon atmosphere and the reaction mixture was stirred for 4–5 h at 40 °C. The reaction mixture turned deep red upon addition of the osmium dimer. The solvent was evaporated under reduced pressure and the solid residue was redissolved in dichloromethane and filtered. Hexane was added for precipitation in the fridge. The product was obtained after filtration and drying under vacuum at 40 °C.

[Chlorido(η^6 -p-cymene)(*N*-phenyl-2-pyridinecarbothioamide)osmium(II)] chloride (1B).

The compound was prepared following the general procedure using *N*-phenyl-2-pyridinecarbothioamide (54 mg, 0.253 mmol) and [Os(η^6 -p-cymene)Cl₂]₂ (100 mg, 0.127 mmol). The reaction mixture was stirred for 5 h at 40 °C. After work-up and precipitation with hexane, the solvent was decanted and the product was dried *in vacuo* to yield a deep red solid. Yield: 87 mg (57%). Elemental analysis, found: C, 42.41; H, 4.02; N, 4.73; S, 4.70, calculated for C₂₂H₂₄Cl₂N₂SOs·H₂O: C, 42.03; H, 4.17; N, 4.46; S, 5.09. ¹H NMR (500.10 MHz, CDCl₃, 25 °C): δ = 14.32 (s, 1H, -NH), 9.85 (d, ³ $J_{(H3,H4)} = 8$ Hz, 1H, H-4), 9.32 (d, ³ $J_{(H1,H2)} = 5$ Hz, 1H, H-1), 8.13 (t, ³ $J_{(H2,H3)/(H3,H4)} = 7.5$ Hz, 1H, H-3), 7.92 (d, ³ $J_{(H8,H9)/(H11,H12)} = 8$ Hz, 2H, H-8/H-12), 7.60 (t, ³ $J_{(H1,H2)/(H2,H3)} = 6$ Hz, 1H, H-2), 7.53 (t, ³ $J_{(H8,H9)/(H11,H12)} = 8$ Hz, 2H, H-9/H-11), 7.41 (t, ³ $J_{(H9,H10)/(H10,H11)} = 8$ Hz, 1H, H-10), 5.92 (d, ³ $J_{(H14,H15)} = 5.5$ Hz, 1H, H-15), 5.83 (d, ³ $J_{(H17,H18)} = 5.5$ Hz, 1H, H-17), 5.81 (d, ³ $J_{(H17,H18)} = 5.5$ Hz, 1H, H-18), 5.62 (d, ³ $J_{(H14,H15)} = 5.5$ Hz, 1H, H-14), 2.71 (sept, ³ $J_{(H20,H21)/(H21,H22)} = 7$ Hz, 1H, H-21), 2.32 (s, 3H, H-19), 1.24 (d, ³ $J_{(H20,H21)} = 7$ Hz, 3H,

H-20), 1.15 (d, $^3J_{(H20,H22)} = 7$ Hz, 3H, H-22) ppm. $^{13}\text{C}\{^1\text{H}\}$ NMR (125.75 MHz, CDCl_3 , 25 °C): $\delta = 193.52$ (C-6), 159.15 (C-1), 153.81 (C-5), 140.43 (C-3), 137.57 (C-7), 130.59 (C-2), 129.27 (C-9/C-11), 128.74 (C-10), 128.33 (C-4), 125.59 (C-8/C-12), 97.71 (C-16), 95.99 (C-13), 79.66 (C-15), 79.19 (C-16), 76.85 (C-17), 74.66 (C-14), 31.16 (C-21), 23.04 (C-20), 22.16 (C-22), 18.69 (C-19) ppm. MS (ESI⁺): m/z 539.01 [M – Cl – H]⁺ ($m_{\text{ex}} = 539.12$).

[Chlorido(η^6 -p-cymene)(*N*-{4-hydroxyphenyl}-2-pyridinecarbothioamide)osmium(II)]

chloride (2B). The compound was prepared following the general procedure using *N*-(4-hydroxyphenyl)-2-pyridinecarbothioamide (58 mg, 0.253 mmol) and $[\text{Os}(\eta^6\text{-p-cymene})\text{Cl}_2]_2$ (100 mg, 0.127 mmol). The reaction time was 4 h and the product was obtained as a dark red crystalline solid. Yield: 75 mg (47%). Elemental analysis, found: C, 41.49; H, 3.76; N, 4.45; S, 4.80; O, 3.52, calculated for $\text{C}_{22}\text{H}_{24}\text{Cl}_2\text{N}_2\text{OSOs}\cdot 0.5\text{H}_2\text{O}$: C, 41.63; H, 3.97; N, 4.41; S, 5.05; O, 3.78. ^1H NMR (500.10 MHz, d_4 -MeOD, 25 °C): $\delta = 9.57$ (d, $^3J_{(H1,H2)} = 5$ Hz, 1H, H-1), 8.47 (d, $^3J_{(H3,H4)} = 8$ Hz, 1H, H-4), 8.26 (t, $^3J_{(H2,H3)/(H3,H4)} = 7.5$ Hz, 1H, H-3), 7.79 (t, $^3J_{(H1,H2)/(H2,H3)} = 7.5$ Hz, 1H, H-2), 7.46 (d, $^3J_{(H8,H9)/(H11,H12)} = 9$ Hz, 2H, H-9/H-11), 6.96 (d, $^3J_{(H8,H9)/(H11,H12)} = 9$ Hz, 2H, H-8/H-12), 6.21 (d, $^3J_{(H14,H15)} = 5.5$ Hz, 1H, H-15), 6.11 (d, $^3J_{(H17,H18)} = 5.5$ Hz, 1H, H-17), 6.06 (d, $^3J_{(H17,H18)} = 5.5$ Hz, 1H, H-18), 5.80 (d, $^3J_{(H14,H15)} = 5.5$ Hz, 1H, H-14), 2.65 (sept, $^3J_{(H20,H21)/(H21,H22)} = 7$ Hz, 1H, H-21), 2.28 (s, 3H, H-19), 1.20 (d, $^3J_{(H20,H21)} = 7$ Hz, 3H, H-20), 1.09 (d, $^3J_{(H21,H22)} = 7$ Hz, 3H, H-22) ppm. $^{13}\text{C}\{^1\text{H}\}$ NMR (125.75 MHz, d_4 -MeOD, 25 °C): $\delta = 196.25$ (C-6), 161.26 (C-1), 159.57 (C-10), 154.97 (C-5), 141.23 (C-3), 131.70 (C-2), 130.40 (C-7), 127.71 (C-9/C-11), 125.21 (C-4), 117.27 (C-8/C-12), 98.74 (C-16), 98.69 (C-13), 81.38 (C-15), 81.01 (C-18), 78.55 (C-17), 75.42 (C-14), 32.54 (C-21), 23.35 (C-20), 22.19 (C-22), 18.72 (C-19) ppm. MS (ESI⁺): m/z 555.05 [M – Cl – H]⁺ ($m_{\text{ex}} = 555.11$).

[Chlorido(η^6 -p-cymene)(*N*-{4-fluorophenyl}-2-pyridinecarbothioamide)osmium(II)]

chloride (3B). The compound was prepared following the general procedure using *N*-(4-fluorophenyl)-2-pyridinecarbothioamide (59 mg, 0.253 mmol) and $[\text{Os}(\eta^6\text{-p-cymene})\text{Cl}_2]_2$

(100 mg, 0.127 mmol). The reaction time was 4 h and the product was obtained as a dark red solid. Yield: 117 mg (74%). Elemental analysis, found: C, 40.94; H, 3.81; N, 4.33; S, 4.75, calculated for $C_{22}H_{23}Cl_2FN_2SO_2 \cdot H_2O$: C, 40.93; H, 3.90; N, 4.34; S, 4.97. 1H NMR (500.10 MHz, $CDCl_3$, 25 °C): δ = 14.36 (s, 1H, -NH), 9.80 (d, $^3J_{(H3,H4)} = 7.5$ Hz, 1H, H-4), 9.29 (brs, 1H, H-1), 8.14 (br t, $^3J_{(H2,H3)/(H3,H4)} = 8$ Hz, 1H, H-3), 7.90 (t, $^3J_{(H8,H9)/(H11,H12)} = 6.5$ Hz, 2H, H-9/H-11), 7.60 (brs, 1H, H-2), 7.18 (t, $^3J_{(H8,H9)/(H11,H12)} = 6.5$ Hz, 2H, H-8/H-12), 5.90 (brs, 1H, H-15), 5.79 (brs, 1H, H-17), 5.77 (brs, 1H, H-18), 5.60 (brs, 1H, H-14), 2.70 (sept, $^3J_{(H20,H21)/(H21,H22)} = 6.5$ Hz, 1H, H-21), 2.31 (s, 3H, H-21), 1.22 (d, $^3J_{(H20,H21)} = 7$ Hz, 3H, H-20), 1.14 (d, $^3J_{(H21,H22)} = 7$ Hz, 3H, H-22) ppm. $^{13}C\{^1H\}$ NMR (125.75 MHz, $CDCl_3$, 25 °C): δ = 193.73 (C-6), 162.05 (C-10), 158.88 (C-1), 153.77 (C-5), 140.59 (C-3), 133.49 (C-7), 130.60 (C-2), 128.37 (C-4), 127.75 (C-9/C-11), 116.29 (C-8/C-12), 97.84 (C-16), 96.00 (C-13), 79.70 (C-15), 79.08 (C-18), 76.85 (C-17), 74, 78 (C-14), 31.19 (C-21), 23.06 (C-20), 22.20 (C-22), 18.76 (C-19) ppm. MS (ESI⁺): m/z 557.08 [$M - Cl - H$]⁺ ($m_{ex} = 557.11$).

[Chlorido(η^6 -p-cymene)(*N*-{2,4,6-trimethylphenyl}-2-pyridinecarbothioamide)osmium(II)] chloride (4B). The compound was prepared following the general procedure using *N*-(2,4,6-trimethylphenyl)-2-pyridinecarbothioamide (66 mg, 0.258 mmol) and $[Os(\eta^6\text{-p-cymene})Cl_2]_2$ (102 mg, 0.129 mmol). The reaction time was 4 h and the product was obtained as a deep violet powder. Yield: 127 mg (76%). Elemental analysis, found: C, 45.15; H, 4.57; N, 4.30; S, 4.73, calculated for $C_{25}H_{30}Cl_2N_2SO_2 \cdot 0.5H_2O$: C, 45.44; H, 4.73; N, 4.24; S, 4.85. 1H NMR (500.10 MHz, $CDCl_3$, 25 °C): δ = 14.19 (s, 1H, -NH), 10.05 (brs, 1H, H-4), 9.35 (brs, 1H, H-1), 8.15 (brs, 1H, H-3), 7.56 (brs, 1H, H-2), 7.02 (s, 1H, H-9), 6.97 (s, 1H, H-11), 5.86 (s, 1H, H-15), 5.80 (brs, 2H, H-17/H-18), 5.46 (s, 1H, H-14), 2.64 (sept, $^3J_{(H20,H21)/(H21,H22)} = 7.5$ Hz, 1H, H-21), 2.34 (s, 3H, H-19), 2.32 (s, 3H, C_{ar}-CH₃), 2.31 (s, 3H, C_{ar}-CH₃), 2.24 (s, 3H, C(10)-CH₃), 1.18 (d, $^3J_{(H20,H21)} = 7$ Hz, 3H, H-20), 1.07 (d, $^3J_{(H21,H22)} = 7$ Hz, 3H, H-22) ppm. $^{13}C\{^1H\}$ NMR (125.75 MHz, $CDCl_3$, 25 °C): δ = 195.38 (C-6), 159.45 (C-1), 152.92 (C-5), 140.61 (C-3), 139.05 (C-7), 134.90 (C_{ar}), 133.98 (C_{ar}), 133.13 (C_{ar}), 130.74 (C-2), 129.91 (C-11), 129.57 (C-9), 128.20 (C-4), 97.61 (C-16),

96.82 (C-13), 79.88 (C-18), 78.97 (C-15), 77.25 (C-17), 72.41 (C-14), 31.28 (C-21), 23.09 (C-20), 22.14 (C-22), 21.19 (CH₃), 18.81 (CH₃), 18.25 (C-19), 18.18 (CH₃) ppm. MS (ESI⁺): *m/z* 581.08 [M – Cl – H]⁺ (*m*_{ex} = 581.17), *m/z* 616.98 [M]⁺ (*m*_{ex} = 617.14).

[Chlorido(η^6 -p-cymene)(*N*-{4-morpholinophenyl}-2-pyridinecarbothioamide)osmium(II)] chloride (5B). The compound was prepared following the general procedure using *N*-(4-morpholinophenyl)-2-pyridinecarbothioamide (76 mg, 0.253 mmol) and [Os(η^6 -p-cymene)Cl₂]₂ (100 mg, 0.127 mmol). The reaction time was 4 h and the product was obtained as a black microcrystalline solid. Yield: 130 mg (74%). Elemental analysis, found: C, 43.66; H, 4.58; N, 5.86; S, 4.26, calculated for C₂₆H₃₁Cl₂N₃OSO₂·H₂O: C, 43.75; H, 4.66; N, 5.89; S, 4.48. ¹H NMR (500.10 MHz, CDCl₃, 25 °C): δ = 14.41 (s, 1H, -NH), 9.75 (brs, 1H, H-4), 9.21 (brs, 1H, H-1), 8.11 (brs, 1H, H-3), 7.97 (d, ³*J*_{(H8,H9)/(H11,H12)} = 8 Hz, 2H, H-9/H-11), 7.51 (brs, 1H, H-2), 7.26 (brs, 2H, H-8/H-12), 5.89 (d, ³*J*_(H14,H15) = 5 Hz, 1H, H-15), 5.76 (brs, 1H, H-17), 5.73 (brs, 1H, H-18), 5.59 (brs, 1H, H-14), 4.01 (brs, 4H, H²-2/H³-3), 3.34 (brs, 4H, H¹-1/H⁴-4), 2.70 (sept, ³*J*_{(H20,H21)/(H21,H22)} = 7 Hz, 1H, H-21), 2.29 (s, 3H, H-19), 1.23 (d, ³*J*_(H20,H21) = 7 Hz, 1H, H-20), 1.14 (d, ³*J*_(H21,H22) = 7 Hz, 1H, H-22) ppm. ¹³C{¹H} NMR (125.75 MHz, CDCl₃, 25 °C): δ = 157.90 (C-1), 154.10 (C-5), 147.99 (C-7), 140.16 (C-3), 129.58 (C-2), 127.77 (C-4), 126.54 (C-9/C-11), 116.97 (C-8/C-12), 97.57 (C-16), 95.65 (C-13), 79.63 (C-15), 78.46 (C-18), 76.75 (C-17), 74.51 (C-14), 65.92 (C²-2/C³-3), 50.25 (C¹-1/C⁴-4), 31.12 (C-21), 23.03 (C-20), 22.11 (C-22), 18.57 (C-19) ppm. MS (ESI⁺): *m/z* 624.04 [M – Cl – H]⁺ (*m*_{ex} = 624.17).

[Chlorido(η^6 -p-cymene)(*N*-{4-benzoylphenyl}-2-pyridinecarbothioamide)osmium(II)] chloride (6B). The compound was prepared following the general procedure using *N*-(4-morpholinophenyl)-2-pyridinecarbothioamide (81 mg, 0.253 mmol) and [Os(η^6 -p-cymene)Cl₂]₂ (100 mg, 0.127 mmol). The reaction time was 4 h and the product was obtained as black crystals. Yield: 150 mg (83%). Elemental analysis, found: C, 47.82; H, 3.80; N, 3.96; S, 4.16, calculated for C₂₉H₂₈Cl₂N₂OSO₂·0.5H₂O: C, 48.13; H, 4.04; N, 3.87; S, 4.42. ¹H NMR (500.10 MHz,

CDCl_3 , 25 °C): $\delta = 14.67$ (s, 1H, -NH), 9.88 (d, ${}^3J_{(H3,H4)} = 8$ Hz, 1H, H-4), 9.28 (d, ${}^3J_{(H1,H2)} = 5$ Hz, 1H, H-1), 8.16 (t, ${}^3J_{(H2,H3)/(H3,H4)} = 8$ Hz, 1H, H-3), 8.09 (d, ${}^3J_{(H8,H9)/(H11,H12)} = 7.5$ Hz, 2H, H-9/H-11), 7.93 (d, ${}^3J_{(H8,H9)/(H11,H12)} = 7.5$ Hz, 2H, H-8/H-12), 7.83 (d, ${}^3J_{(H'3,H'4)/(H'6,H'7)} = 7$ Hz, 2H, H^c-3/H^c-7), 7.62 (m, 1H, H-2), 7.60 (m, 1H, H^c-5), 7.51 (t, ${}^3J_{(H'3,H'4)/(H'4,H'5)} = 8$ Hz, 2H, H^c-4/H^c-6), 5.91 (d, ${}^3J_{(H14,H15)} = 5.5$ Hz, 1H, H-15), 5.81 (d, ${}^3J_{(H17,H18)} = 5.5$ Hz, 1H, H-18), 5.77 (d, ${}^3J_{(H17,H18)} = 5.5$ Hz, 1H, H-17), 5.62 (d, ${}^3J_{(H14,H15)} = 5.5$ Hz, 1H, H-14), 2.71 (sept, ${}^3J_{(H20,H21)/(H21,H22)} = 7.5$ Hz, 1H, H-21), 2.31 (s, 3H, H-19), 1.23 (d, ${}^3J_{(H20,H21)} = 7$ Hz, 3H, H-20), 1.15 (d, ${}^3J_{(H20,H21)} = 7$ Hz, 3H, H-22) ppm. ${}^{13}\text{C}\{{}^1\text{H}\}$ NMR (125.75 MHz, CDCl_3 , 25 °C): $\delta = 195.60$ (C⁻-1), 194.36 (C-6), 158.19 (C-1), 153.84 (C-5), 140.99 (C-7), 140.34 (C-3), 137.34 (C-10), 137.08 (C⁻-2), 132.78 (C-2), 130.98 (C-8/C-12), 130.13 (C⁻-5), 130.11 (C⁻-3/C⁻-7), 128.44 (C⁻-4/C⁻-6), 128.32 (C-4), 125.29 (C-9/C-11), 98.12 (C-16), 96.14 (C-13), 79.71 (C-15), 78.71 (C-17), 76.65 (C-18), 74.82 (C-14), 31.18 (C-21), 23.02 (C-20), 22.13 (C-22), 18.61 (C-19) ppm. MS (ESI⁺): m/z 643.02 [M - Cl - H]⁺ ($m_{\text{ex}} = 643.15$).

Hydrolysis experiments

Compounds **1A** and **1B** (1–5 mM) were investigated on their hydrolysis behavior. The compounds were dissolved in a mixture of D₂O/H₂O (90/10) or in 104 mM NaCl solution in D₂O/H₂O (90/10), and the samples were analyzed by ¹H NMR spectroscopy by suppressing the water signal. Following a preparation time of *ca.* 10 min, spectra were recorded every 10 min for 14 h using 32 scans/spectrum. UV-vis experiments were used to verify the NMR experiments. For this purpose, solutions of **1A** and **1B** in H₂O or in 104 mM NaCl solution were prepared at 20–50 μM concentrations and UV-vis spectra were recorded every 20 min for 24 h after a preparation time of 15 min.

Lipophilicity measurements

The lipophilicity of compounds **1A–6B** was determined using HPLC methods,^{10, 11} following OECD guidelines.¹² The HPLC system (TM100, Dionex) was equipped with a reversed-phased column (Zorbax Eclipse Plus C18, Agilent, 5 μm pore size, 4.6 μm inner diameter and 250 mm column length) that was thermostatted at 25 °C and a UV detector (UVD 170U, Dionex). Potassium iodide (0.1 mM) was used as an internal standard for the determination of the column dead-time. For delineating the lipophilicity, the capacity factors of each compound (250 μM) were measured at three different methanol : water ratios using isocratic methods and 0.5 % formic acid. Measurements were carried out in duplicate and fitted to the equation $\log k = S \cdot \varphi + \log k_w$, where $\log k$ is the logarithmic capacity factor, S the slope, φ the organic solvent concentration and $\log k_w$ the intercept at zero organic solvent concentration. Capacity factors were only considered if detected within the working limits of $-0.5 < \log k < 1.5$, where the mentioned linear relationship is valid.¹⁰ The corresponding correlation factors were all found at $R^2 > 0.9979$. The quotient of the intercept and the slope gives the chromatographic lipophilicity index $\varphi_0 = -\log k_w/S$, which shows a better correlation with lipophilicity than extrapolated $\log k_w$ values.¹³ The index φ_0 is compound

specific and gives the concentration of organic solvent needed to obtain a retention time that is exactly the two-fold column dead-time, *i.e.* $\log k = 0$.

Interaction with biomolecules and stability in hydrochloric acid

The stability of **1A** and **1B** in the presence of biological nucleophiles and in hydrochloric acid was investigated by electrospray ionization mass spectrometry (ESI-MS). Compound **1A** and **1B** were dissolved in aqueous solution and incubated in equimolar ratios with Cys, His, Met, ub, cyt or 5'-dGMP at 37 °C. Spectra were recorded up to 7 d. The samples containing amino acids or 5'-dGMP were diluted with methanol, whereas protein samples were diluted with water : methanol : formic acid (50 : 50 : 0.1) prior to direct infusion into the MS. Furthermore, both **1A** and **1B** (200 µM) were dissolved in 60 mM HCl (pH = 1.2) and incubated at 37 °C. Spectra were recorded after 1, 3 and 19 h at final concentrations of 10 µM. For comparison purposes, **2A** and **2B** were also incubated with Cys and Met and spectra were recorded after 1, 3 and 19 h at final concentrations of 10 µM.

Cytotoxicity in cancer cell lines

Cell lines and culture conditions. CH1 cells (adenocarcinoma of the ovary, human) were provided by Lloyd R. Kelland (CRC Centre for Cancer Therapeutics, Institute of Cancer Research, Sutton, U.K). SW480 (adenocarcinoma of the colon, human) and A549 (non-small cell lung cancer, human) cells were from Brigitte Marian (Institute of Cancer Research, Department of Medicine I, Medical University of Vienna, Austria). All cell culture reagents were purchased from Sigma-Aldrich. Cells were grown in 75 cm² culture flasks (Starlab) as adherent monolayer cultures in complete culture medium, *i.e.* Eagle's minimal essential medium (MEM) supplemented with 10% heat-inactivated fetal calf serum, 1 mM sodium pyruvate, 4 mM L-glutamine, and 1% non-essential amino acids (from 100× ready-to-use stock) without antibiotics. Cultures were maintained at 37 °C in a humidified atmosphere containing 95% air and 5% CO₂.

MTT assay conditions. Cytotoxicity was determined by the colorimetric MTT (3-(4,5-dimethyl-2-thiazolyl)-2,5-diphenyl-2H-tetrazolium bromide, purchased from Fluka) microculture assay. For this purpose, cells were harvested from culture flasks by trypsinization and seeded in 100 μ L/well aliquots of complete culture medium into 96-well microculture plates (Starlab). Cell densities of 1.5×10^3 cells/well (CH1), 2.5×10^3 cells/well (SW480) and 4×10^3 cells/well (A549) were chosen in order to ensure exponential growth of untreated controls throughout the experiment. For 24 h, cells were allowed to settle and resume exponential growth. The test compounds were dissolved in DMSO, serially diluted in complete culture medium (such that the DMSO content in actual test solutions did not exceed 0.5%) and added in 100 μ L/well aliquots for an exposure time of 96 hours. At the end of exposure, the medium was replaced with 100 μ L/well RPMI1640 culture medium (supplemented with 10% heat-inactivated fetal calf serum) plus 20 μ L/well MTT solution in phosphate-buffered saline (5 mg/ml). After incubation for 4 h, the supernatants were removed, and the formazan crystals formed by vital cells were dissolved in 150 μ L DMSO per well. Optical densities at 550 nm were measured with a microplate reader (Tecan Spectra Classic), using a reference wavelength of 690 nm to correct for unspecific absorption. The quantity of vital cells was expressed in terms of T/C values by comparison to untreated control microcultures, and 50% inhibitory concentrations (IC_{50}) were calculated from concentration-effect curves by interpolation. Evaluation is based on means from at least three independent experiments, each comprising at least three replicates per concentration level.

Adduct formation on the nucleosome core particle

NCP crystals were produced and stabilized in harvest buffer (37 mM $MnCl_2$, 40 mM KCl, 20 mM K-cacodylate [pH 6.0], 24% 2-methyl-2,4-pentanediol and 2% trehalose) as previously described.^{14, 15} The 37 mM $MnCl_2$ buffer component was subsequently eliminated by gradual replacement with 10 mM $MgSO_4$ followed by thorough rinsing of crystals with the $MgSO_4$ -containing buffer to remove any residual $MnCl_2$.¹⁶ The crystal structures reported here stems from 44–48 hour incubation of crystals with 1 mM **1A**, **3A**, **1B** or **3B** included in the buffer. Single

crystal X-ray diffraction data were recorded as described previously¹⁵ at beam line X06DA of the Swiss Light Source (Paul Scherrer Institute, Villigen, Switzerland) using a Mar225 CCD detector and an X-ray wavelength of 1.14 Å (NCP-1B, NCP-3B) or 1.50 Å (NCP-1A, NCP-3A). Data were processed with MOSFLM¹⁷ and SCALA from the CCP4 package.¹⁸ The native 2.5 Å resolution NCP145 model (*pdb* code 3REH)¹⁹ was used for initial structure solution by molecular replacement. Structural refinement and model building were carried out with routines from the CCP4 suite.¹⁸ Restraint parameters for the adducts were based on the small molecule crystal structure of **2B** reported here. Data collection and structure refinement statistics are given in Table S3.

Atomic coordinates and structure factors have been deposited in the RCSB Protein Data Bank under accession codes X, Y, Z and Q. Graphic figures were prepared with PyMOL (DeLano Scientific LLC, San Carlos, CA, USA).

Table S1. X-ray diffraction parameters for the measurement of single crystals of **3A** and **2B**^a.

compound	3A	2B
CCDC N ^o	902335	902334
chemical formula	C ₂₂ H ₂₃ Cl ₂ FN ₂ RuS·C ₃ H ₆ O	C ₂₂ H ₂₄ Cl ₂ N ₂ OOsS
<i>M</i> (g mol ⁻¹)	596.53	625.59
temperature (K)	200(2)	100(2)
crystal size (mm)	0.20 × 0.10 × 0.06	0.20 × 0.10 × 0.08
crystal color, habit	red, block	red, block
crystal system	monoclinic	monoclinic
space group	P21n	P21/c
<i>a</i> (Å)	14.0346(9)	14.4797(14)
<i>b</i> (Å)	8.6278(5)	11.9305(11)
<i>c</i> (Å)	22.7026(13)	13.1126(13)
<i>V</i> (Å ³)	2749.0(3)	2239.8(4)
β (deg)	90.353(3)	98.591(3)
<i>Z</i>	4	4
<i>D_c</i> (g cm ⁻³)	1.441	1.855
μ (mm ⁻¹)	0.87	6.041
F(000)	1216.0	1216.0
Θ range (deg)	2.91 to 30.18	2.60 to 30.20
<i>h</i> range	-19/19	-20/20
<i>k</i> range	-11/12	-16/16
<i>l</i> range	-31/32	-18/18
no. unique refls.	7964	6623
no. parameters	301	266
<i>R</i> _{int}	0.082	0.057
<i>R</i> ₁ (obs.)	0.0469	0.0425
<i>wR</i> ₂ (all data)	0.1031	0.0547
<i>S</i>	0.98	1.031

^a $R_1 = \frac{\sum ||F_o| - |F_c||}{\sum w|F_o|}$, ^b $wR_2 = \frac{\{\sum [w(F_o^2 - F_c^2)^2] / \sum [w(F_o^2)^2]\}^{1/2}}$, ^c $S = \frac{\{\sum [w(F_o^2 - F_c^2)^2] / (n - p)\}^{1/2}}$, where *n* is the number of reflections and *p* is the total number of parameters refined

Table S2. Selected bond lengths (Å), angles (°) and torsion angles (°) of **3A** and **2B**.

Bond Lengths (Å)	3A (M = Ru)	2B (M = Os)
M–S	2.3414(9)	2.3468(8)
M–N1	2.095(3)	2.105(2)
M–Cl	2.3924(4)	2.3987(9)
M–centroid	1.687(3)	1.682(3)
Bond Angles (°)	3A	2B
S–M–N1	81.28(8)	80.89(7)
S–M–Cl	89.81(3)	88.04(3)
N1–M–Cl	83.68(8)	82.41(8)
Torsion Angles (°)	3A	2B
C6–N2–C7–C8	52.7(5)	74.8(4)
N1–C5–C6–S	15.9(4)	4.1(4)

Table S3. Data collection and refinement statistics for NCP treated with **1A**, **3A**, **1B** and **3B**.

	NCP-1A	NCP-3A	NCP-1B	NCP-3B
Data collection*				
Space group	P2 ₁ 2 ₁ 2 ₁	P2 ₁ 2 ₁ 2 ₁	P2 ₁ 2 ₁ 2 ₁	P2 ₁ 2 ₁ 2 ₁
Cell dimensions				
<i>a</i> (Å)	106.80	106.48	106.71	106.78
<i>b</i> (Å)	109.81	109.82	109.93	109.73
<i>c</i> (Å)	182.38	181.39	181.84	181.91
Resolution (Å)	2.58–60.8 (2.58–2.72)	2.87–60.5 (2.87–3.03)	2.38–60.6 (2.38–2.51)	2.41–58.6 (2.41–2.54)
<i>R</i> _{merge} (%)	6.8 (47.8)	11.7 (32.9)	4.1 (45.9)	7.5 (40.4)
<i>I</i> / σ <i>I</i>	15.8 (2.3)	8.2 (2.0)	21.3 (2.1)	12.8 (2.0)
Completeness (%)	84.2 (46.5)	99.7 (98.5)	82.6 (39.3)	96.5 (81.6)
Redundancy	6.4 (4.2)	6.4 (3.5)	6.1 (3.0)	6.1 (2.9)
Refinement				
Resolution (Å)	2.58–60.8	2.87–60.5	2.38–60.6	2.41–58.6
No. reflections	55962	48147	69745	78440
<i>R</i> _{work} / <i>R</i> _{free} (%)	25.2 / 27.3	23.7 / 28.0	25.2 / 28.0	26.5 / 27.5
No. atoms	12063	12063	12119	12122
Protein	6086	6086	6086	6086
DNA	5939	5939	5939	5939
Solvent	16	16	16	16
Adduct	22	22	78	81
<i>B</i> -factors (Å ²)	77	72	76	75
Protein	51	45	47	48
DNA	105	99	104	102
Solvent	74	85	78	75
Adduct	123	109	119	117
R.m.s. deviations				
Bond lengths (Å)	0.008	0.010	0.009	0.009
Bond angles (°)	1.30	1.50	1.34	1.28

* Values in parentheses are for the highest-resolution shell.

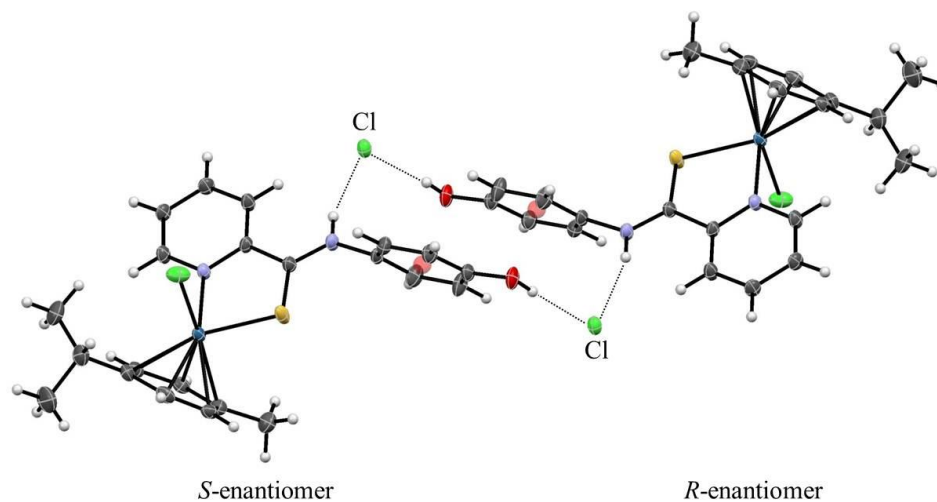


Figure S1. The hydrogen bonding network of two independent molecules in the crystal structure lattice of **2B** is shown, featuring both stereoisomers in a 1 : 1 ratio. The phenol rings are aligned in a parallel offset fashion.

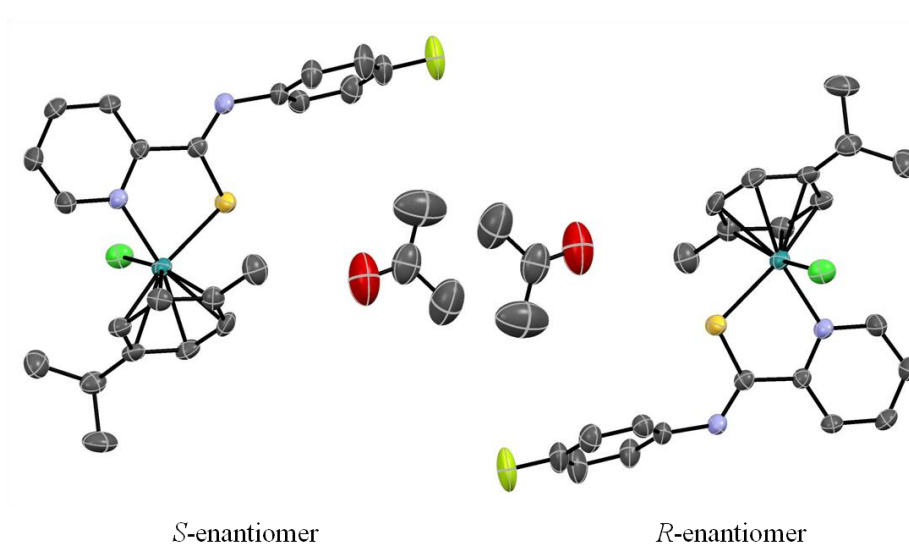


Figure S2. The *S*- (left) and *R*-enantiomers (right) in the crystal structure lattice of **3A** with two co-crystallized acetone molecules. Hydrogen atoms and counter anions are omitted for clarity.

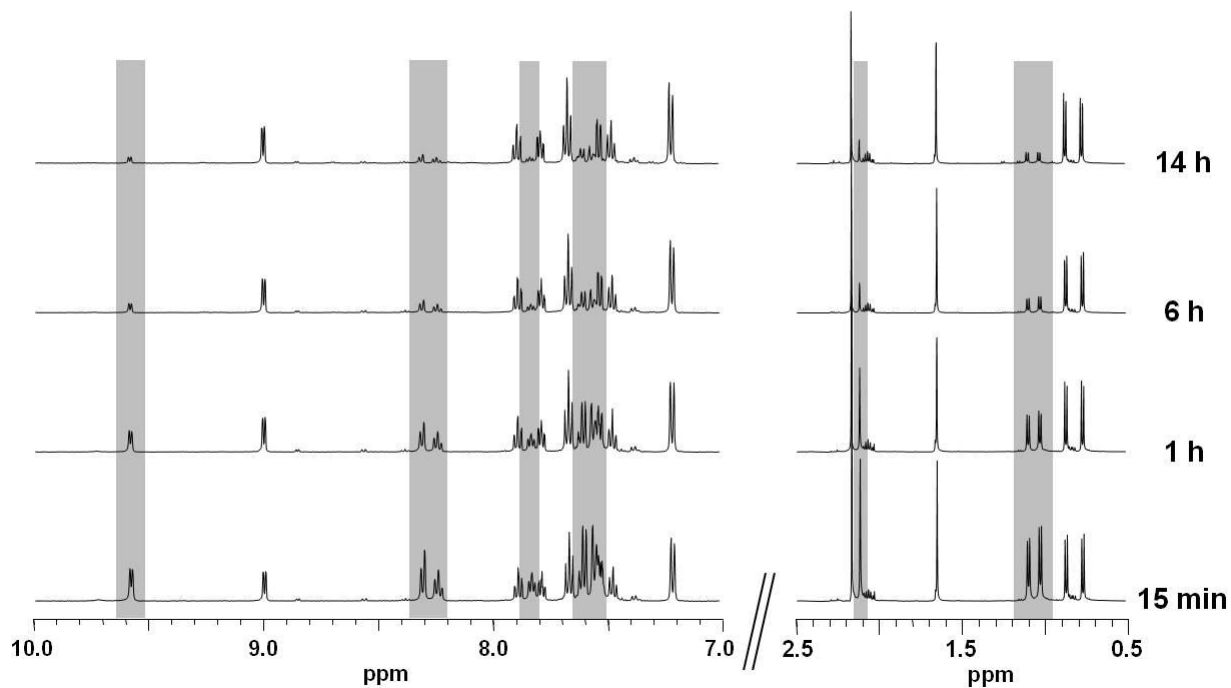


Figure S3. Low- and high-field regions of the NMR experiments monitoring the hydrolysis of **1A** in 104 mM NaCl aqueous solution. The highlighted peaks were assigned to the chlorido species.

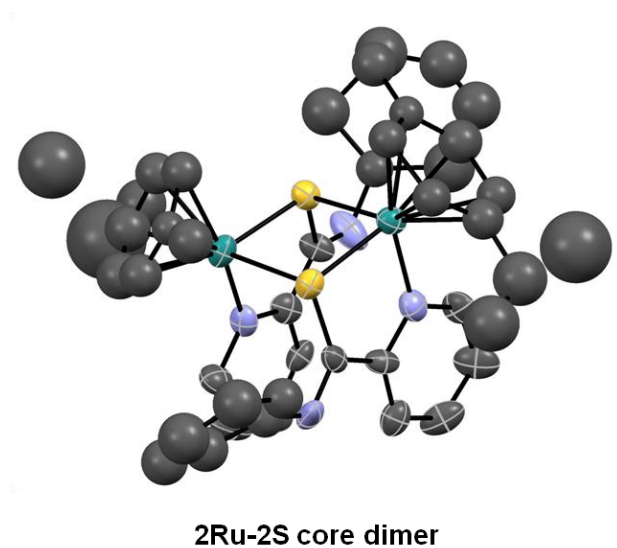


Figure S4. The crystal structure of the 2Ru-2S dimer (top) of **1A** obtained from basic aqueous solution is shown. The hydrogen atoms and counter ions as well as solvent molecules are omitted for clarity.

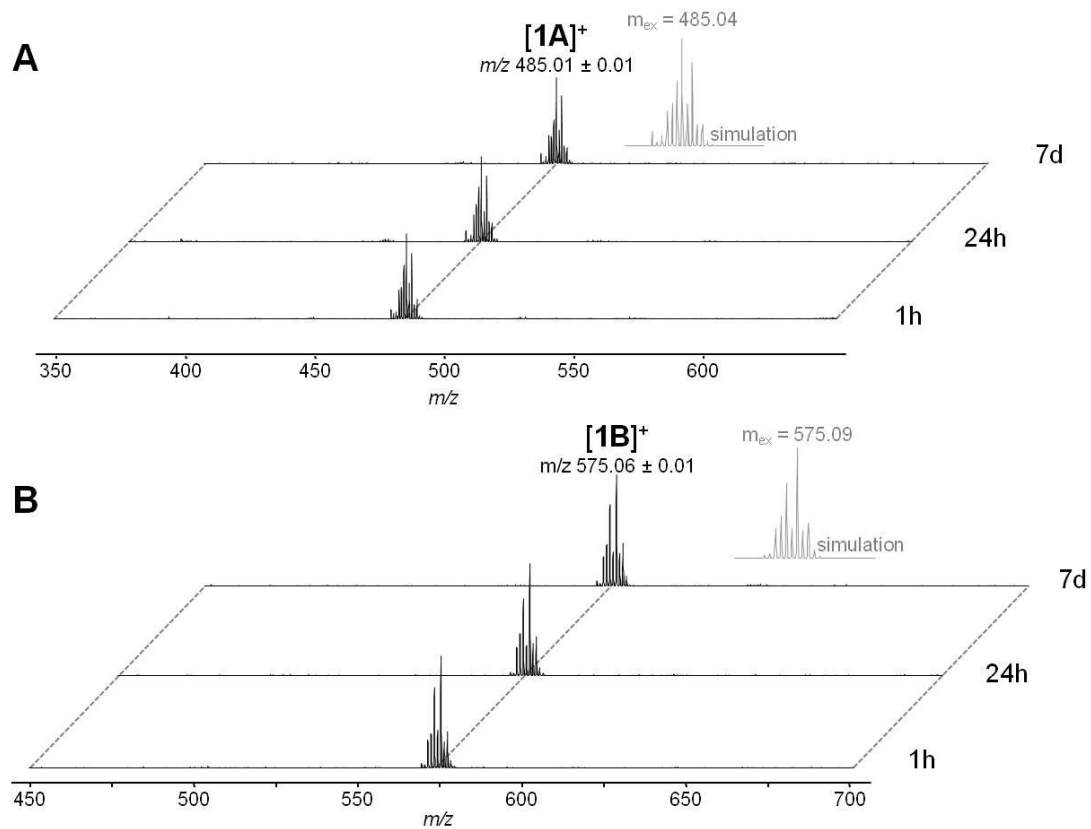


Figure S5. Time-dependent stability determined for **1A** (A) and **1B** (B) in HCl (60 mM, pH 1.2) by ESI-MS. The compounds do not hydrolyze and are stable over the entire incubation period.

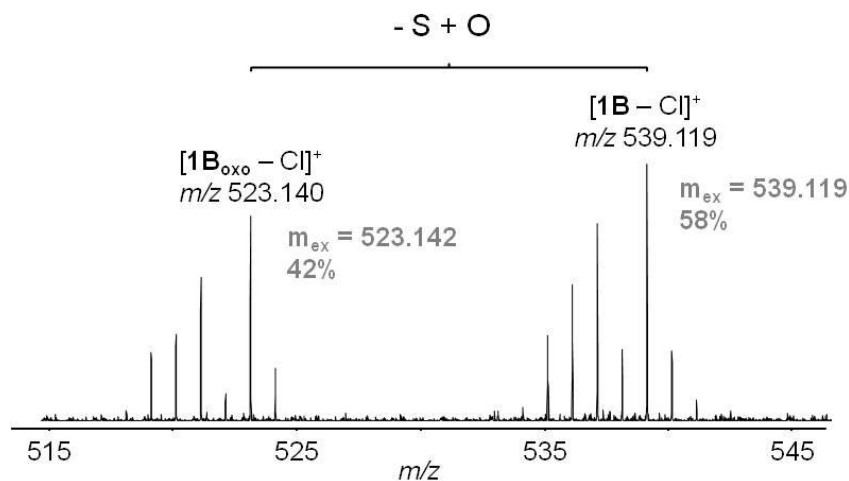


Figure S6. High resolution ESI-TOF mass spectrum of **1B** and its associated S→O exchange. The mass accuracy of the oxo-species is 4 ppm. Stock solutions of **1B** in DMSO were prepared, which inhibits dimer formation.

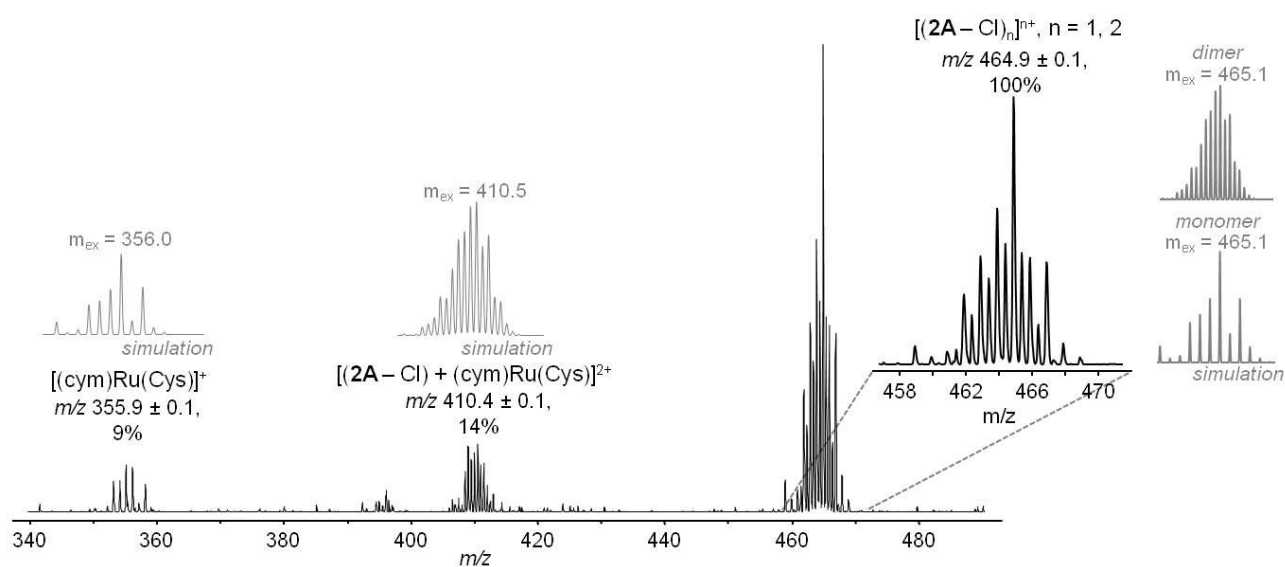


Figure S7. ESI IT mass spectrum of the reaction between **2A** and Cys after 24 h. Adduct formation with Cys is characterized by ligand cleavage.

Table S4. The pre-calculated molecular properties of the chlorido complexes are listed for the quantitative estimate of drug-likeness (QED): MW (molecular weight), LogD (distribution coefficient), HBA (hydrogen bond acceptor), HBD (hydrogen bond donor), PSA (polar surface area), ROTB (rotatable bonds), AROM (number of aromatic rings), ALERTS (number of structural alerts).²⁰ The LogD was calculated from φ_0 according to ref. 13. PSA was calculated using ChemBio3D 12.0 software (CambridgeSoft). In fact, Bickerton *et al.* used a calculated LogP (octanol-water coefficient) in their report. However, LogD was employed for calculating QED in the present study since the organometallics are charged. Calculation of the weighted QED for maximum information content (QED_w^{mo}) was carried out according to ref. 20.

Compound	MW	LogD	HBA	HBD	PSA	ROTB	AROM	ALERTS
1A	485.03	-0.52	2	1	15.27	3	3	0
2A	501.03	-1.13	2	2	23.67	3	3	0
3A	503.02	-0.38	3	1	15.27	3	3	0
4A	527.11	2.9	2	1	15.27	3	3	0
5A	570.13	-0.13	4	1	27.74	4	3	0
1B	574.19	-0.35	2	1	15.27	3	3	0
2B	590.19	-1.03	2	2	23.67	3	3	0
3B	592.18	-0.21	3	1	15.27	3	3	0
4B	616.27	3.15	2	1	15.27	3	3	0
5B	659.29	-0.06	4	1	27.74	4	3	0

References

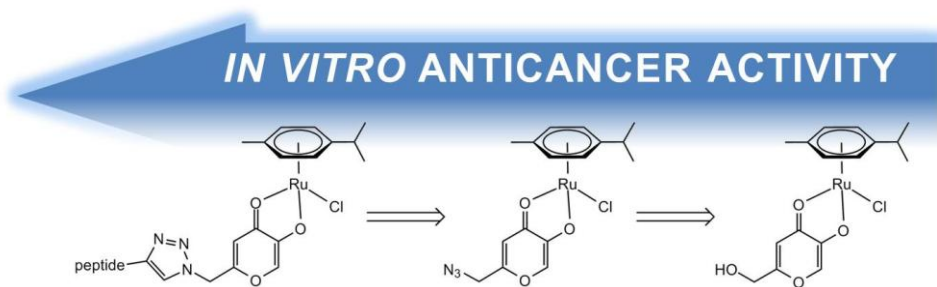
1. M. A. Bennett and A. K. Smith, *J. Chem. Soc., Dalton Trans.*, 1974, 233-241.
2. M. A. Bennett, T. N. Huang, T. W. Matheson and A. K. Smith, *Inorg. Synth.*, 1982, **21**, 74-78.
3. W. A. Kiel, R. G. Ball and W. A. G. Graham, *J. Organomet. Chem.*, 1990, **383**, 481-496.
4. J. A. Kitchen, N. G. White, M. Boyd, B. Moubaraki, K. S. Murray, P. D. W. Boyd and S. Brooker, *Inorg. Chem.*, 2009, **48**, 6670-6679.
5. B. Emmert and M. Groll, *Chem. Ber.*, 1953, **86**, 208-213.
6. W. A. Kinney, N. E. Lee, R. M. Blank, C. A. Demerson, C. S. Sarnella, N. T. Scherer, G. N. Mir, L. E. Borella, J. F. Dijoseph and C. Wells, *J. Med. Chem.*, 1990, **33**, 327-336.
7. M. H. Klingele and S. Brooker, *Eur. J. Org. Chem.*, 2004, 3422-3434.
8. M. R. Pressprich and J. Chambers, Bruker Analytical X-ray systems, Madison, 2004.
9. G. M. Sheldrick, *Acta Crystallogr., Sect. A: Found. Crystallogr.*, 2008, **64**, 112-122.
10. K. Valko, *J. Chromatogr. A*, 2004, **1037**, 299-310.
11. M. J. McKeage, S. J. Berners-Price, P. Galettis, R. J. Bowen, W. Brouwer, L. Ding, L. Zhuang and B. C. Baguley, *Cancer Chemother. Pharmacol.*, 2000, **46**, 343-350.
12. Organisation for Economic Co-operation and Development (OECD), 1989, **117**.
13. K. Valko and P. Slegel, *J. Chromatogr.*, 1993, **631**, 49-61.
14. C. A. Davey, D. F. Sargent, K. Luger, A. W. Maeder and T. J. Richmond, *J. Mol. Biol.*, 2002, **319**, 1097-1113.
15. M. S. Ong, T. J. Richmond and C. A. Davey, *J. Mol. Biol.*, 2007, **368**, 1067-1074.
16. B. Wu, M. S. Ong, M. Groessl, Z. Adhireksan, C. G. Hartinger, P. J. Dyson and C. A. Davey, *Chem. Eur. J.*, 2011, **17**, 3562-3566.
17. A. G. Leslie, *Acta Crystallogr., Sect. D: Biol. Crystallogr.*, 2006, **62**, 48-57.
18. S. Bailey, A. H. Fairlamb and W. N. Hunter, *Acta Crystallogr., Sect. D: Biol. Crystallogr.*, 1994, **50**, 139-154.
19. B. Wu, G. E. Davey, A. A. Nazarov, P. J. Dyson and C. A. Davey, *Nucleic Acids Res.*, 2011, **39**, 8200-8212.
20. G. R. Bickerton, G. V. Paolini, J. Besnard, S. Muresan and A. L. Hopkins, *Nat. Chem.*, 2012, **4**, 90-98.

5.2. Identification of the Structural Determinants for Anticancer Activity of an Organometallic Ru^{II}(Arene)–Peptide Conjugate

Electronic supplementary information available

Samuel M. Meier, Maria Novak, Wolfgang Kandioller, Michael A. Jakupec, Vladimir B. Arion, Nils Metzler-Nolte, Bernhard K. Keppler, Christian G. Hartinger

Chemistry – A European Journal, submitted.



Supporting Information

**Identification of the Structural Determinants for Anticancer
Activity of an Organometallic Ru(Arene)–Peptide Conjugate**

Samuel M. Meier, Maria Novak, Wolfgang Kandioller, Michael A. Jakupec,

Vladimir B. Arion, Nils Metzler-Nolte, Bernhard K. Keppler, Christian G. Hartinger

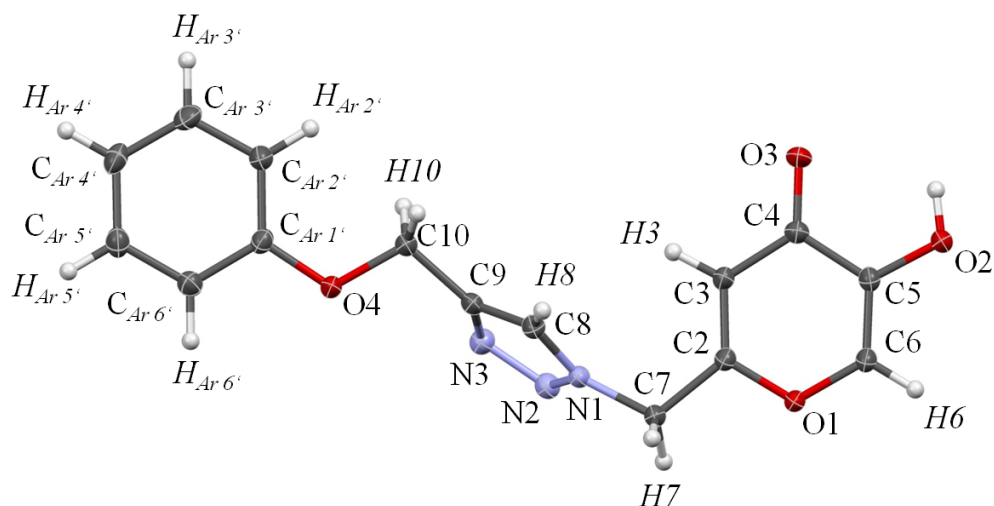


Figure S1. Molecular structure of 5-hydroxy-2-((4-(phenoxy)methyl)-1H-1,2,3-triazol-1-yl)methyl)-4H-pyran-4-one (**2**) and the numbering scheme used for characterization. Details on the X-ray diffraction experiment are listed in Table S1 and S2.

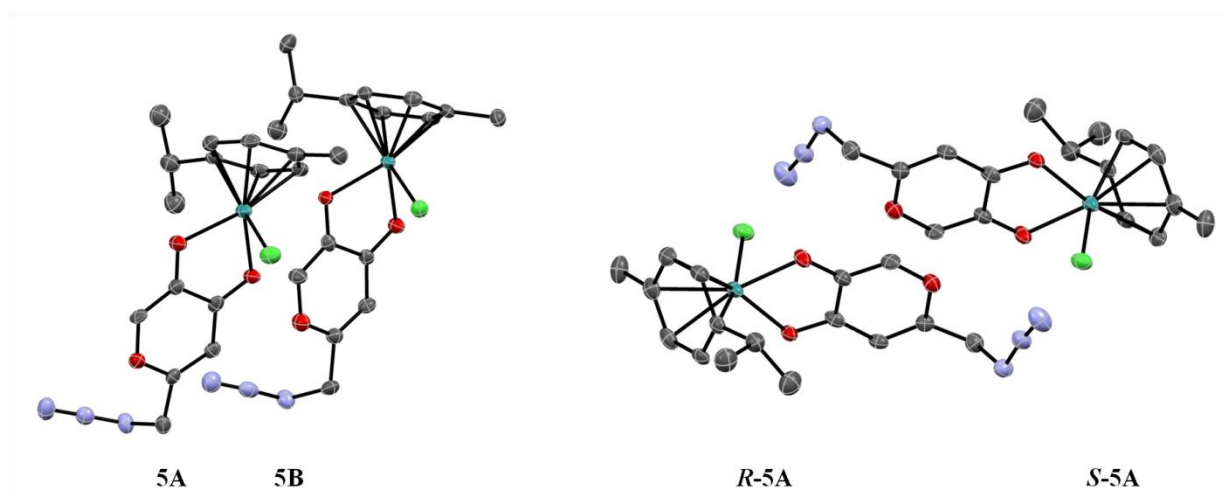


Figure S2. The two conformers of **5** (left) as well as the *R*- and *S*-enantiomers (right), which co-crystallized in the single crystal. Hydrogen atoms are omitted for clarity.

Table S1. Details on X-ray diffraction measurements and associated crystal cell parameters of **2** and **5**.

compound	2	5
CCDC N°	902337	902338
chemical formula	C ₃₀ H ₂₆ N ₆ O ₈	C ₁₂₈ H ₁₄₄ N ₂₄ O ₂₄ Cl ₈ Ru ₈
<i>M</i> (g mol ⁻¹)	598.57	3494.83
temperature (K)	100(2)	100(2)
crystal size (mm)	0.03 × 0.10 × 0.17	0.03 × 0.04 × 0.30
crystal color, habit	transparent, block	red, block
crystal system	triclinic	monoclinic
space group	P-1	P21/n
<i>a</i> (Å)	7.2018(9)	12.6311(5)
<i>b</i> (Å)	8.6385(10)	15.1054(6)
<i>c</i> (Å)	11.7485(6)	18.387(8)
<i>V</i> (Å ³)	663.71(13)	3397.0(2)
<i>α</i> (deg)	108.616(6)	90.00
<i>β</i> (deg)	94.151(7)	104.473(2)
<i>γ</i> (deg)	103.840(7)	90.00
<i>Z</i>	2	8
<i>D_c</i> (g cm ⁻³)	1.50	1.71
<i>μ</i> (mm ⁻¹)	0.11	1.10
F(000)	312.0	1760.0
Θ range (deg)	2.59–30.16	2.14–25.50
<i>h</i> range	-10/9	-15/15
<i>k</i> range	-12/12	-18/18
<i>l</i> range	-16/16	-22/22
no. unique refls.	3905	6310
no. parameters	202	435
<i>R</i> _{int}	0.0924	0.1320
<i>R</i> ₁ (obs.)	0.0534	0.0446
<i>wR</i> ₂ (all data)	0.1480	0.1109
<i>S</i>	1.018	1.049

Table S2. Selected bond lengths (Å), angles (°) and torsion angles (°) of **5**. The asymmetric unit of **5** contains two non-equivalent conformers denoted as **5A** and **5B**.

Bond Length (Å)	5A	5B
Ru–Cl	2.4183(13)	2.4051(14)
Ru–O2	2.074(3)	2.102(3)
Ru–O3	2.154(5)	2.132(3)
Ru–centroid	1.647(5)	1.652(5)
C6–O2	1.317(6)	1.321(6)
C5–O3	1.277(6)	1.287(6)
N1–P1	–	–
Bond Angles (°)		
O2–Ru–O3	77.88(12)	78.41(13)
O2–Ru–Cl	84.07(10)	85.55(11)
O3–Ru–Cl	84.24(10)	84.32(10)
N1–N2–N3	171.2(5)	171.2(5)
Torsion Angle (°)		
Ru–O3–C4–C5	11.0(5)	1.4(5)
C _{Cym4'} –Ru–O3–C4	162.5(3)	170.3(3)
C3–C2–C7–N1	-113.8(6)	-108.7(6)

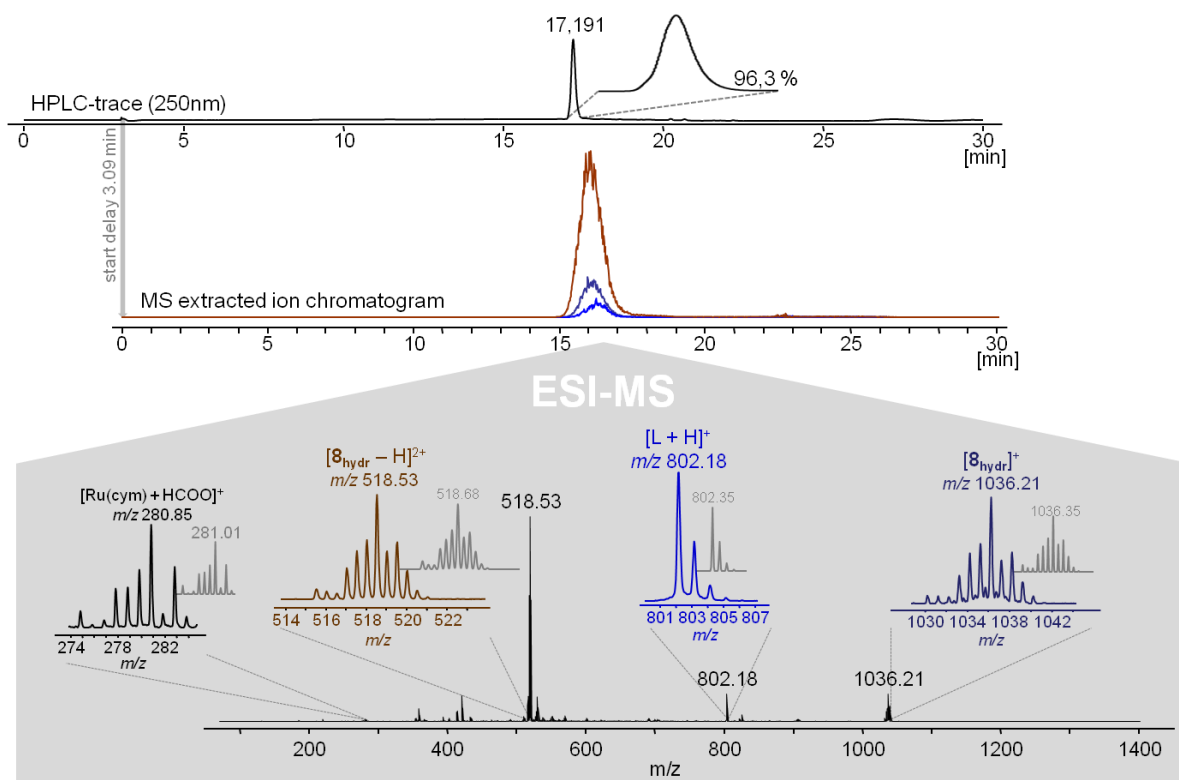


Figure S3. Liquid chromatogram and the corresponding ESI-IT MS trace of the purified peptide bioconjugate **8**. The magnification shows the ESI-IT-mass spectrum and the calculated isotope patterns for the identified species.

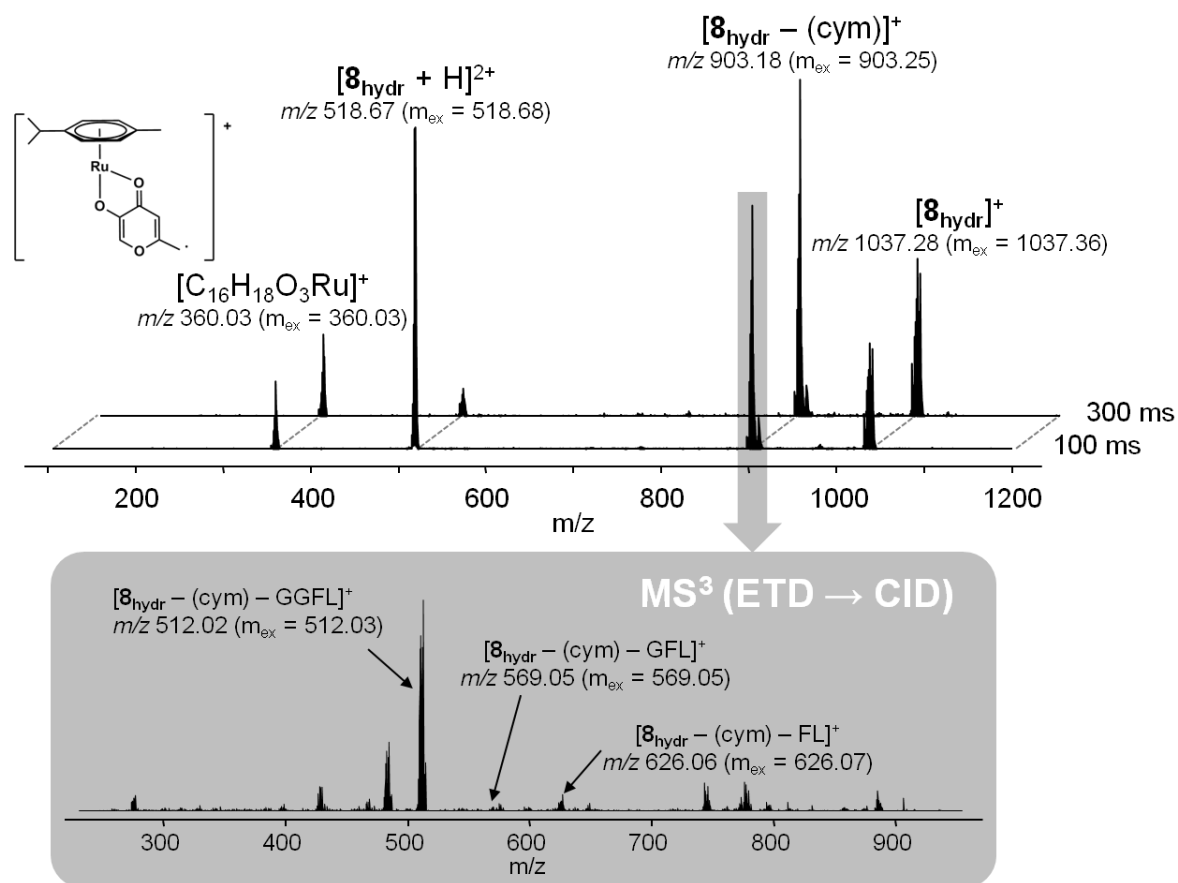


Figure S4. ESI-IT tandem mass spectrum (ETD, above) using 100 and 300 ms reaction time and CRCID MS^3 (gray below) of $[8_{hydr} - (cym)]^+$ underlining arene cleavage as a major reaction mode of Ru^{II} organometallics during ETD fragmentation.

Table S3. Experimental and theoretical ESI-IT mass signals of the detected metal-containing metabolites, which are discussed in the text. ESI-IT-MS include a standard deviation of $m/z \pm 0.03$.

Analysis	Detected Ion	m/z	m_{theor}
stability and top-down	$\mathbf{5}_{\text{hydr}}$	401.94	402.04
	$[\mathbf{5}_{\text{hydr}} - \text{N}_2]^+$	373.94	374.03
	$\mathbf{6}_{\text{hydr}}$	533.96	534.10
	$\mathbf{8}_{\text{hydr}}$	1036.34	1036.35
	$[\mathbf{8}_{\text{hydr}} + \text{H}]^{2+}$	518.70	518.67
	$[\mathbf{8}_{\text{hydr}} + \text{Na}]^{2+}$	529.69	529.67
	$[\mathbf{8}_{\text{hydr}} + \text{H}]^+$	1037.28	1037.36
	$[\mathbf{8}_{\text{hydr}} - (\text{cym})]^+$	903.18	903.25
	$[\mathbf{8}_{\text{hydr}} - (\text{cym}) - \text{GGFL}]^+$	512.02	512.03
	$[\text{Ru}(\text{cym})(\text{C}_6\text{H}_4\text{O}_3)]^+$	360.03	360.03
	$[\text{Ru}_2(\text{cym})_2(\mu\text{-OCH}_3)_3]^+$	564.92	565.08
small biomolecules	$[\text{Ru}(\text{cym})(\text{Cys})]^+$	355.90	356.03
	$[\text{Ru}(\text{cym})(\text{His})]^+$	389.96	390.08
	$[\text{Ru}(\text{cym})(\text{Gly})]^+$	309.92	310.04
	$[\text{Ru}(\text{cym})(\text{Gly})_2]^+$	387.90	388.09
	$[\text{Ru}(\text{cym})(\text{EtG})(\text{Gly})]^+$	489.11	489.12
proteins	$[\text{ub} + \text{Ru}(\text{cym})]^+$	8798.56	8798.58
	$[\text{ub} + 2\text{Ru}(\text{cym})]^+$	9031.54	9031.63
	$[\text{cyt} + \text{Ru}(\text{cym})]^+$	12593.25	12593.35
	$[\text{cyt} + \mathbf{5}_{\text{hydr}}]^+$	12760.25	12760.25

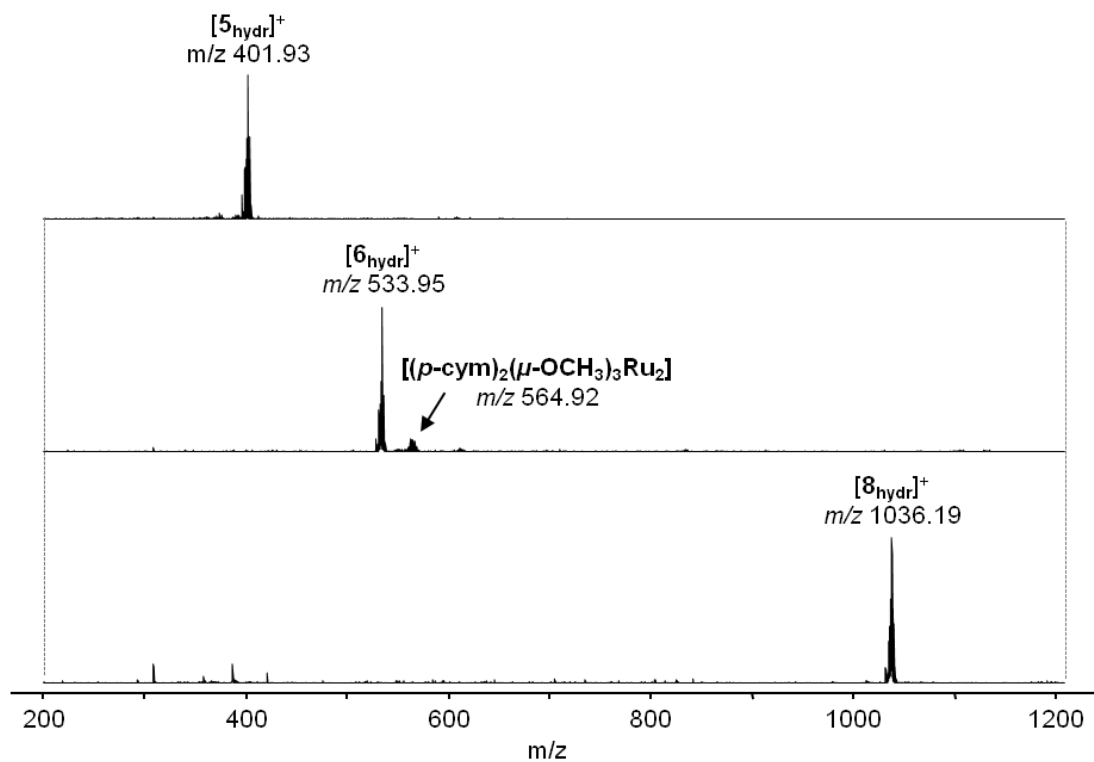
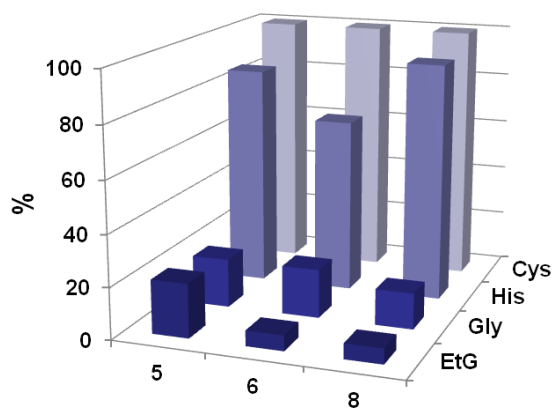
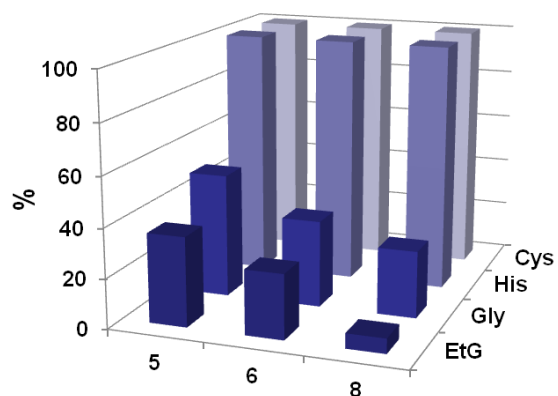


Figure S5. ESI-IT mass spectra recorded in stability experiments of **5**, **6** and **8** in aqueous solution after 48 h. The compounds are stable and dinuclear hydrolysis species were only detected in small amounts in the mass spectrum of **6** (arrow).



1 h incubation



48 h incubation

Figure S6. The percentage of adduct formation between complexes **5**, **6** and **8** and the biomolecules Cys, His, Gly and EtG are shown after 1 h (*left*) and 48 h (*right*) of incubation. The metallodrug and amino acids were incubated at a molar ratio of 1 : 1 while the molar ratio was 1 : 2 in the case of EtG.

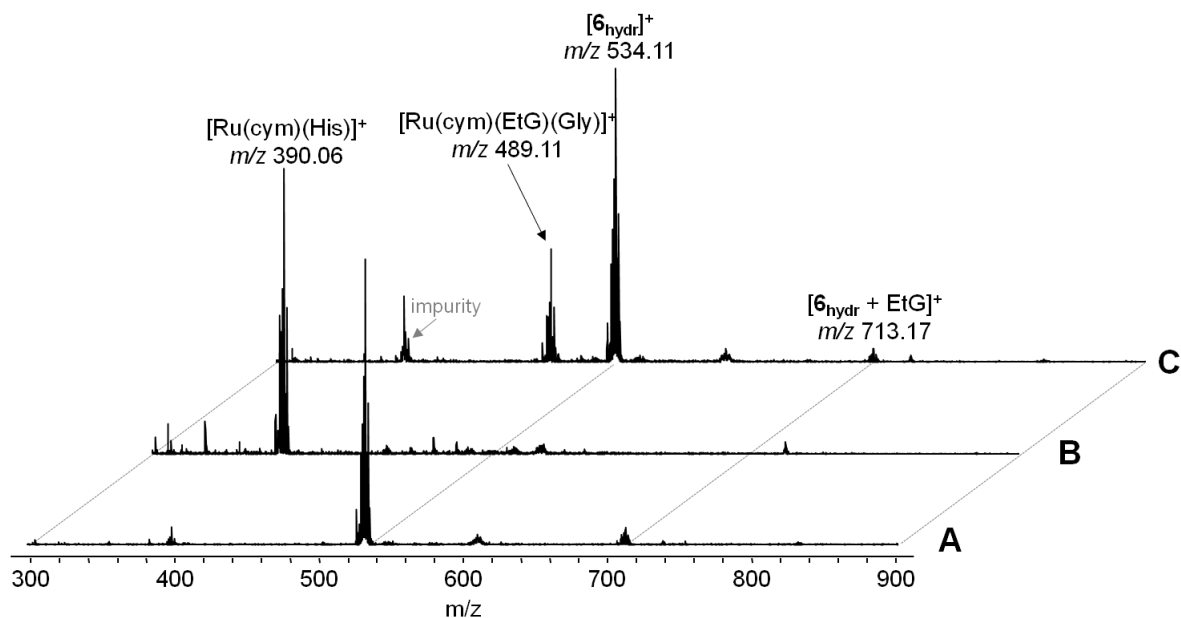


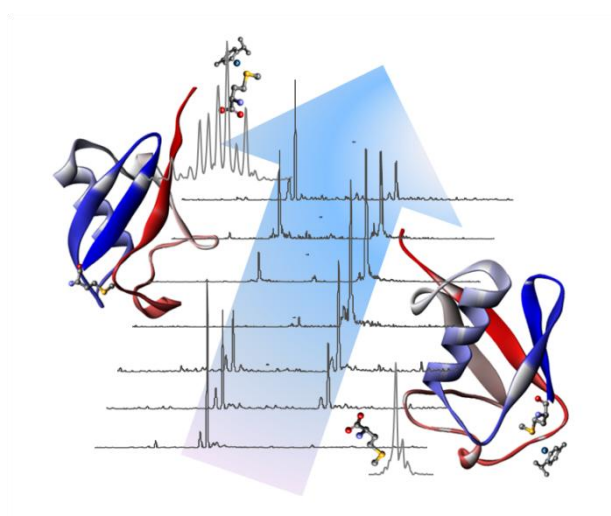
Figure S7. Mass spectra recorded during the reactivity study of **6** and of the $[\mathbf{6} + \text{EtG} - \text{Cl}]^+$ adduct. Compound **6** and EtG were pre-incubated for 5 days at a 1 : 2 molar ratio (**A**). L-Histidine addition to the mixture leads to quantitative $[\text{Ru}(\text{cym})(\text{His})]^+$ adduct formation within 3 h (**B**), whereas glycine cannot induce ligand cleavage in the $[\mathbf{6}_{\text{hydr}} + \text{EtG}]^+$ adduct during the same time period (**C**). However, free **6** slowly converts to the Gly adduct and a mixed glycine/9-ethylguanine adduct is obtained from the EtG–**6** adduct. The absence of a similar adduct in **B** suggests a tridentate binding mode of His to the Ru(cym) moiety.

5.3. Biomolecule Binding vs. Anticancer Activity: Reactions of Ru(arene)[(thio)pyr(id)one] Compounds with Amino Acids and Proteins

Publication does not contain electronic supplementary information

Samuel M. Meier, Muhammad Hanif, Wolfgang Kandioller, Bernhard K. Keppler, Christian G. Hartinger

Journal of Inorganic Biochemistry, **2012**, *108*, 91-95.

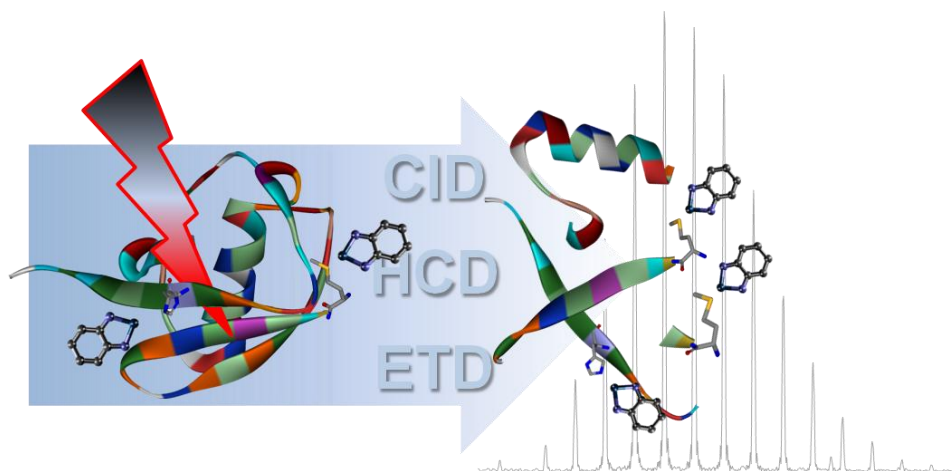


5.4. Fragmentation Methods on the Balance: Unambiguous Top-Down Mass Spectrometric Characterization of Oxaliplatin-Ubiquitin Binding Sites

Electronic supplementary information available

Samuel M. Meier, Yury O. Tsybin, Paul J. Dyson, Bernhard K. Keppler, Christian G. Hartinger

Analytical and Bioanalytical Chemistry, **2012**, *402*, 2655-2662.



Analytical and Bioanalytical Chemistry

Electronic Supplementary Material

**Fragmentation methods on the balance: Unambiguous top-down
mass spectrometric characterization of oxaliplatin–ubiquitin
binding sites**

Samuel M. Meier, Yury O. Tsybin, Paul J. Dyson, Bernhard K. Keppler, Christian
G. Hartinger

Table S1. Numbers of detected metallated peptide fragments in the respective tandem mass spectra of the [Ub + Pt(chxn)] adduct.

Fragment type	FT ICR	FT orbitrap		
	QCID	CID	HCD	ETD
b	9	16	13	-
c	-	-	-	46
y	6	7	14	-
z	-	-	-	4
Total	15	23	27	50

Table S2. Mass list of detected metallated peptide fragments from ESI-CID-orbitrap-MS/MS measurements after isolation of the [Ub + Pt(chxn)] adduct at charge state 12+.

Fragment	Accurate Mass	Exact Mass	Δppm	%	Resolution
Pt(chxn) B ₁₆ ⁴⁺	528.77774	528.77780	0.11	0.6	124000
Pt(chxn) B ₁₇ ⁴⁺	553.54489	553.54491	0.03	2.2	123000
Pt(chxn) B ₂ ⁺	567.17141	567.17126	0.27	4.2	117000
Pt(chxn) B ₁₈ ⁴⁺	586.05618	586.05600	0.31	8.6	116000
Pt(chxn) Y ₂₄ ⁵⁺	607.72079	607.72048	0.51	2.5	113000
Pt(chxn) B ₂₀ ⁴⁺	632.07760	632.07722	0.60	0.5	103000
Pt(chxn) Y ₅₈ ⁹⁺	760.73654	760.73635	0.25	50.0	102000
Pt(chxn) B ₁₁ ²⁺	777.89578	777.89524	0.70	1.3	100000
Pt(chxn) B ₁₈ ³⁺	781.07284	781.07224	0.77	20.3	101000
Pt(chxn) Y ₇₄ ¹¹⁺	783.97048	783.97053	0.06	4.2	95000
Pt(chxn) Y ₆₀ ⁹⁺	785.97073	785.97064	0.11	1.7	96000
Pt(chxn) Y ₇₅ ¹¹⁺	795.61227	795.61222	0.06	1.3	99000
Pt(chxn) Y ₅₆ ⁸⁺	832.69180	832.69188	0.10	1.4	92000
Pt(chxn) Y ₅₇ ⁸⁺	843.57089	843.57089	0.00	0.9	94000
Pt(chxn) B ₅₈ ⁸⁺	847.82082	847.82125	0.51	1.3	90000
Pt(chxn) Y ₅₉ ⁸⁺	871.95834	871.95811	0.26	0.5	93000
Pt(chxn) B ₅₂ ⁷⁺	878.74881	878.74879	0.02	12.5	99000
Pt(chxn) B ₁₃ ²⁺	885.46267	885.46188	0.89	0.9	96000
Pt(chxn) B ₃₉ ⁵⁺	924.28115	924.28076	0.42	1.4	96000
Pt(chxn) B ₅ ⁺	926.39364	926.39284	0.86	0.4	91000
Pt(chxn) B ₁₄ ²⁺	936.48879	936.48846	0.35	0.5	91000
Pt(chxn) B ₃₂ ⁴⁺	971.00496	971.00539	0.44	0.4	97000
Pt(chxn) B ₁₅ ²⁺	992.52835	992.52783	0.53	0.5	85000
Pt(chxn) B ₆ ⁺	1054.48898	1054.48727	1.62	0.9	87000
Pt(chxn) B ₃₆ ⁴⁺	1078.06704	1078.06675	0.27	0.2	88000
Pt(chxn) B ₄₇ ⁵⁺	1107.18484	1107.18384	0.90	0.3	82000

Table S3. Mass list of detected metallated peptide fragments from ESI-CID-FT-ICR-MS/MS measurements after isolation of the [Ub + Pt(chxn)] adduct at charge state 11+.

Fragment	Accurate Mass	Exact Mass	Δppm	%	Resolution
Pt(chxn)B ₂ ⁺	567.17120	567.17126	0.10	13.2	109000
Pt(chxn)B ₁₇ ³⁺	738.05832	738.05802	0.40	3.3	87000
Pt(chxn)Y ₂₄ ⁴⁺	759.39872	759.39878	0.08	12.4	80000
Pt(chxn)B ₁₁ ²⁺	777.89594	777.89524	0.90	2.0	77000
Pt(chxn)B ₁₈ ³⁺	781.07240	781.07224	0.20	5.7	79000
Pt(chxn)Y ₁₈ ³⁺	802.09087	802.09084	0.04	2.3	79000
Pt(chxn)Y ₄₀ ⁶⁺	812.59407	812.59385	0.27	1.3	85000
Pt(chxn)Y ₅₈ ⁸⁺	855.70277	855.70249	0.33	55.5	73000
Pt(chxn)Y ₇₄ ¹⁰⁺	862.26700	862.26686	0.17	4.1	73000
Pt(chxn)B ₅₂ ⁷⁺	878.74914	878.74879	0.40	25.0	71000
Pt(chxn)B ₃₉ ⁵⁺	924.28130	924.28076	0.58	4.1	69000
Pt(chxn)Y ₅₇ ⁷⁺	963.79414	963.79392	0.23	3.5	69000
Pt(chxn)B ₆ ⁺	1054.48800	1054.48727	0.69	9.9	59000
Pt(chxn)B ₁₆ ²⁺	1057.04947	1057.04916	0.30	5.1	59000
Pt(chxn)B ₃₆ ⁴⁺	1077.81665	1077.81599	0.61	2.1	65000

Table S4. Mass list of detected metallated peptide fragments from ESI-HCD-orbitrap-MS/MS

measurements after isolation of the [Ub + Pt(chxn)] adduct at charge state 12+.

Fragment	Accurate Mass	Exact Mass	Δ ppm	%	Resolution
Y_8^{2+}	442.29486	442.29544	1.31	8.2	131000
Pt(chxn) B_2^+	567.17130	567.17126	0.08	22.7	116000
Pt(chxn) B_7^{2+}	578.27121	578.27112	0.15	3.0	113000
Pt(chxn) Y_{24}^{5+}	607.72073	607.72048	0.41	2.3	112000
Pt(chxn) B_{14}^{3+}	623.99265	623.99241	0.39	3.6	111000
Pt(chxn) Y_{14}^{3+}	629.34134	629.34118	0.26	1.1	111000
Pt(chxn) B_8^{2+}	634.81345	634.81317	0.44	2.5	111000
Pt(chxn) Y_{40}^{7+}	696.79636	696.79610	0.37	2.5	105000
Pt(chxn) B_{16}^{3+}	705.03580	705.03520	0.86	28.2	103000
Pt(chxn) B_{17}^{3+}	738.05850	738.05802	0.65	16.8	102000
Pt(chxn) Y_{58}^{9+}	760.73648	760.73635	0.17	36.4	99000
Pt(chxn) B_{11}^+	777.89578	777.89524	0.70	3.6	95000
Pt(chxn) B_{18}^{3+}	781.07285	781.07224	0.78	8.2	95000
Pt(chxn) Y_{25}^{4+}	788.15598	788.15552	0.58	1.1	94000
Pt(chxn) Y_{26}^{4+}	820.66690	820.66675	0.19	1.8	98000
Pt(chxn) B_{12}^{2+}	828.41959	828.41909	0.61	3.6	87000
Pt(chxn) Y_{27}^{4+}	848.68747	848.68721	0.31	3.6	97000
[Pt(chxn) $Y_{59} - OH$] $^{8+}$	869.58164	869.58149	0.17	2.5	92000
Pt(chxn) Y_{13}^{2+}	879.46072	879.46064	0.09	2.3	91000
Pt(chxn) Y_{28}^{4+}	880.70230	880.70186	0.50	2.5	94000
Pt(chxn) B_{13}^{2+}	885.46292	885.46188	1.18	4.1	87000
Pt(chxn) B_5^+	926.39316	926.39229	0.94	5.0	88000
Pt(chxn) Y_{56}^{7+}	951.36075	951.36077	0.02	2.0	95000
Pt(chxn) Y_{39}^{5+}	955.70151	955.70108	0.46	1.8	84000
Pt(chxn) Y_{57}^{7+}	963.79404	963.79392	0.13	3.6	87000
Pt(chxn) B_{15}^{2+}	992.52884	992.52783	1.02	3.6	86000
Pt(chxn) Y_{15}^{2+}	1007.53793	1007.53742	0.50	1.1	96000
Pt(chxn) B_6^+	1054.48880	1054.48727	1.45	3.9	82000

Table S5. Mass list of detected metallated peptide fragments from ESI-ETD-orbitrap-MS/MS

measurements after isolation of the [Ub + Pt(chxn)] adduct at charge state 12+.

Fragment	Accurate Mass	Exact Mass	Δppm	%	Resolution
Z ₈ ²⁺	434.28512	434.28607	2.19	7.1	138000
Pt(chxn)C ₆ ²⁺	536.26058	536.26054	0.07	16.7	129000
Pt(chxn)C ₂ ⁺	584.19808	584.19779	0.50	3.6	102000
Pt(chxn)C ₇ ²⁺	586.78469	586.78439	0.51	28.6	116000
Pt(chxn)C ₁₃ ³⁺	596.31978	596.31919	0.99	3.6	110000
Pt(chxn)C ₁₄ ³⁺	629.66842	629.66792	0.79	8.3	110000
Pt(chxn)C ₈ ²⁺	643.32692	643.32644	0.75	47.6	110000
Pt(chxn)C ₂₁ ⁴⁺	665.09072	665.0906	0.18	2.4	100000
Pt(chxn)C ₁₅ ³⁺	667.69692	667.69649	0.65	3.6	101000
Pt(chxn)C ₉ ²⁺	693.85091	693.85029	0.90	26.2	105000
Pt(chxn)C ₃ ⁺	697.28225	697.2819	0.50	3.6	95000
Pt(chxn)Z ₁₀ ²⁺	713.89467	713.89475	0.11	6.0	103000
Pt(chxn)C ₁₀ ²⁺	722.36184	722.36102	1.14	52.4	103000
Pt(chxn)C ₃₀ ⁵⁺	731.79458	731.7938	1.07	4.8	96000
Pt(chxn)Z ₃₁ ⁵⁺	752.99080	752.99038	0.56	6.0	97000
Pt(chxn)C ₅₁ ⁸⁺	756.78127	756.78105	0.29	2.4	100000
Pt(chxn)C ₅₃ ⁸⁺	778.28713	778.2871	0.04	2.4	107000
Pt(chxn)C ₃₂ ⁵⁺	780.41085	780.410912	0.08	4.8	105000
Pt(chxn)C ₁₁ ²⁺	786.40932	786.40851	1.03	7.1	103000
Pt(chxn)C ₄₇ ⁷⁺	793.56582	793.56582	0.00	4.8	94000
Pt(chxn)C ₅₄ ⁸⁺	797.92519	797.92502	0.21	3.6	107000
Pt(chxn)C ₄₈ ⁷⁺	811.86593	811.86511	1.01	2.9	93000
Pt(chxn)C ₄₁ ⁶⁺	816.09353	816.09283	0.86	6.0	95000
Pt(chxn)C ₁₉ ³⁺	819.09908	819.09869	0.47	6.0	90000
Pt(chxn)C ₆₃ ⁹⁺	827.4385	827.43804	0.56	6.0	101000
Pt(chxn)C ₅₇ ⁸⁺	835.57046	835.57050	0.05	8.3	89000
Pt(chxn)C ₂₇ ⁴⁺	836.18564	836.18582	0.22	19.0	94000
Pt(chxn)C ₄₂ ⁶⁺	842.11031	842.10969	0.74	9.5	102000
Pt(chxn)C ₃₅ ⁵⁺	843.24349	843.24273	0.90	8.3	94000
Pt(chxn)C ₅₈ ⁸⁺	849.82357	849.82359	0.02	7.1	85000
Pt(chxn)C ₂₈ ⁴⁺	853.94619	853.94655	0.42	14.3	95000
Pt(chxn)C ₄₄ ⁶⁺	879.80532	879.80533	0.01	19.0	98000
Pt(chxn)C ₆₀ ⁸⁺	884.58791	884.58717	0.84	9.5	81000
Pt(chxn)C ₆₁ ⁸⁺	898.72292	898.72268	0.27	9.5	94000
Pt(chxn)Z ₄₅ ⁶⁺	900.63704	900.63745	0.46	4.8	101000
Pt(chxn)C ₄₅ ⁶⁺	904.14907	904.14877	0.33	23.8	96000

Table S5 con't. Continued mass list of detected metallated peptide fragments from ESI-ETD-orbitrap-MS/MS measurements after isolation of the [Ub + Pt(chxn)] adduct at charge state 12+.

Fragment	Accurate Mass	Exact Mass	Δ ppm	%	Resolution
Pt(chxn) C_{38}^{5+}	904.88192	904.88224	0.36	16.7	88000
Pt(chxn) C_{22}^{3+}	920.13527	920.13428	1.08	4.8	92000
Pt(chxn) C_{39}^{5+}	927.68661	927.68607	0.58	9.5	90000
Pt(chxn) C_{31}^{4+}	946.50570	946.50508	0.66	26.2	95000
Pt(chxn) C_{23}^{3+}	957.82949	957.82899	0.53	10.7	89000
Pt(chxn) C_{59}^{7+}	994.52120	994.52102	0.18	21.4	95000
Pt(chxn) C_{24}^{3+}	1000.84420	1000.84320	1.00	38.1	92000
Pt(chxn) C_{33}^{4+}	1007.53621	1007.53608	0.13	8.3	96000
Pt(chxn) C_{25}^{3+}	1038.85854	1038.85752	0.99	9.5	90000
Pt(chxn) Z_{25}^{3+}	1045.53567	1045.53465	0.98	3.6	50000
Pt(chxn) C_{16}^{2+}	1065.56264	1065.56243	0.20	6.0	92000
Pt(chxn) C_{26}^{3+}	1071.88112	1071.88033	0.73	9.5	87000
Pt(chxn) C_{75}^{8+}	1102.84218	1102.8437	1.38	16.7	86000
Pt(chxn) C_{40}^{4+}	1191.37185	1191.37042	1.20	8.3	80000
Pt(chxn) C_{20}^{2+}	1272.16286	1272.16146	1.10	4.8	66000

6. Personal Information

Samuel M. Meier, MSc.
University of Vienna
Institute of Inorganic Chemistry, 2H14
Währinger Str. 42
A – 1090 Vienna

T: +43 (1) 4277 52 666
samuel.meier@univie.ac.at

6.1. Curriculum Vitae

6.1.1. Education

2011 Sept	Short scientific mission at the Ruhr University Bochum in the group of Prof. N. Metzler-Nolte Topic: Synthesis of metal-peptide conjugates
2009 – now	Ph.D. studies in chemistry at the University of Vienna in the group of Prof. B.K. Keppler Field: Bioinorganic medicinal chemistry Title: Novel concepts and strategies in anticancer metallodrug development: Towards oral activity, peptide conjugation and mass spectrometric applications
2009 Aug	Master's degree in chemistry at the ETH Zurich
2008 Sep – 2009 Feb	Master's thesis at the University of Zurich in the group of Prof. R. Alberto Field: Inorganic medicinal chemistry Title: Extension of the synthetic route to access Re ^I and Re ^{II} dicarbonyl complexes <i>via</i> ligand-mediated decarbonylation
2007 – 2009	Master's programme in chemistry at the ETH Zurich
2007 Aug	Bachelor's degree in chemistry at the EPF Lausanne
2006 – 2007	SOCRATES student exchange year at the University of Edinburgh Semester project in the group of Prof. P.J. Sadler Field: Inorganic medicinal chemistry Title: Characterisation and photoactivation of dinuclear Ru ^{II} arene complexes
2004 – 2007	Undergraduate studies in chemistry at the EPF Lausanne
2003 Jun	Matura (qualification for university entrance)
1999 – 2003	Secondary school at the Kantonsschule Pfäffikon / Nuolen, Standort Nuolen Major: Chemistry and biology

6.1.2. Grants

2011 myGÖCH-grant for short scientific missions

6.2. List of Publications

6.2.1. Original Articles

- [9] Samuel M. Meier, Maria Novak, Wolfgang Kandioller, Michael A. Jakupec, Vladimir B. Arion, Nils Metzler-Nolte, Bernhard K. Keppler, Christian G. Hartinger
Identification of the Structural Determinants for Anticancer Activity of an Organometallic Ru^{II}(Arene)-Peptide Conjugate
Chemistry – A European Journal, submitted.
- [8] Samuel M. Meier, Muhammad Hanif, Zenita Adhireskan, Verena Pichler, Maria Novak, Elisabeth Jirkovsky, Michael A. Jakupec, Vladimir B. Arion, Curt A. Davey, Bernhard K. Keppler, Christian G. Hartinger
Novel Metal(II) Arene 2-Pyridinecarbothioamides: A Rationale to Orally Active Organometallic Anticancer Agents
Chemical Science, **2013**, *4*, 1837-1846.
- [7] Maria V. Babak, Samuel M. Meier, Alexander Roller, Michael A. Jakupec, Bernhard K. Keppler, Christian G. Hartinger
Am(m)ines make the Difference: Organometallic Ruthenium Am(m)ine Complexes and Their Chemistry in Anticancer Drug Development
Chemistry – A European Journal, **2012**,
DOI:10.1002/chem.201202657.
- [6] Gerlinde Grabmann, Samuel M. Meier, Yulia Y. Scaffidi-Domianello, Markus Galanski, Bernhard K. Keppler, Christian G. Hartinger
CZE and CZE-ESI-MS Studies on the Stability of Anticancer *cis*- and *trans*-[bis(2-propanone oxime)dihalidoplatinum(II)] Complexes
Journal of Chromatography A, **2012**, *1267*, 156-161.
- [5] Samuel M. Meier, Yury O. Tsybin, Paul J. Dyson, Bernhard K. Keppler, Christian G. Hartinger
Fragmentation Methods on the Balance: Unambiguous Top-Down Mass Spectrometric Characterization of Oxaliplatin-Ubiquitin Binding Sites
Analytical and Bioanalytical Chemistry, **2012**, *402*, 2655-2662.
- [4] Samuel M. Meier, Muhammad Hanif, Wolfgang Kandioller, Bernhard K. Keppler, Christian G. Hartinger
Biomolecule Binding vs. Anticancer Activity: Reactions of Ru(arene)[(thio)pyr(id)one] Compounds with Amino Acids and Proteins
Journal of Inorganic Biochemistry, **2012**, *108*, 91-95.
- [3] Muhammad Hanif, Samuel M. Meier, Wolfgang Kandioller, Anna Bytzek, Michaela Hejl, Christian G. Hartinger, Alexey A. Nazarov, Vladimir B. Arion, Michael A. Jakupec, Paul J. Dyson, Bernhard K. Keppler
From Hydrolytically Labile to Hydrolytically Stable Ru(II)-Arene Anticancer Complexes with Carbohydrate-Derived co-Ligands
Journal of Inorganic Biochemistry, **2011**, *105(2)*, 224-231.
- [2] Muhammad Hanif, Helena Henke, Samuel M. Meier, Sanela Martić, Mahmoud Labib, Wolfgang Kandioller, Michael A. Jakupec, Vladimir B. Arion, Heinz-Bernhard Kraatz, Bernhard K. Keppler, Christian G. Hartinger
Is the Reactivity of M(II)-Arene Complexes of 3-Hydroxy-2(1H)-pyridones to Biomolecules the Anticancer Activity Determining Parameter?
Inorganic Chemistry, **2010**, *49(17)*, 7953-7963.

- [1] Steven W. Magennis, Abraha Habtemariam, Olga Novakova, John B. Henry, Samuel Meier, Simon Parsons, Iain D. H. Oswald, Viktor Brabec, Peter J. Sadler
Dual Triggering of DNA Binding and Fluorescence via Photoactivation of a Dinuclear Ruthenium(II) Arene Complex
Inorganic Chemistry, **2007**, *46(12)*, 5059-5068.

6.2.2. Review Articles

- [2] Christian G. Hartinger, Michael Groessl, Samuel M. Meier, Angela Casini, Paul J. Dyson,
Application of Mass Spectrometric Techniques to Delineate the Modes-of-Action of Anticancer Metalloodrugs
Chemical Society Reviews, submitted.
- [1] Wolfgang Kandioller, Andrea Kurzwernhart, Muhammad Hanif, Samuel M. Meier, Helena Henke, Bernhard K. Keppler, Christian G. Hartinger
Pyrone Derivatives and Metals: From Natural Products to Metal-Based Drugs
Journal of Organometallic Chemistry, **2011**, *696(5)*, 999-1010.

6.3. List of Oral Contributions

- [3] Samuel M. Meier, Muhammad Hanif, Wolfgang Kandioller, Bernhard K. Keppler, Christian G. Hartinger
Biomolecule Binding vs. Anticancer Activity: Reactions of Organometallic Ruthenium(II) Arene Metalloodrugs with Amino Acids and Proteins
7th ASAC JunganalytikerInnen Forum, September 25-26, 2011, Linz, Austria.
- [2] Samuel M. Meier, Yury O. Tsybin, Paul J. Dyson, Bernhard K. Keppler, Christian G. Hartinger
Top-Down High Resolution Mass Spectrometry of Ubiquitin-Oxaliplatin Adducts
MassSpec-Forum-Vienna, February 22-23, 2011, Vienna, Austria.
- [1] Samuel M. Meier, Yury O. Tsybin, Paul J. Dyson, Bernhard K. Keppler, Christian G. Hartinger
Investigation of the Binding Interaction of Oxaliplatin to Ubiquitin by Mass Spectrometric Methods
6th Workshop Anorganische Chemie Österreich, March 29-30, 2010, Linz, Austria.

6.4. List of Poster Contributions

- [2] Samuel M. Meier, Yury O. Tsybin, Paul J. Dyson, Bernhard K. Keppler, Christian G. Hartinger
Fragmentation Methods on the Balance: Unambiguous Top-Down Mass Spectrometric Characterization of Oxaliplatin-Ubiquitin Binding Sites
International Symposium of Applied Bioinorganic Chemistry – ISABC11, December 2-5, 2011, Barcelona, Spain.
- [1] Samuel M. Meier, Muhammad Hanif, Wolfgang Kandioller, Bernhard K. Keppler, Christian G. Hartinger
Biomolecule Binding vs. Anticancer Activity: Reactions of Organometallic Ruthenium(II) Arene Metalloodrugs with Amino Acids and Proteins
14th Austrian Chemistry Days, September 26-29, 2011, Linz, Austria.

Ich habe mich bemüht, sämtliche Inhaber der Bildrechte ausfindig zu machen und ihre Zustimmung zur Verwendung der Bilder in dieser Arbeit eingeholt. Sollte dennoch eine Urheberrechtsverletzung bekannt werden, ersuche ich um Meldung bei mir.

– S.M.M
März, 2013